UNIVERSITAT POLITÈCNICA DE CATALUNYA BARCELONATECH

# *BEST: Bézier-Enhanced Shell Triangle A new rotation-free thin shell finite element*


## Pere-Andreu Ubach de Fuentes

UNIVERSITAT POLITÈCNICA DE CATALUNYA BARCELONATECH

*PhD program in Structural Analysis*

# BEST: Bézier-Enhanced Shell Triangle

A NEW ROTATION-FREE THIN SHELL FINITE ELEMENT

A thesis submitted in partial fulfillment of the requirements for the degree of PhD in Civil and Environmental Engineering by the Polytechnic University of Catalonia

This thesis
was partially supported by
the International Center
for Numerical Methods
in Engineering

CIMNE

**Doctoral thesis by:**
Pere-Andreu Ubach de Fuentes

**Thesis Advisors:**
Eugenio Oñate Ibáñez de Navarra
Julio García-Espinosa

Departament d'Enginyeria Civil i Ambiental
Departament de Resistència de Materials i Estructures en Enginyeria

Barcelona, December 2019

# Abstract

A new thin shell finite element is presented. This new element doesn't have rotational degrees of freedom. Instead, in order to overcome the $\mathcal{C}^1$ continuity requirement across elements, the author resorts to enhance the geometric description of the flat triangles of a mesh made out of linear triangles, by means of Bernstein polynomials and triangular Bernstein-Bézier patches.

The author estimates the surface normals at the nodes of a mesh of triangles, in order to use them to define the Bernstein-Bézier patches. Ubach, Estruch and García-Espinosa performed a comprehensive statistical comparison of different weighting factors, including other weights previously used in the literature. The conclusion of that work (included as an appendix to this thesis) is that the inverse of the area of the circumscribed circle to the triangle and the internal angle of the triangle at the node considered, should be used as weighting factor. Using this new weighting factor, we reduce by about 10% the root mean square error in the estimation of normals of randomly generated surfaces with respect to the previous best weighting factor found in the literature.

The author uses the information of the normal vectors at the nodes and the triangular Bernstein-Bézier patches to build cubic Bézier triangles. These cubic Bézier triangles are surface interpolants; $\mathcal{C}^1$ continuous at the nodes and $\mathcal{C}^0$ continuous across the edges. Owing to this approach, the new element is called Bézier-enhanced shell triangle (BEST).

The BEST element takes advantage of all the nodes' connectivities in each triangle of the mesh. The computation of the normal vectors at the nodes doesn't depend on the number of triangles surrounding each node of the mesh. The BEST element is independent from the mesh topology.



# *Resumen*

*Se presenta un nuevo elemento finito de lámina delgada. Este nuevo elemento no usa rotaciones como grados de libertad. En su lugar, para satisfacer el requisito de mantener continuidad $\mathcal{C}^1$ entre elementos, el autor recurre a mejorar la descripción geométrica de los triángulos planos de una malla formada por triángulos lineales, por medio de polinomios de Bernstein y particiones triangulares de Bernstein-Bézier.*

*Para definir dichas particiones de Bernstein-Bézier, el autor realiza una estimación de las normales a la superficie en los nodos de una malla de triángulos. Ubach, Estruch y García-Espinosa realizaron una comparación estadística exhaustiva entre distintos factores de ponderación, incluyendo otros usados previamente en la literatura. La conclusión de dicho trabajo (que se incluye como anejo de esta tesis) conduce a usar como factor de ponderación para calcular una media de los vectores normales de los triángulos: el inverso del área de la circunferencia circunscrita al triángulo y el ángulo interno del triángulo en el nodo considerado. Usando este nuevo factor de ponderación, se reduce en aproximadamente un 10 % el error medio cuadrático cometido en la estimación de las normales de superficies generadas aleatoriamente, respecto del mejor factor de ponderación usado previamente en la literatura.*

*Con la información de los vectores normales en los nodos y las particiones triangulares de Bernstein-Bézier, el autor construye triángulos cúbicos de Bézier. Estos triángulos cúbicos de Bézier interpolan la superficie; con continuidad $\mathcal{C}^1$ en los nodos y $\mathcal{C}^0$ a través de las aristas. Debido a este planteamiento, el nuevo elemento recibe el nombre de BEST.*

*El elemento BEST aprovecha todas las conectividades de los nodos de cada triángulo de la malla. El cálculo de los vectores normales en los nodos no depende del número de triángulos que rodean cada nodo de la malla. El elemento BEST es independiente de la topología de la malla.*

A new paradigm is presented consisting on the reconstruction of the geometry of a cubic triangular element. This geometric reconstruction exploits the properties of cubic B-spline functions (cubic Bézier triangle). This way, the author builds a conforming shell finite element.

The BEST element tackles the problem of rotation-free shell elements' precision dependency with respect to mesh distortion. The BEST element defines the curvature as a 2D tensor. This definition is consistent with the definition of curvature obtained by differential geometry.

The construction of the cubic Bézier triangle requires fixing 30 parameters (3 coordinates for each of the 10 control points). Therefore it needs to apply 30 independent conditions. 15 of these conditions are given directly by the positions of the 3 vertices of the triangle and the orientations of the normal vectors at the 3 vertices. With these 15 conditions the triangles maintain $\mathcal{C}^1$ continuity at the vertices.

8 of the remaining conditions are imposed introducing energy minimization considerations. These energy minimization considerations serve also to define a well-posed element. A set of reduced problems, which are sufficiently representative and general, is defined in order to avoid imposing the energy minimization considerations globally. More specifically, the author defines 3 different reduced problems for the 3 different shell deformation modes: bending deformation, membrane (in-plane extension) deformation and in-plane shear (drilling rotation) deformation.

Built in this manner, the only degrees of freedom of the BEST element are the vertices' coordinates (9 variables). The remaining 21 parameters are solved internally. In order to fix the values of these 21 internal parameters, each BEST element solves 9 systems of linear equations of rank 3.

The BEST element is successfully applied to the analysis of thin shells in linear and geometrically non-linear regimes using an implicit method. The non-linearity is solved using a *Total Lagrangian* formulation.

The author shows how to perform a decomposition of the description of the deformation (including all the higher order terms) and the matrices of change of coordinates; granting a computationally efficient and geometrically

*Se presenta un nuevo paradigma que consiste en reconstruir la geometría de un elemento triangular cúbico. Esta reconstrucción geométrica aprovecha las propiedades de las funciones cúbicas B-spline (triángulo cúbico de Bézier). De esta forma, el autor crea un elemento de lámina conforme.*

*El elemento BEST trata de resolver el problema de la dependencia de la precisión de los elementos de lámina sin rotaciones con respecto a la distorsión de la malla. El elemento BEST define la curvatura como un tensor 2D. Esta definición es consistente con la definición de la curvatura obtenida de la geometría diferencial.*

*La construcción del triángulo cúbico de Bézier requiere determinar 30 parámetros (3 coordenadas para cada uno de los 10 puntos de control). Para ello es necesario aplicar 30 condiciones independientes. 15 de estas condiciones se deducen de manera directa de la posición de los 3 vértices del triángulo y de las orientaciones de los vectores normales en los 3 vértices. Con estas 15 condiciones se asegura que los triángulos mantienen continuidad $\mathcal{C}^1$ en los vértices.*

*De las otras 15 condiciones que quedan por imponer, 8 de ellas se obtienen a partir de criterios de minimización de la energía interna de deformación del elemento. Estos criterios de minimización de la energía interna del elemento sirven para construir un elemento bien planteado. Para no tener que imponer las consideraciones de minimización de la energía sobre el problema global, el autor desarrolla un conjunto de problemas reducidos que son lo suficientemente representativos y generales. Concretamente se definen 3 problemas reducidos para los 3 modos de deformación de la lámina: deformación de flexión, deformación de membrana (extensión en el plano) y deformación de cortante en el plano (rotación de taladro).*

*El elemento BEST construido de esta manera mantiene únicamente como incógnitas las posiciones de los vértices (9 variables). Los 21 parámetros restantes se resuelven internamente. La determinación de estos 21 parámetros internos del elemento implica la resolución de 9 sistemas de ecuaciones lineales de rango 3 para cada elemento BEST.*

*Se ha conseguido aplicar con éxito el elemento BEST al cálculo de láminas delgadas en régimen lineal y geométricamente no-lineal con un método implícito. La no-linealidad se plantea con una formulación* Lagrangiana total.

*El autor demuestra cómo descomponer los términos de la descripción de la deformación y de las ma-*

accurate through-the-thickness pre-integration. The through-the-thickness integrals are evaluated just once: at the reference configuration. There are just 14 through-the-thickness scalar integrals to perform for each Gauss point.

The numerical examples results show that the BEST element has the potential to achieve cubic convergence. Although they also cast doubts on the possibility of reproducing this result for a wide range of problems. For in-plane shear dominated problems, the formulation used in this thesis only achieves linear convergence. For membrane oriented tests with curvature, the convergence is quadratic.

The BEST element exhibits membrane locking behavior. The author suggests exploiting further the drilling rotations kinematics in order to solve membrane locking.

*trices de cambio de coordenadas; permitiendo así una pre-integración en el espesor computacionalmente eficiente y geométricamente precisa. Solo es preciso evaluar las integrales a través del espesor una vez: en la configuración de referencia. Las integrales en el espesor se han reducido a 14 integrales escalares distintas para cada punto de Gauss.*

*Los resultados de los ejemplos numéricos muestran que el elemento BEST tiene potencial para alcanzar convergencia cúbica. Pero al mismo tiempo también existen dudas sobre la posibilidad de reproducir de manera consistente este resultado para un amplio rango de problemas. Para problemas dominados por la deformación de cortante en el plano, la formulación utilizada en esta tesis solo alcanza convergencia lineal. Para ejemplos orientados a la deformación de membrana que incluyen curvatura, la convergencia es cuadrática.*

*El elemento BEST presenta problemas de bloqueo por membrana. El autor sugiere desarrollar más profundamente la cinemática de las rotaciones de taladro para resolver el bloqueo por membrana.*

A mis hermanos David y Jesus, compañeros de vida.
A mi madre Mª Teresa, a quien debo mucho más que mi vida.
Al record carinyós del meu pare, Pere.

# Agradecimientos

Quiero agradecer en primer lugar a mis profesores Eugenio Oñate y Juan Miquel el que me desvelaran el mundo de la investigación y me abrieran sus puertas invitándome a perseguir mis estudios de doctorado. De no ser por ellos y por su oferta, mi vida hubiera seguido un rumbo muy distinto. Tengo que decir que la vida de investigador me atraía de pequeño, pero nunca había soñado con que me la ofrecieran con tanta generosidad.

Quiero dedicar un agradecimiento aparte y muy especial a mi tutor y mentor Don Eugenio Oñate. Eugenio, como familiarmente le llamamos en CIMNE, ha mantenido una confianza en mis capacidades que según como se mire, rayaría la temeridad. Su paciencia para conmigo, en lo que a la elaboración de mi tesis se refiere, no ha tenido límites; y ha sabido entender en todo momento cómo manifestarme ese estímulo que me pudiera faltar para reemprender y proseguir el esfuerzo. Además, su ejemplo de dedicación y trabajo generoso ha sido una de las mejores enseñanzas que he recibido en estos años de trabajo juntos.

A MIS PADRES vaya un GRACIAS en mayúsculas por haber querido compartir conmigo la aventura que decidí emprender al tomar la decisión de completar mis estudios de doctorado. Ellos han sido al tiempo, y durante muchos años: un soporte incondicional, la infraestructura de mi actividad (permitiendo multiplicar mi rendimiento), y los interlocutores ideales con quien reflexionar y compartir mis logros y preocupaciones. Todo esto no es en modo alguno una tarea sencilla y ellos la han resuelto con la mejor nota posible.

A Julio García, quien ha ejercido de tutor de mi tesis en lo que se refiere a la parte naval y todo aquello relacionado con la mecánica de fluidos, quiero reconocer también la infinita paciencia que ha tenido con mis tímidos avances cuando mi dedicación era mayoritariamente a tareas ajenas a mi doctorado. Sus aportaciones e ideas han sido valiosísimas para hacer que mi trabajo tuviera mayor rendimiento; y he tratado humildemente de desarrollarlas en la medida de mis posibilidades. La mayor parte de las aportaciones que esta tesis doctoral incluye en lo relacionado con la mecánica de fluidos y la interacción fluido-estructura, cabe atribuírselas a él.

También quiero reservar un espacio en este apartado de agradecimientos a los doctores Ramón Ribó y [de nuevo a] Julio García por poner a mi disposición las herramientas que habían elaborado ellos previamente: **`RAMSeries`** y **`Tdyn`**; y en el marco de las cuales yo he elaborado mis partes de programa que implementan los desarrollos teóricos expuestos en la tesis. Este agradecimiento es por haber compartido los mismos ide-

ales que yo considero necesarios para revolucionar el conocimiento; y que pasan necesariamente por la colaboración entre todos aquellos actores que pueden aportar su trabajo y su conocimiento.

Quiero manifestar mi agradecimiento a Carles Estruch por su implicación en el trabajo sobre estimación de las normales en los nodos de las mallas de triángulos planos. Ha sido un privilegio contar con su colaboración y rigor para la realización de las varias decenas de millones de casos que hubo que evaluar para demostrar de manera convincente una de las principales aportaciones de esta tesis. Pero su participación no fue meramente de ejecutor. La búsqueda de la excelencia de Carles queda perfectamente reflejada en la presentación de resultados del artículo que publicamos conjuntamente y que se incluye como anejo de esta tesis.

Finalmente quiero agradecer a todo el personal de CIMNE, profesores adscritos del Departamento de Resistencia de Materiales y Estructuras en Ingeniería de la UPC, personal de administración y compañeros de estudios por la camaradería mostrada en todo momento. La experiencia de CIMNE fue extraordinaria desde el primer momento en que me invitaron y todavía manifiesto esa sensación del primer día en que si te lo propones puedes conseguir tus objetivos. Muy especialmente quiero manifestar mi agradecimiento a:

- Pooyan Dadvand por introducirme al mundo de la programación del Método de los elementos Finitos. Junto a Pooyan, empecé mis primeros meses en CIMNE ideando y programando el entorno de desarrollo de los *solvers* de **KRATOS**, la obra maestra de Pooyan.

- Miquel Pasenau por aguantar todas mis preguntas de programación en **C++**. Si bien no fue el único, Miquel me facilitó muchísimo la curva de aprendizaje del lenguaje de programación en el que he implementado los desarrollos teóricos y algoritmos expuestos en esta tesis.

- Enrique Escolano y Aleix Valls por compartir conmigo los análisis a fondo en innumerables *descansos* vespertinos de mis teorías geométricas y matemáticas.

- El equipo de desarrollo de **GiD** por poner a nuestra disposición una muy potente herramienta que nos facilita desarrollar día a día nuevos métodos numéricos y algoritmos cada vez más potentes.

- Javier Mora por saber alentarme en los momentos de frustración y hacerme ver el mérito en aquello que a veces he considerado accesorio.

Suele decirse que los individuos incorporamos a nuestra personalidad facetas o rasgos de aquellos otros con quienes interactuamos. Yo me siento orgulloso de haber interaccionado con todos ellos y sería un honor identificar en mí aquello que he valorado en ellos.

# Contents

# List of Figures

# List of Tables

# Acronyms

**BEST** This is the shell triangle element developed in this PhD thesis. And stands for Bézier-enhanced shell triangle. i–iii, xvi, xix, 62, 63, 74, 75, 77, 87, 99, 101–104, 106, 116, 118–120, 123, 125, 140, 143, 145, 147, 150, 151, 154–156, 158–161, 163–165, 167–169, 171–173, 176–179, 183, 185–192

**BPT** basic plate triangle. 29

**BSN** basic shell node. 33, 41, 186

**BST** basic shell triangle. 28, 29, 33, 165, 186

**CAD** computer aided design. 30, 31, 44

**CAE** computer aided engineering. 30

**CAGD** computer aided geometric design. 30

**CIMNE** International Center for Numerical Methods in Engineering using the initials of the catalan name. xxix, 1, 4, 16, 204, 206

**EBST** enhanced basic shell triangle. 165, 168, 169, 197

**FEM** finite element method. 43, 47, 57

**IGA** Isogeometric Analysis. 31, 43, 44, 62

**NURBS** non-uniform rational B-Spline. 30, 31, 43, 44

# Notation

$\Psi$ fraction of the cordal lenght of an element's edge used to position the boundary control points minimizing the deformation energy of the element. xvii, 51, 52, 55–61, 105–114, 116, 135–137, 139, 156, 159, 162, 172, 189, 190, 234, 238, 239

$\boldsymbol{\delta}$ Kronecker delta. Its value is 1 if the indices are repeated. 0 in any other case. The indices can be subscripts or superscripts. Not to be confused with the symbol $\delta$ used to identify the variational of a magnitude. 72, 79, 80, 83, 85, 235, 236, 238, 242–247

$\boldsymbol{\kappa}$ curvature tensor. Defined in terms of differential geometry of surfaces. See references [67, 122]. 34

$\lambda$ thickness stretch factor of the shell considering the Poisson effect of the material. A subscript can refer to a specific layer. 67, 69, 70, 73, 78, 79, 83, 84

$\nu$ Poisson coefficient. xvii, 108, 110

$\theta$ angle of drilling rotation of a node. This angle is emulated and not included as a variable of the system. The rotation is measured with respect a given edge of the mesh. The first superindex indicates the node whose drilling rotation is being measured. The second superindex indicates which of all the edges converging to that node is taken as a reference. For example, if the superindices are $\theta^{ij}$, then it refers to the angle about the normal at $i$ ($\boldsymbol{n}^i$) and with respect to the edge $\boldsymbol{x}^i - \boldsymbol{x}^j$. xvii, xviii, 104–116, 118–121, 127, 135–137, 139, 140, 143, 147, 149–151, 154, 156, 159, 162, 164, 165, 171, 172, 244, 245

$\varphi$ angle of inclination of the normal vector at the node with respect to the normal of the flat triangle. The angle is measured between the normal at the node and the plane perpendicular to the edge being considered. For example, if the superindices are $\varphi^{ij}$, then it refers to the angle between $\boldsymbol{n}^i$ and the plane perpendicular to the edge $\boldsymbol{x}^i - \boldsymbol{x}^j$. xvii, 55–57, 59–61, 105, 107, 110–116, 135–137, 139, 156, 162, 234, 247

$\boldsymbol{\varphi}$ function that defines a surface in $\mathbb{R}^3$. Not to be confused with $\varphi$. 34, *see* $\varphi$

$\xi$ first one of the parametric coordinates of the element. It can also be referred to as $\xi_1$. xvi, 34, 35, 46–50, 66, 68–73, 78–81, 83–86, 235–237

$\eta$ second one of the parametric coordinates of the element. It can also be referred to as $\xi_2$. xvi, 34, 35, 46–50, 66, 68–73, 78–80, 83–86, 235–237

$\zeta$ third one of the parametric coordinates of the element. It can also be referred to as $\xi_3$. xvi, 34, 35, 47, 66, 69–73, 78, 79, 82–86, 194

$\boldsymbol{A}$ matrix of change of coordinates from the local axes in the reference configuration to the parametric coordinates of the element. 70–72, 85, 194

$\boldsymbol{B}$ matrix containing the partial derivatives of $\boldsymbol{g}$ with respect to the coordinates of the nodes that define the shape of the element. 74, 75, 78, 79, 83, 85, 127, 155, 156

$\boldsymbol{C}$ Cauchy-Green deformation tensor. 35, 37, 69, 70

$\mathcal{C}^0$ mathematic classification of functions which means that the functions belonging to this group are continuous in a given domain. i, 23, 51, 105, 134, 137

$\mathcal{C}^1$ mathematic classification of functions which means that the functions belonging to this group are continuous and their first derivatives are also continuous in a given domain. i, ii, 23, 25–29, 31, 33, 52–54, 63, 107, 188, 189

$\boldsymbol{D}$ fourth order constitutive tensor, or its corresponding second order tensor in Voigt notation taking advantage of the major and minor symmetries. 35, 37, 38, 67, 70, 74, 75, 78, 83–85

$\boldsymbol{E}$ Green-Lagrange strain tensor, or its corresponding vector in Voigt notation. 35, 37, 38, 67, 69, 70, 72–74, 78, 120–123

$\boldsymbol{F}$ deformation gradient tensor. 35, 69, 70, 122, 123

$\boldsymbol{G}$ inverse of the jacobian tensor in the reference configuration ($\boldsymbol{J}^{-1}$). 35, 37, 70, 71, *see* $\boldsymbol{J}$

$G$ Shear modulus. 146

$\boldsymbol{g}$ pseudo deformation tensor. This tensor contains the deformation metrics of the current (deformed) configuration. It cannot be named a deformation tensor because it lacks the information of the reference configuration. xxvi, 70, 72–75, 78, 79, 83, 85, 194

$\mathcal{G}^1$ mathematic classification of functions which means that the functions belonging to this group are geometrically continuous and their first derivatives are also geometrically continuous in a given domain. xv, xvii, 23, 44, 52, 53, 107, 136, 137

$\boldsymbol{H}$ matrix containing the linearized external loads. A subscript may specify whether it corresponds to the loads defined over the volume in the reference configuration ($\boldsymbol{H}_{V^0}$), or the loads defined over the surface in the reference or current configurations ($\boldsymbol{H}_{S^0}$ and $\boldsymbol{H}_{S}$, respectively), or the loads defined over the boundary in the reference or current configurations ($\boldsymbol{H}_{\Gamma^0}$ and $\boldsymbol{H}_{\Gamma}$, respectively). 85, 86

$h$ thickness of the shell in the reference configuration. A subscript can refer to a specific layer. 67, 69–73, 78, 79, 84, 86

$\boldsymbol{I}$ identity matrix of the convenient dimension, or its corresponding vector in Voigt notation. 35, 37, 38, 68–70, 72–75, 78, 84, 104, 106, 120–123, 129–132, 136, 139

$\boldsymbol{J}$ jacobian tensor of the change of coordinates function from parametric coordinates to global coordinates in the reference configuration. xxvi, xxvii, 35, 69–71, 84

$J$ determinant of the reference jacobian tensor ($\boldsymbol{J}$). 71, 78, 84–86

$\boldsymbol{j}$ jacobian tensor of the change of coordinates function from parametric coordinates to global coordinates in the current configuration. 35, 69, 70

$\boldsymbol{K}$ tangent stiffness matrix of the element. A subscript may specify whether it corresponds to the material stiffness matrix ($\boldsymbol{K}_M$), or to the geometric stiffness matrix ($\boldsymbol{K}_G$). 78, 83

$\boldsymbol{L}$ derivative of the shape function ($N$) corresponding to the node of the element indicated by the superscript. It is derived with respect to the coordinate indicated in the subscript. 35, 48, 49, 69–73, 84, 235–237

$\boldsymbol{\mathcal{N}}$ normal vector to the surface of the shell in the reference configuration. 49, 69, 71, 73, 84, 126, 128–132

$N$ shape function corresponding to the node of the element indicated by the superscript. xxvii, 34, 35, 46–48, 69, 81, 86

$\boldsymbol{n}$ normal vector to a surface (in general refers to the current configuration). xvi, xviii, xxv, 34, 35, 45, 46, 49, 51, 54, 66, 68–70, 73, 80, 86, 104–107, 113, 120, 126–132, 134–140, 235, 236, 238, 240, 246

$\boldsymbol{P}$ tensor containing the coordinates of the 10 control points of the cubic Bézier triangle in the reference configuration. 49, 69, 71–73, 84

$\boldsymbol{p}$ tensor containing the coordinates of the 10 control points of the cubic Bézier triangle. The tensor is arranged as an array of 10 column vectors. Each column contains the 3 coordinates of each control point. When affected by a superindex, it refers to the coordinates of the indicated control point. 47, 49, 51, 53, 54, 69, 70, 73, 78–81, 86, 106, 136, 137, 235–237, 239

$\boldsymbol{Q}$ matrix of change of coordinates, for tensors expressed as vectors in Voigt notation, from the parametric coordinates of the element to the local axes in the reference configuration. 72–75, 78, 84, 194

$\boldsymbol{R}$ residual vector resulting from the difference between the external forces and the internal forces of the structure. 75, 77

$\boldsymbol{S}$ second Piola-Kirchhoff stress tensor, or its corresponding vector in Voigt notation. 35, 37, 38, 70, 73, 74

$\boldsymbol{T}$ matrix of change of coordinates from local axis in the reference configuration to global axis. 68, 70, 71

$\boldsymbol{X}$ position vector of a material point in the reference configuration. 34, 35, 49, 68, 69, 123, 128

$\boldsymbol{x}$ position vector of a material point in the current configuration. When affected by a tilde sign ($\tilde{}$), it indicates a collection of position vectors for different material points. In this case, the author refers to each coordinate of the composite vector using a superindex to refer to the material point, and a subindex to refer to each of the three coordinates. xxv, 34, 35, 38, 47, 49, 51, 54, 66, 69, 70, 74, 75, 77–81, 83, 85, 86, 104, 106, 113, 114, 120, 121, 123, 126–129, 131, 132, 136–139, 155, 156, 238, 242–244, 247

# Foreword

FOR OVER 25 YEARS the International Center for Numerical Methods in Engineering (Centre Internacional de Mètodes Numèrics en Enginyeria (CIMNE))[1] has grown a genuine interest for naval issues and sailboats in particular. Many students and world-renowned researchers fond of the topic (naval engineers, sailors, captains, etc.) have worked and studied at CIMNE. This has left a mark in the institution. All these people approached CIMNE with the vision of developing the numerical techniques that could allow a better understanding on the functioning of sailboats.

Resulting from this historical background, nowadays CIMNE has become one of the research centers on numerical methods better prepared and with a greater knowledge on the issues affecting sailboats in the world. It isn't bold to say that a sailboat encloses one of the trickiest functionings amongst all the machines conceived by mankind in history. This is because the very tight degree of interaction that exists between the different elements that make a sailboat and the high sensibility of the performance of the boat to this interaction. At the same time all these elements are of very different nature and each of them is subject to a wide range of working regimes depending on the sailing scenarios of a sailboat.

I can't think of another research center better suited in which to develop this PhD thesis because the topic fits perfectly within the goals pursued by CIMNE and in various of its most prominent research lines. For example, I mention a few: the research line on *Multiphysics Simulation*, the research line on *Struc-*

[1]The acronym corresponds to the original name in catalan "Centre Internacional de Mètodes Numèrics en Enginyeria". www.cimne.com

# *Preámbulo*

DESDE HACE MÁS DE 25 AÑOS *el Centro Internacional de Métodos Numéricos en Ingeniería (CIMNE)*[1] *ha incorporado en sus líneas de investigación el interés por el mundo naval; y en particular, por los barcos de vela. Por CIMNE han pasado una cantidad importante de estudiantes y científicos de prestigio con una vocación especial en este ámbito (ingenieros navales, regatistas, capitanes de yate, etc.) y ello ha dejado una notable impronta en CIMNE. Toda esta gente se acercó a CIMNE con la visión de desarrollar técnicas numéricas que facilitaran la comprensión acerca del funcionamiento de los barcos de vela.*

*Como fruto de este historial CIMNE es hoy en día uno de los centros de investigación en métodos numéricos con una mejor preparación y mayor grado de conocimiento de la problemática de los barcos de vela de cuantos existen en el mundo. No es arriesgado afirmar que, como máquina, un barco de vela tiene uno de los funcionamientos más complejos de cuantas ha concebido el hombre a lo largo de la historia. Esto es debido al altísimo grado de interacción que tienen los distintos elementos que la componen y de lo sensible que es el rendimiento del barco a dicha interacción. A su vez, todos estos componentes son de muy distinta naturaleza; y cada uno de ellos está sometido a gran disparidad de regímenes en la casuística de navegación de un barco a vela.*

*No se me ocurre otro centro de investigación mejor indicado en el que desarrollar mi tesis doctoral, pues el tema se enmarca plenamente en los objetivos perseguidos por CIMNE y en varias de sus líneas de investigación más destacadas. Se nombran a modo de ejemplo: la línea de investigación en* Simulación Multifísica*, la línea de investigación en* Análisis de

[1]Las siglas corresponden al nombre original en catalán "Centre Internacional de Mètodes Numèrics en Enginyeria". www.cimne.com

*tural Shell Analysis*, the research line on *Composite Materials* and the research line on *Fluid Mechanics*. This thesis has the objective of developing a *New Rotation-Free Thin Shell Element*. The advances achieved with this development shall enable significant improvements in the computations performed nowadays and which are so necessaray to target in the end the full simulation, in three dimensions, and in transient dynamic regime, of a sailboat. That challenge is yet to be solved efficiently in order to make a leap in the improvement of the analysis and design tools for sailboats. Solving this challenge will in turn enable substantial benefits to the performance of sailboats as it will reduce the number of non-trivial simplifications made for their simulation and analysis. Chapter 1 includes a detailed explanation on why the calculation of shells is relevant for the analysis of sailboats.

I hope that along the reading of this PhD thesis I can share with you the good experiences, findings and intelectual satisfactions that my dedication to it has provided me all the time.

Láminas Estructurales*, la línea de investigación en el* Estudio de Materiales Compuestos *y la línea de investigación en* Mecánica de Fluidos*. La presente tesis doctoral tiene por objetivo el desarrollo de un* Nuevo Elemento Finito de Lámina Delgada Sin Rotaciones*. Los avances obtenidos con este desarrollo deben permitir significativas mejoras en los cálculos que se realizan hoy en día; y son en buena parte necesarios para abordar en última instancia la simulación completa, en tres dimensiones, y en régimen dinámico transitorio, de un barco de vela. Este es un desafío pendiente de resolver de manera eficiente para que se puedan mejorar las herramientas de análisis y de diseño de barcos de vela; y sin embargo se considera que podrá aportar ventajas sustanciales al rendimiento de los barcos de vela por cuanto reduzca el número de simplificaciones no inocuas a la hora de simularlos. En el capítulo 1 se explica en detalle la importancia que tiene el cálculo de láminas para el análisis de barcos de vela.*

*Confío que con la lectura de esta tesis doctoral puedan compartir las agradables experiencias, hallazgos, y satisfacciones intelectuales que mi dedicación a ella me han supuesto en todo momento.*

# Chapter 1

# Motivation

# *Motivación*

WHEN I FINISHED MY ENGINEERING STUDIES in 2001 I had the opportunity to combine for the first time my knowledge on structural analysis with my passion for the sport of sailing. The goal of that study was to explore the options of using membrane analysis for the calculation of sails. During the months that preceded my study, a project related to sails manufacturing had been conducted at the International Center for Numerical Methods in Engineering (CIMNE). For that project, the sails were studied as shells. The topic raised my interest immediately. In section 1.4 I summarize some of the aspects of the beginnings of my research.

After many considerations and after realizing the validity of the problem still today in the scientific community and in the industry, I decided to relaunch the study of the analysis of sailboats.

AL TERMINAR MIS ESTUDIOS DE INGENIERÍA *en el año 2001 tuve la ocasión de combinar por primera vez mis conocimientos de cálculo de estructuras con mi gran afición al deporte de la vela. El objeto de aquél estudio era explorar las opciones que ofrecía el análisis de estructuras de membrana para el cálculo de velas. En los meses previos a mi estudio, se había llevado a cabo en el Centro Internacional de Métodos Numéricos en Ingeniería (CIMNE) un proyecto relacionado con la fabricación de velas de barcos en el que éstas se habían estudiado como estructuras tipo lámina. El tema despertó mi interés de manera inmediata. En el apartado 1.4 resumo algunos aspectos de los inicios de mi investigación.*

*Después de numerosas reflexiones y tras constatar la vigencia que todavía tiene el problema en la comunidad científica y en el ámbito industrial, decidí relanzar el estudio del análisis de barcos de vela.*

## 1.1 The importance of shell analysis for sailboats

Studying the behavior of a sailboat requires detailed understanding of its response to the actions and forces acting on it. Therefore it is necessary to analyze the dynamics of the fluids in which the boat is immersed (air and water) and at the same time the static and dynamic equilibrium of the structural ensemble. In the following sections the main elements that conform the structure of a sailboat are described. And the role played by shell structures in each of these elements is specified.

## *Importancia del análisis de láminas para barcos de vela*

*El estudio del comportamiento de un barco de vela requiere de la comprensión en detalle de su respuesta ante las acciones y fuerzas a las que está sometido. Para ello es preciso analizar la dinámica de los fluidos en los que está inmerso el barco (aire y agua) al mismo tiempo que considerar el equilibrio estático y dinámico del conjunto estructural. En los siguientes apartados se describen cada uno de los principales elementos que configuran la estructura de un barco de vela y el papel que en cada elemento juegan las estructuras de lámina.*

## 1.2 The hull

When looking at the structure of a modern sailboat, we can realize that the technology of its construction differs a lot from that used just half a century ago. While in the past the structure was composed mainly of linear elements (frames and planks) crisscrossed in order to configure a frame that could support the external skin of the boat, nowadays the use of plastics and more specifically the fiber reinforced plastics (FRP) in sandwich or laminate have enabled combining the structural and skin functions in a single element with the characteristic of being inherently bidimensional. The curvature used to design the boats in order to optimize the hydrodynamics as well as the slenderness required in order to optimize the use of materials, lead inevitably to consider the hull of a modern boat as a thin shell.

## *El casco*

*Si nos fijamos en la estructura del casco de un barco de vela podemos observar que su tecnología de construcción actual se diferencia bastante de la utilizada hace apenas medio siglo. Si en el pasado la estructura estaba compuesta principalmente por elementos lineales (baos y cuadernas) entrecruzados para componer un emparrillado que actuase de soporte de la piel exterior del casco, hoy en día la aplicación de los plásticos, y más concretamente de los plásticos reforzados con fibras (FRP según sus siglas en inglés) en sándwich o en laminado han permitido combinar la función estructural con la de la piel del casco en un único elemento de características inherentemente bidimensionales. La curvatura con que se diseñan los cascos de barcos para optimizar su hidrodinámica así como la esbeltez que se requiere para optimizar el uso de los materiales conducen necesariamente a considerar el casco de un barco moderno como una lámina delgada.*

## 1.3 Spars

Unlike other kinds of boats, a sailboat's structure continues above the deck of the hull (or hulls in the case of multihulls). Sailboats include one or more masts, booms and poles which are used to support and deploy multiple sails. Moreover the span of contemporary yachts' masts (up to 40 meters tall or more) requires them to be cable-stayed by a sophisticated system of cables and spreaders named standing rigging which comprises: stays, shrouds, back-stays, spreaders, etc.

Technology has also affected how the masts are made. Solid wood masts has been replaced by hollow and thin walled sections of extruded metal (generally aluminum alloys), and more recently of FRP (generally epoxy resin reinforced with carbon fibers). It's with the use of advanced composites that masts have reached spectacular proportions thanks also by the design of the laminates. Even though the mast is an inherently linear piece, a detailed study of the mast requires considering the piece as a cylindric or conic shell with sections of variable geometry.

## *La arboladura*

*Un barco de vela, a diferencia de otros tipos de barcos, tiene la peculiaridad de que su estructura no finaliza en el casco (o los cascos en el caso de multicascos); sino que a éste hay que añadir uno o más mástiles, botavaras y tangones que sirven de soporte para multitud de velas. Por si fuera poco, la envergadura que adquieren los mástiles contemporáneos (alturas de hasta 40 metros o más) requiere en general que éstos estén atirantados por un complejo sistema de cables llamado jarcia y que está compuesto por estayes, obenques, burdas, crucetas, etc. El conjunto del mástil o mástiles con la jarcia que los acompaña recibe el nombre de arboladura.*

*También en el caso de los mástiles la tecnología de construcción ha permitido sustituir el material con el que se construyen: pasando de la madera maciza a secciones huecas de paredes delgadas formadas por metal extruido en primer lugar (generalmente aleaciones de aluminio), y más recientemente por plásticos reforzados con fibras (generalmente resina epoxi reforzada con fibra de carbono). Es en este último caso donde los mástiles están alcanzando su máxima expresión, con arboladuras espectaculares por su altura y donde sus prestaciones vienen favorecidas por la construcción en laminado. Si bien*

## 1.4 Sails

A sailboat requires sails! My research work started studying the funicular shape of a sail under a set of loads.[133] In that study the main hypothesis was that the behavior of a sail could be represented structurally by a membrane. This implies that the bending energy is negligible. The goal was to obtain an initial approximation to the the shape of the sail allowing to accelerate the computation of the structural response of the sail.

One of the conclusions reached during that study was that calculating a membrane is not in *strictu sensu* the calculation of a structure. The argument lies in that lacking bending stiffness, the membrane turns into a mechanism with infinite swivels. In order to tackle the problem posed (from the structural and numerical point of view [133]) by the fact that a membrane is a mechanism, it is required to apply strategies to add energy and complete the system to full rank.

Many authors have applied artificial bending stiffnesses to the swivels between elements (either at the vertices or at the edges). In a previous work by R.L. Taylor [123] he uses another technique to add the necessary energy by considering the dynamic effects into the problem. That is, by avoiding to solve the solution to the static problem the authors acknowledge the existence of a transient state during which the membrane makes the transition from a state out of equilibrium to the configuration that counterbalances the loads applied upon it. By means of including the effects of the inertia and damping forces, we end up adding enough energy to the problem to avoid the numerical issues caused by the mechanism and hence solve the problem.

This discussion kept my interest during the years past after I completed my undergraduate studies in 2001 and until I restarted my PhD studies in 2006. The reasoning that summa-

*la pieza elástica del mástil es inherentemente lineal, un estudio detallado del mismo requiere considerar la pieza como una lámina cilíndrica o cónica con sección de geometría variable.*

## *El velamen*

*Para completar el conjunto de un barco de vela es indispensable contemplar las velas! Mi trabajo de investigación empezó precisamente estudiando la forma funicular de una vela sometida a un conjunto de cargas.[133] En aquél estudio la principal hipótesis de trabajo era que el comportamiento de la vela se podía asemejar estructuralmente al de una membrana. Es decir, que la energía de deformación por flexión es despreciable. Lo que se pretendía era obtener una aproximación inicial de la forma de la vela que permitiese acelerar el cálculo de la respuesta estructural de la vela.*

*Una de las conclusiones obtenidas de aquél estudio fue la certeza de que el cálculo de una membrana no es en* strictu sensu *el cálculo de una estructura. El argumento reside en que al carecer de rigidez a flexión, la membrana se convierte en un mecanismo con múltiples rótulas. Para atajar el problema que supone (desde el punto de vista estructural y numérico [133]) el hecho de que la membrana sea un mecanismo es preciso aplicar técnicas que añadan energía para que la matriz del sistema de ecuaciones sea de rango completo.*

*Muchos autores han recurrido a la asignación de rigideces artificiales en las rótulas de unión entre elementos (ya sea en los vértices o en las aristas). En un trabajo contemporáneo de R.L. Taylor [123] se utiliza otra técnica para añadir la energía necesaria mediante la introducción de la dinámica en el problema. Es decir, huyendo de buscar directamente la solución estática del problema, se reconoce la existencia de un estado transitorio en el que la membrana transita dinámicamente de un estado en desequilibrio a la configuración estable que equilibra las cargas aplicadas sobre ella. Mediante la consideración de las fuerzas de inercia y de amortiguamiento en el problema, asignamos suficiente energía al problema para evitar los inconvenientes numéricos del mecanismo y poder así resolver el problema.*

*Toda esta problemática ha mantenido despierto mi interés durante los años que han transcurrido desde que terminé la carrera en 2001 hasta que*

rizes my thinking is as follows.

1. If the transient dynamic solution leads to a static stationary result, then such static stationary result exists and should be reachable by means of a static calculation. Note that in [123], when the solution converges towards the static solution, the dynamic conditions of the calculation are dropped and a final static step is performed.

2. If there is a need to add modes or energy to complete the system to full rank in order to reach the static result, it's because such energy actually exists and it has been stripped in our classical hypothesis. The main of which is considering the sail as a membrane.

Can the sail indeed resist bending? What if the bending energy is not negligible? Why adding artificial bending energy instead of taking it into account naturally? These were questions that kept pounding me.

In section 1.5 the author attempts to provide an answer to these questions from an intuitive and engineering point of view.

*reemprendí mis estudios de doctorado en 2006. El pensamiento que resume mis reflexiones es el que sigue.*

1. *Si la solución dinámica y transitoria conduce a un resultado estacionario, es que dicho resultado estacionario existe y se debe poder alcanzar mediante un cálculo estático. Nótese que en [123], cuando la solución transitoria converge y se aproxima a la solución estática, se relajan las condiciones del cálculo dinámico y se realiza un último cálculo estático.*

2. *Si para obtener el resultado estático es preciso añadir modos o energía que completen el rango del sistema, es porque dicha energía existe en realidad y la estamos quitando en nuestras hipótesis. La principal de todas ellas es considerar la vela como una membrana.*

*¿Y si la vela efectivamente es capaz de resistir flexiones? ¿Y si en definitiva la energía de flexión no es despreciable? ¿Porqué añadir energía de flexión artificialmente en lugar de considerarla naturalmente? Estas eran preguntas que una y otra vez resurgían y me inquietaban.*

*En el apartado 1.5 se trata de dar respuesta a estas preguntas desde un punto de vista intuitivo e ingenieril.*

## 1.5 Shells vs Membranes

## *Láminas versus Membranas*

Let's revisit the decision to model sails as membranes. Despite this consideration was not documented in my undergraduate thesis [133] truth is that the main reason behind considering the sails as membranes was because they had been modeled as shells without much success in a previous work by Lara Pellegrini [99] also at CIMNE.[1] At the time I had the chance to discuss with Ms. Pellegrini her experiences on the study of sails, and one of them were that the shell elements used did not provide satisfactory results. The shell element used for those simulations was the DKT element. The main reason behind this lack of performance was locking of the elements. That is, the dis-

*Revisitemos la decisión de modelar las velas como membranas. Aunque esta reflexión no quedase documentada en mi tesina de final de carrera [133], lo cierto es que la principal motivación para considerar las velas como membranas es que se había hecho sin demasiado éxito como láminas en un trabajo anterior de Lara Pellegrini [99] también en CIMNE.*[1] *Tuve la ocasión en su momento de comentar con la Sra. Pellegrini sus experiencias del estudio de velas y una de ellas era que los elementos de lámina utilizados no ofrecían resultados suficientemente satisfactorios. El elemento de lámina utilizado para aquellos cálculos era el elemento DKT. El principal motivo era el bloqueo de la solución. Es decir, que los desplazamientos obtenidos mediante cálcu-*

[1] The decision was also affected by the trend set by North Sails with the program MemBrain. See appendix A.1.

[1] La decisión también estuvo influenciada por la tendencia iniciada por North Sails con su programa MemBrain. Ver el apéndice A.1.

placements obtained by calculation were far smaller than the displacements expected because other deformation modes where absorbing all the energy instead of allocating the energy adequately to the membrane deformation mode. That's why my undergraduate thesis tried to start with a geometric configuration closer to the final shape by means of the funicular shape of the loads.

*lo eran muy inferiores a los esperados debido a que otros modos de energía absorbían toda la energía de deformación al modo de energía por deformación de membrana. Por ello se pretendía partir de una configuración geométrica más cercana a la final con el cálculo de la forma funicular de las cargas.*

### 1.5.1 The shell-like nature of sails

### *La naturaleza laminar de las velas*

During this chapter I have repeatedly mentioned how the introduction of new materials and new construction technologies have affected the development of boats. Sails are not different. While in the old times sails were manufactured using textiles only —in [57] Ickert illustrates how cotton was used was still used to make sails in mid of the $20^{th}$ century— and this technology determines making the consideration that there are indeed an infinite number of swivels in the *dis*-continuum material of the sail; more recently FRP have disrupted the sail's manufacturing technology. In the beginning the textile material was treated to make it airtight and thus increase its aerodynamic efficiency as it decreases the losses of the pressure gradient generated by the sails as they deflect the airflow. This technique has evolved and nowadays the resin matrices used allow the use of a coarser fabric or even the use of unwoven fibers. In the limit, for the more demanding situations, the sails are no longer manufactured by joining together different panels (sewn at first and glued later) but instead by laying the fibers one by one onto a mold that provides the shape to the sail and laminating both sides with the resin matrix chosen. Precisely, the technique described constitutes the most popular advance in the technology of sail-making in the last decades. This was object of a controverted patent named 3DL [7].

Therefore, the technology used to manufacture the sails provides the answer to the dilemma between *shells* and *membranes*. Looking at the technological evolution there aren't fundamental differences between the manufacturing methods used for hulls, masts, or sails.

*En este capítulo se ha mencionado reiteradamente como la introducción de nuevos materiales y nuevas tecnologías de construcción han afectado el desarrollo de los barcos. El caso de las velas no es distinto. Si bien primitivamente las velas se confeccionaban a partir de tejidos exclusivamente —en [57] Ickert ilustra como todavía en los años 50 del siglo XX las velas se confeccionaban a partir de tejido de algodón— y esta tecnología invitaba a la consideración de que en efecto existían un sinfín de rótulas en el* dis*-continuo del material que componía la vela; más recientemente los materiales reforzados con fibras también han hecho su irrupción en la tecnología de fabricación de velas. Inicialmente se aplicaban tratamientos que impermeabilizaban el tejido, permitiendo aumentar su eficiencia aerodinámica al evitar pérdidas del gradiente de presión que las velas generan cuando deflectan el flujo de aire. La técnica se fue depurando y hoy en día las matrices de resina que se utilizan permiten que el entramado de fibras no tenga que ser tupido y mucho menos que tenga que ser tejido. Hasta el extremo de que las velas en los casos más exigentes ya no se fabrican mediante paños unidos (cosidos primero y soldados después) sino que se fabrican disponiendo las fibras una a una sobre el molde que da la forma a la vela y se laminan ambas caras con la matriz de resina elegida. El avance más popular de los últimos años en lo que a tecnología de fabricación de velas concierne es precisamente el último descrito, y que fue objeto de la patente denominada 3DL [7].*

*Así pues, la respuesta al dilema entre* láminas *y* membranas *nos la da la tecnología utilizada para fabricar las velas. A la vista de la evolución tecnológica, ya no existen diferencias fundamentales entre el modo como se fabrican el casco, el mástil, o las velas, y por lo tanto tampoco debería haberlas en el modo como las concebimos estructuralmente.*

And thus there shouldn't be differences either between the ways we conceive them structurally.

### 1.5.2 Spinnakers: a different case

There is a kind of sails that deserves a special consideration that given their characteristics and behavior are different from the other sails hoisted in a sailboat. The spinnakers (symmetric or asymmetric) are a family of sails designed to propel the boat when the wind blows in favor. This very circumstance makes their use uncompromising for the stability of the boat because they don't generate large lateral forces that could tip the boat over. As a result, these sails reach gigantic dimensions. Given the enormous area of these sails it becomes necessary to minimize their surface density as much as possible. —In fact, it is not uncommon to see these sails "explode" when the wind pressure overcomes their structural resistance.— This design restriction has thus far implied a *de facto* barrier to the introduction of the laminate manufacturing technology in spinnakers. Not just because of weight considerations, but also because of another more pragmatic consideration: in order to stack these sails they need to take as little volume as possible and therefore they have to withstand being folded and pressed with little regard. The delicate materials used to manufacture laminated sails cannot withstand such careless manipulation without affecting the durability of the material. This consideration has allowed the woven textile manufacturing technology to survive for the case of spinnakers. The future evolution of this situation is uncertain. The recent appearance of new and radical sail designs such as *Code Zero* [43] opens an opportunity to start thinking on the manufacturing of spinnakers using composite materials.

However it be, it is not incorrect to consider the analysis of a spinnaker sail as a membrane. But it wouldn't be erroneous neither to analyze it as a thin shell. If the extreme slenderness of the sail can be taken into account and accurately represented by a thin shell model, the differences between the results using one model or the other should be neg-

### *Los spinnaker: un caso aparte*

*Merecen una mención aparte una familia de velas que por sus características y prestaciones se diferencian del resto de velas que enarbola un barco de vela. Los spinnaker (simétricos o asimétricos) son una familia de velas diseñadas para empujar la embarcación en rumbos portantes, esto es, favorecidos por la dirección del viento. Debido a esto, su uso no suele causar peligrosas fuerzas laterales de escora en el barco y estas velas alcanzan proporciones gigantescas. Dado el enorme metraje de estas colosales velas es imprescindible minimizar su gramaje todo lo posible. —De hecho no es extraño ver "explotar" estas velas cuando la presión del viento vence su resistencia estructural—. Esta restricción de diseño ha supuesto hasta ahora una barrera a la introducción de la tecnología de fabricación laminada en los spinnaker. No únicamente por consideraciones de peso sino también de cariz más práctico: cuando se tienen que plegar estas velas es necesario que ocupen muy poco espacio una vez estibadas y por ello tienen que poder permitir ser replegadas en desmesura. Los delicados materiales utilizados para laminar velas no permiten un tratamiento tan desconsiderado sin afectar a la durabilidad del material y ello ha permitido a la tecnología textil sobrevivir en la fabricación de los spinnaker. Está por ver la evolución futura de esta situación, ya que la aparición de los novedosos y extremos* Códigos Cero *[43] abre una brecha para que se empiece a pensar en la fabricación de spinnakers a base de materiales compuestos.*

*Por ahora, sin embargo, no es incorrecto concebir el análisis de un spinnaker como una membrana. Sin embargo, tampoco sería muy incorrecto analizar un spinnaker como una lámina delgada. Dada la extrema esbeltez de la vela, si esta puede ser reproducida por el modelo de lámina delgada, las diferencias en los resultados analizando con un modelo u otro serán prácticamente inexistentes. Con la diferencia de que el modelo de membrana requerirá en todo caso un enfoque dinámico transitorio (u otra técnica equivalente), mientras que el modelo de lámina podrá abordar directamente el problema estático. Esta es bajo mi punto de vista una ventaja*

ligible. But while the membrane model will inevitably require a dynamic transient analysis (or another analogous technique), the shell model can tackle the static problem straight away. This is, in my opinion, a clear advantage that tips the balance clearly in favor of the rotation-free shell elements with respect to the membrane elements.

*que decanta la balanza claramente en favor de los elementos de lámina sin rotaciones en frente de los elementos de membrana.*

## 1.6 Justification of the use of high technology in sailing

## *Justificación del uso de alta tecnología en el deporte de la vela*

The discussion I am about to present has mainly economic reasons, and the reader might not understand that a scientific work with an engineering tone is justified by economic motivations —besides, this is not exactly the case—. But it is true that the author is not indifferent to the arguments set forth below.

*La justificación que voy a exponer tiene motivaciones principalmente económicas, y no se entendería que un trabajo científico de carácter ingenieril se justificase de inicio por motivos económicos — cuando por añadidura no es exacto—. Pero sí que es cierto que el autor no es insensible a los argumentos que presenta a continuación.*

### 1.6.1 The competition rules between boats of diferent kind

### *Las reglas de competición entre barcos de vela distintos*

Despite how strange it may sound, the creation of the Chesapeake Sailing Yacht Symposium (CSYS) doesn't happen in response the the interests of the scientific community around the America's Cup as the pinnacle of sailing. When reviewing the topics presented during the first editions of the symposium, it's revealing to realize that the large majority discusses about the rules that allow comparing different boats competing together. At that moment, the rule that had been created shortly before was the International Offshore Rule (IOR). From a market standpoint there is a great economic interest in enabling different boats to compete together between them, grouped by classes or similarities; and hence this focus on the rules. Enabling this possibility implies that more yacht owners can compete with their general purpose yacht. And the economic value of this market is huge.

Therefore it's interesting to review, albeit briefly, how these rules have evolved. The first rules dominated globally because the first efforts were scarce. However the rules were imperfect, allowing the designers to exploit their defects. This implies that the rules haven't

*Por extraño que pueda parecer, el nacimiento del Chesapeake Sailing Yacht Symposium (CSYS) no responde a los intereses de la comunidad científica alrededor de la Copa del América como pináculo del deporte de la vela. Si repasamos los asuntos tratados en sus primeras ediciones resulta revelador que en su mayoría se hable de las reglas que permiten comparar distintos barcos que compiten entre sí. En ese momento, la regla que se había creado recientemente era la International Offshore Rule (IOR). Este énfasis en las reglas se entiende fácilmente por el gran interés económico y de mercado que tiene permitir que distintos barcos puedan competir entre sí; agrupados por clases/similitud. Abrir esa posibilidad implica que más propietarios de barcos puedan competir con sus utilitarios y por lo tanto tengan un mayor incentivo para poseer una embarcación. Y el valor económico que tiene este mercado es enorme.*

*Por lo tanto tiene interés repasar aunque sea muy someramente cuál ha sido la evolución de estas reglas de comparación para que distintos barcos puedan competir entre sí. Las primeras reglas dominaban internacionalmente, pues estos esfuerzos primitivos eran escasos. Sin embargo las reglas eran imperfectas, permitiendo a los diseñadores explotar los defectos de las reglas. Esto implica*

always promoted a positive technological evolution of the sailboats. On the contrary, in many cases boats with worse characteristics can result winners in front of better boats because of the errors in the rules[2]. Nevertheless, market drivers tend to prevail and the designs —taken in average— have evolved positively with time; which has forced a review of the rules in order to take into account the design innovations —see the recent modifications to the latest version of the VPP (Velocity Prediction Program) used for the International ORC rule [91]—. Moreover, as the global sailing competition market has grown, different regions of the planet have developed specific rules. To the point that nowadays the rules are established and administrated by the national authorities of each country or group of countries. It is not completely ridiculous to think that each club might end up with its specific competition rule.

There is another explanation for this proliferation of organisms that manage a particular competition rule. It consists in the acceptance of the obligation to possess a certificate complying with a given rule in order to compete in a regatta administered by that specific rule. This certificate has a cost that has to be renewed periodically even if the boat has not undergone any change. This paradigm is reaching undesirable situations because the last decade has seen a drastic decline in the number of boats competing in regattas open to boats different between them. Thus loosing a great market opportunity.

The hope brought by science is the possibility of aligning the interests of yacht owners willing to compete between them despite having different boats and the unstoppable technological advance of the newer designs. This objective shall be achieved without generating absurd scenarios as science's goal can never be the absurdity. Therefore, unlike the large majority of sports where the use of high-end technology is only justified for high performance competition; high technology in

[2]DeBord et al. [59, p. 4] explain very eloquently how this paradox can occur in their paper on the America's Cup designs and the IACC rule.

*que las reglas no siempre han conseguido promover una evolución tecnológica positiva de los diseños de los barcos. Al contrario, en numerosos casos, barcos con peores características pueden resultar vencedores frente a mejores barcos debido a los defectos de las reglas*[2]*. A pesar de ello, las fuerzas del mercado siempre terminan triunfando y los diseños —tomados en promedio— han ido evolucionando positivamente con el tiempo; lo que ha ido obligando a revisiones de las reglas para tener en cuenta las innovaciones en los diseños —véanse las recientes modificaciones a la última versión del programa VPP (Velocity Prediction Program) para la regla ORC International [91]—. Más aún, con el crecimiento de lo que podríamos llamar el mercado de la competición de la vela a nivel mundial, varias regiones del mundo fueron desarrollando reglas específicas. Hasta el punto que hoy en día, las reglas son reguladas y administradas por las autoridades nacionales de cada país o conjunto de estados. No es descabellado pensar en el extremo de que cada club tenga su propia regla de competición.*

*Existe otro motivo que explica esta proliferación de organismos que se erigen como administradores de una regla de competición particular. Y consiste en la aceptación de que para poder participar en una regata administrada bajo una determinada regla de competición cada barco participante debe estar en posesión de un certificado de acuerdo con esa determinada regla. Certificado que tiene un coste y que es preciso renovar periódicamente, aunque el barco no haya sufrido ninguna modificación. Esta situación está llegando a extremos indeseables, pues se ha visto en la última década una drástica reducción en el número de embarcaciones participantes en regatas abiertas a barcos distintos entre sí. Por lo que se está perdiendo una gran oportunidad de mercado.*

*La esperanza que trae la ciencia es poder unir los intereses de los propietarios de barcos que quieren competir entre sí aunque tengan barcos distintos, y el irrefrenable avance tecnológico de los diseños de barcos. Conseguir este objetivo es hacerlo sin por ello generar oportunidad para situaciones absurdas, pues no es nunca el objetivo de la ciencia producir un absurdo. Por lo tanto, a diferencia de*

[2]DeBord et al. [59, p. 4] explican de manera concisa cómo se puede producir esta paradoja en su artículo sobre los diseños en la Copa del América y la regla IACC.

sailing —besides being applied to the elite competition— is absolutely necessary in order to compete at amateur level. This peculiarity happens because the yachts (the required equipment to practice the sport) has an economic cost that surpasses in several orders of magnitude the cost of the equipment necessary in the majority of sports. Science makes the promise to make comparable boats that perform differently and therefore make it possible to evaluate the sportsman minimizing the differences established by the equipment. The present thesis attempts to bring just some of the elements that can be necessary in order for science to fulfill its promise.

*la gran mayoría de deportes, en los que la aplicación de alta tecnología solo se justifica para la práctica de la competición de élite; en el deporte de la vela la alta tecnología —además de aplicarse en la competición de élite— es imprescindible para poder practicar la competición a nivel amateur. Esta peculiaridad es debida a que los barcos (el equipamiento necesario para la práctica de la vela) tienen un coste económico que supera en varios órdenes de magnitud al equipamiento necesario en la mayoría de los deportes. La ciencia nos ofrece la promesa de hacer comparables barcos que rinden distintamente y por lo tanto poder valorar al deportista minimizando las diferencias debidas al equipamiento. La presente tesis pretende aportar solo algunas de las piezas que pueden ser necesarias para que la ciencia cumpla su promesa.*

# Chapter 2

# Objectives

IN ORDER TO RESPOND TO THE MOTIVATIONS set forth in chapter 1 and state the objectives of this thesis, let's analyze which are the computational tools (capabilities) needed to increase the level of detail in the simulation and enable a further understanding and analysis of the response of sailboats. An enumeration of some of them follows:

- Dynamic simulation of membranes in 3D
  - Large displacements non-linear theory.
  - Orthotropic materials model.
- Dynamic simulation of shells in 3D
  - Large displacements non-linear theory.
  - Large strains non-linear theory.
  - Anisotropic laminated composite materials model.
  - Assign the principal directions of the material properties.
- Dynamic simulation of beams in 3D
  - Large displacements non-linear theory.
  - Large strains non-linear theory.
  - Anisotropic laminated composite materials model.
- Dynamic simulation of cables in 3D
  - Large displacements non-linear theory.
  - Non-linear materials model.
- Dynamic simulation of 3D fluids

# *Objetivos*

PARA PODER DAR RESPUESTA A LAS MOTIVACIONES *expuestas en el capítulo 1 y enunciar los objetivos de la presente tesis, veamos qué herramientas computacionales (capacidades) se precisan para simular con un nivel de detalle que permita dar un paso más allá en el análisis y comprensión del comportamiento de barcos de vela. A continuación se enumeran algunas de ellas:*

- *Simulación dinámica de membranas en 3D*
  - *Teoría no lineal con grandes desplazamientos.*
  - *Modelo de materiales ortótropos.*
- *Simulación dinámica de láminas en 3D*
  - *Teoría no lineal con grandes desplazamientos.*
  - *Teoría no lineal con grandes deformaciones.*
  - *Modelo de materiales laminares compuestos anisótropos.*
  - *Asignación de direcciones principales.*
- *Simulación dinámica de vigas en 3D*
  - *Teoría no lineal con grandes desplazamientos.*
  - *Teoría no lineal con grandes deformaciones.*
  - *Modelo de materiales compuestos laminares anisótropos.*
- *Simulación dinámica de cables en 3D*
  - *Teoría no lineal con grandes desplazamientos.*

  - Non compressible Newtonian fluids.
  - Free surface problem.
- Fluid-Structure interaction
  - Strong coupling Air $\rightleftarrows$ Boat $\rightleftarrows$ Water.
  - Coupling interfaces in 3D.
  - Large deformations of the fluid mesh.
- Dynamic control of the boat
  - Equilibrium with several degrees of freedom to satisfy both static or dynamic conditions.
- Parallel computing
  - Preferably implemented in shared memory (OpenMP protocol).
- Sailboats singularities
  - The boat is a prestressed structure, and thus it is necessary to reproduce the different states of prestress of the structure imposing the compatibility of uncoupled relative displacements.
    * Loading of the spars and standing rigging (tensioning of stays and shrouds).
    * Setting the battens (compatibility of the batten geometry with that of its bag in the sail).
    * Hoisting the sails (compatibility of the geometry of the sail with that of the spars).
    * Trimming the rig: sheets, vang, outhaul, downhaul, etc.

Appendix A presents succinctly the evolution of the use of numerical methods in the calculation and design of high performance sailboats; while also signaling the principal tools used by the industry. Undoubtedly the argument of this historical review uses the America's Cup as a backdrop, although the author uses also other top level references to enrich the argument with a particular point of view like the ocean going round-the-world regattas and the advances of the industrial leaders in the field.

  - *Modelo de materiales no lineales.*
- *Simulación dinámica de fluidos en 3D*
  - *Fluidos newtonianos no compresibles.*
  - *Problema de superficie libre.*
- *Interacción Fluido-Estructura*
  - *Acoplamiento fuerte Aire $\rightleftarrows$ Barco $\rightleftarrows$ Agua.*
  - *Interfases de acoplamiento en 3D.*
  - *Grandes deformaciones de la malla del fluido.*
- *Control dinámico del barco*
  - *Equilibrio de varios grados de libertad para satisfacer restricciones estáticas o dinámicas.*
- *Cálculo en paralelo*
  - *Preferiblemente en memoria compartida (protocolo OpenMP).*
- *Singularidades de los barcos de vela*
  - *El barco es una estructura pretensada, y por ello es preciso reproducir los distintos estados de pretensado de la estructura mediante la compatibilización de desplazamientos relativos desacoplados.*
    * *Puesta en carga de la jarcia (tensado de estayes y obenques).*
    * *Colocación de sables forzados (compatibilización de la geometría del sable con la de su funda en la vela).*
    * *Izado de las velas (compatibilización de la geometría de la vela con la geometría de la arboladura).*
    * *Trimado del aparejo. Cazado de escotas, contra, pajarín, cunningham, etc.*

*El apéndice A presenta sucintamente cómo ha evolucionado la presencia de los métodos numéricos en el cálculo y diseño de veleros de competición; al tiempo que indica las principales herramientas usadas en la industria. El hilo conductor de esta revisión es sin lugar a dudas la Copa América, aunque también se usan otras referencias de primer nivel que enriquecen el punto de vista como las competiciones oceánicas de vuelta al mundo y los avances de los líderes industriales del sector.*

## 2.1 Narrowing down the objective

In view of the introductory list of the necessary capabilities and the review of the technologies used nowadays by sailboat designers, there is a need to concentrate the efforts in order to develop those which are particularly relevant to improve the calculation tools for sailboats. Therefore let's divide the complex system which is a sailboat into 3 large subsystems from the computational mechanics point of view:

**Structure:** comprising all the solid resisting elements in the boat, including the hull, the appendages, the spars, the sails and the standing rigging.

**Fluid:** comprising both the liquid medium (water) on which the boat floats and the gaseous medium which propels it (air).

**Fluid-Structure interface:** is the part that needs to be accounted for from a computational mechanics point of view when the system is solved tackling its parts separately. This technique is more efficient in general, but implies some difficulties that need to be solved.

The reader will notice that the list above expressly omits some of the capabilities listed in the beginning; like for example the dynamic control of the boat. The capabilities included in the list in the introduction of the present chapter represent beyond any doubt the ensemble of my scientific ambitions in the field of computational mechanics at the moment of starting my academic career (without becoming limited by them), but it would be unrealistic to imagine that all of them are attainable in the framework of a doctoral thesis. In fact, I look forward at progressing in my career solving consecutively the various challenges set forth in this introduction.

Specifically, in this thesis I have set the focus on the first of the three great subsystems described in the previous section: the structure.

The reason for setting aside the subsystem representing the fluid is that it is a field under very quick development within the international computational mechanics community. Including this topic in a doctoral thesis would imply imme-

## *Focalizando el objetivo*

*A la vista de la enumeración anterior de capacidades necesarias, es preciso concentrar los esfuerzos para desarrollar aquellas que resultan especialmente relevantes para mejorar las herramientas de cálculo de barcos de vela. Es por ello que vamos a descomponer el sistema complejo que representa un barco de vela en 3 grandes subsistemas desde el punto de vista de la mecánica computacional:*

***Estructura:*** *que comprende todos los elementos sólidos resistentes en el barco, incluyendo el casco, los apéndices, la arboladura, el velamen y el aparejo.*

***Fluido:*** *que contempla tanto el medio líquido (agua) en el que se soporta la embarcación como el medio gaseoso que lo propulsa (aire).*

***Interfase Fluido-Estructura:*** *es la parte que es preciso tener en cuenta desde un punto de vista de la mecánica computacional cuando se resuelve el sistema abordando sus partes separadas. Esta técnica es por lo general más eficiente, pero tiene algunos inconvenientes que es preciso resolver.*

*Se puede apreciar que en esta clasificación hemos omitido expresamente algunas de las capacidades listadas en un principio como por ejemplo el control dinámico del barco. Las capacidades listadas en la introducción de este capítulo representan sin duda alguna el conjunto de mis ambiciones científicas en el campo de la mecánica computacional en el momento de abordar mi carrera académica (sin limitarme a ellas), pero sería poco realista asumir que todas ellas son alcanzables en el marco de una tesis doctoral. De hecho, confío poder continuar mi carrera académica resolviendo de manera consecutiva los distintos retos planteados en esta introducción.*

*Específicamente en esta tesis me he centrado únicamente en el primero de los tres grandes subsistemas descritos en el punto anterior: la estructura.*

*El motivo para dejar a un lado el subsistema que representa el fluido es que se trata de un campo en muy rápido desarrollo en la comunidad de la mecánica computacional a nivel mundial, e incorporar esta temática en una tesis doctoral implicaría inmediatamente dedicar la totalidad de la tesis a este tema.*

Table 2.1: Summary of tools and technologies used in the industry to simulate sailboats.

| **Subsystem** *Subsistema* | **Part** *Parte* | **Capabilities needed** *Capacidades requeridas* | **Computational tools used** *Herramientas computacionales utilizadas* |
|---|---|---|---|
| Structure | Hull | Static and dynamic simulation of shells. Small displacements. Linear theory. | Fairly well solved using Reissner-Mindlin-type elements. This implies using rotational degrees of freedom. Rotation-free elements haven't reached yet the same level of maturity as elements with rotations. |
| | Spars | Static and dynamic simulation of beams and cables. Small displacements. Linear theory. | |
| | Sails | Static and dynamic simulation of shells and membranes. Large displacements. Non-linear theory. | MemBrain™ (only for membranes and only dynamic). There aren't computational tools to simulate sails as shells. |
| Fluid | Air | Potential flow for upwind, Navier-Stokes for other cases. | Flow™, FLUENT™, etc. Very good existing solvers from the aeronautical industry. |
| | Water | Navier-Stokes equations, free surface. | Panel solvers, FEM solvers (potential flow and RANS). For example: FANS™, FLUENT™, Splash™, etc. |
| Fluid-Structure interaction | Air ⇵ Boat | Strong coupling and mesh deformation. In order to improve coupling it is desirable to use the same kinematic variables $\Longrightarrow$ no rotations. | Structure decomposition: rig separated from hull and considered fix in air flow. |
| | Boat ⇵ Water | | Structure decomposition: hull separated from rig and considered fix in the water. |
| | Air ⇵ Boat ⇵ Water | | Results from Air$\rightleftarrows$Boat and Boat$\rightleftarrows$Water tabulated and entered as input for VPP model and equilibrium obtained for 3 or 4 degrees of freedom. |

diately concentrate all the efforts to this topic. Moreover, the thesis would necessarily concentrate on some very specific aspect of fluid computational mechanics, and this is not the spirit of this research work. For that reason, on anything related to the solution of the fluid domain of the problem, I will rely on previous methods already implemented in existing computational codes.

Likewise, improving the fluid-structure interaction algorithms requires a research work that falls outside of the scope of this thesis. However, the research conducted within the thesis includes

*Además, la tesis se enfocaría necesariamente en algún aspecto muy particular de la mecánica computacional de fluidos, cosa que no es el espíritu de este trabajo. Por ello, en todo lo que hace referencia a la resolución del dominio fluido del problema, me apoyaré en métodos previos y ya implementados en códigos computacionales existentes.*

*Del mismo modo, la mejora de los algoritmos de interacción fluido-estructura requiere de un trabajo de investigación y desarrollo que queda fuera del alcance de la presente tesis. Sin embargo, la investigación realizada incluye aspectos que pueden ser aprovecha-*

some aspects that can be used to improve the simulation algorithms where the geometry smoothness is important for a correct solution of the fluid-structure interaction smoothness.

## 2.2 Rotation-Free Thin Shell Element

Structure-wise, in the previous pages the author has pinpointed different kinds of structural typology: membranes, shells, beams and cables. Out of these types of structural typologies this thesis focuses on shells; more precisely on thin shells. The argument for this election is two-fold. On the one side, the one-dimensional typologies such as beams and cables as well as the typology of membranes have been continuously thoroughly studied and it's fair to say that satisfactory solutions have been achieved in all cases. The implementations considering the non-linear theory of large strains/displacements or anisotropic materials aren't anything more than that: implementations. Their corresponding methodology has been widely developed and its inclusion in a doctoral research work would not be justified. On the other side, shells are prominently used in the construction technology of sailboats. A detailed justification of this statement is presented in section 1.1. Therefore, the selection of the shells structural typology as the object of study of the present thesis is supported by both scientific objectives and technological objectives.

The selection of the thin shells subtypology responds to the challenge presented by the sails of boats. In many cases involving composite laminated materials, there is agreement that the shell needs to be analyzed under the Reissner-Mindlin assumptions (see section 3.2.2). In other words, the shear strain is not negligible. This is why it is questionable to use the thin shells theory to analyze the structural response of the other structural elements of the boat built with composite laminated materials. There will be cases where the Kirchhoff-Love hypotheses suffice, and there will be cases where the Reissner-Mindlin hypotheses are needed.

Therefore, a specific objective of this thesis consists in developing a versatile thin shell element. The author focuses on the rotation-free

## *Elemento de Lámina Delgada sin Rotaciones*

*Por lo que respecta a la estructura, en las páginas anteriores se han distinguido varias tipologías estructurales: membranas, láminas, vigas y cables. De todas ellas, esta tesis se centra en la tipología estructural de láminas; y más concretamente en las láminas delgadas. El motivo de esta elección es doble. Por un lado las tipologías unidimensionales de viga y cable así como la tipología de membranas han sido objeto intenso de estudio de manera continuada y se puede considerar que se han alcanzado soluciones muy satisfactorias en todos los casos. Las implementaciones con teoría no lineal de grandes deformaciones/desplazamientos o con materiales no isótropos no son más que eso: implementaciones. La metodología para las cuales ha sido ampliamente desarrollada y no se justificaría su inclusión en un trabajo de investigación doctoral. Por otro lado las láminas tienen una destacada presencia en la tecnología de construcción de barcos a vela. Desarrollo una justificación detallada de esta afirmación en el apartado 1.1. Por lo tanto, se puede afirmar que la elección de la tipología de láminas como objeto de estudio específico de esta tesis es a la vez una elección motivada por objetivos científicos y objetivos tecnológicos.*

*La elección de la subtipología de láminas delgadas responde al reto que supone el cálculo de las velas de los barcos. En el caso de materiales compuestos laminados, en muchos casos se considera que es necesario analizar las láminas bajo las hipótesis de Reissner-Mindlin (ver apartado 3.2.2). Es decir, que la deformación por cortante no es despreciable. Por ello, la construcción de los otros elementos estructurales del barco con laminados de materiales compuestos pone en duda la idoneidad de la teoría de láminas delgadas para analizar la respuesta estructural de dichos elementos. Habrá casos en los que las hipótesis de Kirchhoff-Love sean suficientes, y habrá otros casos en los que sea preciso recurrir a las hipótesis de Reissner-Mindlin.*

*Por todo lo anterior, un objetivo específico de esta tesis doctoral consiste en el desarrollo de un elemento de lámina delgada versátil. Nos concentraremos en*

shell elements kind. This new rotation-free thin shell element shall permit to include the parallel advances being made by other CIMNE researchers (professor Eugenio Oñate and professor Francisco Zárate [145]) on a new general framework to complement the rotation-free shell elements with the rotation variables enabling the reproduction of the thick shell theory by Reissner and Mindlin.

One of the main advantages of the rotation-free shell elements is their natural combination with solid elements. Moreover, the rotation variables lack the additive property, which makes their use in non-linear theory with large strains and large displacements very difficult.

The present thesis will attempt to solve the following challenges posed by rotation-free thin shell elements:

- To guarantee the accuracy of the membrane response of the element.
- To prevent the dependency of curvature computation on mesh distortion.
- To design the element as simple as possible in order to limit the stiffness matrix bandwidth.
- To simplify the application of boundary conditions.

*la tipología de los elementos de lámina sin rotaciones. Dicho elemento de lámina delgada sin rotaciones deberá poder incorporar los avances que se están realizando en paralelo por otros investigadores de CIMNE (el profesor Eugenio Oñate y el profesor Francisco Zárate [145]) en el desarrollo de un marco general para complementar elementos de lámina sin rotaciones con las variables de rotación que les permita reproducir la teoría de láminas gruesas de Reissner y Mindlin.*

*Una de las ventajas que presentan los elementos de lámina sin rotaciones es que se pueden combinar de manera natural con elementos de sólido. Además, las rotaciones carecen de la propiedad aditiva, por lo que su tratamiento en teoría no-lineal con grandes deformaciones y grandes desplazamientos se hace sumamente complicado.*

*La presente tesis pretende resolver los siguientes retos que presentan los elementos de lámina sin rotaciones:*

- *Garantizar la precisión de la respuesta membranal del elemento.*
- *Evitar la dependencia del cálculo de la curvatura respecto de la distorsión de la malla.*
- *Diseñar el elemento lo más simple posible para limitar el ancho de banda de la matriz.*
- *Simplificar la aplicación de las condiciones de contorno.*

## 2.3 Summary

This chapter has listed the computational tools (capabilities) needed to increase the level of detail in the simulation and enable a further understanding of the response of sailboats. It then narrows down on the computational mechanics domains affected by the sailboat problem (structure, fluid and fluid-structure interface). And starts taking apart the components of the mechanical problem. The author takes advantage of this segmented viewpoint of the boat to analyze which are the current tools in use by the industry and whether there is room for improvement. The reader can find an explanation on the evolution and actual use of all these tools in appendix A. The author justifies that it is worthwhile to focus the efforts of the thesis on the structure system

## *Sumario*

*Este capítulo ha enumerado la lista de las herramientas computacionales (capacidades) necesarias para simular barcos de vela con un nivel de detalle que permita dar un paso más allá en el análisis y comprensión de su comportamiento. A continuación cierra el foco para centrarse únicamente en los aspectos relativos a los dominios de la mecánica computacional del problema del barco de vela (estructura, fluido e interfase fluido-estructura). Y procede a descomponer los componentes del problema mecánico. El autor aprovecha esta visión segmentada del barco de vela para determinar qué herramientas de análisis usa actualmente la industria y si existe margen para mejorarlas. Se puede encontrar una explicación sobre el estado de la técnica de todas estas herramientas en el apéndice A. El autor justifica que es pertinente centrar los*

of the boat. And more specifically on developing a new rotation-free thin shell element. The reasons are two-fold:

Firstly, because there's a need to analyze sails as shells under non-linear assumptions of large strains/displacements. And secondly, because the use of this technology can subsequently be used broadly in the structural analysis of the sailboat.

The new rotation-free thin shell finite element shall comply with the following requirements:

- Non-linear theory for large displacements
- Non-linear theory for large strains
- Transient dynamic analysis
- Account for the intense use of anisotropic materials
- Interact naturally with the CFD analysis

*esfuerzos de la tesis en el sistema de la estructura del barco de vela. Y en particular en desarrollar un nuevo elemento finito de lámina delgada sin rotaciones. Para ello se esgrimen dos motivos:*

*En primer lugar, por la necesidad de analizar las velas como láminas en condiciones de no-linealidad y asumiendo grandes deformaciones/desplazamientos. Y en segundo lugar, porque el uso de esta tecnología se puede aplicar posteriormente al análisis general de la estructura del barco de vela.*

*El nuevo elemento finito de lámina delgada sin rotaciones debería cumplir los siguientes requisitos:*

- *Teoría no-lineal para grandes desplazamientos.*
- *Teoría no-lineal para grandes deformaciones.*
- *Análisis dinámico transitorio.*
- *Considerar el uso intenso de materiales anisótropos.*
- *Interactuar naturalmente con los análisis CFD.*

# Chapter 3

# State of the Art

IN THIS CHAPTER we will review the state of the art regarding the calculation technologies for thin shell structures. Thin shell structures are, as we have justified in section 1.1 the most relevant type for the analysis of the structural behavior of the elements of a sailboat. We have already reviewed in appendix A the state of practice regarding the use of computer programs in the industry to calculate sailboats; both on what relates the sails and on what relates the hulls.

Section 3.1 introduces the different approaches employed to tackle the computation of sails using various computational strategies. Section 3.2 uses a very brief description of the mechanical characteristics of thin shells to support a short list of advantages and disadvantages of the elements based on the Kirchhoff-Love theory with respect those based on the Reissner-Mindlin theory for the analysis of thin shells. The main recent research lines based on the use of rotation-free elements to analyze thin shells under the Kirchhoff-Love assumptions are also introduced.

## 3.1 Academic approaches to computer simulation of sails

It's important referring to the works of the different schools of thought that have tackled the problem of simulating sails. The most simple modeling of sails is presented by Le Maître, Souza de Cursi and Huberson in [78]. It consists on first meshing the sail surface and then taking into account only the edges of the ele-

# *Estado del Arte*

*EN EL PRESENTE CAPÍTULO revisaremos el estado del arte en cuanto a la tecnología de cálculo de estructuras laminares delgadas que como hemos justificado en la apartado 1.1 es la más relevante para el cálculo estructural de los componentes de un velero. Ya hemos revisado también en la apéndice A el estado de la práctica relativo al uso de programas en la industria para el cálculo de veleros, tanto en lo que concierne a las velas como en lo que concierne a los cascos.*

*El apartado 3.1 presenta los enfoques que abordan el cálculo de velas usando distintas estrategias computacionales. Basándose en una brevísima descripción de las características mecánicas de las estructuras de lámina, en el apartado 3.2 se incluye una breve relación de las ventajas y desventajas de los elementos basados en la teoría de Kirchhoff-Love frente a aquellos basados en la teoría de Reissner-Mindlin para analizar láminas delgadas y se comentan las principales líneas de investigación recientes que emplean elementos sin rotaciones para analizar láminas delgadas bajo las hipótesis de Kirchhoff-Love.*

## *Enfoques académicos de la simulación de velas por computador*

*Es importante hacer referencia al trabajo de las distintas escuelas de pensamiento que han abordado el problema de simular las velas de los barcos. La modelización más simplificada de velas de barcos la presentan Le Maître, Souza de Cursi y Huberson en [78], y consiste en mallar primero la superficie de la vela y a continuación considerar únicamente las*

ments in the mesh. Thus modeling them as elastic chords articulated in every node.

An evolution of this method presented by Charvet, Hauville and Huberson [23] consists on dividing the sail response in 2 different steps. The first step is used to find a starting geometry of the sail that balances the wind pressures. In this first step there is the assumption that the sail tissue has no bending resistance and cannot stretch. The structural response is computed in the second step obtaining the sail deformations using a shell model. This method is very similar to the one developed by Ubach in [133] and is summarized in section 1.4 on page 3.

An original contribution for sail analysis was made by Pérez del Castillo and García in [21]. Their method consists on considering the structural response of a sail modeled as a membrane [123] as an energy minimization problem. And for that they solve the system of equations using an optimization method. This approach is also used by Ortigosa in her PhD thesis (see [5] and its references) and in the paper by García, Ortigosa and Fernandez [46].

The problem of membrane simulation, and in particular the phenomenon of wrinkling, is studied in depth by Rossi, Lazzari, Vitaliani and Oñate in [111]. However, wrinkling modeling in membranes results in a smooth simulated geometry instead of a wrinkled one. That is because the model simulates the effect of the wrinkle on the overall shape of the membrane as argue Razenbach and Xu [106]. Another kind of sails, solar sails, do require a detailed analysis of the wrinkles formed in the mirror. Tessler, Sleight and Wang [125] proceed to simulate solar sails modeling them as shells in order to capture their wrinkling behavior.

Finally, scientists from Southampton University and INRIA (France) have also suggested recently the need to model the sails of boats as thin shells [128].

With respect to shell analysis, a short review of the calculation methods of both shells and membranes was written by Valdés in [134]. For more thorough reviews the author recommends the books by Zienkiewicz and Taylor [144] and by Oñate [93]. Some authors have done reviews from a historical viewpoint; that's

*aristas de los elementos de la malla; modelizándolas como cuerdas elásticas articuladas en todos los nodos.*

*Una evolución de este método y propuesto por Charvet, Hauville y Huberson [23] consiste en dividir la respuesta de la vela en 2 partes diferenciadas. En un primer paso se calcula una forma inicial de la geometría de la vela que equilibra las presiones ejercidas por el viento. En este primer paso se considera que el tejido de la vela no tiene resistencia a flexión y que es inextensible. En un segundo paso se calcula la respuesta estructural en deformaciones de la vela a partir de un modelo de lámina. Este enfoque es muy similar al que desarrolló Ubach en [133] que se resume en el apartado 1.4 en la página 3.*

*Una propuesta original para el cálculo de velas la hacen Pérez del Castillo y García en [21]. La propuesta consiste en considerar la respuesta estructural de la vela modelizada como membrana [123] como un problema de minimización de energía y para ello resolver las ecuaciones mediante un método de optimización. Este enfoque también lo utiliza Ortigosa en su tesis doctoral (véase [5] y sus referencias) y en el artículo publicado por García, Ortigosa y Fernández [46].*

*El problema de resolución del cálculo de membranas, y en particular del tratamiento de las arrugas, está tratado en profundidad por Rossi, Lazzari, Vitaliani y Oñate en [111]. A pesar de todo, la modelización de las arrugas en una membrana conduce a una solución suave de la geometría en vez de una geometría arrugada. Ello se debe a que el modelo de arrugas simula el efecto que tiene la arruga sobre la geometría global de la membrana, tal y como explican Razenbach y Xu [106]. Tenemos que irnos a otro tipo de velas, las velas solares, para encontrar simulaciones que capturen el detalle de las arrugas que se forman en el espejo. Para conseguirlo, Tessler, Sleight y Wang [125] analizan las velas solares como láminas.*

*Finalmente, científicos en la Universidad de Southampton y en el INRIA (Francia) han propuesto también recientemente la necesidad de calcular las velas de barcos directamente como láminas delgadas [128].*

*En lo que respecta al cálculo de láminas, una breve revisión de métodos de cálculo tanto de láminas como de membranas fue realizada por Valdés en [134]. Para revisiones más exhaustivas se reco-*

the case of Stolarski et al. [121], MacNeal [73], Yang et al. [141] and Gal and Levy [45].

*miendan los libros de Zienkiewicz y Taylor [144] y de Oñate [93]. Autores que han realizado distintas revisiones desde una perspectiva histórica son Stolarski et al. [121], MacNeal [73], Yang et al. [141] y Gal y Levy [45].*

## 3.2 Thin shell finite elements

## *Elementos finitos de lámina delgada*

The need for modeling sails as thin shell structures has been discussed in detail in chapters 1 and 2. Next we will review briefly what are the finite element methods developed to perform this kind of calculations, but before that the reader needs to understand the nature of shells as structural elements and how they respond to external loads.

*En los capítulos 1 y 2 ya se trata en detalle la necesidad de modelizar las velas como estructuras de lámina delgada. A continuación vamos a revisar brevemente los métodos de elementos finitos desarrollados para realizar cálculos de este tipo, pero antes el lector debe entender la naturaleza de las láminas en tanto que estructuras y como éstas responden a cargas externas.*

### 3.2.1 Mechanic response of a shell

### *Respuesta mecánica de una lámina*

Shells are a structural typology which differs significantly from the most common structures we are used to see (and thus to understand). The *primadonna of structures* as called by Ramm [103, 104], shells combine in a unique way the possibility of resisting axial stresses as well as bending moments while spanning surfaces of arbitrary shape. There are many classical treaties on the mechanics and theory of shells. Therefore, it is not in the scope of this thesis to cover those contents. I will here just pinpoint the main traits that are relevant for understanding the mechanics and kinematics of shells in order to design a finite element successfully.

A shell can be defined as a structure in which one dimension is much smaller than the other two and which can exhibit [double] curvature. Considering the section of the surface, a shell can exhibit a *membrane*-like load carrying mechanism. That is, the shell will oppose a resistance to exterior forces acting aligned to the midsurface of the shell. Also, it can resist external moments acting on the shell's midsurface via a non-uniform distribution of stresses across the thickness (*bending*/plate-like load carrying mechanism). As for external moments orthogonal to the shell's midsurface, the shell resists exhibiting in-plane shear stresses. Finally, regarding forces perpendicular to the

*Las láminas representan un tipo de estructura que se diferencia sustancialmente del resto de estructuras que estamos acostumbrados a ver (y por consiguiente a entender). Ramm las llama la* primadonna de las estructuras *[103, 104], y es que las láminas combinan de manera única la posibilidad de resistir tensiones en su plano y momentos flectores; al tiempo que cubren superficies con formas arbitrarias. Existen varios tratados clásicos sobre la mecánica y teoría de láminas. Sin embargo no encaja en el ámbito de esta tesis cubrir dichos contenidos. Simplemente señalaré los aspectos principales que son necesarios para entender la mecánica y cinemática de las láminas para así poder diseñar un elemento finito con éxito.*

*Una lámina se define como una estructura en la que una dimensión es mucho menor a las otras 2 y que puede manifestar curvatura [doble]. Si analizamos la sección de la superficie que representa la lámina, ésta puede resistir cargas en su plano (mecanismo resistente tipo-membrana). Es decir, la lámina ofrece resistencia a fuerzas externas que actúan alineadas a la superficie media de la lámina. Pero la lámina también puede resistir momentos externos actuando en la superficie media de la lámina gracias a una distribución no-uniforme de las tensiones a través del espesor (flexión/mecanismo resistente tipo-placa). En lo que atañe a momentos*

*perpendiculares a la superficie media de la lámina,*

shell's midsurface, these will generate a combination of in-plane axial stresses (uniform and non-uniform) —activating both the membrane and bending modes— according to the curvature characteristics of the shell. All these resisting mechanisms —and in particular their combinations— a shell is capable of, confer them with their highly regarded stiffness yet lightness so valuable for structural engineers.

For a complete review (if anyone can ever claim completeness in any given field of knowledge) the reader can refer to the following references:

**Timoshenko [127]:** Probably the most cited book for classic analysis of plates and shells.

**Flügge [44]:** This is another excellent book by one of the most relevant engineers of the fine tradition of German scholars.

**Ventsel and Krauthammer [135]:** For a more contemporary publication focused specifically on thin shells and containing a wealth of information and references to the historic understanding of shells, I unreservedly recommend this work. This encyclopædic effort cannot be thanked enough by those students who want to dig in the field of thin shell structures and use a single point of reference to start with.

*la lámina los resiste en la forma de tensiones de cortante en el plano. Y por último, en el caso de fuerzas perpendiculares a la superficie media de la lámina, estas fuerzas generarán una combinación de tensiones axiales en el plano de la lámina (uniformes y no-uniformes) —de manera que se activan los modos de membrana y de flexión de la lámina— según las características de curvatura de la superficie de la lámina. Son todos estos mecanismos resistentes —y particularmente sus combinaciones—, los que confieren a las láminas una gran rigidez aún a pesar de su esbeltez. Esta es una característica sumamente apreciada por los ingenieros de estructuras.*

*Para una revisión completa (si es que alguien puede hablar de completitud en cualquier campo del conocimiento) el lector puede acudir a las siguientes referencias:*

***Timoshenko [127]:*** *Se trata probablemente del libro de mecánica clásica de placas y láminas más citado de cuantos existen.*

***Flügge [44]:*** *Este es otro libro excelente escrito por uno de los ingenieros más relevantes de la magnífica escuela alemana.*

***Ventsel y Krauthammer [135]:*** *Para una publicación más contemporánea, enfocada específicamente en láminas delgadas y que contiene una cantidad ingente de información y referencias para la seguir la evolución histórica de la comprensión de las láminas, recomiendo sin ninguna reserva esta obra. Este esfuerzo enciclopédico no se puede agradecer lo suficiente por parte de aquellos estudiantes que deseen profundizar en el campo de las láminas delgadas y quieran usar un único punto de referencia para empezar.*

### 3.2.2 A glimpse on the development of thin shell finite elements

Modern theories for thin shells are based on Kirchhoff's hypothesis [65] for the kinematics of plate bending and translated into shells by Love [72]. Many theories refining or improving those hypotheses have been formulated to solve classical problems of shells. The *Kirchhoff-Love* kinematic hypotheses for thin shells are:

### *Un vistazo rápido al desarrollo de elementos finitos de lámina delgada*

*Las teorías modernas de láminas delgadas se desarrollan a partir de las hipótesis de Kirchhoff [65] sobre la cinemática de la flexión de placas y aplicadas por Love para láminas [72]. Han sido muchos los autores que han aportado diversas teorías que refinan y mejoran en uno u otro aspecto las teorías para resolver problemas clásicos de láminas. Las hipótesis cinemáticas de* Kirchhoff-Love *para*

- The thickness of the shell remains constant after the deformation.
- A straight fiber perpendicular to the shell midsurface remains straight after the deformation.
- A straight fiber perpendicular to the shell midsurface remains perpendicular after the deformation.

The first finite elements based on the Kirchhoff-Love hypotheses for thin shells had to face the challenge of maintaining $\mathcal{C}^1$ continuity across different elements. This condition arises from the need to compute the curvature of the shell's midsurface as this is essential in order to reproduce the bending mode of the shell. More precisely the challenge is to maintain $\mathcal{G}^1$ continuity, which is a relaxation over $\mathcal{C}^1$, but still hard for finite elements to comply across element boundaries. This condition resulted in overly complex elements. A good example is the tri-cubic triangle by Clough and Tocher [27, 37, 73].

The use of the *Reissner-Mindlin* hypotheses [81, 107, 108] soon gathered popularity among those scholars developing new shell finite elements. Reissner developed a theory for plates and shells dropping the third hypothesis of those stated above. The objective is to try to increase the range of validity of the theory also for thick shells. It was clear that as the thickness of the shell increases, the third hypothesis is no longer valid. Translated into finite elements, the Reissner-Mindlin hypotheses require to take into account the rotations of the transverse fibers as additional degrees of freedom. But maybe the main reason for the popularity of Reissner-Mindlin elements is that only $\mathcal{C}^0$ continuity is required. However, the scholars soon found out that using the Reissner-Mindlin hypothesis had numerical drawbacks. By including the rotations as independent degrees of freedom, the elements did not have control over how much energy the shear mode absorbs as the thickness tends to 0; leading to what is known as shear locking[1]. Some of

[1]The reader can find a full chapter devoted to the discussion of shear locking and the advantages/disadvantages of Reissner-Mindlin elements in [93].

*láminas delgadas son las siguientes:*

- *El espesor de la lámina se mantiene constante después de la deformación.*
- *Las fibras rectas y perpendiculares a la superficie media de la lámina se mantienen rectas después de la deformación.*
- *Las fibras rectas y perpendiculares a la superficie media de la lámina se mantienen perpendiculares después de la deformación.*

*Los primeros desarrollos de elementos finitos de lámina delgada basados en las hipótesis de Kirchhoff-Love tenían que enfrentarse al desafío de mantener continuidad $\mathcal{C}^1$ entre los elementos. Este condicionante surge de la necesidad de calcular la curvatura de la superficie media de la lámina; ya que esta magnitud es esencial para reproducir el modo de flexión de la lámina. Siendo más exactos, el desafío consiste en mantener continuidad $\mathcal{G}^1$, que es una relajación con respecto a la continuidad $\mathcal{C}^1$, pero aún complicada de imponer por los elementos finitos entre elementos. De hecho, este condicionante dio lugar a elementos enormemente complejos. Un buen ejemplo de ello es el elemento triangular tricúbico de Clough y Tocher [27, 37, 73].*

*Ante esta dificultad los científicos que desarrollaban nuevos elementos de lámina popularizaron rápidamente el uso de las hipótesis de* Reissner-Mindlin *[81, 107, 108]. Reissner desarrolló una teoría de placas y láminas en las que obviaba la tercera de las hipótesis indicadas anteriormente. La intención de Reissner era aumentar el rango de validez de la teoría para poder incluir láminas gruesas. Resultaba evidente que a medida que aumentaba el espesor de la lámina, la tercera hipótesis dejaba de ser válida. Al trasladarlas a los elementos finitos, las hipótesis de Reissner-Mindlin implican tomar en cuenta las rotaciones de las fibras transversales como nuevos grados de libertad. Pero la principal razón por la que los elementos de Reissner-Mindlin obtuvieron tanta popularidad fue seguramente porque ya no se requería continuidad $\mathcal{C}^0$. Sin embargo los científicos pronto se percataron de que usar las hipótesis de Reissner-Mindlin tenía efectos numéricos indeseados. Al incluir las rotaciones como grados de libertad independientes, los elementos dejan de discernir cuanta energía debe absorber el modo de cortante a medida que el espesor tiende a 0; lo*

the strategies developed to overcome this problem are reduced [selective] integration and assumed strain fields. Although these techniques were thought initially to solve the shear locking problems, nowadays it is known that they only partially alleviate the problem [35]. Besides, there are many more challenges associated. For a complete historic review of the challenges and difficulties faced by scholars in the development of shell finite elements, the following references and the ones contained therein are recommended: [73, 141]. It is important to note that 50 years have passed by since the development of the first shell finite elements.

*que conduce a lo que se denomina bloqueo por cortante*[1]*. Algunas de las estrategias que se aplicaron para resolver este problema es la integración reducida [selectiva] o los campos de deformación condicionados. A pesar de que en un inicio se pensó que estas técnicas servían para resolver los problemas de bloqueo por cortante, hoy en día se sabe que sólo sirven para aliviar el problema parcialmente [35]. A parte, existen muchas otras dificultades asociadas. Para una revisión histórica completa de los desafíos confrontados y las dificultades encontradas por los científicos que desarrollan elementos finitos de lámina, el lector puede acudir a las siguientes referencias y las contenidas en ellas: [73, 141]. Es oportuno recordar que han pasado 50 años desde el desarrollo de los primeros elementos finitos de lámina.*

### Rotation-free elements as a resort to develop thin shell elements

Recently, the interest for using Kirchhoff-Love hypotheses has picked-up with the advent of rotation-free elements. Gärdsback and Tibert offer a comparison of various elements of this kind [49]. In their paper they discuss the advantages offered by the rotation-free shell elements with respect to other families of thin shell elements. The following are highlighted:

- Reduced number of degrees of freedom in the model.
- As the span/thickness ratio increases, using rotation-free elements results in system matrices with a lower condition number than if regular shell elements with rotations were used.
- The same applies when the meshes are refined.
- 3D rotations don't have the commutative property. Moreover, rotations are difficult to derive for large displacements applications.

With respect to the disadvantages mentioned in [49]:

- The precision of the membrane response of the element becomes limited. This is because the elements reviewed are using

### *Elementos sin rotaciones como recurso para desarrollar elementos de lámina delgada*

*Recientemente, el interés por la resolución adecuada de las láminas delgadas modelizadas con la teoría de Kirchhoff-Love ha experimentado un resurgimiento con la aparición de los elementos sin rotaciones. Gärdsback y Tibert ofrecen una comparación de varios de estos métodos en [49]. En dicho artículo se presentan las ventajas que ofrecen los elementos de lámina delgada sin rotaciones frente a otras familias de elementos. De entre ellas destaco las siguientes:*

- *Menos grados de libertad en el modelo.*
- *A medida que la relación de esbeltez de la lámina se acentúa, la aplicación de los elementos de lámina sin rotaciones resulta en sistemas matriciales mejor condicionados que si aplicamos elementos con grados de libertad de rotaciones.*
- *Sucede lo mismo a medida que se refinan las mallas de cálculo.*
- *Las rotaciones carecen de la propiedad conmutativa en el espacio 3D. Más aún, en aplicaciones con grandes desplazamientos, las grandes rotaciones son difíciles de derivar.*

[1] El lector encontrará un capítulo entero dedicado al tema del bloqueo por cortante y las ventajas en inconvenientes de los elementos de Reissner-Mindlin en [93].

low order interpolations to describe the membrane kinematics.

- The computation of the curvature of the element is sensible to mesh distortion.
- The bandwidth of the stiffness matrix increases because now the connectivities are increased in order to compute the curvatures.
- Connecting rotation-free elements to other element typologies is not always trivial.

The present thesis tackles and tries to solve the problems encountered by Gärdsback and Tibert, and other additional issues found in previous efforts (i.e. simplifying the application of boundary conditions, which may be cumbersome in some cases [142]).

Aside from the family of rotation-free shell elements developed by Oñate et al. [41, 95, 96] other element families are cited in the references of [49]. In fact, there are not many rotation-free shell elements in the literature. And very few have been applied for geometrically nonlinear problems. The reader is referred on the one side to the works by Gärdsback and Tibert [49], Zhou and Sze [142], Linhard et al. [71], and Oñate, Flores and Zárate [41, 95, 96] and references therein. On the other side, Cirak, Ortiz et al. [24] have developed a new paradigm to simulate rotation-free shells. This paradigm is based on the application of developments in the field of computer graphics, so that mesh subdivision algorithms are used to obtain new meshes suitable to interpolate a cubic function in regular patches of elements. Finally, a new trend with a broad support has emerged from the group led by T.J.R. Hughes based on the paradigm of isogeometric analysis [56]. The first application of the isogeometric analysis to the simulation of shells is the one by Benson [11] using the Reissner-Mindlin hypotheses. However, a great advantage of the isogeometric analysis is the possibility of representing the geometry with $\mathcal{C}^\infty$ continuity. Therefore, it should now be possible to achieve $\mathcal{C}^1$ continuity in the geometric representation of shells and use the Kirchhoff-Love

*En cuanto a las desventajas que se anuncian en [49]:*

- *Limitación de la precisión a la precisión de la parte membranal del elemento. Esto se debe a que los elementos revisados usan interpolaciones de bajo orden para describir la cinemática asociada al modo de membrana.*
- *Sensibilidad a la distorsión de la malla para la parte de flexión del elemento.*
- *Aumenta el ancho de banda de la matriz de rigidez debido a que para calcular las curvaturas es preciso incrementar las conectividades.*
- *La conexión de los elementos de lámina sin rotaciones a otras tipologías de elementos no siempre es trivial.*

*En la presente tesis se procura resolver o minimizar los inconvenientes encontrados por Gärdsback y Tibert y otros inconvenientes encontrados en trabajos anteriores, como por ejemplo simplificar la aplicación de las condiciones de contorno, que puede ser rebuscado en algunos casos [142]).*

*Aparte de la familia de elementos de lámina sin rotaciones desarrollada por Oñate y colaboradores [41, 95, 96] se pueden encontrar otras familias de elementos en las referencias de [49]. Aunque de hecho no existen muchos elementos de lámina sin rotaciones en la literatura. Y de ellos, muy pocos se han llevado a problemas geométricamente no lineales. El lector puede acudir por un lado a los trabajos de: Gärdsback y Tibert [49], Zhou y Sze [142], Linhard, Wüchner y Bletzinger [71], Oñate, Flores y Zárate [41, 95, 96] y las referencias contenidas en ellos. Y por otro lado Cirak, Ortiz y otros colaboradores han desarrollado un nuevo paradigma para el cálculo de láminas sin rotaciones [24]. Este paradigma se basa en aplicar desarrollos propios del campo de la gráfica computacional, de modo que usando algoritmos de subdivisión de mallas se obtienen nuevas mallas que son útiles para interpolar una función cúbica sobre parcelas regulares de elementos. Finalmente, otra nueva tendencia surge desde el grupo liderado por Tomas J.R. Hughes y que cuenta con un seguimiento muy amplio. La idea consiste en el paradigma del análisis isogeométrico [56]. La primera aplicación del análisis isogeométrico a la simulación de lámina es la realizada*

assumptions. The first group to achieve it are Kiendl, Bletzinger et al. [63]. However, philosophical issues with isogeometric analysis remain still unsettled. For example, there is not a direct way to apply boundary conditions on boundaries defined by trimmed surfaces [102]. A more in depth review of the rotation-free elements with their advantages and disadvantages is provided in section 4.1.1.

*por Benson [11] utilizando las hipótesis de Reissner-Mindlin. No obstante, una de las grandes ventajas del análisis isogeométrico consiste en la posibilidad de representar la geometría de cálculo con continuidad $\mathcal{C}^\infty$. Por ello, debería ser posible alcanzar continuidad $\mathcal{C}^1$ en la representación geométrica de las láminas y usar las hipótesis de Kirchhoff-Love. El primer grupo en conseguirlo ha sido Kiendl, Bletzinger et al. [63]. Sin embargo, todavía existen aspectos sin zanjar; como por ejemplo la asignación de condiciones de contorno a bordes definidos por superficies trimadas [102]. Una revisión más profunda de los elementos de lámina sin rotaciones con sus ventajas e inconvenientes se encuentra en el apartado 4.1.1.*

# Chapter 4

# Ideas for a new rotation-free shell element

IN THIS CHAPTER I will introduce the core ideas on which the new element is based. I will provide evidences of the first failures as well as explanations for those. The objective of this chapter is to introduce the reader into the difficulties entrenched and provide the foundations to understand the solution adopted in chapter 5.

The following sections are based on the work reported in [132] published by Ubach and Oñate, and provide a broader introduction to the work than the one reported in the paper itself.

In the following pages the author presents the original ideas that support the development of the new shell element formulation. The triangle presented in this chapter is flawed: it exhibits hourglassing. That is, *spurious* or zero energy modes that affect the solution. In spite of it, this chapter serves to present the fundamental ideas that support the advantages of the final formulation: simplicity and generality. Simplicity, because the formulation is free from rotation degrees of freedom. Generality, because the triangle here presented can be used regardless of the mesh topology, thus generality is conserved for any mesh-represented surface (see the topology requirements by other previous rotation-free shell elements in the literature in section 4.1.1). The element uses the neighboring elements (sharing the nodes) in order to enrich the information about the normals, but it does not require them nor a minimum number of them to perform the computations.

Section 4.1 presents the design requirements for the new element and the different strategic decisions made to build the new element. These decisions will hold throughout this thesis development. Section 4.2 presents the geometric principle that allows computing the curvature as a product of first derivatives while defining the normal orientation of the shell surface in a continuous way, and thus opening a door to overcome the $C^1$ condition. Section 4.3 develops this idea into a first concept triangular element. This development already shows the use of the design guidelines introduced in section 4.1. In section 4.4 the author reports several attempts to control the spurious energy modes detected in the previous section. Finally, in section 4.5 the author reflects on the root cause for the

zero energy modes and presents the path that will ultimately lead to the successful development of a new rotation-free shell element.

## 4.1 Design requirements for the new shell element

It is common to specify a number of design requirements for any new shell element. It is no different in this case. The motivation already establishes some hard conditions. First of all, the new element should combine easily with other elements solving different physics like fluids, but also other structural typologies like beams or solids. Also, it is required that the element solves geometrically nonlinear problems. The dynamics of the shell should also be taken into account. Finally, many modern shell structures are made out of composite materials. This renders them highly anisotropic properties.

### 4.1.1 Going *rotation-free*

The first and most important design decision made early on has been to opt for a rotation-free element. Avoiding the use of rotations ensures parting from the possibility of suffering shear locking. It also has the advantage of not having to deal with the difficult topic of finite rotations in the geometrically nonlinear regime. Chapter 3 provides an overview of the different rotation-free shell element approaches adopted to the date. Let's analyze them in more detail in order to draw some conclusions for this new development. We classify the different methods in three main families. We will only include in this review the most contemporary developments, except for the historic case of the Clough-Tocher interpolant.

#### Clough-Tocher interpolant

This element is included here for being the first thin shell element to satisfy the $\mathcal{C}^1$ continuity condition. It was presented in 1965 [27]. It is a complicated element because it is a triangle split into three sub-triangles. Each sub-triangle is cubic and some degrees of freedom are restrained in order to maintain $\mathcal{C}^1$ continuity across the sub-triangles. In order to achieve slope continuity across the macro triangles, it uses the rotations at the nodes as degrees of freedom, but also the cross boundary derivatives at the center of the sides.

#### 4 element patches

This family involves all those elements that overcome the $\mathcal{C}^1$ continuity condition by computing the curvature over an element using a patch of 4 elements (the main element and the 3 elements sharing one edge). This family includes the basic shell triangle (BST) elements developed by Oñate et al. [41, 95, 96], the formulations by Phaal and Calladine [100], Zhou and Sze [142], Sabourin and Brunet [112] and many other formulations reviewed in depth in the works by Gärdsback and Tibert [49] and by Oñate in [92]. These formulations perform a computation of the average curvature in the element. Either they compute a constant two-dimensional

curvature taking into account all 4 elements in the patch, or more usually, they compute a direction-wise curvature for every pair of triangles. It must be noted that most of these shell elements are an evolution of their thin plate formulation counterparts to which a membrane formulation has been added in order to analyze shell structures. This is the case for example with the BST, which evolved from the basic plate triangle (BPT) designed by Oñate and Cervera [94]. Indeed, this is a simplification and can work when the curvature is small or when the mesh is sufficiently fine. All these formulations represent a sincere effort to make a rotation-free element as simple as possible. But in many cases it can lead to errors as reported. There is also a topology requirement in that an element must be surrounded by 3 others. Most authors propose to drop this requirement at the boundary, but [142] maintains it and creates ghost slave elements to fulfill the condition. Some membrane locking issues are also reported which are partially alleviated when using a quadratic interpolation for the membrane behavior of the element and when the mesh is refined.

**Subdivision paradigm**

This is an original development proposed by Cirak, Ortiz et al. [24–26]. They propose to take advantage of subdivision algorithms developed for computer graphics applications to generate regular meshes. They start with a coarse mesh generated using conventional methods. Then, they use subdivision algorithms for surfaces that guarantee $\mathcal{C}^1$ continuity in the limit for all the set of points generated. The practical application for using these subdivision algorithms is that all the new points generated are regular points. A point in a mesh of triangles is regular if it is surrounded exactly by 6 triangles. Using this property, the authors generate cubic representations of the surface using patches of 13 elements (12 nodes). Following this strategy the descriptions for two adjacent triangles are $\mathcal{C}^1$ continuous. This approach, however, has some drawbacks. First, those vertices of the original mesh which are irregular, remain irregular throughout the subdivision process. Therefore, there are regions of the surface for which the new paradigm does not provide a solution. It is true, though, that those regions can be made arbitrarily small by means of successive subdivision steps. Nevertheless, this constitutes a very strong topology requirement. Furthermore, the subdivision process requires the application of edge detection algorithms in order to prevent smoothing of the structure's surface. One of the main contributions of these works is to show that it is possible to generate cubic representations of a surface represented by a tessellation of linear triangles. Most importantly, these works open the path for finally attaining $\mathcal{C}^1$ continuity.

**Discontinuous Galerkin methods**

This methodology has become popular in a number of fields in computational mechanics and also in fluid dynamics problems. The method consists on imposing the continuity of the unknown variables in a weak form. Thus, some authors have found it suitable for enforcing the $\mathcal{C}^1$ continuity condition across elements and avoid the need to use rotational degrees of

freedom. Güzey, Stolarsky, Cockburn and Tamma [50] propose a discontinuous Galerkin formulation to build a new bilinear quadrilateral shell element. This method also depends on the selection of a set of arbitrary constants that modify the behavior of the function jumps in the discontinuous fields. Later, in separate works by Dung and Wells [34] and by Noels and Radovitzky [86] have proposed a discontinuous Galerkin approach to build quadratic and bicubic thin shell elements. The problem with the discontinuous Galerkin method is that in general, by relaxing the continuity requirements, they lose accuracy. It is also cumbersome to implement and computationally expensive because both surface integrals and boundary integrals are required—the latter in order to apply the weak form of the continuity condition—.

**Isogeometric analysis (IGA)**

The last approach is the one proposed by Hughes, Cottrell and Bazilevs [56] and implemented for thin shells by Kiendl, Bletzinger et al. [63]. This approach proposes the use of the non-uniform rational B-Spline (NURBS) description of surfaces that is commonly used in computer aided geometric design (CAGD). This approach has many advantages over conventional finite element formulations. The first one is to avoid the meshing step, which is usually complex and time consuming. Then, the use of NURBS functions allows to attain solutions with $\mathcal{C}^{\infty}$ continuity, attaining the highest orders of convergence with the least number of elements used. However, this approach also has some drawbacks. The first one is having to deal with trimmed surfaces in the geometric description. This is not a big issue in computer aided design (CAD) because trimming NURBS surfaces does not have an impact on visualization. For computer aided engineering (CAE), though, it is paramount to solve this issue. Schmidt, Wüchner and Bletzinger [114] have proposed a solution for this issue.

Let's review for a moment the efforts made to overcome the challenge posed by trimmed surfaces to measure the magnitude and importance of the problem. This has been addressed separately by the group at ICES (University of Texas at Austin)[1] in collaboration with Sederberg reformulating Isogeometric Analysis using T-Splines [8]. Also the group at Technische Universität München (Germany) have formulated a clever approach proposed by Schmidt, Wüchner and Bletzinger [114] to embed trimmed surfaces into the Isogeometric Analysis formulation. This topic had also been addressed previously by Kim, Seo and Youn from KAIST (Korea) splitting trimmed elements using triangles [64].

Besides, other drawbacks of the isogeometric approach are that it departs from the traditional conception of structural analysis in which the points of analysis are material points in the structure. Instead, here the points used for the analysis are control points of the geometry. This requires an important effort regarding the pre- and post-processing tools. Furthermore, dealing with NURBS functions, has intrinsic smoothing properties that brings some precision advantages, but which are also more complex to deal with than the traditional Lagrangian shape functions used

[1]The author considers prof. Bazilevs a scholar of ICES although his affiliation in this work is the University of California.

traditionally in isoparametric analysis. Finally, by directly using the CAD geometry for performing the mechanical analysis, the method is subjected to the CAD definition of the geometry, which may not be well suited for simulation purposes (i.e. it may happen that the geometry features far more geometry patches than actually necessary for the simulation, which can become a burden).

At this point, it is relevant to cite the pioneering work of Rho and Cho [109, 110]. Rho and Cho proposed originally to blend the CAD description of the geometry with the finite element analysis for shell structures. Their work is independent of the developments in Isogeometric Analysis (IGA) but has not gained the momentum that isogeometric analysis has created.

Table 4.1: Main advantages and disadvantages of the different rotation-free finite element technologies in the literature.

| **Rotation-free element family** | **Advantages** | **Disadvantages** |
|---|---|---|
| **Clough-Tocher interpolant** | •Solves $\mathcal{C}^1$ continuity. | •Very sophisticated.<br>•Needs the transverse derivatives at the edges. |
| **4 element patches** | •Simplicity.<br>•Linear elements are used. | •Boundary conditions sometimes complicated.<br>•Membrane locking.<br>•Precision issues. |
| **Subdivision paradigm** | •$\mathcal{C}^1$ continuity achieved.<br>•Linear elements are used for input. | •Strong topological requirement.<br>•Complex process. |
| **Discontinuous Galerkin** | •$\mathcal{C}^1$ continuity is weakly achieved. | •Tuning required.<br>•Requires surface and boundary integrals. |
| **Isogeometric analysis** | •Continuity achieved naturally.<br>•Inherits good approximation properties of NURBS functions.<br>•Does not need to generate a mesh. | •Complexity.<br>•Has to deal with trimmed functions.<br>•Dependency on CAD description. |

Table 4.1 presents a summary of the advantages and disadvantages brought by each of the approaches reported. One advantage that is common to all rotation-free shell elements is that by only having displacement degrees of freedom, they are reducing the number of degrees of freedom in the system. Therefore, it will be a priority not to undermine this advantage by adding degrees of freedom to the element unless absolutely necessary.

It has been shown that each approach has merits and drawbacks. The effort undertaken in the present thesis is to try to gather the experience of all these previous works and combine their strengths while at the same time avoid or provide solutions to tackle the drawbacks.

### 4.1.2 *Implicit* vs *Explicit* time integration

Another of the important design decisions was about the time integration scheme. On the one side, it is common for new finite elements to opt for an explicit time integration scheme. This avoids the difficult task of having to derive the tangent stiffness matrix of the element and the tangent matrix of the loads on the element, and invert them. Explicit finite elements solve first the accelerations of the system taking into account the state of equilibrium of the previous time step and the inertiæ (mass matrix) of the system. The positions are computed by forward integration. Then, the new equilibrium is calculated and a new step starts. The explicit time integration scheme is conditionally stable and therefore very small time steps are required. The advantage of this scheme is that usually a lumped mass matrix is used, which turns the system of equations matrix into a diagonal matrix, and thus trivial to solve and very fast. They are also very robust, albeit their accuracy is conditional. The main disadvantage though, is that only dynamic problems can be solved. The static problems are treated solving the quasi-static problem and considering it solved when the velocities and accelerations are close to zero.

On the other side, implicit integration schemes offer unconditional stability, which means that the time step can be arbitrarily set as large as wanted. Usually to the time scale resolution of the problem at hand. When the time scale resolution of interest is similar to the conditional time step of the explicit time integration scheme, an implicit scheme is not competitive. However for most engineering problems this is not the case and implicit schemes are very competitive for most cases. This scheme requires to invert the tangent stiffness matrix of the element and therefore solving a nontrivial system of equations. In an implicit scheme the mass matrix needs not be anymore lumped (as in the case with explicit time integration schemes) because we already face the challenge of solving a nontrivial system of equations. This offers another opportunity for maintaining accuracy in the analysis.

Another advantage usually claimed in favor of explicit time integration schemes is that they are more accurate when solving problems involving shock waves. In fact, what happens is that the discretization inherent in the finite element method introduces numerical diffusion in the solution. This effect is more severe in implicit time integration schemes than in explicit schemes. In this case both methods benefit from the use of higher order formulations because they enrich the solution space.

For this development, the author decided to opt for an implicit time integration scheme. Having weighted the advantages and disadvantages of both approaches, it seems that the implicit scheme represents a short term investment (in terms of development effort) that will yield many long term benefits. In addition, it is always possible to easily develop the explicit version of the element for those problems whose time scale resolution comes close to the conditional time step requirements. Another advantage in terms of development is that the implicit scheme forces to perform many more checks than the explicit scheme. It would have been harder to identify many of the problems encountered in the development of this research work if the tangent stiffness matrix had not been taken into account and

only dynamic analysis were considered.

### 4.1.3 Advantages of the *total Lagrangian* formulation

The last main design decision was to develop all the formulation in the total Lagrangian framework. The *total lagrangian* framework describes the deformation with respect to the reference configuration. Whereas the *updated lagrangian* framework describes the deformation with respect to the previous equilibrium configuration in the analysis.

The total Lagrangian framework equations are very similar to their counterparts in the updated Lagrangian framework. The main advantage of the total Lagrangian framework is that it can yield some computational savings if there are magnitudes that can be precomputed in the reference configuration and stored throughout the analysis.

On the other hand, the updated Lagrangian framework allows overcoming a problem encountered by the total Lagrangian framework in analysis involving large rotations when angles become larger than $2\pi$. In [85] Mäkinen also claims that the updated Lagrangian framework yields a fully symmetric tangent matrix for conservative loads.

The decision was to develop the formulation in the total Lagrangian framework. The main reasons are to take advantage of the precomputation of magnitudes in the reference configuration and the lack of rotational degrees of freedom in the formulation as explained in section 4.1.1. With respect to the symmetry/asymmetry of the tangent matrix, the author did not consider this a deciding factor, since a wide range of loadings are to be applied to the element, both conservative and non-conservative.

A clear example of the benefit of using the total Lagrangian framework is shown in section 7.2, where the author shows the possibility of preintegrating the expression of the element's Jacobian —maintaining all the terms of the polynomial— through-the-thickness of the shell. This is an original contribution for rotation-free shell elements, it is also the first time it is applied to a shell element in a total Lagrangian formulation and had only been done before in the updated Lagrangian formulation by Stanley [120].

## 4.2 Computing curvatures without second derivatives

Several attempts have been made to overcome the $C^1$ condition that thin-shell finite elements need to satisfy in order to avoid spurious modes [24, 56, 63, 73, 93, 121, 143]. This work builds on the original proposal for rotation-free shell elements reported in [41, 93, 95, 96], and extends those principles in order to gather richer geometrical information from the patch of all the elements—not only those sharing one side—surrounding a given triangle in the mesh.[2] This allows to avoid the need for computing an *averaged* curvature for the element and instead we can obtain precise values

[2]It was reported in [96] that the nodal implementation of the BST, dubbed basic shell node (BSN), was marginally more precise than the elemental implementation. This is taken as an advice and a new way to better exploit the enriched information is sought.

for the curvature at any point in the triangle, in particular at the Gauss points.

The original approach is based on a linear interpolation (i.e. using linear basis functions). The curvatures are computed using the gradient of the surface normal at each element.

In all cases simplicity is of the utmost importance when dealing with boundary conditions. Boundary conditions are managed very easily, both for Dirichlet and Neumann conditions. The normal vector to the surface at every node accounts for this simplicity without the need to use additional degrees of freedom nor virtual nodes.

In the following we write the basic principles on which the formulation is based.

Let [67, 122]:

$$\boldsymbol{X} \in \mathcal{S} \subset \mathbb{R}^3 \mid \boldsymbol{X} = (x, y, z)^T = \boldsymbol{\varphi}(u, v) = \boldsymbol{\varphi} \tag{4.1}$$

$\nabla\boldsymbol{\varphi}$ defines the tangent plane to $\mathcal{S}$ as follows:

$$(\nabla\boldsymbol{\varphi})_1 \equiv \boldsymbol{\varphi}_{,1} = \frac{\partial\boldsymbol{\varphi}}{\partial u} \ , \ (\nabla\boldsymbol{\varphi})_2 \equiv \boldsymbol{\varphi}_{,2} = \frac{\partial\boldsymbol{\varphi}}{\partial v} \tag{4.2}$$

We define:

$$\boldsymbol{n} = \boldsymbol{\varphi}_{,1} \times \boldsymbol{\varphi}_{,2} \tag{4.3}$$

then:

$$\boldsymbol{n} \perp \boldsymbol{\varphi}_{,1} \ , \ \boldsymbol{n} \perp \boldsymbol{\varphi}_{,2} \Rightarrow \nabla(\boldsymbol{n} \cdot \nabla\boldsymbol{\varphi}) = \boldsymbol{0} \tag{4.4}$$

$$\nabla(\boldsymbol{n} \cdot \nabla\boldsymbol{\varphi}) = \nabla\boldsymbol{n} \cdot \nabla\boldsymbol{\varphi} + \boldsymbol{n} \cdot \nabla\nabla\boldsymbol{\varphi} = \boldsymbol{0} \tag{4.5}$$

$$\nabla\boldsymbol{n} \cdot \nabla\boldsymbol{\varphi} = \boldsymbol{\kappa} = -\boldsymbol{n} \cdot \nabla\nabla\boldsymbol{\varphi} \tag{4.6}$$

The means to accomplish the objective of computing the curvature ($\boldsymbol{\kappa}$) at specific locations—using the first equality given by equation (4.6)—is to compute the values of the normal directions at each of the three nodes of the triangle (this process is described in section 5.1). Using the values of the normal at the three nodes of the triangle we can build the following vector field of normal directions for the triangle and obtain its gradient ($\nabla\boldsymbol{n}$):

$$\boldsymbol{n}(\xi, \eta) = \frac{\sum_{i=1}^{3} N^i(\xi, \eta) \cdot \boldsymbol{n}^i}{\| \sum_{i=1}^{3} N^i(\xi, \eta) \cdot \boldsymbol{n}^i \|} \tag{4.7}$$

Using this field of normal vectors we can express the position of any point of the shell as:

$$\boldsymbol{x}(\xi, \eta, \zeta) = \sum_{i=1}^{3} N^i(\xi, \eta) \cdot \boldsymbol{x}^i + h\zeta \cdot \boldsymbol{n}(\xi, \eta) \tag{4.8}$$

where the shape functions are represented by $N$ and $h$ stands for the thickness of the shell. It must be noted that the shape functions used here are linear Lagrangian functions.

## 4.3 Raw approach and why it doesn't work

The development of the formulæ follows a continuum-based approach (very similar to the one presented in [123]), which yields the following expression for the Cauchy-Green strain tensor:

$$\boldsymbol{C} = \boldsymbol{F}^T \cdot \boldsymbol{F} = \left(\boldsymbol{j} \cdot \boldsymbol{J}^{-1}\right)^T \cdot \boldsymbol{j} \cdot \boldsymbol{J}^{-1} = \boldsymbol{G}^T \cdot \boldsymbol{g} \cdot \boldsymbol{G} \tag{4.9}$$

$$\boldsymbol{G} = \boldsymbol{J}^{-1} \tag{4.10}$$

$$\boldsymbol{g} = \boldsymbol{j}^T \cdot \boldsymbol{j} \tag{4.11}$$

$$\boldsymbol{j} = \left[\frac{\partial \boldsymbol{x}}{\partial \xi}\ ,\ \frac{\partial \boldsymbol{x}}{\partial \eta}\ ,\ \frac{\partial \boldsymbol{x}}{\partial \zeta}\right] \tag{4.12}$$

$$\boldsymbol{J} = \left[\frac{\partial \boldsymbol{X}}{\partial \xi}\ ,\ \frac{\partial \boldsymbol{X}}{\partial \eta}\ ,\ \frac{\partial \boldsymbol{X}}{\partial \zeta}\right] \tag{4.13}$$

where $\boldsymbol{G}$ is the Jacobian matrix of the inverse function of change of coordinates from global (in the reference configuration) to parametric of the element, and $\boldsymbol{g}$ contains the information of the deformed configuration. The reminding symbols are standard in the literature and the reader can refer to the **Notation** on page xxv.

The terms of $\boldsymbol{g}$ can be expressed as:

$$\begin{aligned} g_{\alpha\beta} = & \sum_{i=1}^{3} \boldsymbol{L}_{\alpha}^{i} \boldsymbol{x}^{i^T} \cdot \sum_{i=1}^{3} \boldsymbol{L}_{\beta}^{i} \boldsymbol{x}^{i} \\ & + 2\lambda\zeta \sum_{i=1}^{3} \boldsymbol{L}_{\alpha}^{i} \boldsymbol{x}^{i^T} \cdot \boldsymbol{U} \cdot \sum_{i=1}^{3} \boldsymbol{L}_{\beta}^{i} \boldsymbol{n}^{i} \\ & + \lambda^2\zeta^2 \sum_{i=1}^{3} \boldsymbol{L}_{\alpha}^{i} \boldsymbol{n}^{i^T} \cdot \boldsymbol{U} \cdot \boldsymbol{U} \cdot \sum_{i=1}^{3} \boldsymbol{L}_{\beta}^{i} \boldsymbol{n}^{i} \qquad \forall\ \alpha, \beta = \xi, \eta \end{aligned} \tag{4.14}$$

$$\boldsymbol{U} = \frac{1}{\| \sum_{i=1}^{3} N^i \boldsymbol{n}^i \|} \cdot \left[ \boldsymbol{I} - \frac{\left(\sum_{i=1}^{3} N^i \boldsymbol{n}^i\right) \otimes \left(\sum_{i=1}^{3} N^i \boldsymbol{n}^i\right)^T}{\| \sum_{i=1}^{3} N^i \boldsymbol{n}^i \|^2} \right] \tag{4.15}$$

where $\boldsymbol{L}_{\alpha}^{i}$ refers to the derivative of the shape function corresponding to node $i$ with respect to the coordinate $\alpha$, and $\boldsymbol{U}$ contains the information regarding the normalization of the normal vectors. The three terms of equation (4.14) are respectively: the *membranal* deformation, the *bending* deformation and the so-called *second order* deformation terms.

Figures 4.1 and 4.2 depict respectively the global and parametric coordinates that identify the nodes of the triangles, and the relation between the normals at the nodes and the patch of triangles that surround each node.

The relation between strains and stresses in a linear elastic material is established by the constitutive tensor:

$$\boldsymbol{S}' = \boldsymbol{D} : \boldsymbol{E}' \tag{4.16}$$

which is a fourth order tensor. But taking advantage of the major and minor symmetries corresponding to the symmetry of the stress and strain

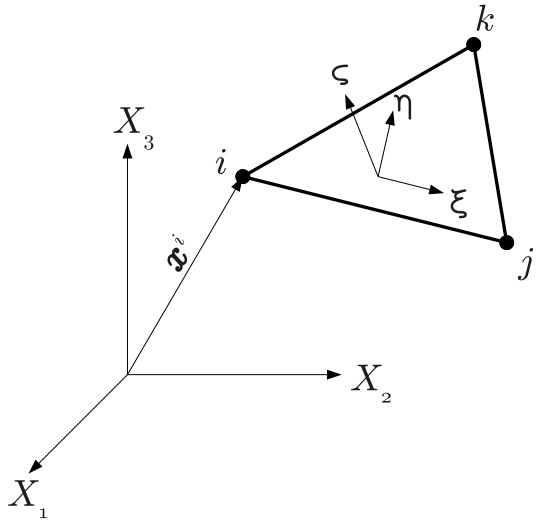


Figure 4.1: Representation of the global and parametric coordinates used to define the positions of each of the nodes of the triangle.

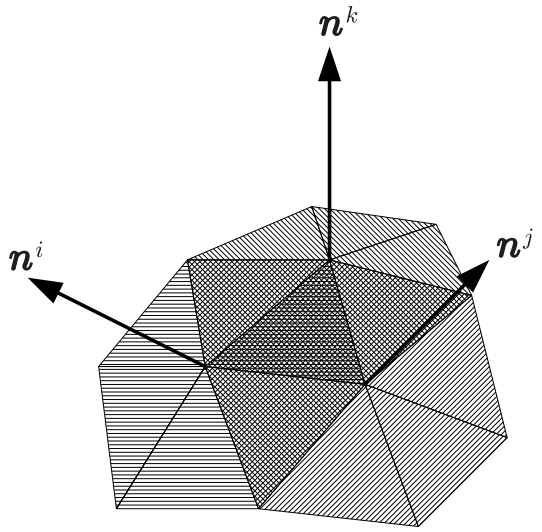


Figure 4.2: In order to compute the curvature inside the central triangle, we use the information of the patch of elements that surround each node. The shading patterns indicate which triangles contribute to the determination of each normal.

tensors—and using Voigt notation—, it can be expressed as a second order tensor. $\boldsymbol{E}$ is the Green-Lagrange strain tensor. $\boldsymbol{S}$ is the second Piola-Kirchhoff stress tensor. And the $'$s indicate that the strain and stress tensors must be expressed in material local coordinates, since that is the base used by the elasticity tensor $\boldsymbol{D}$.

$$\boldsymbol{E} = \frac{1}{2}\left(\boldsymbol{C} - \boldsymbol{I}\right) = \frac{1}{2}\left(\boldsymbol{G}^T \cdot \boldsymbol{g} \cdot \boldsymbol{G} - \boldsymbol{I}\right) \tag{4.17}$$

$$\boldsymbol{E}' = \boldsymbol{T}^T \cdot \boldsymbol{E} \cdot \boldsymbol{T} = \frac{1}{2}\left(\boldsymbol{T}^T \cdot \boldsymbol{G}^T \cdot \boldsymbol{g} \cdot \boldsymbol{G} \cdot \boldsymbol{T} - \boldsymbol{I}\right) = \frac{1}{2}\left(\boldsymbol{A}^T \cdot \boldsymbol{g} \cdot \boldsymbol{A} - \boldsymbol{I}\right) \tag{4.18}$$

$$\boldsymbol{A} = \boldsymbol{G} \cdot \boldsymbol{T} \tag{4.19}$$

$$\delta\boldsymbol{E}' = \frac{1}{2}\,\boldsymbol{A}^T \cdot \delta\boldsymbol{g} \cdot \boldsymbol{A} \tag{4.20}$$

where $\boldsymbol{T}$ is the matrix of change of coordinates from local to global (in the reference configuration). Thus, $\boldsymbol{A}$ results in the matrix of change of coordinates from local of the material to parametric of the element—in any configuration!

The expression for the internal virtual work can be expressed as:

$$\delta\Pi^{int} = \iiint_V \delta E'_{IJ} \cdot S'_{IJ} \cdot dV = \iiint_V \delta\boldsymbol{E}' : \boldsymbol{S}' \cdot dV \tag{4.21}$$

Taking advantage of Voigt's notation we can write the following expressions:

$$\begin{aligned} \delta E'_{IJ} \cdot S'_{IJ} &= \frac{1}{2}\,A^T_{Ii} \cdot \delta g_{ij} \cdot A_{jJ} \cdot S'_{IJ} = \frac{1}{2}\,\delta g_{ij} \cdot A_{iI} \cdot A_{jJ} \cdot S'_{IJ} \\ &= \frac{1}{2}\,\delta g_{ij} \cdot s_{ij} = \frac{1}{2}\,\delta\boldsymbol{g}^T_{Voigt} \cdot \boldsymbol{s}_{Voigt} \end{aligned} \tag{4.22}$$

$$\boldsymbol{g}_{Voigt} = \begin{bmatrix} g_{11} \\ g_{22} \\ g_{12} + g_{21} \end{bmatrix} \overset{Not}{=} \boldsymbol{g} \tag{4.23}$$

$$\boldsymbol{s}_{Voigt} = \begin{bmatrix} s_{11} \\ s_{22} \\ s_{12} \end{bmatrix} \overset{Not}{=} \boldsymbol{s} \tag{4.24}$$

$$\boldsymbol{I}_{Voigt} = \begin{bmatrix} 1 \\ 1 \\ 0 \end{bmatrix} \overset{Not}{=} \boldsymbol{I} \tag{4.25}$$

$$\begin{bmatrix} s_{11} \\ s_{22} \\ s_{12} \end{bmatrix} = \underbrace{\begin{bmatrix} A^2_{11} & A^2_{12} & 2A_{11}A_{12} \\ A^2_{21} & A^2_{22} & 2A_{21}A_{22} \\ A_{11}A_{21} & A_{12}A_{22} & A_{11}A_{22} + A_{12}A_{21} \end{bmatrix}}_{\boldsymbol{Q}^T} \cdot \begin{bmatrix} S'_{11} \\ S'_{22} \\ S'_{12} \end{bmatrix} \tag{4.26}$$

From this point onward, unless specifically indicated by subscripts, Voigt notation will be used for the engineering strains and stresses. Thus, the

$Voigt$ subscript will be dropped from the notation.

$$\boldsymbol{s} = \boldsymbol{Q}^T \cdot \boldsymbol{S}' \tag{4.27}$$

$$\delta E'_{IJ} \cdot S'_{IJ} = \frac{1}{2}\,\delta g_{ij} \cdot s_{ij} = \frac{1}{2}\,\delta \boldsymbol{g}^T \cdot \boldsymbol{Q}^T \cdot \boldsymbol{S}' = \frac{1}{2}\,\delta \boldsymbol{g}^T \cdot \boldsymbol{Q}^T \cdot \boldsymbol{D} \cdot \boldsymbol{E}' \tag{4.28}$$

$$\boldsymbol{E}' = \frac{1}{2}\,(\boldsymbol{Q} \cdot \boldsymbol{g} - \boldsymbol{I}) \tag{4.29}$$

$$\delta \boldsymbol{g} = \frac{\partial \boldsymbol{g}}{\partial \boldsymbol{x}} \cdot \delta \boldsymbol{x} = \boldsymbol{B} \cdot \delta \boldsymbol{x} \tag{4.30}$$

$$\prod^{int} = \frac{1}{4} \iint_S \int_{-\frac{h}{2}}^{\frac{h}{2}} \delta \boldsymbol{x}^T \cdot \boldsymbol{B}^T \cdot \boldsymbol{Q}^T \cdot \boldsymbol{D} \cdot (\boldsymbol{Q} \cdot \boldsymbol{g} - \boldsymbol{I}) \cdot dz' \cdot dA \tag{4.31}$$

where $\boldsymbol{Q}$ is defined in equation (4.26).

The development of this first and raw approach does not lead to satisfactory results. The reason behind it is that zero energy modes affect the solution. The first thing that raises our suspicion is that the element as described above is non-conforming. That is, the normal at each point of the element is not necessarily perpendicular to the surface of the element (see equations (4.7) and (4.8)). We have kept the geometric description of the element intentionally as simple as possible by using linear shape functions. As a consequence, it is possible for the mesh of triangles to fold like an accordion and not develop significant deformation energy. Take for example a simply supported square plate subjected to a point load at its center (figure 4.3). Note that because of the near-symmetry of the folds, the normals barely change direction making their gradient very close to zero. Thus the computed curvature using the first equality in equation (4.6) might be accurate, even if the plane of the triangle differs a lot from the direction of the normals at the nodes. But this does not prevent the system from assigning totally erroneous positions to the nodes.

### 4.3.1 A historical remark

The current approach was first introduced by Ubach and Oñate in [130]. This early proposal was followed by the current framework also by Ubach and Oñate in [131]. However, it must be said that, an almost identical and independent work (with identical results) was presented at the same congress by Linhard et al. [70]. They later published their work in [71]. This coincidence emphasizes the interest that the computation of thin-shells using rotation-free elements enjoys within the computational mechanics community[3]. But it also underscores the difficulty in developing new and original strategies not explored before.

[3]Sabourin and Brunet [112] also report a similar simultaneity of independent research publications on the same topic in 1993.

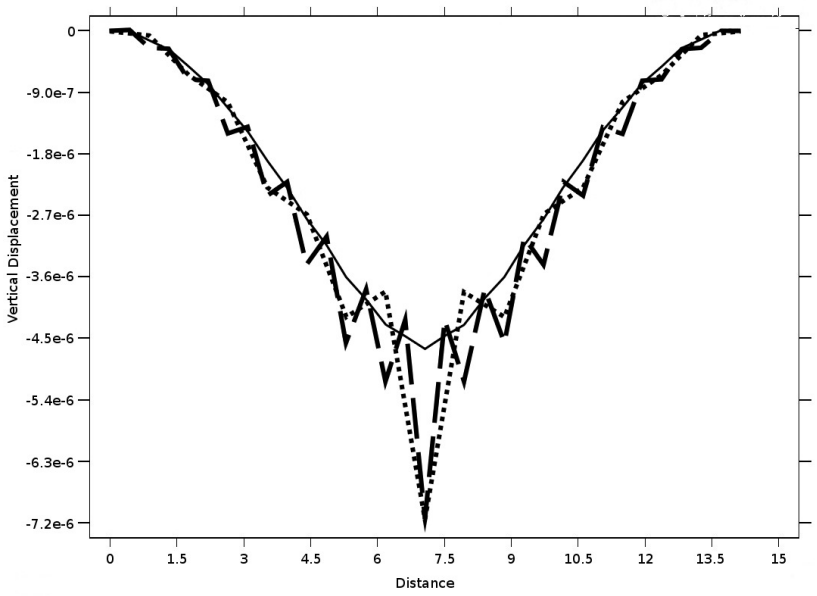


Figure 4.3: Numerical example showing the displacements along the diagonals (discontinuous line and dots) of a simply supported square with central point load. The results are compared to the corresponding solution given by the DKT element (solid line).

## 4.4 Attempts to add energy modes and stabilize the element

We have explored different strategies to neutralize the instabilities caused by the lack of conformity in the description of the element:

- The simplest strategy consisted in making an analogy that assumed that the deviation of the normal from the theoretic perpendicular to the plane at the center of the element represented a rotation due to shear deformation.

- Another strategy consisted in assuming that the missing energy mode in the elements was an antimetric bending mode. Again, the deviation of the normal from the theoretic perpendicular at the center was used to estimate an increased deformation energy (figure 4.4).

- Yet another strategy was devised. In this case the normal at the center of the element was prescribed to remain perpendicular to the element. To achieve this the triangle was further subdivided into three sub-triangles (figure 4.5).

In all cases the resulting finite elements were stable and did not show zero energy modes. However the strategies had secondary effects. The first effect was an increased stiffness of the shell, yielding smaller displacements

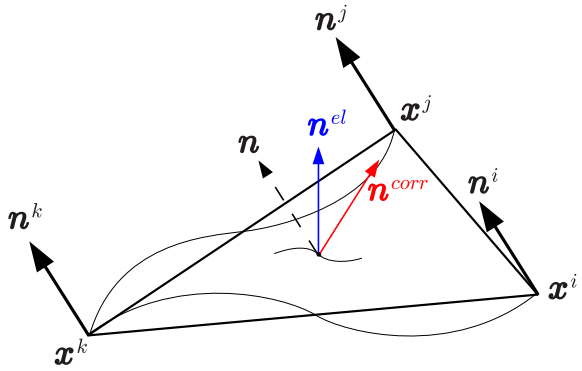


Figure 4.4: Figure depicting the concept of the antimetric bending energy mode to stabilize the element.

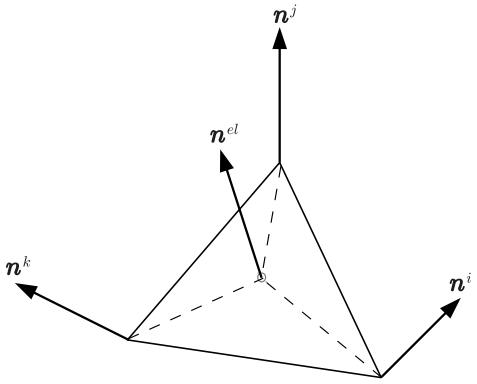


Figure 4.5: Figure depicting the concept for *gently* forcing the normals toward the perpendicular of the element.

than the theoretic ones. The second observation was that the convergence, unlike that of conventional finite element formulations, approached the solution from less stiff solutions. This is suspected to be caused by the underlying non-conforming formulation.

Of the three strategies described, the one that showed better results was the analogy with an antimetric bending mode. However, those results were achieved at the cost of excessive sophistication of the model and yet the errors were still inadmissible.

## 4.5 Evolving to a higher order description of the triangle

In order to neutralize the instabilities caused by the lack of conformity in the description of the element, we have shifted towards a strategy that consists on increasing the order of the geometrical description so that all the

modes of deformation can be represented and thus avoiding the problems associated with the non-conforming formulation. The triangle of lowest order that can interpolate at the same time the positions and the normals at the nodes is a cubic triangle. However, in order to determine unambiguously the ten parameters of a cubic triangle there is not enough data with the three nodes and the three normals. Therefore, choices must be made.

## 4.6 Summary

The design guidelines for the new rotation-free shell element have been presented. The design guidelines are:

- Use only displacement degrees of freedom. Do not add any additional degree of freedom to the element if possible.
- Develop the implicit formulation version of the element. This ensures being able to solve the widest possible range of engineering problems. An explicit version is easy to develop once the implicit is working.
- Use a total Lagrangian framework to exploit its advantages for the computational implementation.
- Develop the formulation for a continuum-based approach. This provides rigor to the formulation.

Using these guidelines and using the left-hand-side of equation (4.6) to compute the curvature on a surface $\mathcal{S} \subset \mathbb{R}^3$ a first formulation is presented. This work takes as starting point the nodal implementation of a basic triangle shell element (BSN; see Oñate and Zárate [96]). In order to use an exact formula for the curvature, the normal directions at each node and the way to characterize them are proposed.

This first development did not result to be a conforming element. Different strategies were sought to solve this problem and control the spurious modes. Finally the decision was made to enhance the geometrical description of the element while keeping the main design features.

# Chapter 5

# Using Bézier triangles

AT THE TIME WHEN THE IDEAS PRESENTED IN THIS CHAPTER were being developed, the Isogeometric Analysis was starting to boom. The author faced the decision of whether to join this new current or stick within a more traditional mesh-based Finite Element Method approach. The decision was to blend some of the advantages brought by both methods using Bézier shape functions, which are of polynomial nature —just as the Lagrange functions used in the finite element method (FEM)—, but also serve as the basis to generate the NURBS functions used in IGA, and also use the versatility provided by the meshes of triangles. A number of challenges have emerged as a consequence of this decision. Chapter 5 presents the framework provided by the Bézier shape functions and explains the geometric construction of the element. Chapter 6 develops all the underlying formulation to obtain the equations that describe the deformation of the element and sets the basis to apply the variational principles used in continuum mechanics. Chapter 7 is devoted to instantiate a general expression of the tangential stiffness matrix of the element considering a linear elastic material, and developing all the expressions which are of particular interest attending the inherent non-linear characteristics of shells' geometries. Chapter 8 determines the most adequate order of integration of the element, while chapter 9 deals with the phenomenon of membrane locking.

Chapter 4 showed the need for enhancing the geometric description of the element. The reasons are the following:

- The idea of computing averaged normals at the nodes and using them to enrich the geometrical description of the element seems a good one. During his presentation at the 9th USNCCM Linhard [70] did report excellent accuracy in the computation of the curvatures using the scheme explained in section 4.2.

- If the shell is to be computed using a conforming representation, then a linear description will not do. We have to increase the polynomial degree of the modeling.

- The Bézier framework fulfills the two requirements above: it allows to use the information provided by the normals and does so

> using higher order polynomials. Furthermore, Bézier shape functions share the same *variation diminishing* and *monotone variation* properties that seem so valuable in IGA which uses NURBS shape functions [56, p. 4149].

As stated in section 4.1, it is a priority not to increase the number of degrees of freedom unless absolutely necessary. Therefore, we will use the simplest possible splines. The minimal spline that interpolates the nodes and the endpoint derivatives of a curve is a cubic. The same happens for a triangle (interpolating vertices and vertex normals). Furthermore, by interpolating the normals at the nodes, $\mathcal{G}^1$ continuity is attained automatically at the nodes (not overall $\mathcal{G}^1$ continuity though).

The challenge then becomes to enhance the geometric description of the triangle without increasing the number of degrees of freedom in the system. A way to precisely define the geometrical parameters for the cubic triangle without increasing the number of degrees of freedom is adopting the concept of Bézier triangles first defined by de Casteljau [19, 20][37, Ch. 17, pp. 309–333]. The different sections in this chapter are devoted to understand this process.

Since one of the main inputs that characterize the geometry of the triangles are the vertex normals, it is of paramount importance to obtain precise normals at the nodes of the mesh. This process is explained in section 5.1. Section 5.2 provides a detailed explanation of the shape functions used in Bézier triangles and their transformation from natural or barycentric coordinates to parametric coordinates. Section 5.3 provides the fundamentals to construct the geometry of the cubic Bézier triangle based on geometric considerations. Up to this point, only geometrical considerations are taken into account for the construction of the enhanced triangle. But a cubic Bézier triangle has more unknowns than data can be obtained from local geometric constraints. Therefore we will also take into account energy minimization in the geometric construction. This process is explained in section 5.4.

## 5.1 Selecting the normals

The computation of the normals at the nodes is an arbitrary choice since this is unprescribed data and we must estimate it from the mesh information. Some might argue that this could be retrieved as exact data from the CAD model. However, that would result in an inconsistency in the process of analysis. There is no way to obtain the information on the normals from CAD in the deformed configuration. If the normals are obtained using different methods in the current and deformed configurations, it can lead to uncontrolled errors in the analysis.

We choose to compute the normal at every node as a weighted average of the normals of all the triangles that surround the node (see figure 5.1). The weights chosen have been determined so that the error is minimized for a wide range of possible surface shapes. The paper [129] by Ubach, Estruch and García-Espinosa presents a specific study conducted to determine those weights. Here the author will only present the conclusions of that paper.

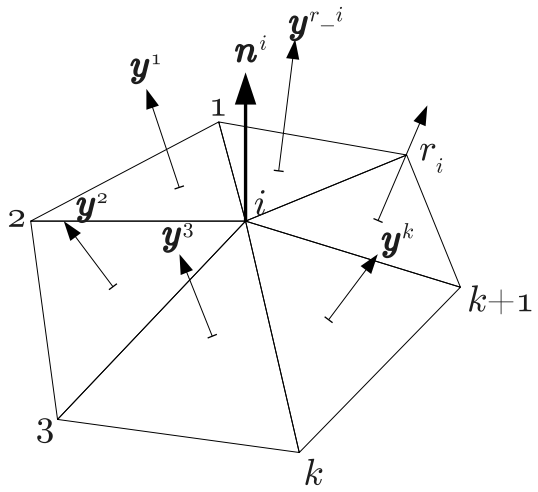


Figure 5.1: Example of a mesh approaching a surface $\mathcal{S}$ in the vicinity of a node $i$. The normal at node $i$ is estimated using the normals at each of the surrounding triangles. $r_i$ is the total number of triangles surrounding node $i$.

The goal of the study is to find the weighting factors:

$$w^k \in \mathbb{R}, k = 1 \div r_i \mid \hat{\boldsymbol{n}}^i = \frac{\sum_{k=1}^{r_i} w^k \hat{\boldsymbol{y}}^k}{\left\| \sum_{k=1}^{r_i} w^k \hat{\boldsymbol{y}}^k \right\|} + \vec{\mathcal{O}} \tag{5.1}$$

where $\hat{\boldsymbol{n}}^i$ is the actual unit normal vector of $\mathcal{S}$ at $i$ and $\vec{\mathcal{O}}$ represents the error made; so that $\vec{\mathcal{O}}$ is minimized. See figure 5.1 for a graphical representation. The study proposes a framework for determining the weights that better characterize the representativity of each triangle's normal vector:

> Let's consider the surface $\mathcal{S}$ and its local Taylor expansion series at the vertex $[i]$. Then, by truncating this series at the second order terms, we will obtain a quadric. So now we have two different approximations to $\mathcal{S}$ at $[i]$, namely:
>
> - the set of triangles with a vertex at $[i]$,
> - and the quadric.
>
> If we now make the assumption that the quadric interpolates all the vertices of the set of triangles, the error we are making is of the order of $h^2$. Being $h$ a measure of the size of the triangles. This allows us to reinterpret the relationship between $[\hat{\boldsymbol{y}}^k]$ and the surface $\mathcal{S}$. The vector $[\hat{\boldsymbol{y}}^k]$ can be thought of as the normal direction of a plane section of the quadric.

> We will still make one more assumption. This is that the conic resulting from the intersection with the quadric is a closed curve. This may seem like a very strong assumption. But in fact it is no more limiting than the restriction which represent the triangles themselves. What this assumption implies is that the section of the quadric is bounded; just like the triangles are.
>
> In no way, are we implying in the current argument that this framework will produce approximations with an error bounded by $\mathcal{O} \propto h^2$. What this analysis provides us is a framework to enrich the information provided by the set of $[\hat{\boldsymbol{y}}^k]$ and their corresponding triangles. (Ubach et al. [129], p. 249)

The study concludes that:

> In order to approximate the normal vectors at the nodes of a triangle mesh using a weighted average rule (see equation (5.1)), the weight consisting on *the interior angle of the triangle at the node considered divided by the area of the circumscribed circle to the triangle* ($w_{\alpha/A_\circ}$) is recommended. The mathematical expression of this weighting factor for the node $A$ as a function of the coordinates of the nodes of the $\widehat{ABC}$ triangle is shown in equation (5.2). (Ubach et al. [129], p. 267)

$$w_{\alpha/A_\circ} = \left( \frac{\|\overrightarrow{AB} \times \overrightarrow{AC}\|}{\|\overrightarrow{AB}\| \cdot \|\overrightarrow{AC}\| \cdot \|\overrightarrow{BC}\|} \right)^2 \cdot \arccos\left( \frac{\overrightarrow{AB} \cdot \overrightarrow{AC}}{\|\overrightarrow{AB}\| \cdot \|\overrightarrow{AC}\|} \right) \tag{5.2}$$

Therefore, the normal at each node is computed using the following formula:

$$\hat{\boldsymbol{n}}^i = \frac{\displaystyle\sum_{k=1}^{r_i} w^k_{\alpha/A_\circ} \hat{\boldsymbol{y}}^k}{\left\| \displaystyle\sum_{k=1}^{r_i} w^k_{\alpha/A_\circ} \hat{\boldsymbol{y}}^k \right\|} \tag{5.3}$$

In this case $\hat{\boldsymbol{n}}^i$ is the approximation to the actual unit normal vector of the surface $\mathcal{S}$, unlike in equation (5.1) where the error term had not been truncated.

## 5.2 Shape Functions

Figure 5.2 shows a barycentric representation of the cubic Bézier triangle along with the corresponding parametric representation. The respective shape functions in barycentric and parametric coordinates are as well written in the figure.

Next we write explicitly the ten shape functions for the element:

$$\begin{array}{lll} N^1 = (1-\xi-\eta)^3 & N^2 = \xi^3 & N^3 = \eta^3 \\ N^4 = 3\cdot\xi\cdot(1-\xi-\eta)^2 & N^5 = 3\cdot\eta\cdot(1-\xi-\eta)^2 & N^6 = 3\cdot\xi^2\cdot\eta \\ N^7 = 3\cdot\xi^2\cdot(1-\xi-\eta) & N^8 = 3\cdot\eta^2\cdot(1-\xi-\eta) & N^9 = 3\cdot\xi\cdot\eta^2 \\ & N^{10} = 6\cdot\xi\cdot\eta\cdot(1-\xi-\eta) & \end{array} \tag{5.4}$$

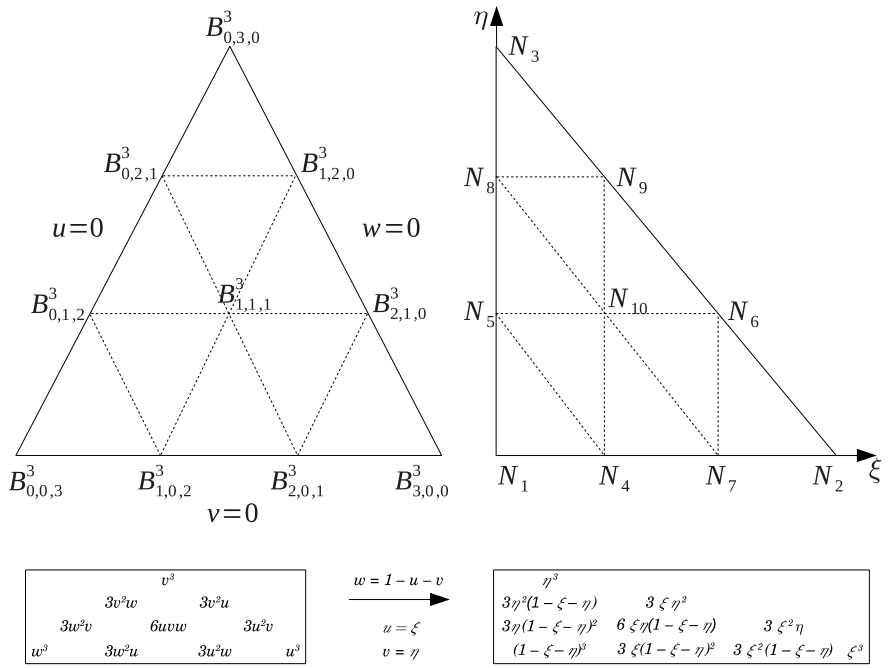


Figure 5.2: Left: barycentric representation of the Bézier triangle along with its shape functions corresponding to each of the control points of the net. The capital $B$s use the Bernstein polynomials notation [38]. Right: equivalent representation using parametric coordinates. The capital $N$s refer to the more traditional FEM notation for the shape functions. The arrow in the center specifies the transformation used from barycentric to parametric coordinates.

These shape functions are represented in figure 5.3 for the *control points* along the diagonal edge of the parametric triangle and the central *control point*. Notice the change of terminology: the points which describe the geometry of the triangle are no longer called *nodes*, and instead they are called *control points* ($\boldsymbol{p}$). As we will see later this doesn't mean that we part away from the concepts of the isoparametric formulations. Even though we only use the vertices of the triangle as mesh and system variables, both the geometric description and the deformation description are done using the same shape functions together with this set of 10 control points.

Using these shape functions the points on the shell's midsurface are computed using equation (5.5).

$$\bar{\boldsymbol{x}}(\xi,\eta) = \boldsymbol{x}(\xi,\eta)|_{\zeta=0} = \sum_{i=1}^{10} \boldsymbol{p}^i \cdot N^i(\xi,\eta) = \boldsymbol{p}^i N^i = \boldsymbol{p}\cdot\boldsymbol{N} \tag{5.5}$$

$$\boldsymbol{p} = \left[\boldsymbol{p}^1\ \boldsymbol{p}^2\ \boldsymbol{p}^3\ \boldsymbol{p}^4\ \boldsymbol{p}^5\ \boldsymbol{p}^6\ \boldsymbol{p}^7\ \boldsymbol{p}^8\ \boldsymbol{p}^9\ \boldsymbol{p}^{10}\right] \tag{5.6}$$

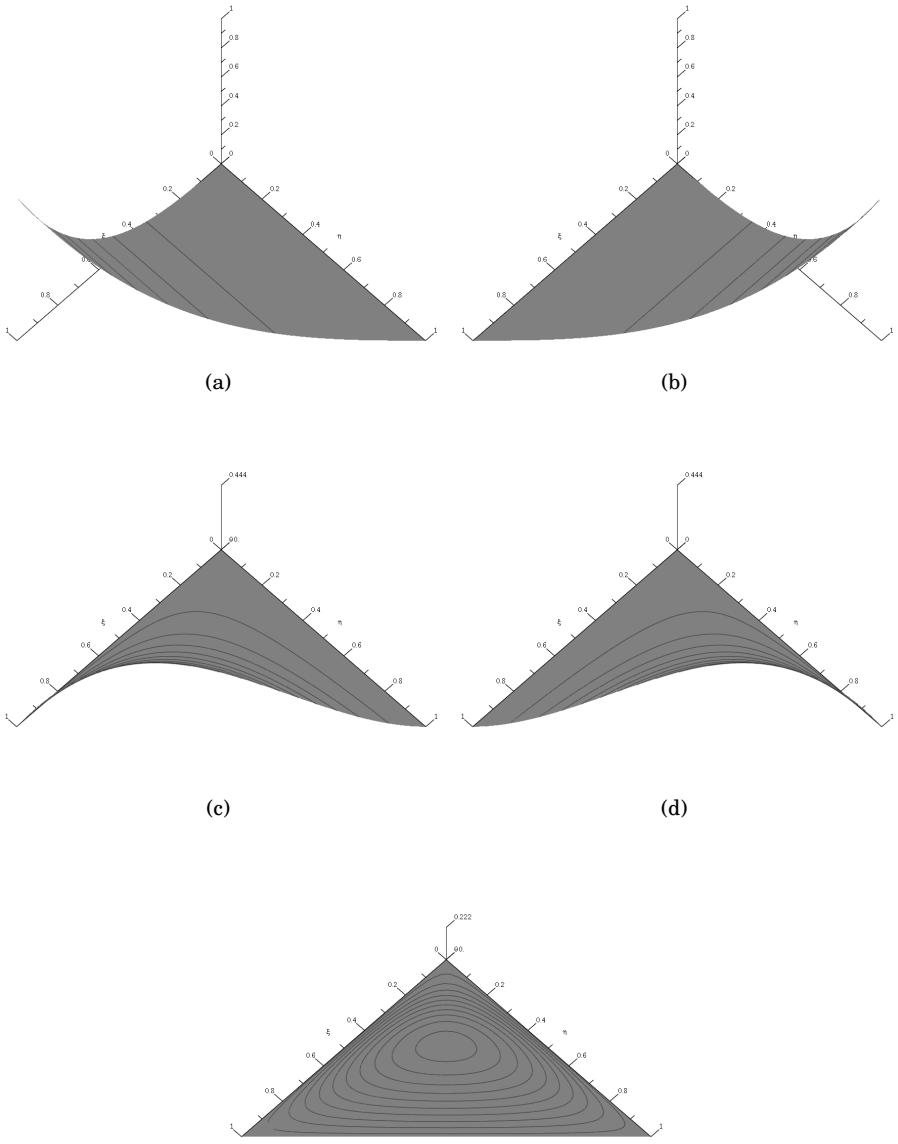

(a) (b)

(c) (d)

(e)

Figure 5.3: Representation of the shape functions corresponding to 5 different control points. Graphs (a), (b), (c), (d) and (e) depict respectively shape functions: $N^2$, $N^3$, $N^6$, $N^9$ and $N^{10}$. The vertical axes indicate the maximum value for each function.

The first derivatives of the shape functions are:

$$\boldsymbol{L}_\xi = \begin{bmatrix} -3(1-\xi-\eta)^2 \\ 3\xi^2 \\ 0 \\ 3(1-\xi-\eta)(1-3\xi-\eta) \\ -6\eta(1-\xi-\eta) \\ 6\xi\eta \\ 3\xi(2-3\xi-2\eta) \\ -3\eta^2 \\ 3\eta^2 \\ 6\eta(1-2\xi-\eta) \end{bmatrix} \qquad \boldsymbol{L}_\eta = \begin{bmatrix} -3(1-\xi-\eta)^2 \\ 0 \\ 3\eta^2 \\ -6\xi(1-\xi-\eta) \\ 3(1-\xi-\eta)(1-\xi-3\eta) \\ 3\xi^2 \\ -3\xi^2 \\ 3\eta(2-2\xi-3\eta) \\ 6\xi\eta \\ 6\eta(1-\xi-2\eta) \end{bmatrix} \tag{5.7}$$

and the second derivatives are:

$$\boldsymbol{L}_{\xi,\xi} = \begin{bmatrix} 6(1-\xi-\eta)^2 \\ 6\xi^2 \\ 0 \\ -6(2-3\xi-2\eta) \\ 6\eta \\ 6\eta \\ 6(1-3\xi-\eta) \\ 0 \\ 0 \\ -12\eta \end{bmatrix} \qquad \boldsymbol{L}_{\xi,\eta} = \begin{bmatrix} 6(1-\xi-\eta)^2 \\ 0 \\ 0 \\ -6(1-2\xi-\eta) \\ -6(1-\xi-2\eta) \\ 6\xi \\ -6\xi \\ -6\eta \\ 6\eta \\ 6(1-2\xi-2\eta) \end{bmatrix} \tag{5.8}$$

$$\boldsymbol{L}_{\eta,\xi} = \begin{bmatrix} 6(1-\xi-\eta) \\ 0 \\ 0 \\ -6(1-2\xi-\eta) \\ -6(1-\xi-2\eta) \\ 6\xi \\ -6\xi \\ -6\eta \\ 6\eta \\ 6(1-2\xi-2\eta) \end{bmatrix} \qquad \boldsymbol{L}_{\eta,\eta} = \begin{bmatrix} 6(1-\xi-\eta) \\ 0 \\ 6\eta \\ 6\xi \\ -6(2-2\xi-3\eta) \\ 0 \\ 0 \\ 6(1-1\xi-3\eta) \\ 6\xi \\ -12\xi \end{bmatrix} \tag{5.9}$$

And therefore, the curvilinear coordinates are expressed as:[1]

$$\bar{\boldsymbol{x}}_{,\xi}(\xi,\eta) = \frac{\partial \bar{\boldsymbol{x}}}{\partial \xi} = \sum_{i=1}^{10} \boldsymbol{p}^i \cdot L^i_\xi(\xi,\eta) = \boldsymbol{p}^i L^i_\xi = \boldsymbol{p} \cdot \boldsymbol{L}_\xi \tag{5.10}$$

$$\bar{\boldsymbol{x}}_{,\eta}(\xi,\eta) = \frac{\partial \bar{\boldsymbol{x}}}{\partial \eta} = \sum_{i=1}^{10} \boldsymbol{p}^i \cdot L^i_\eta(\xi,\eta) = \boldsymbol{p}^i L^i_\eta = \boldsymbol{p} \cdot \boldsymbol{L}_\eta \tag{5.11}$$

Using these expressions, the normal vector to the midsurface can be obtained.

$$\boldsymbol{n}(\xi,\eta) = \frac{\bar{\boldsymbol{x}}_{,\xi} \times \bar{\boldsymbol{x}}_{,\eta}}{\|\bar{\boldsymbol{x}}_{,\xi} \times \bar{\boldsymbol{x}}_{,\eta}\|} = \frac{\boldsymbol{p}^i L^i_\xi \times \boldsymbol{p}^i L^i_\eta}{\|\boldsymbol{p}^i L^i_\xi \times \boldsymbol{p}^i L^i_\eta\|} = \frac{(\boldsymbol{p} \cdot \boldsymbol{L}_\xi) \times (\boldsymbol{p} \cdot \boldsymbol{L}_\eta)}{\|(\boldsymbol{p} \cdot \boldsymbol{L}_\xi) \times (\boldsymbol{p} \cdot \boldsymbol{L}_\eta)\|} \tag{5.12}$$

For the reference configuration, the normal vector $\boldsymbol{\mathcal{N}}$ can also be referred to as $\boldsymbol{t}_3$.

$$\boldsymbol{t}_3 \equiv \boldsymbol{\mathcal{N}}(\xi,\eta) = \frac{\bar{\boldsymbol{X}}_{,\xi} \times \bar{\boldsymbol{X}}_{,\eta}}{\|\bar{\boldsymbol{X}}_{,\xi} \times \bar{\boldsymbol{X}}_{,\eta}\|} = \frac{(\boldsymbol{P} \cdot \boldsymbol{L}_\xi) \times (\boldsymbol{P} \cdot \boldsymbol{L}_\eta)}{\|(\boldsymbol{P} \cdot \boldsymbol{L}_\xi) \times (\boldsymbol{P} \cdot \boldsymbol{L}_\eta)\|} \tag{5.13}$$

See figure 6.2 on page 68 for a graphical representation.

## 5.3 Geometric construction of the Bézier triangle

The mathematical expression of a cubic triangle contains the complete monomial basis up to 3rd order: i.e. 10 monomials (notice the geometric

[1] Notice the use of the Einstein convention for the summation over repeated indices.

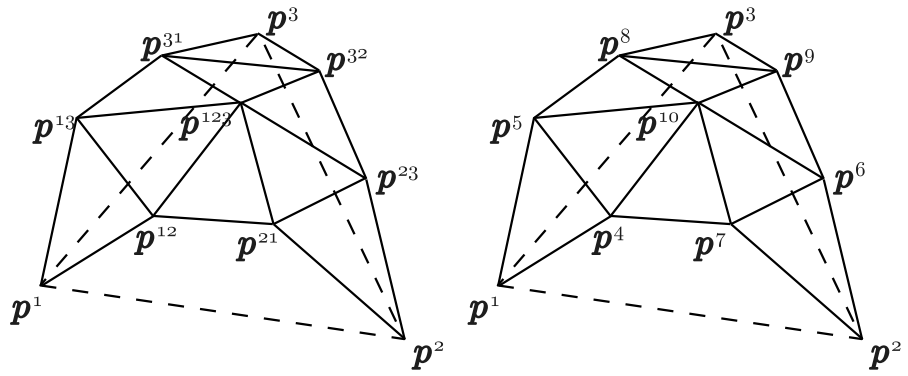


Figure 5.4: The geometry of the cubic Bézier triangle is determined by the position of the 10 control points. Notation used to identify each of the control points in a triangle. Left: barycentric-like notation. Right: natural notation. Notice that there exists a bijective relationship between the two notations.

analogy between Pascal's triangle in table 5.1 and the barycentric representation of the Bernstein polynomials in figure 5.2, which indicates that both sets of polynomial basis span the same polynomial space). Therefore, in order to obtain the expression for a given triangle we have to determine the 10 coefficients for the complete polynomial in the 3 spatial coordinates: 30 in total. There is clearly not enough information in the position of the 3 vertices ($3 \times 3 = 9$ conditions) and the orientation of the 3 vertex normals ($3 \times 2 = 6$ conditions) to uniquely determine these 30 coefficients. I could have opted to simply discard 5 terms of the polynomial and reduce the order of description of the cubic triangle to an incomplete quadratic triangle.

Table 5.1: Pascal's triangle of monomials for bi-variate cubic functions.

$$
\begin{array}{cccc}
 & & 1 & \\
 & \xi & & \eta \\
\xi^2 & & \xi\eta & & \eta^2 \\
\xi^3 & \xi^2\eta & & \xi\eta^2 & & \eta^3
\end{array}
$$

Instead, I seized the opportunity that Bézier triangles provide for constructing higher order triangular surfaces. The bulk of this thesis work consists on finding the geometrical relations that allow to complete the cubic polynomial basis for a Bézier triangle aimed at performing non-linear thin shell analysis. Next I explain the process I have followed and which generates a space of solutions that includes the solution of the discrete problem. Other arbitrary choices do not, in general, generate such a space of solutions[2].

[2]See section 5.4 for a detailed explanation of this issue.

In order to refer to each of the control points in a cubic Bézier triangle, the author uses a dual notation (see figure 5.4). On one side, the author uses a barycentric-like notation to define the position of the control points. On the other side, once the control points have been defined, the author uses a natural notation to use them in conjunction with the shape functions defined in section 5.2. Since this section is focused on the geometric construction of the Bézier triangle, the barycentric-like notation will be used.

The vertex control points are straight forward to evaluate:

$$\boldsymbol{p}^i = \boldsymbol{x}^i \qquad \forall i = 1 \div 3 \tag{5.14}$$

The net's remaining control point coordinates can be evaluated for each point computing the intersection of three planes. For the contour points, the planes are the ones displayed shaded or darkened in figure 5.5:

1. The plane perpendicular to the normal at the vertex —this is a necessary and sufficient condition to interpolate the normals—.

2. The plane that contains the curve of the triangle's contour. In order to maintain $\mathcal{C}^0$ continuity, this has to be a symmetric condition for two adjacent triangles. The selection of the plane is so that one of the directors is the edge of the flat triangle and the other director is the average of the 2 normals at the nodes. In section 9.2 the author will show a variation on this condition to enhance the versatility of the element.

3. And a plane perpendicular to the edge of the flat triangle. the exact location of this plane will be explained in section 5.4. Suffice it to say, that the criterion to position the plane is based on energy minimization and not on geometric considerations.

The mathematical expression of these three planes and their intersection is presented in equation (5.15):

$$\underbrace{\begin{bmatrix} \boldsymbol{n}^{iT} \\ \boldsymbol{d}^{ijT} \\ (\boldsymbol{x}^i - \boldsymbol{x}^j)^T \end{bmatrix}}_{\boldsymbol{A}_{\boldsymbol{p}}^{ij}} \cdot \boldsymbol{p}^{ij} = \underbrace{\begin{bmatrix} \boldsymbol{n}^{iT} \cdot \boldsymbol{x}^i \\ \boldsymbol{d}^{ijT} \cdot \boldsymbol{x}^i \\ (\boldsymbol{x}^i - \boldsymbol{x}^j)^T \cdot \left[(1 - \Psi^{ij})\boldsymbol{x}^i + \Psi^{ij}\boldsymbol{x}^j\right] \end{bmatrix}}_{\boldsymbol{b}_{\boldsymbol{p}}^{ij}} \qquad \forall i, j = 1 \div 3, i \neq j \tag{5.15}$$

So the control points on the contour are computed by solving the system of equations:

$$\boldsymbol{A}_{\boldsymbol{p}}^{ij} \cdot \boldsymbol{p}^{ij} = \boldsymbol{b}_{\boldsymbol{p}}^{ij} \tag{5.16}$$

where $\boldsymbol{d}^{ij}$ represents the vector perpendicular to the plane indicated by item 2 and represented light gray in figure 5.5[3]; and the parameter $\Psi^{ij}$

[3]This definition will change when the author introduces the emulated drilling rotations in chapter 9. Refer to equation (9.7) on page 106.

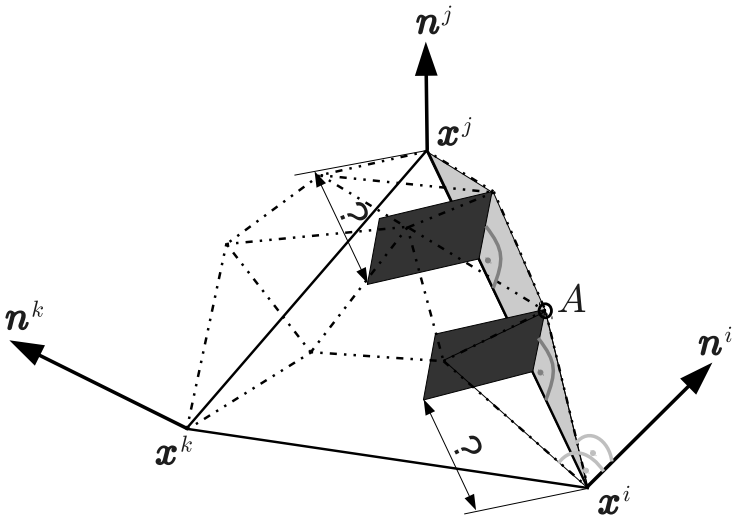


Figure 5.5: Representation of the net of control points (dashed lines) for a cubic Bézier triangle constructed using the nodal positions and normals. Three planes—shaded, light gray and dark gray—define the position of a control point $A$ of the contour. Question marks indicate that the position of the dark gray planes has not been determined yet. Their position will be solved in section 5.4.

specifies the location of the plane indicated by item 3 on page 51 and represented dark gray in figure 5.5. These definitions ($\boldsymbol{d}^{ij}$ and $\Psi^{ij}$) will change in chapter 9.

The central control point is determined by the intersection of the three mid-edge control triangles. There is a geometric condition that can be used. If all the control triangles sharing an edge across two triangles are co-planar, then the two triangles have $\mathcal{G}^1$ continuity [37, pp. 368–371]. This is very desirable as has been discussed in sections 3.2.2 and 4.1.1 on page 22 and on page 28.

Because the control triangles at the corners of each Bézier triangle are orthogonal to the normal vectors at the nodes (see item 1 on page 51), then all the corner control triangles at a given node have already been defined as co-planar. Then, we would only need to enforce co-planarity of the mid-edge control triangles to achieve $\mathcal{C}^1$ continuity (see figure 5.6). However this is a double-edged sword and not always possible. Being a very appealing opportunity to construct a fully $\mathcal{C}^1$ continuous triangle, it would be, alas, a very ill-conditioned equation system. Take for example the case of a flat triangle shape. In this case, all three mid-edge control triangles would be co-planar, and their intersection indefinite. Another undesirable case would be when the three mid-edge control triangles intersect far away from the triangle's domain, or don't intersect at all.

In order to work around the ill-conditioning of the above condition, let's perform a trick. Instead of computing the intersection of the three mid-edge control triangles, I will estimate a *likely* position for this intersection.

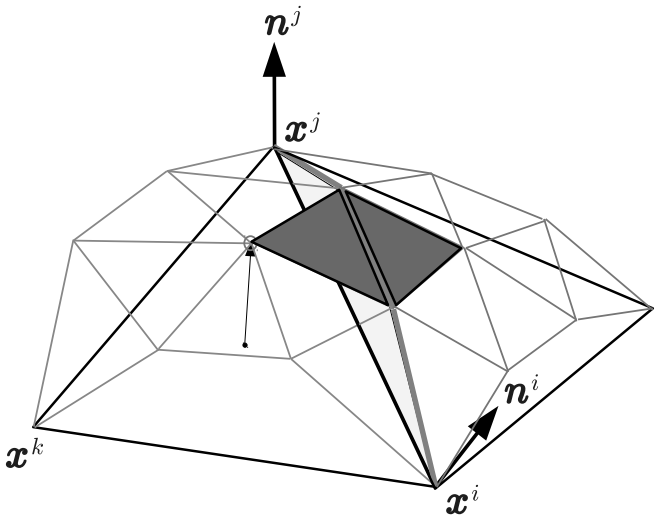


Figure 5.6: Two adjacent Bézier triangles are $\mathcal{G}^1$ continuous if all their adjacent control triangles are co-planar. This condition could be used to enforce $\mathcal{C}^1$ continuity and determine the position of the central control point. The control triangles at the corners are always co-planar since they are perpendicular to the normal at the node. The mid-edge control triangles are colored dark gray.

It is likely that the central control point will be located near the vertical line that runs through the barycenter of the triangle. To be more precise, let's use the barycenter of the 6 control points in the perimeter of the Bézier triangle and the line perpendicular to the flat triangle running through it. Then, let's compute the candidate position for the central control point corresponding to an edge ($\boldsymbol{p}^{0i}$), by intersecting this line with the plane perpendicular to the plane described by item 2 on page 51 and passing through the intermediate control points of the edge. The barycenter of these three candidate positions is taken as the position for the central control point.

$$\boldsymbol{p}^{123} = \frac{1}{3}\sum_{i=1}^{3}\boldsymbol{p}^{0i} \tag{5.17}$$

Thus, the central point of the net is obtained as an average of the three candidate points for this position. Each of the three candidate points is computed solving a system of the form:

$$\boldsymbol{A}_{\boldsymbol{p}}^{0i} \cdot \boldsymbol{p}^{0i} = \boldsymbol{b}_{\boldsymbol{p}}^{0i} \tag{5.18}$$

The definition of $\boldsymbol{A}_{\boldsymbol{p}}^{0i}$ and $\boldsymbol{b}_{\boldsymbol{p}}^{0i}$ is given by equation (5.19). This is an analogous procedure to the one followed for the control points of the contour. So the intersection of three planes is solved:

1. A plane perpendicular to the one described by item 2 on page 51. This is a symmetric condition and thus the same plane will be used for adjacent triangles.

2. A plane perpendicular to one of the edges of the flat triangle and passing through the barycenter of the 6 control points of the perimeter.

3. And a plane perpendicular to another edge of the flat triangle and passing through the barycenter of the 6 control points of the perimeter.

$$\underbrace{\begin{bmatrix} \left[\boldsymbol{n}^{jk} \times (\boldsymbol{p}^{jk} - \boldsymbol{p}^{kj})\right] \times (\boldsymbol{p}^{jk} - \boldsymbol{p}^{kj}) \\ (\boldsymbol{x}^i - \boldsymbol{x}^j)^T \\ (\boldsymbol{x}^i - \boldsymbol{x}^k)^T \end{bmatrix}}_{\boldsymbol{A}_{\boldsymbol{p}}^{0i}} \cdot \boldsymbol{p}^{0i} =$$

$$= \underbrace{\begin{bmatrix} \left\{\left[\boldsymbol{n}^{jk} \times (\boldsymbol{p}^{jk} - \boldsymbol{p}^{kj})\right] \times (\boldsymbol{p}^{jk} - \boldsymbol{p}^{kj})\right\} \cdot \boldsymbol{p}^{jk} \\ (\boldsymbol{x}^i - \boldsymbol{x}^j) \cdot \frac{1}{6}(\boldsymbol{p}^{ij} + \boldsymbol{p}^{ji} + \boldsymbol{p}^{ik} + \boldsymbol{p}^{ki} + \boldsymbol{p}^{jk} + \boldsymbol{p}^{kj}) \\ (\boldsymbol{x}^i - \boldsymbol{x}^k) \cdot \frac{1}{6}(\boldsymbol{p}^{ij} + \boldsymbol{p}^{ji} + \boldsymbol{p}^{ik} + \boldsymbol{p}^{ki} + \boldsymbol{p}^{jk} + \boldsymbol{p}^{kj}) \end{bmatrix}}_{\boldsymbol{b}_{\boldsymbol{p}}^{0i}}$$

$$\forall i = 1 \div 3, (j,k) = combination\{1,2,3\} - \{i\} \quad (5.19)$$

Where $\boldsymbol{n}^{jk}$ refers to the average of the normals $\boldsymbol{n}^j$ and $\boldsymbol{n}^k$.

$$\boldsymbol{n}^{jk} = \frac{\boldsymbol{n}^j + \boldsymbol{n}^k}{2} \quad (5.20)$$

The resulting system of equations above is well posed, and thus a robust method to compute the central control point. Constructing the central control point in this way does not ensure $\mathcal{C}^1$ continuity, but comes close enough. In any case, neighboring triangles are $\mathcal{C}^1$ continuous at the nodes, but not—in general—along the edges.

## 5.4 Determining shape through energy minimization

As reported in [132] by Ubach and Oñate, the construction of the Bézier triangle did not account initially for energy aspects. Some arbitrary decisions were adopted in that work. For example, fixing the boundaries of the triangle to lie in a plane causes the boundaries to be planar curves. Clearly, this does not exploit all the potential of a cubic formulation. This aspect will be treated by the author in section 9.2.

There are, though, two relevant differences between the constructions reported in section 5.3 and in [132]. The first difference is the distance at which the plane specified by item 3 on page 51 is located. The second one is the decision to use the barycenter of the 6 contour control points instead of the triangle's barycenter as the reference to locate the central control point.

Concerning the first case, Ubach and Oñate stated that the value $\Psi = \frac{1}{3}$ was applied always. No issues were detected using this constraint when solving linear problems. A lack of precision was identified, though, for what should be expected in a cubic triangle. Consequently Ubach and Oñate did specify in [132, Section 5. Conclusions]:

> We need to improve the capability of the element to represent constant curvatures not only in the limit of the element's size becoming zero, but for the more general case.

At that time the author was working behind the idea of making the value of the parameter $\Psi$ depend on the angle $\varphi$ between the edge's chord and the tangent of the curved boundary at the vertex.—The definition of $\varphi$ is given in figure 5.7.—The aim was to create boundary curves of approximately constant curvature.

This thinking changed when the author tried to use the construction in [132] to solve non-linear problems. The element formulated in that way was incapable of converging to any solution. This posed a great challenge. The author struggled for several months trying to find the root cause of the problem. A full revision of the code was undertaken to make sure no bugs were present in the software code. And a thorough verification of every derivative was performed numerically. Finally the author got a hint at the problem when performing trials with different numerical quadratures. The element seemed to exhibit a somewhat better convergence behavior (never converging totally) when only one quadrature point was used at the center of the element. This was a very bizarre behavior. So something had to be going on regarding the geometry of the element in the points located far from the center. The author's suspicion was that the decision to assign a value of $\frac{1}{3}$ to the parameter $\Psi$ was playing a role. Furthermore, the fact that even using a Newton-Raphson nonlinear solving scheme it was impossible to obtain convergence, made the author suspect that the space of solutions created did not include the solution to the problem.

Let's go deeper into this idea for a second. In the Finite Element Method, the continuous domain is modeled by a discrete domain. Therefore, the space of solutions generated by the mesh of finite elements is a reduced version of the space in which the solution for the continuous problem lies. Furthermore, by including arbitrary constrains to the construction of the Bézier triangle, we had not checked for the existence of the solution in the constrained space of finite elements we had generated. Indeed, by constraining the geometric construction of the element with the arbitrary decision of placing the dark grayed plane in figure 5.5 at $\frac{1}{3}$ of the edge's chordal length, we were modifying the shape of the deformed triangle away from the solution that minimizes the deformation energy with respect to the nodal forces. So it was as if we were imposing virtual forces and/or moments in the interior of the element. These virtual forces and moments did not belong to the discrete model of the problem and therefore it was impossible for the element to obtain a converged solution. To put it in another way, the non-linear problem was not well-posed.

It was at this point that the author acknowledged the need to take into account the energy associated with the deformation of the element

if the element had to solve non-linear problems. In particular, in order to obtain the conditions to determine the location of the Bézier control points, those conditions which cannot be determined via geometric considerations, should be obtained considering an energy minimization problem.

### 5.4.1 Reduction of the problem

In order to tackle the energy minimization problem associated to the value of $\Psi$ (i.e. the location of the dark grayed plane in figure 5.5), the author had to simplify the general 3D problem to something more manageable. The general problem can be solved with optimization algorithms. However this approach has two drawbacks. On the one side, optimization algorithms are computationally expensive. On the other side, they do not provide information on the derivatives of the solution, which are needed to solve the non-linear problem. Since the general 3D solution cannot be obtained analytically, the author performed a reduction of the problem in order to obtain an analytic solution that could be used to approximate the general solution.

First, instead of finding an analytic solution concerning the whole triangle, only the edge of the triangle was considered. So that the bending and membrane deformation energies of the triangle were assimilated to the bending and axial (membrane) deformation energies of a 2D line (Bernoulli beam). Having previously considered that the edges of the triangle were flat curves came in handy.

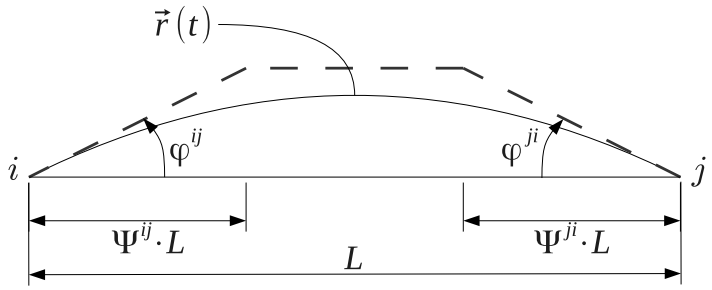


Figure 5.7: Representation of the 2D problem simplification. The edge of the triangle between nodes $i$ and $j$ is represented as a flat curve defined by the parametrization $\vec{r}(t)$. The angle $\varphi^{ij}$ is defined here for flat curved edges. For the more general case of 3D curved edges, refer to the definitions provided in figure 9.3 and equation (9.18) on page 105 and on page 113.

Second, the problem of minimizing the total energy was split into the two separate problems: minimization of the energy associated to bending deformation; and minimization of the energy associated to axial (membrane) deformation. We know from the works of Chapelle and Bathe [22] and Briassoulis [15–17], that the asymptotic behavior of shell structures as their thickness tends to zero can be membrane dominant, shell dominant, or mixed; depending on the geometry, the loads and the boundary

conditions. Therefore, by considering the two energy modes separately we create the opportunity for taking into account the different combinations of bending energy and membrane energy modes in our study.

Clearly, by simplifying the problem it is impossible to account for every particular case and for the different material properties and distributions in the shell. Nevertheless, the solutions provided are only local and therefore they do not reduce the validity of the discretization strategy using the FEM. On the other hand, by taking into account separately the bending and axial (membrane) energy, we are effectively decoupling the effect that layered composite materials could have on the ratio of these energies in the shell laminate. Finally, by changing the overall minimization problem into the analysis of a reduced problem, we have to carefully analyze and *adjust*, not minimize, the deformation energy of the shell.[4] It is the author's conviction that this approach yields a sufficiently good approximation for every particular case.

### Bending energy

The problem of bending energy minimization (adjustment) was the easiest of the two and was tackled first. The study started by acknowledging that a necessary condition for the absence of any virtual moments along the 2D curve of the edge was that the resulting shape of the curve shall be a spiral. That is, a 2D beam with only endpoint moments has a law of moments which varies monotonically (strictly speaking the law of moments varies linearly in the absence of axial forces). Considering that the effect of moments induced by axial forces should not affect the monotonicity of the law of moments if the shell is shallow enough, this condition is accepted.

Since for a 2D Bernoulli beam the curvature at any point is proportional to the bending moment, a monotonic law of bending moments results in a monotonic law of curvatures along the beam. Therefore, the construction of the cubic Bézier curve shall result in all cases in a spiral. Figure 5.8 shows in red the region of pairs of angles at the endpoints of a 2D cubic Bézier curve for which spirals are obtained fixing the value $\Psi = \frac{1}{3}$.

At this point the author implemented the idea of improving the capability of the element to represent constant curvatures. The idea was that the analytic solution of the value of $\Psi$ for representing constant curvatures was a better approximation than fixing this value to $\frac{1}{3}$; and thus a solution candidate. This value is found for a symmetric curve (the start and end point angles are the same) by forcing the center point of the cubic Bézier spline to coincide with the circular arc spanning the same chord with the same start and endpoint tangents. The value of $\Psi$ that satisfies this condition for any given angle $\varphi$ is specified in equation (5.21).

$$\Psi^{ij}_{\varphi}(\varphi^{ij}) = \frac{1}{3} \cdot \frac{2 \cdot \cos \varphi^{ij}}{1 + \cos \varphi^{ij}} \tag{5.21}$$

[4]The author is knowledgeable of the bad press for *adjustments* in the FEM literature. Fear not. The process followed is fully rigorous and maintains the objective of minimizing the overall deformation energy. However, taking into account compatibility considerations, this problem is converted into a locally-defined energy-adjustment problem.

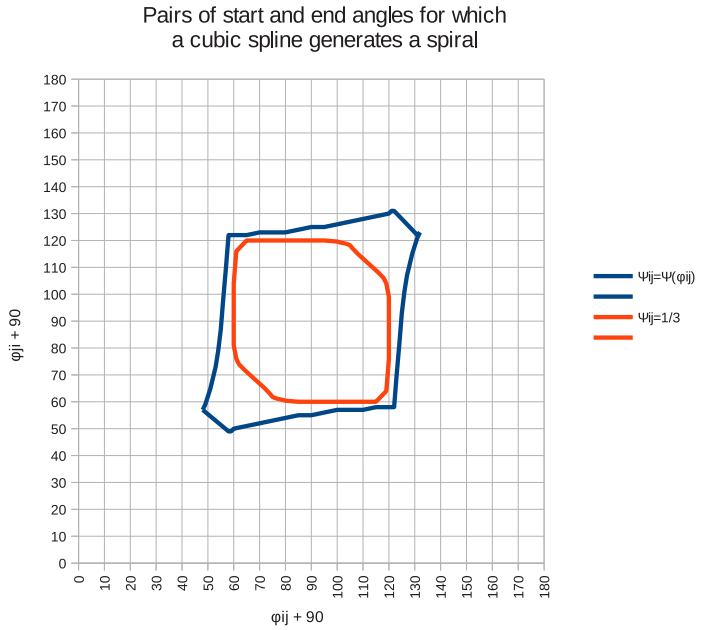


(a)

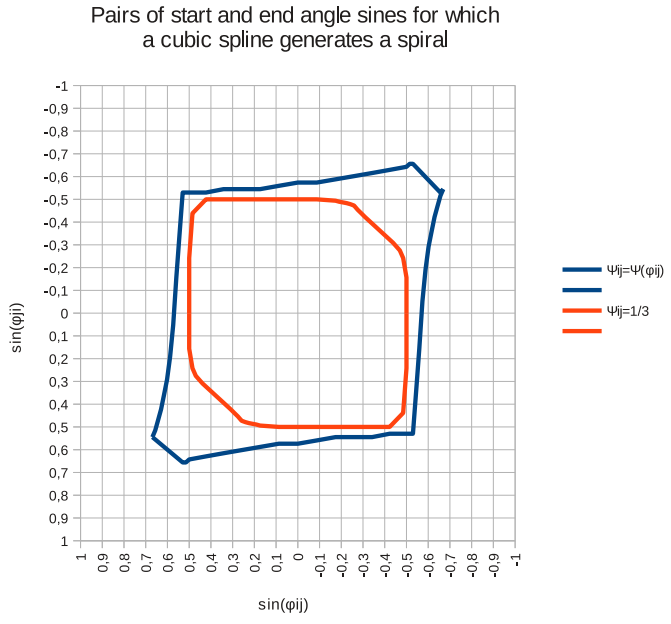


(b)

Figure 5.8: Regions of start and endpoint angles of a cubic spline for which spirals are generated. The red line indicates the region corresponding to a construction of the cubic Bézier spline using $\Psi = \frac{1}{3}$. The blue line indicates the region corresponding to a construction of the cubic Bézier spline using equation (5.21). (a) Variables in the axis expressed in terms of the angle of the normal with respect to the chord. (b) Variables in the axis expressed in terms of the sinus of the angles represented in (a).

With this formula we are ensuring to comply with the patch test and therefore to satisfy the accurate representation of constant curvatures. How about non-symmetric curves? Figure 5.8 shows in blue the the region of pairs of angles at the endpoints of a 2D cubic Bézier curve for which spirals are obtained plugging the value of $\Psi^{ij}_{\varphi}$ of equation (5.21) into equation (5.15). The improvement is clear in all the quadrants of the domain. The improvement is more significant when the sign of the curvature doesn't change than when the sign of the curvature does change.

Taking into account this result, the author considers that equation (5.21) constitutes a good approximate solution for the minimization of the bending energy. Furthermore, this is a very simple equation that is easy to differentiate and thus does not add extra complexity to the problem.

**Axial (membrane) energy**

While the bending problem was the easiest to solve, the membrane energy problem is the least evident or intuitive to lay out. Following the same simplification procedure explained in section 5.4.1 on page 56, the author developed a thorough analytic solution for this reduced problem. The complete development can be followed in appendix C.

The key aspect of this development is to understand that we are not so interested in minimizing the total strain energy as in minimizing the variation of the density of strain energy along the beam. The main reason that justifies this approach is that, in order to satisfy the patch test, the element has to be able to represent constant states of deformation. Therefore, we are interested in designing an element which represents constant states of deformation and thus letting the energy be what it ought to be.

Let's make an analogy: the analogy shall be between the axial strain of the Bernoulli beam and the celerity ($c$) of the curve parameter ($t$). Let,

$$\vec{r}(t) = (x(t), y(t)) \tag{5.22}$$

be the equation of a parametric curve in the Cartesian coordinates $(x, y)$. $\vec{r}(t)$ represents the generatrix of the 2D Bernoulli beam. Then, $c$ is defined as:

$$\vec{r}'(t) = \frac{\partial \vec{r}(t)}{\partial t} \tag{5.23}$$

$$c = \|\vec{r}'(t)\| \tag{5.24}$$

Following this analogy, the density of axial deformation energy is proportional to $c^2$. Then, we are interested in finding the values of $\Psi$ which minimize the variation of $c^2$ along the curve. In equation (5.25) we take the square of the value to minimize in order to avoid the effect of the sign.

$$\left.\begin{aligned} \frac{\partial}{\partial \Psi^{ij}} \int_0^1 \left(\frac{\partial c^2}{\partial t}\right)^2 dt = 0 \\ \frac{\partial}{\partial \Psi^{ji}} \int_0^1 \left(\frac{\partial c^2}{\partial t}\right)^2 dt = 0 \end{aligned}\right\} \tag{5.25}$$

The system in equation (5.25) is a system of 2 cubic equations, with two unknowns: $\Psi^{ij}$ and $\Psi^{ji}$; and taking the angles $\varphi^{ij}$ and $\varphi^{ji}$ as variables (see

appendix C). The author has programmed this system of equations into the Maple® symbolic manipulation software. The analytic solution obtained by Maple® has over 1 million characters. This makes it almost impossible to verify and very hard to program efficiently. But most importantly, its evaluation would be very costly computationally.

Since the analytic solution is incomprehensible, the author sought a graphical solution of the problem. Each of the two equations in equation (5.25) represents a 2D curve in the coordinate space $(\Psi^{ij}, \Psi^{ji})$. Therefore, the intersection of these two curves is the solution of the problem. The author plotted these intersections using Maple® for different pairs of angles $(\varphi^{ij}, \varphi^{ji})$. The results are shown in figure 5.9.

Figure 5.9 deserves some comments. First of all, the reader must notice how close the solution provided by $\Psi_\varphi$ in equation (5.21) is to the symmetric cases, even for values of $\varphi$ up to 27°. This is a very encouraging result, because it opens the door to use a very simple and uncoupled expression (equation (5.21)), and obtain a good approximation of a very complex and coupled equation (equation (5.25)). Secondly, the reader can also observe that the exact solution exhibits strong coupling for the non-symmetric cases. This limits effectively the applicability of the approximation provided by $\Psi_\varphi$ to small values of $\varphi$ where the coupling effect is not so severe. Combining both observations, the author concludes that the formula provided by equation (5.21) can be used to solve also the membrane energy aspects of the element as long as the values of $\varphi$ do not exceed 18°. This is consistent and well within the limits of the validity of the formula regarding the construction of spirals shown in figure 5.8. After all 18° is not so small, as it allows an element to confidently span an arc of up to 36°; which is very interesting.

### 5.4.2 Location of the central control point

The decision to locate the central control point near the the barycenter of the 6 control points of the contour also responds to an energy minimization criterion. However in this case the reasoning is heuristic. The author observed that the solution for both the bending and axial energy minimization problems in the 2D Bernoulli beam tends to make Bézier splines which have control segments of similar length. That is, the higher the value of $\varphi$, the smaller the corresponding value of $\Psi_\varphi$, to compensate for the extra length of the control path. Also, by understanding the parametric construction of a Bézier curve and a Bézier triangle that is well analyzed in the analogy used to pose equation (5.25), the author gains this heuristic knowledge that having the control points equally spaced favors a correct distribution of the deformation energy density.

This is why the author decides to position the central control point in a line that passes through the barycenter of the 6 contour control points. A more sophisticated approach would have been to compute the plane that minimizes the square distances to the 6 contour control points and position the central control point in the line perpendicular to that plane and that passes through the barycenter of these 6 control points. Instead, the author selects another line far easier to compute which is the line perpendicular to the flat shape of the triangle.

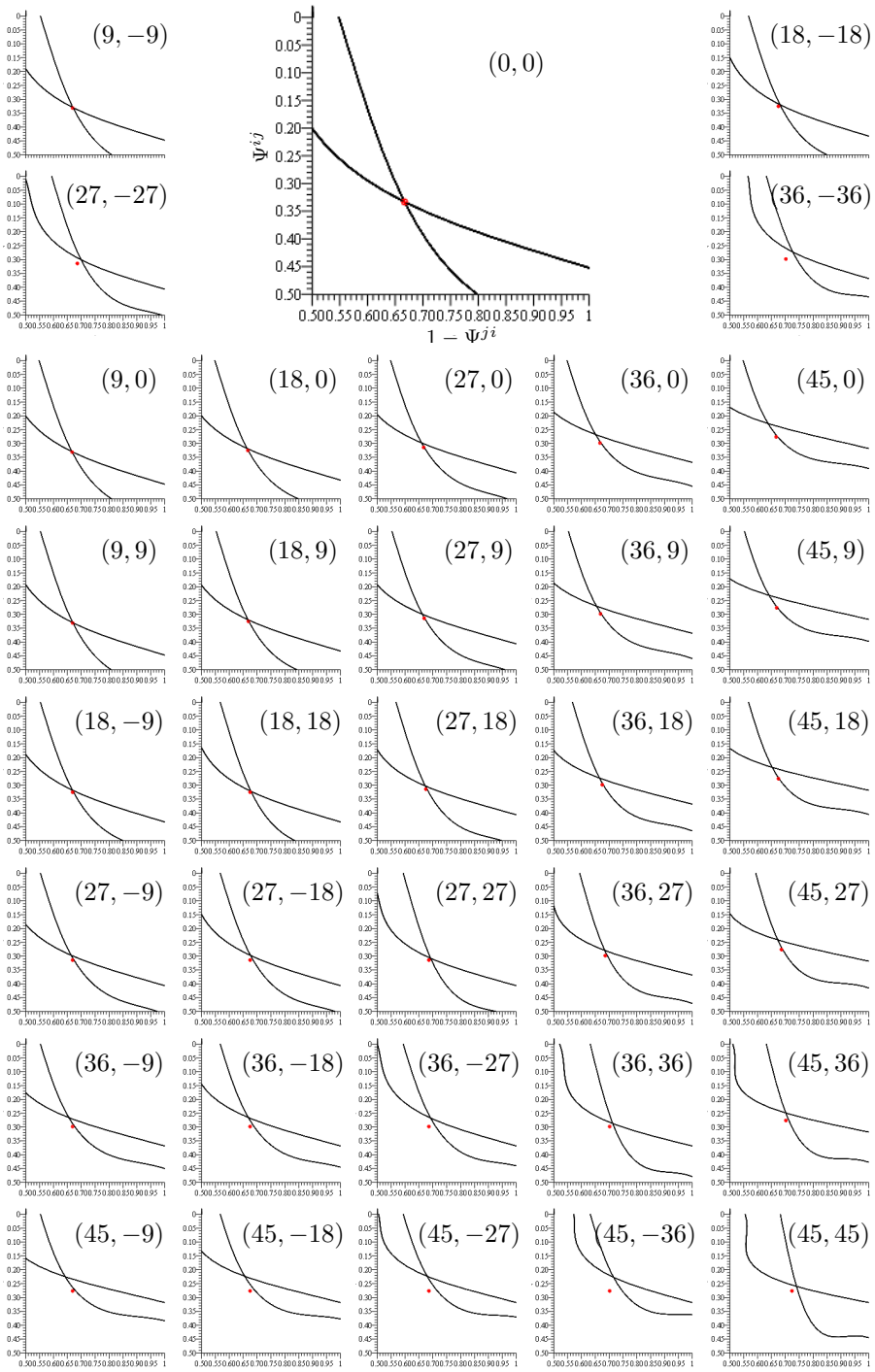


Figure 5.9: Graphical solution of equation (5.25). Each plot solves the system of equations for a given pair of angles $(\varphi^{ij}, \varphi^{ji})$ indicated at the top right corner of each plot. The vertical axis represents the value of $\Psi^{ij}$ and it varies from $0$ at the top and $0.5$ at the bottom. The horizontal axis represents the value of $1 - \Psi^{ji}$, taking values between $0.5$ and $1$. The two black curves represent each of the two expressions in equation (5.25). So their intersection is the exact solution of the system. The red dot in each plot represents the values of $\Psi^{ij}$ and $\Psi^{ji}$ obtained using equation (5.21).

## 5.5 Summary

The process of geometric construction of the cubic Bézier triangle has been presented. First, the need for obtaining accurate normals at the nodes is explained and the best averaging weights have been obtained for a very wide variety of surfaces. This is an original contribution of this thesis.

The shape functions based on the Bernstein polynomials for a cubic triangle have been presented. These shape functions offer very attractive properties like the variation-diminishing property and the monotone-variation property that IGA enjoys and exploits. The reader is encouraged to consult the references for a thorough understanding of the properties of this polynomial basis.

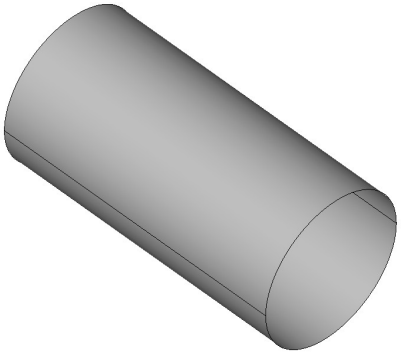

(a) Geometry of a cylinder.

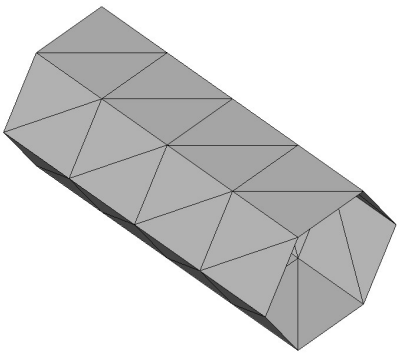

(b) Coarse mesh used to discretize a cylinder.

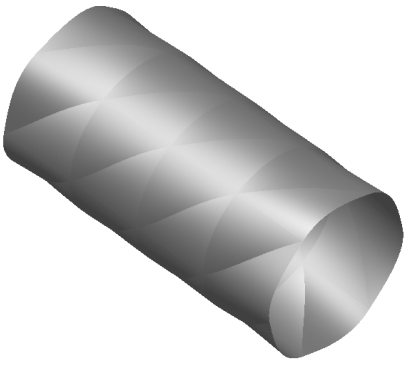

(c) Geometric representation of the BEST elements obtained from the coarse mesh (left) to discretize the cylinder.

Figure 5.10: Example of the enhancement provided by the procedure presented in this chapter to model the geometry obtained from a mesh of linear triangles. The BEST mesh (c) has the same degrees of freedom as the linear mesh (b).

Taking into account these shape functions the geometric construction of the cubic Bézier triangle is performed; control point per control point. First, the corners. Then, the contour. And finally the central control point.

The construction presented is $\mathcal{C}^1$ continuous at the nodes. Following these geometric rules the author has developed a new way to describe a *cubic* triangle using only *linear* unknowns corresponding to the coordinates of the vertices of the triangle. The coordinates of the control points are determined taking into account the coordinates of the neighboring triangles' vertices. This geometric construction for a cubic shell triangle is an original contribution of this thesis.

In order to obtain non-linear convergence, a detailed energy minimization analysis is performed on the geometric construction of the cubic Bézier triangle. The study is performed after a reduction of the dimensional complexity of the problem from 3D to 2D, and uncoupling the bending and membrane energy modes of the shell. This study concludes the determination of the remaining parameters that could not be determined through geometric conditions alone. Using the simple formula (see equation (5.21)) obtained in this study, the author has achieved excellent non-linear convergence in all cases. This analysis is an original contribution of this thesis.

Owing to the construction process followed to create this new finite element, the author decided to name it Bézier-Enhanced Shell Triangle (BEST). Figure 5.10 provides an example showing how using the Bézier enhancement process affects the geometric representation of a curved shell. Taking into account the number of original contributions included in this chapter, the reader will understand that this is a central chapter of the thesis.

# Chapter 6

# Implementation of a continuum-based formulation for the Bézier-enhanced shell triangle

USING THE BÉZIER TRIANGLES DESCRIBED in sections 5.1 to 5.4 we can now develop a conforming formulation based on the continuum-based approach. Continuum-based shell formulations—a term proposed by Stanley [120]—have become popular because of their simplicity. General curved shell theories are complex and difficult to implement, while a continuum-based framework benefits from the general 3D continuum theory of elasticity. There are a number of frameworks that differ in name, but different scholars group them together [9, p. 536][12, p. 76]. This is the case of the *degenerated solid approach*, first proposed by Ahmad, Irons and Zienkiewicz [2], and that of the *geometrically exact shell model* [118]. The author shares the preference stated by Belytschko et al. [9] and refers to this as the *continuum-based* approach.

The formulation here presented is based on the same principles already applied in section 4.3. Here we will develop them further. The author proposes the use of Green-Lagrangian strains and Cauchy stresses[1] instead of generalized strains and generalized stresses because the former are better suited to evaluate the state of strain and stress of the material. In the case of a laminated shell, each layer will be subject to different stress states and evaluating these values at each layer allows to evaluate failure of the structure in a more precise manner than using generalized stresses and strains (for example in the case of evaluating principal strains and stresses and comparing their directions to the directions of the material fibers), which only provide information on the pre-integrated section characteristics and thus cannot account for all the cases. Having said that, the author has applied an efficient and geometrically accurate[2] pre-integration

[1] Cauchy stresses are suggested for engineering analysis. The development presented uses the second Piola-Kirchhoff stress tensor for the computation of elastic energy, since this is the conjugate of the Green-Lagrange strain tensor.

[2] Notice the difference in terminology with respect to the *geometrically exact* term coined

scheme in order to avoid extra computations associated to the volume integrals.

## 6.1 Thickness change due to the Poisson effect and the mild taper assumption

The mild taper assumption for the shell thickness is adopted. This assumption implies that in the case of a shell with varying thickness, where the curvilinear coordinate $\zeta$ in the normal direction changes orientation to adapt to each layer of the shell, it is assumed that its direction remains constant through the thickness and coincident with the normal vector to the midsurface (see figure 6.1). The mild taper assumption is expressed mathematically in equation (6.1). In the case of a shell with steeply varying thickness, this will be considered by changing the nominal thickness from element to element. The mesh can be adaptively refined if necessary.

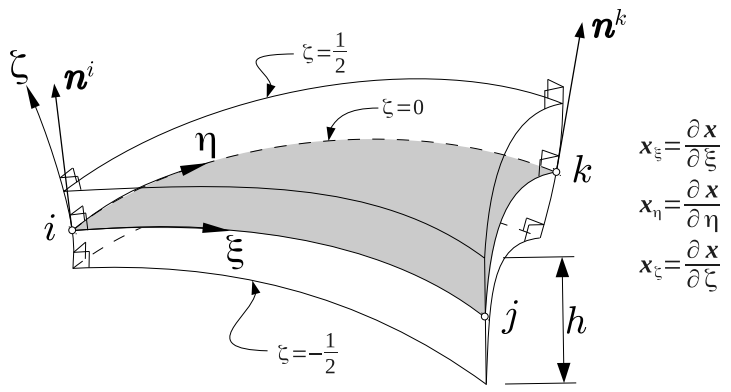


Figure 6.1: Representation of the curved shell element identifying the curvilinear coordinates ($\xi$, $\eta$, $\zeta$) and the effect of the mild taper assumption. The reference midsurface is identified.

$$\boldsymbol{x}_{,\zeta}\,(\xi,\eta,\zeta) = \frac{\partial \boldsymbol{x}}{\partial \zeta} \simeq \left.\frac{\partial \boldsymbol{x}}{\partial \zeta}\right|_{\zeta=0} = \frac{\partial \bar{\boldsymbol{x}}}{\partial \zeta} \parallel \boldsymbol{n}(\xi,\eta) \quad \Rightarrow \quad \boldsymbol{x}_{,\zeta}\,(\xi,\eta,\zeta) \simeq \parallel \boldsymbol{n}(\xi,\eta) \tag{6.1}$$

However, thickness change is considered accounting for the Poisson effect. This does not imply that the zero vertical stress assumption is eliminated. The author wants to include the effect that stretching in the shell's surface has on the thickness of the shell. The classical Kirchhoff-Love kinematic hypotheses have been stated in section 3.2.2 on page 22. We will drop the first one and keep the other two. But unlike other authors that propose 6 and 7 parameter models to account for the full three-dimensional stress state of the shell, the author will simply allow that

$$\varepsilon_3 \neq 0 \tag{6.2}$$

by Simo and Fox in [118].

but maintaining a plane stress state of the material:

$$\sigma_3 = 0 \tag{6.3}$$

By allowing this stretching effect that can affect some thin shells made of hyper-elastic materials due to the Poisson effect, the author increases the range of applicability of the formulation to some particular thin-shell structures like balloons.

Let's thus define the plane stress state constitutive tensor of a linear elastic orthotropic material:

$$\begin{bmatrix} S'_{11} \\ S'_{22} \\ S'_{12} \end{bmatrix} = \underbrace{\frac{1}{1-\nu_{12}\cdot\nu_{21}} \begin{bmatrix} E_1 & \nu_{12}\cdot E_1 & 0 \\ \nu_{21}\cdot E_2 & E_2 & 0 \\ 0 & 0 & (1-\nu_{12}\cdot\nu_{21})\cdot G_{12} \end{bmatrix}}_{\boldsymbol{D}} \cdot \begin{bmatrix} \varepsilon_1 \\ \varepsilon_2 \\ \gamma_{12} \end{bmatrix} \tag{6.4}$$

$$\frac{1}{G_{12}} \simeq \frac{1+\nu_{21}}{E_1} + \frac{1+\nu_{12}}{E_2} \tag{6.5}$$

$$\boldsymbol{E}' = \begin{bmatrix} E'_{11} \\ E'_{22} \\ E'_{12}+E'_{21} \end{bmatrix} = \begin{bmatrix} \varepsilon_1 \\ \varepsilon_2 \\ \gamma_{12} \end{bmatrix} \tag{6.6}$$

$$\varepsilon_3 = -\frac{\nu_{31}\cdot S'_{11} + \nu_{32}\cdot S'_{22}}{E_3} \tag{6.7}$$

$$\lambda = 1 + \varepsilon_3 \tag{6.8}$$

Where $E_1$ and $E_2$, $\nu_{12}$ and $\nu_{21}$, and $G_{12}$ are respectively the Young moduli, the Poisson ratios and the shear modulus of the material in the principal directions of the plane; and $E_3$, $\nu_{31}$ and $\nu_{32}$ are respectively the Young modulus and Poisson ratios associated with the principal direction orthogonal to the plane.

The value of $\lambda$—evaluated after each time-step—can be used to update the thickness of the material.[3] Thus, the total thickness in the deformed configuration will be simply expressed as:

$$\sum_{l=1}^{\sharp\text{layers}} \lambda_l h_l \tag{6.9}$$

Where $h$ is the thickness of the material in the reference configuration.

## 6.2 Definition of local axes

Since the original mesh is defined with linear triangles, the local axes used to define the principal directions of the material $\boldsymbol{e}'_1$ and $\boldsymbol{e}'_2$ are uniform

[3]Notice that combined with equation (6.7) and equation (4.16), equation (6.8) defines an implicit second order equation for $\lambda$. The solution to this equation includes a fraction and a square root with terms that belong to the reference configuration and the deformed configuration and cannot be factored. As a result, the expression of $\lambda$ cannot be linearized like all the other terms. This is why it is much more effective and efficient to evaluate $\lambda$ explicitly instead of implicitly.

over the surface of the flat triangle (see figure 6.2). Therefore a rotation is needed to obtain the material local axes $\boldsymbol{t}_1$ and $\boldsymbol{t}_2$. To that end, the author uses the normal vectors $\hat{\boldsymbol{y}}$ and $\boldsymbol{t}_3$. The rotation vector and the rotation angle are defined as follows:

$$\boldsymbol{\omega} = \frac{\hat{\boldsymbol{y}} \times \boldsymbol{t}_3}{\|\hat{\boldsymbol{y}} \times \boldsymbol{t}_3\|} \tag{6.10}$$

$$\alpha = \arcsin\|\hat{\boldsymbol{y}} \times \boldsymbol{t}_3\| \tag{6.11}$$

where $\boldsymbol{t}_3$ has been defined in equation (5.13) on page 49, and

$$\hat{\boldsymbol{y}} = \frac{(\boldsymbol{X}^j - \boldsymbol{X}^i) \times (\boldsymbol{X}^k - \boldsymbol{X}^i)}{\|(\boldsymbol{X}^j - \boldsymbol{X}^i) \times (\boldsymbol{X}^k - \boldsymbol{X}^i)\|} \tag{6.12}$$

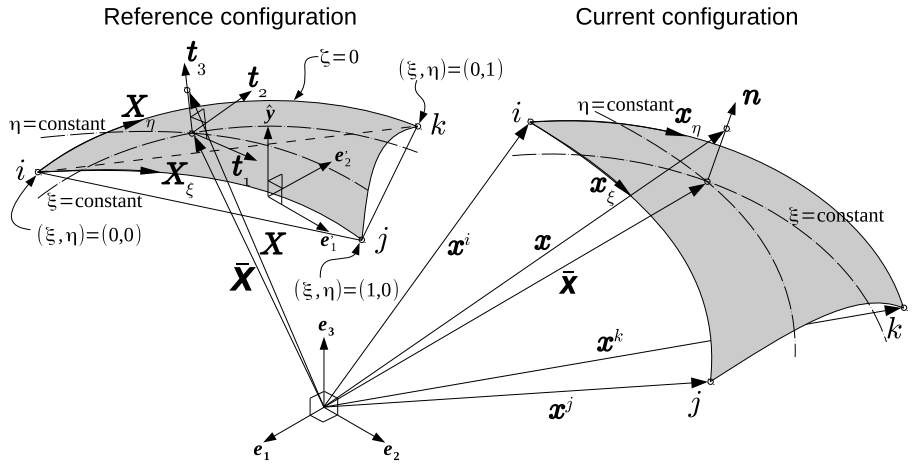


Figure 6.2: A set of orthogonal local axes $(\boldsymbol{t}_1, \boldsymbol{t}_2, \boldsymbol{t}_3)$ is defined in the reference configuration in order to establish the principal directions of the material over the curved surface of the element. The user defines the material local axes $(\boldsymbol{e}'_1, \boldsymbol{e}'_2, \hat{\boldsymbol{y}})$ on the flat triangle geometry. The vector $\boldsymbol{t}_3$ is defined in the same way as $\boldsymbol{n}$ in the current configuration.

Then, using the Rodrigues formula, we can easily compute the other two local vectors on the curved surface. Let $\boldsymbol{R}$ be the rotation matrix defined by the vector $\boldsymbol{\omega}$ and the angle $\alpha$.

$$\boldsymbol{R}(\boldsymbol{\omega}, \alpha) = \cos\alpha \cdot (\boldsymbol{I} - \boldsymbol{\omega} \otimes \boldsymbol{\omega}) + (\boldsymbol{\omega} \otimes \boldsymbol{\omega}) + \sin\alpha \cdot e_{ijk}\omega_j \tag{6.13}$$

Where $e_{ijk}$ stands for the permutation tensor. Then,

$$\boldsymbol{t}_1(\xi, \eta) = \boldsymbol{R} \cdot \boldsymbol{e}'_1 \tag{6.14}$$

$$\boldsymbol{t}_2(\xi, \eta) = \boldsymbol{R} \cdot \boldsymbol{e}'_2 \tag{6.15}$$

and the matrix of change of coordinates from local axes to global axes is

$$\boldsymbol{T} = [\boldsymbol{t}_1\ \boldsymbol{t}_2\ \boldsymbol{t}_3] \tag{6.16}$$

## 6.3 Description of the deformation

In this section the equations and concepts from section 4.3 will be adapted to the Bézier description of the triangle. A point with parametric coordinates ($\xi$,$\eta$,$\zeta$) in the element has the global coordinates given by the position of the midsurface and the orientation of the normal vector to the midsurface.

$$\boldsymbol{x}(\xi,\eta,\zeta) = \bar{\boldsymbol{x}}(\xi,\eta) + \lambda\, h\, \zeta\, \boldsymbol{n}(\xi,\eta) = \boldsymbol{p}\cdot\boldsymbol{N} + \lambda\, h\, \zeta\, \boldsymbol{n} \tag{6.17}$$

$$\boldsymbol{X}(\xi,\eta,\zeta) = \bar{\boldsymbol{X}}(\xi,\eta) + h\, \zeta\, \boldsymbol{\mathcal{N}}(\xi,\eta) = \boldsymbol{P}\cdot\boldsymbol{N} + h\, \zeta\, \boldsymbol{\mathcal{N}} \tag{6.18}$$

Equations (4.9) to (4.13) remain unchanged. Let's develop the expression for the components of equation (4.12).

$$\frac{\partial \boldsymbol{x}}{\partial \xi} = \boldsymbol{p}\cdot\boldsymbol{L}_\xi + \lambda\, h\, \zeta\, \boldsymbol{n}_{,\xi} \tag{6.19}$$

$$\frac{\partial \boldsymbol{x}}{\partial \eta} = \boldsymbol{p}\cdot\boldsymbol{L}_\eta + \lambda\, h\, \zeta\, \boldsymbol{n}_{,\eta} \tag{6.20}$$

$$\frac{\partial \boldsymbol{x}}{\partial \zeta} = \lambda\, h\, \boldsymbol{n} \tag{6.21}$$

where

$$\boldsymbol{n}_{,\xi} = \frac{\partial \boldsymbol{n}}{\partial \xi} = \frac{(\boldsymbol{p}\cdot\boldsymbol{L}_{\xi,\xi})\times(\boldsymbol{p}\cdot\boldsymbol{L}_\eta) + (\boldsymbol{p}\cdot\boldsymbol{L}_\xi)\times(\boldsymbol{p}\cdot\boldsymbol{L}_{\eta,\xi})}{\|(\boldsymbol{p}\cdot\boldsymbol{L}_\xi)\times(\boldsymbol{p}\cdot\boldsymbol{L}_\eta)\|}\cdot(\boldsymbol{I}-\boldsymbol{n}\otimes\boldsymbol{n}) \tag{6.22}$$

$$\boldsymbol{n}_{,\eta} = \frac{\partial \boldsymbol{n}}{\partial \eta} = \frac{(\boldsymbol{p}\cdot\boldsymbol{L}_{\xi,\eta})\times(\boldsymbol{p}\cdot\boldsymbol{L}_\eta) + (\boldsymbol{p}\cdot\boldsymbol{L}_\xi)\times(\boldsymbol{p}\cdot\boldsymbol{L}_{\eta,\eta})}{\|(\boldsymbol{p}\cdot\boldsymbol{L}_\xi)\times(\boldsymbol{p}\cdot\boldsymbol{L}_\eta)\|}\cdot(\boldsymbol{I}-\boldsymbol{n}\otimes\boldsymbol{n}) \tag{6.23}$$

Following the thought expressed in footnote 3 on page 67, the value of $\lambda$ has been considered constant throughout the domain of the element. This is because it is very difficult to obtain a derivative expression of $\lambda$. But in addition, its value is expected to change very little; except for the step variations across the layers of the laminate. These can be taken into account when computing the stiffness matrix of the element (see chapter 7).

Most authors consider that the second order terms of the Green-Lagrange deformation tensor ($\boldsymbol{E}$) are negligible. It is evident that by making that assumption they are making an error that adds to all the other assumptions. The author intends to make as little assumptions as possible in order to reduce the errors in the modeling. Therefore, the second order terms will be fully considered. The author will show that in the current framework, doing so does not increase the complexity of the element. Let's recall the definition of some tensors:

$$\boldsymbol{J} = \left[\frac{\partial \boldsymbol{X}}{\partial \xi} \quad \frac{\partial \boldsymbol{X}}{\partial \eta} \quad \frac{\partial \boldsymbol{X}}{\partial \zeta}\right] \tag{6.24}$$

$$\boldsymbol{j} = \left[\frac{\partial \boldsymbol{x}}{\partial \xi} \quad \frac{\partial \boldsymbol{x}}{\partial \eta} \quad \frac{\partial \boldsymbol{x}}{\partial \zeta}\right] \tag{6.25}$$

$$\boldsymbol{F} = \frac{\partial \boldsymbol{x}}{\partial \boldsymbol{X}} = \boldsymbol{j}\cdot\boldsymbol{J}^{-1} \tag{6.26}$$

$$\boldsymbol{C} = \boldsymbol{F}^T\cdot\boldsymbol{F} = \left(\boldsymbol{j}\cdot\boldsymbol{J}^{-1}\right)^T\cdot\boldsymbol{j}\cdot\boldsymbol{J}^{-1} \tag{6.27}$$

$$\boldsymbol{E} = \frac{1}{2}\left(\boldsymbol{C} - \boldsymbol{I}\right) \tag{6.28}$$

$$\boldsymbol{E}' = \boldsymbol{T}^T \cdot \boldsymbol{E} \cdot \boldsymbol{T} \tag{6.29}$$

$$\boldsymbol{S}' = \boldsymbol{D} : \boldsymbol{E}' \tag{6.30}$$

Now, similarly to the procedure followed in section 4.3, let's define some useful tensors:

$$\boldsymbol{G} = \boldsymbol{J}^{-1} \tag{6.31}$$

$$\boldsymbol{A} = \boldsymbol{G} \cdot \boldsymbol{T} \tag{6.32}$$

$$\boldsymbol{g} = \boldsymbol{j}^T \cdot \boldsymbol{j} \tag{6.33}$$

Notice that $\boldsymbol{G}$ and $\boldsymbol{A}$ are defined in the reference configuration, while $\boldsymbol{g}$ is defined in the current configuration. Using these tensors we can rewrite equations (6.27) to (6.29):

$$\boldsymbol{C} = \boldsymbol{F}^T \cdot \boldsymbol{F} = \left(\boldsymbol{j} \cdot \boldsymbol{J}^{-1}\right)^T \cdot \boldsymbol{j} \cdot \boldsymbol{J}^{-1} = \boldsymbol{G}^T \cdot \boldsymbol{g} \cdot \boldsymbol{G} \tag{6.34}$$

$$\boldsymbol{E} = \frac{1}{2}\left(\boldsymbol{C} - \boldsymbol{I}\right) = \frac{1}{2}\left(\boldsymbol{G}^T \cdot \boldsymbol{g} \cdot \boldsymbol{G} - \boldsymbol{I}\right) \tag{6.35}$$

$$\boldsymbol{E}' = \boldsymbol{T}^T \cdot \boldsymbol{E} \cdot \boldsymbol{T} = \frac{1}{2}\left(\boldsymbol{T}^T \cdot \boldsymbol{G}^T \cdot \boldsymbol{g} \cdot \boldsymbol{G} \cdot \boldsymbol{T} - \boldsymbol{I}\right) = \frac{1}{2}\left(\boldsymbol{A}^T \cdot \boldsymbol{g} \cdot \boldsymbol{A} - \boldsymbol{I}\right) \tag{6.36}$$

The tensor $\boldsymbol{g}$ is a symmetric tensor. Furthermore, since

$$\boldsymbol{x}_{,\xi} \perp \boldsymbol{x}_{,\zeta} \text{ and } \boldsymbol{x}_{,\eta} \perp \boldsymbol{x}_{,\zeta} \Rightarrow g_{13} = g_{23} = g_{31} = g_{32} = 0 \tag{6.37}$$

then $\boldsymbol{g}$ is of the form

$$\boldsymbol{g} = \begin{bmatrix} g_{11} & g_{12} & 0 \\ & g_{22} & 0 \\ sym. & & g_{33} \end{bmatrix} \tag{6.38}$$

The components of $\boldsymbol{g}$ can be expressed in the following way:

$$g_{\alpha\beta} = \boldsymbol{L}_{\xi_\alpha}^T \cdot \boldsymbol{p}^T \cdot \boldsymbol{p} \cdot \boldsymbol{L}_{\xi_\beta} + \lambda\, h\, \zeta\, (\boldsymbol{L}_{\xi_\alpha}^T \cdot \boldsymbol{p}^T \cdot \boldsymbol{n}_{,\xi_\beta} + \boldsymbol{L}_{\xi_\beta}^T \cdot \boldsymbol{p}^T \cdot \boldsymbol{n}_{,\xi_\alpha}) + \lambda^2\, h^2\, \zeta^2\, \boldsymbol{n}_{,\xi_\alpha}^T \cdot \boldsymbol{n}_{,\xi_\beta} \quad \forall \alpha, \beta = 1 \div 2 \tag{6.39}$$

where

$$\boldsymbol{L}_{\xi_1} \equiv \boldsymbol{L}_\xi \qquad\qquad \boldsymbol{L}_{\xi_2} \equiv \boldsymbol{L}_\eta \tag{6.40}$$

and

$$\boldsymbol{n}_{,\xi_1} \equiv \boldsymbol{n}_{,\xi} \qquad\qquad \boldsymbol{n}_{,\xi_2} \equiv \boldsymbol{n}_{,\eta} \tag{6.41}$$

The explicit value of $g_{33}$ is not of interest because given the structure of $\boldsymbol{A}$ it is only meaningful towards the determination of $\varepsilon_3$. In fact, the value of $\varepsilon_3$ can only be obtained using equation (6.7), because it does not generate any work in the plane stress assumption.

## 6.4 Decomposition into thickness-independent tensors

This section provides the necessary proofs to decompose the tensors that govern the deformation of the shell element into sums of tensors that are constant in the thickness direction and which eventually may be affected by scalar components that provide the variation in the thickness direction. This is useful in order to subsequently pre-integrate through-the-thickness, which is invaluable in order to reduce the computational cost of the calculations.

It can be proved that $\boldsymbol{A}$ is of the form

$$\boldsymbol{A} = \begin{bmatrix} A_{11} & A_{12} & 0 \\ A_{21} & A_{22} & 0 \\ 0 & 0 & A_{33} \end{bmatrix} \tag{6.42}$$

Let's proceed with the demonstration. In order to analyze $\boldsymbol{A}$ we will use it's inverse $\boldsymbol{A}^{-1}$:

$$\begin{aligned} \boldsymbol{A}^{-1} &= (\boldsymbol{G}\cdot\boldsymbol{T})^{-1} = \boldsymbol{T}^{-1}\cdot\boldsymbol{G}^{-1} = \boldsymbol{T}^{T}\cdot\boldsymbol{J} = \\ &= \begin{pmatrix} \uparrow & \uparrow & \uparrow \\ \boldsymbol{t}_1 & \boldsymbol{t}_2 & \boldsymbol{t}_3 \\ \downarrow & \downarrow & \downarrow \end{pmatrix}^{T} \cdot \begin{pmatrix} \uparrow & \uparrow & \uparrow \\ \boldsymbol{P}\cdot\boldsymbol{L}_\xi + h\zeta\boldsymbol{\mathcal{N}}_{,\xi} & \boldsymbol{P}\cdot\boldsymbol{L}_\eta + h\zeta\boldsymbol{\mathcal{N}}_{,\eta} & h\,\boldsymbol{t}_3 \\ \downarrow & \downarrow & \downarrow \end{pmatrix} = \\ &= \begin{pmatrix} \boldsymbol{t}_1\cdot(\boldsymbol{P}\cdot\boldsymbol{L}_\xi + h\,\zeta\,\boldsymbol{\mathcal{N}}_{,\xi}) & \boldsymbol{t}_1\cdot(\boldsymbol{P}\cdot\boldsymbol{L}_\eta + h\,\zeta\,\boldsymbol{\mathcal{N}}_{,\eta}) & 0 \\ \boldsymbol{t}_2\cdot(\boldsymbol{P}\cdot\boldsymbol{L}_\xi + h\,\zeta\,\boldsymbol{\mathcal{N}}_{,\xi}) & \boldsymbol{t}_2\cdot(\boldsymbol{P}\cdot\boldsymbol{L}_\eta + h\,\zeta\,\boldsymbol{\mathcal{N}}_{,\eta}) & 0 \\ 0 & 0 & h \end{pmatrix} \end{aligned} \tag{6.43}$$

$$\boldsymbol{A}^{-1}_{\substack{1\,1\\2\,2}} \coloneqq \begin{pmatrix} \boldsymbol{t}_1\cdot(\boldsymbol{P}\cdot\boldsymbol{L}_\xi + h\,\zeta\,\boldsymbol{\mathcal{N}}_{,\xi}) & \boldsymbol{t}_1\cdot(\boldsymbol{P}\cdot\boldsymbol{L}_\eta + h\,\zeta\,\boldsymbol{\mathcal{N}}_{,\eta}) \\ \boldsymbol{t}_2\cdot(\boldsymbol{P}\cdot\boldsymbol{L}_\xi + h\,\zeta\,\boldsymbol{\mathcal{N}}_{,\xi}) & \boldsymbol{t}_2\cdot(\boldsymbol{P}\cdot\boldsymbol{L}_\eta + h\,\zeta\,\boldsymbol{\mathcal{N}}_{,\eta}) \end{pmatrix} \tag{6.44}$$

$$\det\boldsymbol{A}^{-1} = \det(\boldsymbol{T}^{T}\cdot\boldsymbol{J}) = \det\boldsymbol{T}^{T}\,\det\boldsymbol{J} = \det\boldsymbol{J} \coloneqq J \tag{6.45}$$

but also ... $$\det\boldsymbol{A}^{-1} = \det\boldsymbol{A}^{-1}_{\substack{1\,1\\2\,2}}\,\det\boldsymbol{A}^{-1}_{33} = h\,\det\boldsymbol{A}^{-1}_{\substack{1\,1\\2\,2}} \tag{6.46}$$

then: $$\det\boldsymbol{A}^{-1}_{\substack{1\,1\\2\,2}} = \frac{J}{h} \tag{6.47}$$

$$\begin{aligned} \boldsymbol{A}_{\substack{1\,1\\2\,2}} &= \left(\boldsymbol{A}^{-1}_{\substack{1\,1\\2\,2}}\right)^{-1} = \frac{h}{J}(\boldsymbol{A}_0 + h\,\zeta\,\boldsymbol{A}_1) = \\ &= \frac{h}{J}\begin{pmatrix} \boldsymbol{t}_2\cdot(\boldsymbol{P}\cdot\boldsymbol{L}_\eta + h\,\zeta\,\boldsymbol{\mathcal{N}}_{,\eta}) & -\boldsymbol{t}_1\cdot(\boldsymbol{P}\cdot\boldsymbol{L}_\eta + h\,\zeta\,\boldsymbol{\mathcal{N}}_{,\eta}) \\ -\boldsymbol{t}_2\cdot(\boldsymbol{P}\cdot\boldsymbol{L}_\xi + h\,\zeta\,\boldsymbol{\mathcal{N}}_{,\xi}) & \boldsymbol{t}_1\cdot(\boldsymbol{P}\cdot\boldsymbol{L}_\xi + h\,\zeta\,\boldsymbol{\mathcal{N}}_{,\xi}) \end{pmatrix} \end{aligned} \tag{6.48}$$

$$\boldsymbol{A}_0 = \begin{pmatrix} \boldsymbol{t}_2^{T}\cdot\boldsymbol{P}\cdot\boldsymbol{L}_\eta & -\boldsymbol{t}_1^{T}\cdot\boldsymbol{P}\cdot\boldsymbol{L}_\eta \\ -\boldsymbol{t}_2^{T}\cdot\boldsymbol{P}\cdot\boldsymbol{L}_\xi & \boldsymbol{t}_1^{T}\cdot\boldsymbol{P}\cdot\boldsymbol{L}_\xi \end{pmatrix} \tag{6.49}$$

$$\boldsymbol{A}_1 = \begin{pmatrix} \boldsymbol{t}_2\cdot\boldsymbol{\mathcal{N}}_{,\eta} & -\boldsymbol{t}_1\cdot\boldsymbol{\mathcal{N}}_{,\eta} \\ -\boldsymbol{t}_2\cdot\boldsymbol{\mathcal{N}}_{,\xi} & \boldsymbol{t}_1\cdot\boldsymbol{\mathcal{N}}_{,\xi} \end{pmatrix} \tag{6.50}$$

$$A_{33} = \frac{1}{h} \tag{6.51}$$

This concludes the demonstration. This demonstration is going to proof very useful in the coming sections because not only have we provided the explicit expression for $\boldsymbol{A}$, but we have also found a decomposition with matrices that are constant in the thickness direction.

By rearranging the terms of equation (6.36) we can define a new tensor $\boldsymbol{Q}$ that permits the use of Voigt notation.

$$E'_{IJ} = \frac{1}{2}(A^T_{Ii}\, g_{ij}\, A_{jJ} - \boldsymbol{\delta}_{IJ}) = \frac{1}{2}(A_{iI}\, A_{jJ}\, g_{ij} - \boldsymbol{\delta}_{IJ}) \tag{6.52}$$

$$\boldsymbol{E}'_{Voigt} = \begin{bmatrix} E'_{11} \\ E'_{22} \\ E'_{12} + E'_{21} \end{bmatrix} = \frac{1}{2}(\boldsymbol{Q} \cdot \boldsymbol{g}_{Voigt} - \boldsymbol{I}_{Voigt}) \overset{not}{=} \frac{1}{2}(\boldsymbol{Q} \cdot \boldsymbol{g} - \boldsymbol{I}) =$$

$$= \frac{1}{2}\left( \underbrace{\begin{bmatrix} A^2_{11} & A^2_{21} & A_{11}\, A_{21} \\ A^2_{12} & A^2_{22} & A_{12}\, A_{22} \\ 2\, A_{11}\, A_{12} & 2\, A_{22}\, A_{21} & A_{11}\, A_{22} + A_{12}\, A_{21} \end{bmatrix}}_{\boldsymbol{Q}} \cdot \begin{bmatrix} g_{11} \\ g_{22} \\ g_{12} + g_{21} \end{bmatrix} - \begin{bmatrix} 1 \\ 1 \\ 0 \end{bmatrix} \right) \tag{6.53}$$

However, since $\boldsymbol{Q}$ contains only the components of $\boldsymbol{A}_{\frac{1}{2}\frac{1}{2}}$, we can make use of its decomposition in equation (6.48) to also decompose $\boldsymbol{Q}$:

$$\begin{aligned} \boldsymbol{E}'_{\frac{1}{2}\frac{1}{2}} &= \frac{1}{2}\left( \boldsymbol{A}^T_{\frac{1}{2}\frac{1}{2}} \cdot \boldsymbol{g}_{\frac{1}{2}\frac{1}{2}} \cdot \boldsymbol{A}_{\frac{1}{2}\frac{1}{2}} - \boldsymbol{I}_{\frac{1}{2}\frac{1}{2}} \right) = \\ &= \frac{1}{2}\left[ \frac{h^2}{J^2}(\boldsymbol{A}_0 + h\,\zeta\,\boldsymbol{A}_1)^T \cdot \boldsymbol{g}_{\frac{1}{2}\frac{1}{2}} \cdot (\boldsymbol{A}_0 + h\,\zeta\,\boldsymbol{A}_1) - \boldsymbol{I}_{\frac{1}{2}\frac{1}{2}} \right] = \\ &= \frac{1}{2}\left[ \frac{h^2}{J^2}\,\boldsymbol{A}_0^T \cdot \boldsymbol{g}_{\frac{1}{2}\frac{1}{2}} \cdot \boldsymbol{A}_0 + \right. \\ &\quad + \frac{h^3\,\zeta}{J^2}\left( \boldsymbol{A}_0^T \cdot \boldsymbol{g}_{\frac{1}{2}\frac{1}{2}} \cdot \boldsymbol{A}_1 + \boldsymbol{A}_1^T \cdot \boldsymbol{g}_{\frac{1}{2}\frac{1}{2}} \cdot \boldsymbol{A}_0 \right) + \\ &\quad \left. + \frac{h^4\,\zeta^2}{J^2}\,\boldsymbol{A}_1^T \cdot \boldsymbol{g}_{\frac{1}{2}\frac{1}{2}} \cdot \boldsymbol{A}_1 - \boldsymbol{I}_{\frac{1}{2}\frac{1}{2}} \right] \end{aligned} \tag{6.54}$$

$$\left( \boldsymbol{A}_0^T \cdot \boldsymbol{g}_{\frac{1}{2}\frac{1}{2}} \cdot \boldsymbol{A}_0 \right)_{Voigt} = \boldsymbol{Q}_0 \cdot \boldsymbol{g} \tag{6.55}$$

$$\left( \boldsymbol{A}_0^T \cdot \boldsymbol{g}_{\frac{1}{2}\frac{1}{2}} \cdot \boldsymbol{A}_1 + \boldsymbol{A}_1^T \cdot \boldsymbol{g}_{\frac{1}{2}\frac{1}{2}} \cdot \boldsymbol{A}_0 \right)_{Voigt} = \boldsymbol{Q}_1 \cdot \boldsymbol{g} \tag{6.56}$$

$$\left( \boldsymbol{A}_1^T \cdot \boldsymbol{g}_{\frac{1}{2}\frac{1}{2}} \cdot \boldsymbol{A}_1 \right)_{Voigt} = \boldsymbol{Q}_2 \cdot \boldsymbol{g} \tag{6.57}$$

$$\boldsymbol{E}' = \frac{1}{2}\left[ \frac{h^2}{J^2}\left( \boldsymbol{Q}_0 + h\,\zeta\,\boldsymbol{Q}_1 + h^2\,\zeta^2\,\boldsymbol{Q}_2 \right) \cdot \boldsymbol{g} - \boldsymbol{I} \right] \tag{6.58}$$

$$\boldsymbol{Q} = \frac{h^2}{J^2}\,\boldsymbol{Q}_0 + \frac{h^3\,\zeta}{J^2}\,\boldsymbol{Q}_1 + \frac{h^4\,\zeta^2}{J^2}\,\boldsymbol{Q}_2 \tag{6.59}$$

$$\boldsymbol{Q}_0 = \begin{bmatrix} (\boldsymbol{t}_2^T \cdot \boldsymbol{P} \cdot \boldsymbol{L}_\eta)^2 & (\boldsymbol{t}_2^T \cdot \boldsymbol{P} \cdot \boldsymbol{L}_\xi)^2 & -(\boldsymbol{t}_2^T \cdot \boldsymbol{P} \cdot \boldsymbol{L}_\eta)(\boldsymbol{t}_2^T \cdot \boldsymbol{P} \cdot \boldsymbol{L}_\xi) \\ (\boldsymbol{t}_1^T \cdot \boldsymbol{P} \cdot \boldsymbol{L}_\eta)^2 & (\boldsymbol{t}_1^T \cdot \boldsymbol{P} \cdot \boldsymbol{L}_\xi)^2 & -(\boldsymbol{t}_1^T \cdot \boldsymbol{P} \cdot \boldsymbol{L}_\eta)(\boldsymbol{t}_1^T \cdot \boldsymbol{P} \cdot \boldsymbol{L}_\xi) \\ -2(\boldsymbol{t}_2^T \cdot \boldsymbol{P} \cdot \boldsymbol{L}_\eta)\cdot & -2(\boldsymbol{t}_2^T \cdot \boldsymbol{P} \cdot \boldsymbol{L}_\xi)\cdot & (\boldsymbol{t}_2^T \cdot \boldsymbol{P} \cdot \boldsymbol{L}_\eta)(\boldsymbol{t}_1^T \cdot \boldsymbol{P} \cdot \boldsymbol{L}_\xi) + \\ \cdot(\boldsymbol{t}_1^T \cdot \boldsymbol{P} \cdot \boldsymbol{L}_\eta) & \cdot(\boldsymbol{t}_1^T \cdot \boldsymbol{P} \cdot \boldsymbol{L}_\xi) & +(\boldsymbol{t}_1^T \cdot \boldsymbol{P} \cdot \boldsymbol{L}_\eta)(\boldsymbol{t}_2^T \cdot \boldsymbol{P} \cdot \boldsymbol{L}_\xi) \end{bmatrix} \tag{6.60}$$

$$\boldsymbol{Q}_1 = \begin{bmatrix} 2(\boldsymbol{t}_2^T \cdot \boldsymbol{P} \cdot \boldsymbol{L}_\eta)\cdot & 2(\boldsymbol{t}_2^T \cdot \boldsymbol{P} \cdot \boldsymbol{L}_\xi)\cdot & -[(\boldsymbol{t}_2^T \cdot \boldsymbol{P} \cdot \boldsymbol{L}_\eta)(\boldsymbol{t}_2 \cdot \boldsymbol{\mathcal{N}}_{,\xi}) + \\ \cdot(\boldsymbol{t}_2 \cdot \boldsymbol{\mathcal{N}}_{,\eta}) & \cdot(\boldsymbol{t}_2 \cdot \boldsymbol{\mathcal{N}}_{,\xi}) & +(\boldsymbol{t}_2^T \cdot \boldsymbol{P} \cdot \boldsymbol{L}_\xi)(\boldsymbol{t}_2 \cdot \boldsymbol{\mathcal{N}}_{,\eta})] \\ 2(\boldsymbol{t}_1^T \cdot \boldsymbol{P} \cdot \boldsymbol{L}_\eta)\cdot & 2(\boldsymbol{t}_1^T \cdot \boldsymbol{P} \cdot \boldsymbol{L}_\xi)\cdot & -[(\boldsymbol{t}_1^T \cdot \boldsymbol{P} \cdot \boldsymbol{L}_\eta)(\boldsymbol{t}_1 \cdot \boldsymbol{\mathcal{N}}_{,\xi}) + \\ \cdot(\boldsymbol{t}_1 \cdot \boldsymbol{\mathcal{N}}_{,\eta}) & \cdot(\boldsymbol{t}_1 \cdot \boldsymbol{\mathcal{N}}_{,\xi}) & +(\boldsymbol{t}_1^T \cdot \boldsymbol{P} \cdot \boldsymbol{L}_\xi)(\boldsymbol{t}_1 \cdot \boldsymbol{\mathcal{N}}_{,\eta})] \\ -2[(\boldsymbol{t}_2^T \cdot \boldsymbol{P} \cdot \boldsymbol{L}_\eta)\cdot & -2[(\boldsymbol{t}_2^T \cdot \boldsymbol{P} \cdot \boldsymbol{L}_\xi)\cdot & [(\boldsymbol{t}_2^T \cdot \boldsymbol{P} \cdot \boldsymbol{L}_\eta)(\boldsymbol{t}_1 \cdot \boldsymbol{\mathcal{N}}_{,\xi}) + \\ \cdot(\boldsymbol{t}_1 \cdot \boldsymbol{\mathcal{N}}_{,\eta}) + & \cdot(\boldsymbol{t}_1 \cdot \boldsymbol{\mathcal{N}}_{,\xi}) + & +(\boldsymbol{t}_1^T \cdot \boldsymbol{P} \cdot \boldsymbol{L}_\xi)(\boldsymbol{t}_2 \cdot \boldsymbol{\mathcal{N}}_{,\eta}) + \\ +(\boldsymbol{t}_1^T \cdot \boldsymbol{P} \cdot \boldsymbol{L}_\eta)\cdot & +(\boldsymbol{t}_1^T \cdot \boldsymbol{P} \cdot \boldsymbol{L}_\xi)\cdot & +(\boldsymbol{t}_1^T \cdot \boldsymbol{P} \cdot \boldsymbol{L}_\eta)(\boldsymbol{t}_2 \cdot \boldsymbol{\mathcal{N}}_{,\xi}) + \\ \cdot(\boldsymbol{t}_2 \cdot \boldsymbol{\mathcal{N}}_{,\eta})] & \cdot(\boldsymbol{t}_2 \cdot \boldsymbol{\mathcal{N}}_{,\xi})] & +(\boldsymbol{t}_2^T \cdot \boldsymbol{P} \cdot \boldsymbol{L}_\xi)(\boldsymbol{t}_1 \cdot \boldsymbol{\mathcal{N}}_{,\eta})] \end{bmatrix} \tag{6.61}$$

$$\boldsymbol{Q}_2 = \begin{bmatrix} (\boldsymbol{t}_2 \cdot \boldsymbol{\mathcal{N}}_{,\eta})^2 & (\boldsymbol{t}_2 \cdot \boldsymbol{\mathcal{N}}_{,\xi})^2 & -(\boldsymbol{t}_2 \cdot \boldsymbol{\mathcal{N}}_{,\eta})(\boldsymbol{t}_2 \cdot \boldsymbol{\mathcal{N}}_{,\xi}) \\ (\boldsymbol{t}_1 \cdot \boldsymbol{\mathcal{N}}_{,\eta})^2 & (\boldsymbol{t}_1 \cdot \boldsymbol{\mathcal{N}}_{,\xi})^2 & -(\boldsymbol{t}_1 \cdot \boldsymbol{\mathcal{N}}_{,\eta})(\boldsymbol{t}_1 \cdot \boldsymbol{\mathcal{N}}_{,\xi}) \\ -2(\boldsymbol{t}_2 \cdot \boldsymbol{\mathcal{N}}_{,\eta})\cdot & -2(\boldsymbol{t}_2 \cdot \boldsymbol{\mathcal{N}}_{,\xi})\cdot & (\boldsymbol{t}_2 \cdot \boldsymbol{\mathcal{N}}_{,\eta})(\boldsymbol{t}_1 \cdot \boldsymbol{\mathcal{N}}_{,\xi}) + \\ \cdot(\boldsymbol{t}_1 \cdot \boldsymbol{\mathcal{N}}_{,\eta}) & \cdot(\boldsymbol{t}_1 \cdot \boldsymbol{\mathcal{N}}_{,\xi}) & +(\boldsymbol{t}_1 \cdot \boldsymbol{\mathcal{N}}_{,\eta})(\boldsymbol{t}_2 \cdot \boldsymbol{\mathcal{N}}_{,\xi}) \end{bmatrix} \tag{6.62}$$

But $\boldsymbol{g}$ can also be decomposed and equation (6.39) is rewritten as:

$$\boldsymbol{g} = \boldsymbol{g}_m + 2\,\lambda\,h\,\zeta\,\boldsymbol{g}_b + \lambda^2\,h^2\,\zeta^2\,\boldsymbol{g}_n \tag{6.63}$$

$$\boldsymbol{g}_m = \begin{bmatrix} \boldsymbol{L}_\xi^T \cdot \boldsymbol{p}^T \cdot \boldsymbol{p} \cdot \boldsymbol{L}_\xi \\ \boldsymbol{L}_\eta^T \cdot \boldsymbol{p}^T \cdot \boldsymbol{p} \cdot \boldsymbol{L}_\eta \\ 2\,\boldsymbol{L}_\xi^T \cdot \boldsymbol{p}^T \cdot \boldsymbol{p} \cdot \boldsymbol{L}_\eta \end{bmatrix} \tag{6.64}$$

$$\boldsymbol{g}_b = \begin{bmatrix} \boldsymbol{L}_\xi^T \cdot \boldsymbol{p}^T \cdot \boldsymbol{n}_\xi \\ \boldsymbol{L}_\eta^T \cdot \boldsymbol{p}^T \cdot \boldsymbol{n}_\eta \\ \boldsymbol{L}_\xi^T \cdot \boldsymbol{p}^T \cdot \boldsymbol{n}_\eta + \boldsymbol{L}_\eta^T \cdot \boldsymbol{p}^T \cdot \boldsymbol{n}_\xi \end{bmatrix} \tag{6.65}$$

$$\boldsymbol{g}_n = \begin{bmatrix} \boldsymbol{n}_\xi \cdot \boldsymbol{n}_\xi \\ \boldsymbol{n}_\eta \cdot \boldsymbol{n}_\eta \\ 2\,\boldsymbol{n}_\xi \cdot \boldsymbol{n}_\eta \end{bmatrix} \tag{6.66}$$

where $\boldsymbol{g}_m$, $\boldsymbol{g}_b$ and $\boldsymbol{g}_n$ contain respectively the *membrane*, *bending* and *second order* terms of the deformation. Finally, by combining equation (6.63) into equation (6.58), we obtain a fully decomposed expression for the Green-Lagrange strain tensor in local coordinates of the material. All the vectors and tensors in equation (6.67) are constant in the thickness direction. We shall remark again that the Green-Lagrange strain tensor ($\boldsymbol{E}$') is defined in the reference configuration.

$$\boldsymbol{E}' = \frac{1}{2}\left[\frac{h^2}{J^2}\left(\boldsymbol{Q}_0 + h\,\zeta\,\boldsymbol{Q}_1 + h^2\,\zeta^2\,\boldsymbol{Q}_2\right) \cdot \left(\boldsymbol{g}_m + 2\,\lambda\,h\,\zeta\,\boldsymbol{g}_b + \lambda^2\,h^2\,\zeta^2\,\boldsymbol{g}_n\right) - \boldsymbol{I}\right] \tag{6.67}$$

## 6.5 Principle of virtual work

The second Piola-Kirchhoff stress tensor ($\boldsymbol{S}$) is work-conjugate of the Green-Lagrange strain tensor ($\boldsymbol{E}$). So the density of work produced by the defor-

mation is expressed as:

$$U = \boldsymbol{E} \colon \boldsymbol{S} = \boldsymbol{E}' \colon \boldsymbol{S}' \tag{6.68}$$

The expression of the virtual work principle for the internal virtual work of an element is:

$$\begin{aligned} \delta W_e^{int} = \iiint_{\Omega_e^0} \delta \boldsymbol{E}' \colon \boldsymbol{S}' \, \mathrm{d}\Omega^0 = \iiint_{\Omega_e^0} \delta \boldsymbol{E}'^T \cdot \boldsymbol{D} \cdot \boldsymbol{E}' \, \mathrm{d}\Omega^0 = \\ = \frac{1}{4} \iiint_{\Omega_e^0} \delta \boldsymbol{g}^T \cdot \boldsymbol{Q}^T \cdot \boldsymbol{D} \cdot (\boldsymbol{Q} \cdot \boldsymbol{g} - \boldsymbol{I}) \, \mathrm{d}\Omega^0 \end{aligned} \tag{6.69}$$

and the external virtual work is:

$$\delta W_e^{ext} = \iiint_{V_e} \delta \boldsymbol{x} \cdot \boldsymbol{q}_V \, \mathrm{d}V + \iint_{S_e} \delta \boldsymbol{x} \cdot \boldsymbol{q}_S \, \mathrm{d}S + \int_{\Gamma_e} \delta \boldsymbol{x} \cdot \boldsymbol{q}_\Gamma \, \mathrm{d}\Gamma + \sum_{i=1}^{r_{\text{total}}} \delta \boldsymbol{x}^i \cdot \boldsymbol{q}^i \tag{6.70}$$

where $\boldsymbol{q}_V$, $\boldsymbol{q}_S$, $\boldsymbol{q}_\Gamma$ and $\boldsymbol{q}^i$ refer to the volume loads, surface loads, linear loads and nodal loads, respectively. Notice that the integrals in equation (6.70) do not specify whether the integral is defined in the reference or in the current configuration. That is because some loads will be defined in the reference configuration (e.g. self weight) and some other loads will be defined in the deformed configuration (e.g. a follower pressure load).

Because the BEST element uses neighboring nodes to define the geometry, the author refers to the set of nodes that surround the triangle as $\tilde{\boldsymbol{x}}^r$. This is a column vector which has the different vector coordinates of each of the surrounding nodes stacked one after the other (with the coordinates of the three nodes of the triangle taking the first 9 positions).

$$\tilde{\boldsymbol{x}}^r := \begin{bmatrix} x_1^1 \\ x_2^1 \\ x_3^1 \\ \vdots \\ x_1^k \\ x_2^k \\ x_3^k \\ \vdots \\ x_1^{r_{\text{total}}} \\ x_2^{r_{\text{total}}} \\ x_3^{r_{\text{total}}} \end{bmatrix} \tag{6.71}$$

Where $r_{\text{total}}$ is the total number of nodes in the patch of elements that surrounds the triangle. For a regular mesh, $r_{\text{total}} = 12$.

When taking derivatives of the different magnitudes with respect to the coordinates of the nodes of the BEST element, all the coordinates of the neighboring nodes need to be accounted for. For example:

$$\delta \boldsymbol{g} = \frac{\partial \boldsymbol{g}}{\partial \tilde{\boldsymbol{x}}^r} \delta \tilde{\boldsymbol{x}}^r = \boldsymbol{B} \cdot \delta \tilde{\boldsymbol{x}}^r \tag{6.72}$$

$$\delta \boldsymbol{x} = \frac{\partial \boldsymbol{x}}{\partial \tilde{\boldsymbol{x}}^r} \delta \tilde{\boldsymbol{x}}^r \tag{6.73}$$

$\boldsymbol{B}$ is a matrix with 3 rows and three times as many columns as nodes exist in the patch of the element. Usually, in the literature, other authors use this notation for the matrix relating the nodal displacements with the deformation tensor. The author is not using a formulation based on displacements but based on nodal coordinates, so this possibility is forfeited in this work. Besides, in terms of derivatives, the product of $\boldsymbol{Q}$ and $\boldsymbol{B}$ would be equivalent to the matrix $\boldsymbol{B}$ used in the literature. The author prefers to keep them separated in order to simplify the decomposed expression with respect to the thickness coordinate.

Now we can rewrite equations (6.69) and (6.70) using the expressions above:

$$\delta W_e^{int} = \frac{1}{4}\delta\tilde{\boldsymbol{x}}^{rT} \iiint_{\Omega_e^0} \boldsymbol{B}^T \cdot \boldsymbol{Q}^T \cdot \boldsymbol{D} \cdot (\boldsymbol{Q} \cdot \boldsymbol{g} - \boldsymbol{I})\, \mathrm{d}\Omega^0 \tag{6.74}$$

$$\begin{aligned} \delta W_e^{ext} = \delta\tilde{\boldsymbol{x}}^{rT} \Bigg[ & \iiint_{V_e} \left(\frac{\partial \boldsymbol{x}}{\partial \tilde{\boldsymbol{x}}^r}\right)^T \cdot \boldsymbol{q}_V \,\mathrm{d}V + \iint_{S_e} \left(\frac{\partial \boldsymbol{x}}{\partial \tilde{\boldsymbol{x}}^r}\right)^T \cdot \boldsymbol{q}_S \,\mathrm{d}S + \\ & + \int_{\Gamma_e} \left(\frac{\partial \boldsymbol{x}}{\partial \tilde{\boldsymbol{x}}^r}\right)^T \cdot \boldsymbol{q}_\Gamma \,\mathrm{d}\Gamma + \tilde{\boldsymbol{q}}^r \Bigg] \end{aligned} \tag{6.75}$$

Equaling the expression for the internal virtual work and the external virtual work we establish a condition for equilibrium. Since the equality must hold for any arbitrary value of $\delta\tilde{\boldsymbol{x}}^r$, then we can write:

$$\begin{aligned} \frac{1}{4} \iiint_{\Omega_e^0} \boldsymbol{B}^T \cdot \boldsymbol{Q}^T \cdot \boldsymbol{D} \cdot (\boldsymbol{Q} \cdot \boldsymbol{g} - \boldsymbol{I})\, \mathrm{d}\Omega^0 = & \iiint_{V_e} \left(\frac{\partial \boldsymbol{x}}{\partial \tilde{\boldsymbol{x}}^r}\right)^T \cdot \boldsymbol{q}_V \,\mathrm{d}V + \\ & + \iint_{S_e} \left(\frac{\partial \boldsymbol{x}}{\partial \tilde{\boldsymbol{x}}^r}\right)^T \cdot \boldsymbol{q}_S \,\mathrm{d}S + \int_{\Gamma_e} \left(\frac{\partial \boldsymbol{x}}{\partial \tilde{\boldsymbol{x}}^r}\right)^T \cdot \boldsymbol{q}_\Gamma \,\mathrm{d}\Gamma + \tilde{\boldsymbol{q}}^r \end{aligned} \tag{6.76}$$

The left hand side contains what is commonly referred to as the vector of equivalent nodal loads to the internal stresses of the element ($\boldsymbol{F}_e^{int}$). The right hand side contains what is commonly referred to as the vector of equivalent external nodal loads ($\boldsymbol{F}_e^{ext}$).

Equation (6.76) is a nonlinear equation. In order to solve it, we use the Newton-Raphson method.

$$\boldsymbol{R}_e^k = \boldsymbol{F}_e^{int}(\tilde{\boldsymbol{x}}^r)^k - \boldsymbol{F}_e^{ext}(\tilde{\boldsymbol{x}}^r)^k \tag{6.77}$$

$$\boldsymbol{R}_e^{k+1} \approx \frac{\partial \boldsymbol{R}_e^k}{\partial \tilde{\boldsymbol{x}}^r} \cdot \Delta\tilde{\boldsymbol{x}}^r = \boldsymbol{0} \tag{6.78}$$

$$(\tilde{\boldsymbol{x}}^r)^{k+1} = (\tilde{\boldsymbol{x}}^r)^k + \Delta\tilde{\boldsymbol{x}}^r \tag{6.79}$$

## 6.6 Summary

This chapter presents the description of the deformation of the BEST element for a total Lagrangian formulation and for a modified version of the Kirchhoff-Love hypothesis of the shell mechanics in which the constraint on the thickness change has been relaxed while assuming a plane stress state of the material.

Under the above conditions the author has obtained a decomposition of the Green-Lagrange strain tensor in local coordinates (see equation (6.58)),

where the components are independent through the thickness except for scalar coefficients. This will prove very valuable in the next chapter in order to perform the efficient and geometrically accurate through-the-thickness pre-integration of the stiffness matrix in the total Lagrangian framework.

# Chapter 7

# Construction of the tangent stiffness matrix

THIS CHAPTER PRESENTS THE CONSTRUCTION of the tangent stiffness matrix of the BEST element as required per equation (6.78), which implies the solution of a linear system of equations. On the one side, the linearization of the expression of the equivalent internal nodal loads leads to obtaining the classical stiffness matrix of the element. On the other side, the linearization of the equivalent external nodal loads leads to the tangent matrix of the nodal loads. In many cases, the external loads are constant, but it is not infrequent that an engineer faces a structure with varying loads.

$$\frac{\partial \boldsymbol{R}_e}{\partial \tilde{\boldsymbol{x}}^r} = \frac{\partial \boldsymbol{F}_e^{int}(\tilde{\boldsymbol{x}}^r)}{\partial \tilde{\boldsymbol{x}}^r} - \frac{\partial \boldsymbol{F}_e^{ext}(\tilde{\boldsymbol{x}}^r)}{\partial \tilde{\boldsymbol{x}}^r} \tag{7.1}$$

Section 7.1 presents the computation of the material and the geometric stiffness matrices of the element. The geometric stiffness matrix appears only in geometrically nonlinear problems. This is the case of shells. This is accentuated in the case of very thin shells whose structures can undergo very large displacements. An efficient integration of the stiffness matrix is necessary in order to keep the computational cost competitive with other finite elements. This issue is presented in section 7.2. Finally, the computation of the tangent loads matrix is presented in section 7.3. The BEST element is also different in this aspect, because the shape of the element depends not only on the element's nodal positions, but also on the positions of the patch of nodes surrounding the element.

## 7.1 Material and geometric stiffness matrices

The stiffness matrix stems from the linearization of the equivalent internal nodal loads.

$$\begin{aligned}\frac{\partial \boldsymbol{F}_e^{int}(\tilde{\boldsymbol{x}}^r)}{\partial \tilde{\boldsymbol{x}}^r} &= \frac{1}{4}\frac{\partial}{\partial \tilde{\boldsymbol{x}}^r}\iiint_{\Omega_e^0} \boldsymbol{B}^T\cdot\boldsymbol{Q}^T\cdot\boldsymbol{D}\cdot(\boldsymbol{Q}\cdot\boldsymbol{g}-\boldsymbol{I})\,\mathrm{d}\Omega^0 = \\ &= \underbrace{\frac{1}{4}\iiint_{\Omega_e^0}\boldsymbol{B}^T\cdot\boldsymbol{Q}^T\cdot\boldsymbol{D}\cdot\boldsymbol{Q}\cdot\boldsymbol{B}\,\mathrm{d}\Omega^0}_{\boldsymbol{K}_M} + \\ &\quad + \underbrace{\frac{1}{2}\iiint_{\Omega_e^0}\frac{\partial \boldsymbol{B}^T}{\partial \tilde{\boldsymbol{x}}^r}\cdot\boldsymbol{Q}^T\cdot\boldsymbol{D}\cdot\boldsymbol{E}'\,\mathrm{d}\Omega^0}_{\boldsymbol{K}_G}\end{aligned} \tag{7.2}$$

Where $\boldsymbol{K}_M$ is the material stiffness matrix, and $\boldsymbol{K}_G$ is the geometric stiffness matrix. Let's proceed with the details of the computations in the parametric space of coordinates.

$$\begin{aligned}\boldsymbol{K}_M &= \frac{1}{4}\iiint_{\Omega_e^0}\boldsymbol{B}^T\cdot\boldsymbol{Q}^T\cdot\boldsymbol{D}\cdot\boldsymbol{Q}\cdot\boldsymbol{B}\,\mathrm{d}\Omega^0 = \\ &= \frac{1}{4}\int_0^1\int_0^{1-\xi}\int_{-\frac{1}{2}}^{\frac{1}{2}}\boldsymbol{B}^T\cdot\boldsymbol{Q}^T\cdot\boldsymbol{D}\cdot\boldsymbol{Q}\cdot\boldsymbol{B}\cdot J\,\mathrm{d}\xi\,\mathrm{d}\eta\,\mathrm{d}\zeta\end{aligned} \tag{7.3}$$

$$\begin{aligned}\boldsymbol{K}_G &= \frac{1}{2}\iiint_{\Omega_e^0}\frac{\partial \boldsymbol{B}^T}{\partial \tilde{\boldsymbol{x}}^r}\cdot\boldsymbol{Q}^T\cdot\boldsymbol{D}\cdot\boldsymbol{E}'\,\mathrm{d}\Omega^0 \\ &= \frac{1}{2}\int_0^1\int_0^{1-\xi}\int_{-\frac{1}{2}}^{\frac{1}{2}}\frac{\partial \boldsymbol{B}^T}{\partial \tilde{\boldsymbol{x}}^r}\cdot\boldsymbol{Q}^T\cdot\boldsymbol{D}\cdot\boldsymbol{E}'\cdot J\,\mathrm{d}\xi\,\mathrm{d}\eta\,\mathrm{d}\zeta\end{aligned} \tag{7.4}$$

The matrix $\boldsymbol{B}$ and the tensor in 3 dimensions $\dfrac{\partial \boldsymbol{B}}{\partial \tilde{\boldsymbol{x}}^r}$ have not been thoroughly defined, yet. Let's recall the first time $\boldsymbol{B}$ has been introduced in equation (6.72) and the decomposition of $\boldsymbol{g}$ in equation (6.63):

$$\begin{aligned}\boldsymbol{B} = \frac{\partial \boldsymbol{g}}{\partial \tilde{\boldsymbol{x}}^r} &= \frac{\partial \boldsymbol{g}_m}{\partial \tilde{\boldsymbol{x}}^r} + 2\,\lambda\,h\,\zeta\,\frac{\partial \boldsymbol{g}_b}{\partial \tilde{\boldsymbol{x}}^r} + \lambda^2\,h^2\,\zeta^2\,\frac{\partial \boldsymbol{g}_n}{\partial \tilde{\boldsymbol{x}}^r} = \\ &= \boldsymbol{B}_m + 2\,\lambda\,h\,\zeta\,\boldsymbol{B}_b + \lambda^2\,h^2\,\zeta^2\,\boldsymbol{B}_n\end{aligned} \tag{7.5}$$

$$\boldsymbol{B}_m = \frac{\partial \boldsymbol{g}_m}{\partial \tilde{\boldsymbol{x}}^r} = \frac{\partial \boldsymbol{g}_m}{\partial \boldsymbol{p}} : \frac{\partial \boldsymbol{p}}{\partial \tilde{\boldsymbol{x}}^r} \tag{7.6}$$

$$\boldsymbol{B}_b = \frac{\partial \boldsymbol{g}_b}{\partial \tilde{\boldsymbol{x}}^r} = \frac{\partial \boldsymbol{g}_b}{\partial \boldsymbol{p}} : \frac{\partial \boldsymbol{p}}{\partial \tilde{\boldsymbol{x}}^r} \tag{7.7}$$

$$\boldsymbol{B}_n = \frac{\partial \boldsymbol{g}_n}{\partial \tilde{\boldsymbol{x}}^r} = \frac{\partial \boldsymbol{g}_n}{\partial \boldsymbol{p}} : \frac{\partial \boldsymbol{p}}{\partial \tilde{\boldsymbol{x}}^r} \tag{7.8}$$

For the sake of brevity, the author will request from the reader an effort of abstraction. The formulæ will try to be presented in condensed form whenever possible. For example, the above expressions can be jointly presented as:

$$\boldsymbol{B}_\chi = \frac{\partial \boldsymbol{g}_\chi}{\partial \tilde{\boldsymbol{x}}^r} = \frac{\partial \boldsymbol{g}_\chi}{\partial \boldsymbol{p}} : \frac{\partial \boldsymbol{p}}{\partial \tilde{\boldsymbol{x}}^r} \quad \forall \chi = \{m, b, n\} \tag{7.9}$$

And the terms included in the following expression

$$\begin{aligned}\frac{\partial \boldsymbol{B}}{\partial \tilde{\boldsymbol{x}}^r} = \frac{\partial^2 \boldsymbol{g}}{(\partial \tilde{\boldsymbol{x}}^r)^2} = \frac{\partial^2 \boldsymbol{g}_m}{(\partial \tilde{\boldsymbol{x}}^r)^2} + 2\,\lambda\,h\,\zeta\,\frac{\partial^2 \boldsymbol{g}_b}{(\partial \tilde{\boldsymbol{x}}^r)^2} + \lambda^2\,h^2\,\zeta^2\,\frac{\partial^2 \boldsymbol{g}_n}{(\partial \tilde{\boldsymbol{x}}^r)^2} = \\ = \frac{\partial \boldsymbol{B}_m}{\partial \tilde{\boldsymbol{x}}^r} + 2\,\lambda\,h\,\zeta\,\frac{\partial \boldsymbol{B}_b}{\partial \tilde{\boldsymbol{x}}^r} + \lambda^2\,h^2\,\zeta^2\,\frac{\partial \boldsymbol{B}_n}{\partial \tilde{\boldsymbol{x}}^r}\end{aligned} \tag{7.10}$$

can be further expanded as follows:

$$\begin{aligned}\frac{\partial \boldsymbol{B}_\chi}{\partial \tilde{\boldsymbol{x}}^r} = \frac{\partial^2 \boldsymbol{g}_\chi}{(\partial \tilde{\boldsymbol{x}}^r)^2} = \left(\frac{\partial^2 \boldsymbol{g}_\chi}{(\partial \boldsymbol{p})^2} : \frac{\partial \boldsymbol{p}}{\partial \tilde{\boldsymbol{x}}^r}\right) : \frac{\partial \boldsymbol{p}}{\partial \tilde{\boldsymbol{x}}^r} + \frac{\partial \boldsymbol{g}_\chi}{\partial \boldsymbol{p}} : \frac{\partial^2 \boldsymbol{p}}{(\partial \tilde{\boldsymbol{x}}^r)^2} = \\ = \left(\frac{\partial^2 g_{\chi(i)}}{\partial p_{(jq)}\,\partial p_{(ls)}} : \frac{\partial p_{(ls)}}{\partial \tilde{x}^r_{(w)}}\right) : \frac{\partial p_{(jq)}}{\partial \tilde{x}^r_{(v)}} + \frac{\partial g_{\chi(i)}}{\partial p_{(jq)}} : \frac{\partial^2 p_{(jq)}}{\partial \tilde{x}^r_{(v)}\,\partial \tilde{x}^r_{(w)}} = \\ = \frac{\partial B_{\chi(iv)}}{\partial \tilde{x}^r_{(w)}} \quad \forall \chi = \{m, b, n\} \quad \forall i = 1 \div 3 \quad \forall v, w = 1 \div 3\, r_{total}\end{aligned} \tag{7.11}$$

Since these matrices start to get rather large in the number of dimensions, the author prefers to express some of the definitions using indicial notation for further clarity. Indices are written in parentheses to distinguish them from subscripts.

$$\frac{\partial \boldsymbol{g}_\chi}{\partial \boldsymbol{p}} = \frac{\partial g_{\chi(k)}}{\partial p_{(lv)}} \quad \forall \chi = \{m, b, n\} \quad \forall k, l = 1 \div 3 \quad \forall v = 1 \div 10 \tag{7.12}$$

$$\frac{\partial g_{m(1)}}{\partial p_{(lv)}} = 2\,p_{(lj)} L_{\xi(j)} L_{\xi(v)} \tag{7.13}$$

$$\frac{\partial g_{m(2)}}{\partial p_{(lv)}} = 2\,p_{(lj)} L_{\eta(j)} L_{\eta(v)} \tag{7.14}$$

$$\frac{\partial g_{m(3)}}{\partial p_{(lv)}} = 2\,(p_{(lj)} L_{\xi(j)} L_{\eta(v)} + p_{(lj)} L_{\eta(j)} L_{\xi(v)}) \tag{7.15}$$

Again, the author makes an abuse of notation and switches indistinctively between tensorial notation and Voigt notation for the components of $\boldsymbol{g}$ (see equation (4.23) on page 37); in order to condense the above expressions in the following manner:

$$\frac{\partial g_{m(\alpha\beta)}}{\partial p_{(lv)}} = 2\,p_{(lj)} L_{\xi_\alpha(j)} L_{\xi_\beta(v)} \qquad \forall \alpha, \beta = 1, 2 \tag{7.16}$$

$$\frac{\partial g_{b(\alpha\beta)}}{\partial p_{(lv)}} = n_{,\xi_\alpha(l)}\, L_{\xi_\beta(v)} + p_{(ji)} L_{\xi_\beta(i)} \frac{\partial n_{,\xi_\alpha(j)}}{\partial p_{(lv)}} \qquad \forall \alpha, \beta = 1, 2 \tag{7.17}$$

$$\frac{\partial g_{n(\alpha\beta)}}{\partial p_{(lv)}} = 2\,n_{,\xi_\alpha(i)}\, \frac{\partial n_{,\xi_\beta(i)}}{\partial p_{(lv)}} \qquad \forall \alpha, \beta = 1, 2 \tag{7.18}$$

$$\frac{\partial^2 g_{m(\alpha\beta)}}{\partial p_{(jq)}\,\partial p_{(ls)}} = 2\boldsymbol{\delta}_{(jl)} L_{\xi_\alpha(q)} L_{\xi_\beta(s)} \qquad \forall \alpha, \beta = 1, 2 \tag{7.19}$$

$$\frac{\partial^2 g_{b(\alpha\beta)}}{\partial p_{(jq)}\,\partial p_{(ls)}} = \frac{\partial n_{,\xi_\alpha(j)}}{\partial p_{(ls)}} L_{\xi_\beta(q)} + \frac{\partial n_{,\xi_\beta(l)}}{\partial p_{(jq)}} L_{\xi_\alpha(s)} + p_{(jk)} L_{\xi_\alpha(k)} \frac{\partial^2 n_{,\xi_\beta(j)}}{\partial p_{(jq)}\,\partial p_{(ls)}} \qquad \forall \alpha, \beta = 1, 2 \tag{7.20}$$

$$\frac{\partial^2 g_{n(\alpha\beta)}}{\partial p_{(jq)}\,\partial p_{(ls)}} = 2\left(\frac{\partial n_{,\xi_\alpha(i)}}{\partial p_{(jq)}}\frac{\partial n_{,\xi_\beta(i)}}{\partial p_{(ls)}} + n_{,\xi_\beta(i)}\,\frac{\partial^2 n_{,\xi_\alpha(i)}}{\partial p_{(jq)}\,\partial p_{(ls)}}\right) \quad \forall \alpha,\beta = 1,2 \tag{7.21}$$

The expressions for $\frac{\partial \boldsymbol{n}_{,\xi}}{\partial \boldsymbol{p}}$, $\frac{\partial \boldsymbol{n}_{,\eta}}{\partial \boldsymbol{p}}$, $\frac{\partial^2 \boldsymbol{n}_{,\xi}}{(\partial \boldsymbol{p})^2}$ and $\frac{\partial^2 \boldsymbol{n}_{,\eta}}{(\partial \boldsymbol{p})^2}$ become rather complex. For this reason the author prefers to present them in appendix D.

### 7.1.1 Derivatives of the control points' coordinates

Similarly to the procedure followed in section 5.3, the derivatives of the control points' coordinates will be determined by groups. First, the corner control points, which are coincident with the triangle's nodes. Second, the control points in the boundaries of the Bézier triangle. And third, the central control point.

Using equation (5.14), it is straight forward to find the derivatives of the corner control points.

$$\frac{\partial \boldsymbol{p}^i}{\partial \tilde{\boldsymbol{x}}^r} = \frac{\partial \boldsymbol{x}^i}{\partial \tilde{\boldsymbol{x}}^r} = \frac{\partial x^i_{(l)}}{\partial x^h_{(v)}} = \boldsymbol{\delta}^{ih}\boldsymbol{\delta}_{(lv)} \quad \forall\, i,l,v = 1 \div 3 \quad \forall\, h = 1 \div r_{total} \tag{7.22}$$

$$\frac{\partial^2 \boldsymbol{p}^i}{(\partial \tilde{\boldsymbol{x}}^r)^2} = \boldsymbol{0} \tag{7.23}$$

The control points of the Bézier triangle's boundary are determined by solving a linear system of 3 equations. In order to reduce the computational cost, we will take advantage of the fact that the system matrix has to be inverted. We will not invert any other system matrix for the determination of the derivatives. So deriving by parts equation (5.16) and solving for $\frac{\partial \boldsymbol{p}^{ij}}{\partial \tilde{\boldsymbol{x}}^r}$ we obtain:

$$\frac{\partial \boldsymbol{p}^{ij}}{\partial \tilde{\boldsymbol{x}}^r} = \frac{\partial p^{ij}_{(m)}}{\partial x^h_{(v)}} = A^{ij-1}_{p(ml)}\left(\frac{\partial b^{ij}_{p(l)}}{\partial x^h_{(v)}} - \frac{\partial A^{ij}_{p(ln)}}{\partial x^h_{(v)}} p^{ij}_{(n)}\right) \tag{7.24}$$

$$\forall\, i,j = 1 \div 3 \mid i \neq j \qquad \forall\, l,m,n,v = 1 \div 3 \qquad \forall\, h = 1 \div r_{total}$$

$$\boldsymbol{A}^{ij}_{\boldsymbol{p}} \cdot \frac{\partial \boldsymbol{p}^{ij}}{\partial \tilde{\boldsymbol{x}}^r} = \frac{\partial \boldsymbol{b}^{ij}_{\boldsymbol{p}}}{\partial \tilde{\boldsymbol{x}}^r} - \frac{\partial \boldsymbol{A}^{ij}_{\boldsymbol{p}}}{\partial \tilde{\boldsymbol{x}}^r} \cdot \boldsymbol{p}^{ij} \tag{7.25}$$

Deriving again by parts equation (7.25) and solving for $\frac{\partial^2 \boldsymbol{p}^{ij}}{(\partial \tilde{\boldsymbol{x}}^r)^2}$ we obtain:

$$\begin{aligned}\frac{\partial^2 \boldsymbol{p}^{ij}}{(\partial \tilde{\boldsymbol{x}}^r)^2} = \frac{\partial^2 p^{ij}_{(m)}}{\partial x^h_{(v)}\,\partial x^s_{(w)}} = A^{ij-1}_{p(ml)}\Bigg(&\frac{\partial^2 b^{ij}_{p(l)}}{\partial x^h_{(v)}\,\partial x^s_{(w)}} - \frac{\partial^2 A^{ij}_{p(ln)}}{\partial x^h_{(v)}\,\partial x^s_{(w)}} p^{ij}_{(n)} \\ &- \frac{\partial A^{ij}_{p(ln)}}{\partial x^h_{(v)}}\frac{\partial p^{ij}_{(n)}}{\partial x^s_{(w)}} - \frac{\partial A^{ij}_{p(ln)}}{\partial x^s_{(w)}}\frac{\partial p^{ij}_{(n)}}{\partial x^h_{(v)}}\Bigg)\end{aligned} \tag{7.26}$$

$$\forall\, i,j = 1 \div 3 \mid i \neq j \qquad \forall\, l,m,n,v,w = 1 \div 3 \qquad \forall\, h,s = 1 \div r_{total}$$

The expressions for $\frac{\partial \boldsymbol{A}^{ij}_{\boldsymbol{p}}}{\partial \tilde{\boldsymbol{x}}^r}$, $\frac{\partial^2 \boldsymbol{A}^{ij}_{\boldsymbol{p}}}{(\partial \tilde{\boldsymbol{x}}^r)^2}$, $\frac{\partial \boldsymbol{b}^{ij}_{\boldsymbol{p}}}{\partial \tilde{\boldsymbol{x}}^r}$ and $\frac{\partial^2 \boldsymbol{b}^{ij}_{\boldsymbol{p}}}{(\partial \tilde{\boldsymbol{x}}^r)^2}$ become rather complex. For this reason the author prefers to present them in appendix D.

The central control point of the Bézier triangle is computed as an average of three candidate points (see equation (5.17)). The derivatives of the central control point will then be the average of the candidate points' derivatives.

$$\frac{\partial \boldsymbol{p}^{123}}{\partial \tilde{\boldsymbol{x}}^r} = \frac{1}{3}\sum_{i=1}^{3}\frac{\partial \boldsymbol{p}^{0i}}{\partial \tilde{\boldsymbol{x}}^r} \tag{7.27}$$

$$\frac{\partial^2 \boldsymbol{p}^{123}}{(\partial \tilde{\boldsymbol{x}}^r)^2} = \frac{1}{3}\sum_{i=1}^{3}\frac{\partial^2 \boldsymbol{p}^{0i}}{(\partial \tilde{\boldsymbol{x}}^r)^2} \tag{7.28}$$

Each of the candidate points is determined by solving a linear system of 3 equations. To compute their derivatives, an analogous procedure as the one used for the control points in the contour can be used. Therefore, we will derive by parts equation (5.18) and solve for $\dfrac{\partial \boldsymbol{p}^{0i}}{\partial \tilde{\boldsymbol{x}}^r}$ to obtain:

$$\frac{\partial \boldsymbol{p}^{0i}}{\partial \tilde{\boldsymbol{x}}^r} = \frac{\partial p^{0i}_{(m)}}{\partial x^h_{(v)}} = A^{0i-1}_{p(ml)}\left(\frac{\partial b^{0i}_{p(l)}}{\partial x^h_{(v)}} - \frac{\partial A^{0i}_{p(ln)}}{\partial x^h_{(v)}} p^{0i}_{(n)}\right) \tag{7.29}$$
$$\forall\, i,l,m,n,v = 1 \div 3 \qquad \forall\, h = 1 \div r_{total}$$

$$\boldsymbol{A}^{0i}_{\boldsymbol{p}} \cdot \frac{\partial \boldsymbol{p}^{0i}}{\partial \tilde{\boldsymbol{x}}^r} = \frac{\partial \boldsymbol{b}^{0i}_{\boldsymbol{p}}}{\partial \tilde{\boldsymbol{x}}^r} - \frac{\partial \boldsymbol{A}^{0i}_{\boldsymbol{p}}}{\partial \tilde{\boldsymbol{x}}^r} \cdot \boldsymbol{p}^{0i} \tag{7.30}$$

Deriving again by parts equation (7.30) and solving for $\dfrac{\partial^2 \boldsymbol{p}^{0i}}{(\partial \tilde{\boldsymbol{x}}^r)^2}$ we obtain:

$$\frac{\partial^2 \boldsymbol{p}^{0i}}{(\partial \tilde{\boldsymbol{x}}^r)^2} = \frac{\partial^2 p^{0i}_{(m)}}{\partial x^h_{(v)}\,\partial x^s_{(w)}} = A^{0i-1}_{p(ml)}\left(\frac{\partial^2 b^{0i}_{p(l)}}{\partial x^h_{(v)}\,\partial x^s_{(w)}} - \frac{\partial^2 A^{0i}_{p(ln)}}{\partial x^h_{(v)}\,\partial x^s_{(w)}} p^{0i}_{(n)} - \frac{\partial A^{0i}_{p(ln)}}{\partial x^h_{(v)}}\frac{\partial p^{0i}_{(n)}}{\partial x^s_{(w)}} - \frac{\partial A^{0i}_{p(ln)}}{\partial x^s_{(w)}}\frac{\partial p^{0i}_{(n)}}{\partial x^h_{(v)}}\right) \tag{7.31}$$
$$\forall\, i,l,m,n,v,w = 1 \div 3 \qquad \forall\, h,s = 1 \div r_{total}$$

The expressions for $\dfrac{\partial \boldsymbol{A}^{0i}_{\boldsymbol{p}}}{\partial \tilde{\boldsymbol{x}}^r}$, $\dfrac{\partial^2 \boldsymbol{A}^{0i}_{\boldsymbol{p}}}{(\partial \tilde{\boldsymbol{x}}^r)^2}$, $\dfrac{\partial \boldsymbol{b}^{0i}_{\boldsymbol{p}}}{\partial \tilde{\boldsymbol{x}}^r}$ and $\dfrac{\partial^2 \boldsymbol{b}^{0i}_{\boldsymbol{p}}}{(\partial \tilde{\boldsymbol{x}}^r)^2}$ become rather complex. For this reason the author prefers to present them in appendix D.

## 7.2 Efficient and geometrically accurate through-the-thickness pre-integration

Equations (7.3) and (7.4) are to be integrated numerically. The author proposes to decouple the through-the-thickness integration ($\int_{-\frac{1}{2}}^{\frac{1}{2}}$) from the area integration ($\int_0^1 \int_0^{1-\xi}$).

Regarding the integration over the area of the triangle, the first thing to figure out is the order of integration necessary. Since the shape functions ($N$) are cubic, the deformation has a quadratic description. Therefore, the internal virtual energy is being described with fourth order functions. The numerical quadrature that needs the least number of integration points

for a fourth order polynomial is a Gaussian quadrature, which needs 6 integration points over the triangle. The author uses the quadrature obtained by Dunavant in [33]. There are other authors who have also obtained fourth order quadratures for the triangle. The reader can refer to the references in [29] for a complete review on numerical quadratures on different domains.

The beauty of Dunavant's quadrature is that it is symmetric, all the weights are positive and all the points are inside the triangle (see table 7.1).

Table 7.1: Weights and coordinates for fourth order integration using Gaussian quadrature over a triangle.

| Gauss point | Weight | Parametric coordinates |
|---|---|---|
| 1 | $w_1$ | $(\alpha_1, \beta_1)$ |
| 2 | $w_1$ | $(\beta_1, \alpha_1)$ |
| 3 | $w_1$ | $(\beta_1, \beta_1)$ |
| 4 | $w_2$ | $(\alpha_2, \beta_2)$ |
| 5 | $w_2$ | $(\beta_2, \alpha_2)$ |
| 6 | $w_2$ | $(\beta_2, \beta_2)$ |
| $w_1 = 0.223381589678011$ | | |
| $\alpha_1 = 0.108103018168070$ | | |
| $\beta_1 = 0.445948490915965$ | | |
| $w_2 = 0.109951743655322$ | | |
| $\alpha_2 = 0.816847572980459$ | | |
| $\beta_2 = 0.091576213509771$ | | |

Regarding the integration through the thickness of the triangle, there are two options. The first one, is to also perform a Gaussian integration through the thickness and multiply each point in the triangle quadrature by the number of evaluation points through the thickness. The problem with this approach is that at least 5 evaluation points in the thickness direction are necessary. This implies a total of not less than 30 evaluation points. The number of evaluation points is a direct measure of the cost of building the stiffness matrix of the element. Fortunately, the decision for developing a total Lagrangian formulation comes in very handy. As it has been shown in equations (6.59), (6.63), (6.67), (7.5) and (7.10); the tensors that conform the material stiffness matrix and the geometric stiffness matrix in equations (7.3) and (7.4) can be decomposed into constant tensors in the thickness direction and scalar factors that are affected by the thickness coordinate $\zeta$. Furthermore, these scalar factors that have variation in the thickness direction, are defined in the reference configuration and do not change in the current configuration. Therefore, the author follows what other scholars have done for other elements [120][1] and proposes a through-the-thickness pre-integration of all the terms, which can

[1]Stanley is regarded as the first scholar to have successfully introduced this kind of decomposition in the through-the-thickness direction in order to pre-integrate the stiffness matrix. Oñate also cites different authors who have followed this approach, see [93, p. 640] and references therein.

be pre-computed in the reference configuration. To the author's knowledge, however, nobody has performed this through-the-thickness pre-integration taking into account all the higher order terms of the Jacobian and the deformation tensors for a rotation-free shell element[2]. This approach has a signifficant computational advantage over the Updated Lagrangian formulations, as the preintegration is performed only once, instead of performing it at every time-step or load-step. Performing a little bit of arithmetic, all of this results in the following expressions for the material and geometric stiffness matrices.

$$\boldsymbol{K}_M = \sum_{\forall\,\alpha=\{m,b,n\}} \sum_{\forall\,\beta=\{m,b,n\}} \boldsymbol{K}_{M\alpha\beta} \tag{7.32}$$

$$\boldsymbol{K}_G = \sum_{\forall\,\alpha=\{m,b,n\}} \sum_{\forall\,\beta=\{m,b,n\}} \boldsymbol{K}_{G\alpha\beta} \tag{7.33}$$

$$\boldsymbol{K}_{M\alpha\beta} = \int_0^1 \int_0^{1-\xi} \boldsymbol{B}_\alpha^T \cdot \hat{\boldsymbol{D}}_{\alpha\beta} \cdot \boldsymbol{B}_\beta \,\mathrm{d}\xi\,\mathrm{d}\eta \tag{7.34}$$

$$\boldsymbol{K}_{G\alpha\beta} = \int_0^1 \int_0^{1-\xi} \frac{\partial \boldsymbol{B}_\alpha^T}{\partial \tilde{\boldsymbol{x}}^r} \cdot (\hat{\boldsymbol{D}}_{\alpha\beta} \cdot \boldsymbol{g}_\beta - \boldsymbol{\delta}_{\alpha\beta} \cdot \hat{\boldsymbol{D}}_\beta)\,\mathrm{d}\xi\,\mathrm{d}\eta \tag{7.35}$$

$$\hat{\boldsymbol{D}}_{\alpha\beta} = \sum_{l=1}^{\sharp layers} (\lambda_l)^{\kappa+\chi}\, \hat{\boldsymbol{D}}^l_{\alpha\beta} \tag{7.36}$$

$$\hat{\boldsymbol{D}}_{\beta} = \sum_{l=1}^{\sharp layers} (\lambda_l)^{\chi}\, \hat{\boldsymbol{D}}^l_{\beta} \tag{7.37}$$

$$\kappa = \begin{cases} 0 & \text{if } \alpha = m, \\ 1 & \text{if } \alpha = b, \\ 2 & \text{if } \alpha = n. \end{cases} \qquad \chi = \begin{cases} 0 & \text{if } \beta = m, \\ 1 & \text{if } \beta = b, \\ 2 & \text{if } \beta = n. \end{cases} \tag{7.38}$$

Notice that in equations (7.34) and (7.35), all the terms that do not depend on the thickness coordinate $\zeta$ have been taken out of the through-the-thickness integral. All the other terms, including those that are constant in the current configuration have been condensed into the $\hat{\boldsymbol{D}}^l_{\alpha\beta}$ tensors and the $\hat{\boldsymbol{D}}^l_{\beta}$ vectors; which can be computed in the reference configuration once and for all in the simulation/analysis if the material is linear elastic. In the case of non-linear behavior of the materials (e.g. plasticity, damage, etc.) these tensors need to be reevaluated in the current configuration; but the integrals are not reevaluated.

[2]Yang et al. [141] explain that many shell elements are based on moderate rotation assumptions. Since rotations lead to rational expressions that imply complicated derivatives, researchers have sought for ways to circumvent those rational expressions and use aproximated polynomial expressions instead [9, pp. 545–549]. In addition, in order to compensate for the errors introduced by the approximations of the large rotations, most finite element developers favored the Updated Lagrangian formulation, this was also the reason behind the development of the co-rotational shell elements [138].

Another important consideration has been introduced. Since there can be different materials in the thickness direction, the through-the-thickness integral has been split into a summation over the different layers of the laminate. The stretch factor ($\lambda$) is taken into account evaluating it once per each material layer. So the author considers that it is sufficient to consider a piece-wise constant variation of the stretch factor through the thickness.

$$\hat{\boldsymbol{D}}^l_{mm} = \frac{h}{4}\sum_{i=0}^{2}\sum_{j=0}^{2} h^{i+j}\,\boldsymbol{Q}_i^T\cdot\boldsymbol{D}^l\cdot\boldsymbol{Q}_j\cdot\left(\int_{\zeta_{l-1}}^{\zeta_l}\frac{\zeta^{i+j}}{(\hat{J})^3}\,\mathrm{d}\zeta\right) \tag{7.39}$$

$$\hat{\boldsymbol{D}}^l_{mb} = \frac{h^2}{2}\sum_{i=0}^{2}\sum_{j=0}^{2} h^{i+j}\,\boldsymbol{Q}_i^T\cdot\boldsymbol{D}^l\cdot\boldsymbol{Q}_j\cdot\left(\int_{\zeta_{l-1}}^{\zeta_l}\frac{\zeta^{i+j+1}}{(\hat{J})^3}\,\mathrm{d}\zeta\right) \tag{7.40}$$

$$\hat{\boldsymbol{D}}^l_{mn} = \frac{h^3}{4}\sum_{i=0}^{2}\sum_{j=0}^{2} h^{i+j}\,\boldsymbol{Q}_i^T\cdot\boldsymbol{D}^l\cdot\boldsymbol{Q}_j\cdot\left(\int_{\zeta_{l-1}}^{\zeta_l}\frac{\zeta^{i+j+2}}{(\hat{J})^3}\,\mathrm{d}\zeta\right) \tag{7.41}$$

$$\hat{\boldsymbol{D}}^l_{bb} = 4\,\hat{\boldsymbol{D}}^l_{mn} \tag{7.42}$$

$$\hat{\boldsymbol{D}}^l_{bn} = \frac{h^2}{2}\sum_{i=0}^{2}\sum_{j=0}^{2} h^{i+j}\,\boldsymbol{Q}_i^T\cdot\boldsymbol{D}^l\cdot\boldsymbol{Q}_j\cdot\left(\int_{\zeta_{l-1}}^{\zeta_l}\frac{\zeta^{i+j+3}}{(\hat{J})^3}\,\mathrm{d}\zeta\right) \tag{7.43}$$

$$\hat{\boldsymbol{D}}^l_{nn} = \frac{h^5}{4}\sum_{i=0}^{2}\sum_{j=0}^{2} h^{i+j}\,\boldsymbol{Q}_i^T\cdot\boldsymbol{D}^l\cdot\boldsymbol{Q}_j\cdot\left(\int_{\zeta_{l-1}}^{\zeta_l}\frac{\zeta^{i+j+4}}{(\hat{J})^3}\,\mathrm{d}\zeta\right) \tag{7.44}$$

$$\hat{\boldsymbol{D}}^l_{m} = \frac{h}{4}\sum_{i=0}^{2} h^{i}\,\boldsymbol{Q}_i^T\cdot\boldsymbol{D}^l\cdot\boldsymbol{I}\cdot\left(\int_{\zeta_{l-1}}^{\zeta_l}\frac{\zeta^{i}}{\hat{J}}\,\mathrm{d}\zeta\right) \tag{7.45}$$

$$\hat{\boldsymbol{D}}^l_{b} = \frac{h^2}{2}\sum_{i=0}^{2} h^{i}\,\boldsymbol{Q}_i^T\cdot\boldsymbol{D}^l\cdot\boldsymbol{I}\cdot\left(\int_{\zeta_{l-1}}^{\zeta_l}\frac{\zeta^{i+1}}{\hat{J}}\,\mathrm{d}\zeta\right) \tag{7.46}$$

$$\hat{\boldsymbol{D}}^l_{n} = \frac{h^3}{4}\sum_{i=0}^{2} h^{i}\,\boldsymbol{Q}_i^T\cdot\boldsymbol{D}^l\cdot\boldsymbol{I}\cdot\left(\int_{\zeta_{l-1}}^{\zeta_l}\frac{\zeta^{i+2}}{\hat{J}}\,\mathrm{d}\zeta\right) \tag{7.47}$$

$$J = \det\boldsymbol{J} = h\,J_0 + h^2\,\zeta\,J_1 + h^3\,\zeta^2\,J_2 \tag{7.48}$$

$$\hat{J} = \frac{J}{h} = J_0 + h\,\zeta\,J_1 + h^2\,\zeta^2\,J_2 \tag{7.49}$$

$$J_0 = \left|\begin{matrix}\uparrow & \uparrow & \uparrow\\ \boldsymbol{P}\cdot\boldsymbol{L}_\xi & \boldsymbol{P}\cdot\boldsymbol{L}_\eta & \boldsymbol{\mathcal{N}}\\ \downarrow & \downarrow & \downarrow\end{matrix}\right| \tag{7.50}$$

$$J_1 = \left|\begin{matrix}\uparrow & \uparrow & \uparrow\\ \boldsymbol{P}\cdot\boldsymbol{L}_\xi & \boldsymbol{\mathcal{N}}_{,\eta} & \boldsymbol{\mathcal{N}}\\ \downarrow & \downarrow & \downarrow\end{matrix}\right| + \left|\begin{matrix}\uparrow & \uparrow & \uparrow\\ \boldsymbol{P}\cdot\boldsymbol{L}_\eta & \boldsymbol{\mathcal{N}}_{,\xi} & \boldsymbol{\mathcal{N}}\\ \downarrow & \downarrow & \downarrow\end{matrix}\right| \tag{7.51}$$

$$J_2 = \left|\begin{matrix}\uparrow & \uparrow & \uparrow\\ \boldsymbol{\mathcal{N}}_{,\xi} & \boldsymbol{\mathcal{N}}_{,\eta} & \boldsymbol{\mathcal{N}}\\ \downarrow & \downarrow & \downarrow\end{matrix}\right| \tag{7.52}$$

Where $\boldsymbol{D}^l$ denotes the constitutive tensor defined in equation (6.4) for the material layer $l$. All the other superindices in the above equations

mean exponents. The limits of the thickness integrals are the bottom and top coordinates of each layer $l$. Thus, $\zeta_0 = -\frac{1}{2}$, and $\zeta_{\sharp layers} = \frac{1}{2}$.

Now, the advantage of these expressions is that all the through-the-thickness integrals contain only scalar values and are completely defined in the reference configuration. There are in total 14 $(9 + 5)$ scalar integrals to perform. The integrands are rational, because the expression of the Jacobian $(J)$ is polynomic. However, most authors perform a Taylor series expansion on the jacobian $J$ in the thickness direction[3] —dropping the quadratic terms in the thickness direction[4]— and take only into account the maximum exponent in the numerators to evaluate the polynomial order of the integrands. The maximum exponent in the numerator is 8. This is why the author suggests using a 5 points Gaussian quadrature to numerically evaluate the integrals of the shell in the thickness direction. However, because these expressions are so cheap, it is possible to select an arbitrary precision for the thickness integrals at a marginal increment of the computational cost. The author suggests to use at least 5 integration points per material layer in the laminate.

We can now take advantage of all this notation and perform also a through-the-thickness pre-integration of the equivalent internal nodal loads:

$$\boldsymbol{F}_e^{int} = \sum_{\forall\, \alpha=\{m,b,n\}} \sum_{\forall\, \beta=\{m,b,n\}} \boldsymbol{F}_{\alpha\beta}^{int} \tag{7.53}$$

$$\boldsymbol{F}_{\alpha\beta}^{int} = \int_0^1 \int_0^{1-\xi} \boldsymbol{B}_\alpha^T \cdot (\hat{\boldsymbol{D}}_{\alpha\beta} \cdot \boldsymbol{g}_\beta - \boldsymbol{\delta}_{\alpha\beta} \cdot \hat{\boldsymbol{D}}_\beta)\, \mathrm{d}\xi\, \mathrm{d}\eta \tag{7.54}$$

## 7.3 Tangent loads matrix

The tangent loads matrix stems from the linearization of the equivalent external nodal loads.

$$\begin{aligned}
\frac{\partial \boldsymbol{F}_e^{ext}}{\partial \tilde{\boldsymbol{x}}^r} = \frac{\partial}{\partial \tilde{\boldsymbol{x}}^r} \Bigg[ \iiint_{V_e} \left(\frac{\partial \boldsymbol{x}}{\partial \tilde{\boldsymbol{x}}^r}\right)^T \cdot \boldsymbol{q}_V \,\mathrm{d}V + \iint_{S_e} \left(\frac{\partial \boldsymbol{x}}{\partial \tilde{\boldsymbol{x}}^r}\right)^T \cdot \boldsymbol{q}_S \,\mathrm{d}S + \\
+ \int_{\Gamma_e} \left(\frac{\partial \boldsymbol{x}}{\partial \tilde{\boldsymbol{x}}^r}\right)^T \cdot \boldsymbol{q}_\Gamma \,\mathrm{d}\Gamma + \tilde{\boldsymbol{q}}^r \Bigg] = \\
= \underbrace{\frac{\partial}{\partial \tilde{\boldsymbol{x}}^r} \iiint_{\Omega^0} \frac{\partial \boldsymbol{x}^T}{\partial \tilde{\boldsymbol{x}}^r} \cdot \boldsymbol{q}_V^0 \,\mathrm{d}\Omega^0}_{\boldsymbol{H}_{V^0}} + \underbrace{\frac{\partial}{\partial \tilde{\boldsymbol{x}}^r} \iiint_{\Omega} \frac{\partial \boldsymbol{x}^T}{\partial \tilde{\boldsymbol{x}}^r} \cdot \boldsymbol{q}_V \,\mathrm{d}\Omega}_{\boldsymbol{H}_V} + \\
+ \underbrace{\frac{\partial}{\partial \tilde{\boldsymbol{x}}^r} \iint_{\partial\Omega^0} \frac{\partial \boldsymbol{x}^T}{\partial \tilde{\boldsymbol{x}}^r} \cdot \boldsymbol{q}_S^0 \,\mathrm{d}S^0}_{\boldsymbol{H}_{S^0}} + \underbrace{\frac{\partial}{\partial \tilde{\boldsymbol{x}}^r} \iint_{\partial\Omega} \frac{\partial \boldsymbol{x}^T}{\partial \tilde{\boldsymbol{x}}^r} \cdot \boldsymbol{q}_S \,\mathrm{d}S}_{\boldsymbol{H}_S} +
\end{aligned}$$

[3] Also a Taylor series expansion or other approximations of the shell shifter are common in the literature on shell finite elements [12, p. 94]

[4] Büchter and Ramm in [18, pp. 44–46] describe the different proposed approaches to perform the through-the-thickness integration in continuum based (degenerated) shell elements. Bischoff et al. in [12, p. 101] further explain that using an exact shifter ($\boldsymbol{A}$ in our case) yields better results than using an aproximated shifter that facilitates performing an analytic integration through-the-thickness.

$$+\underbrace{\frac{\partial}{\partial\tilde{\boldsymbol{x}}^r}\int_{\partial^2\Omega^0}\frac{\partial\boldsymbol{x}^T}{\partial\tilde{\boldsymbol{x}}^r}\cdot\boldsymbol{q}_\Gamma^0\,\mathrm{d}\Gamma^0}_{\boldsymbol{H}_{\Gamma^0}}+\underbrace{\frac{\partial}{\partial\tilde{\boldsymbol{x}}^r}\int_{\partial^2\Omega}\frac{\partial^2\boldsymbol{x}^T}{\partial\tilde{\boldsymbol{x}}^r}\cdot\boldsymbol{q}_\Gamma\,\mathrm{d}\Gamma}_{\boldsymbol{H}_{\Gamma}} \tag{7.55}$$

Each of the tangent matrices above can be developed for each particular case considered. Here, the author will only develop as an example the self-weight loads (equation (7.56)), which are a case of loads defined over the volume in the reference configuration, and then two different surface loads. One for dead loads (equation (7.57)), which are also defined in the reference configuration. And another one for follower pressure loads (equation (7.58)), which are defined in the deformed configuration and the direction changes with the geometry.

$$\begin{aligned}\boldsymbol{H}_{V^0}&=\frac{\partial}{\partial\tilde{\boldsymbol{x}}^r}\iiint_{\Omega^0}\rho\,g\,\boldsymbol{e}_3^T\cdot\frac{\partial\boldsymbol{x}}{\partial\tilde{\boldsymbol{x}}^r}\,\mathrm{d}\Omega^0=\int_0^1\int_0^{1-\xi}\int_{-\frac{1}{2}}^{\frac{1}{2}}\rho\,g\,\boldsymbol{e}_3^T\cdot\frac{\partial^2\boldsymbol{x}}{(\partial\tilde{\boldsymbol{x}}^r)^2}J\,\mathrm{d}\xi\,\mathrm{d}\eta\,\mathrm{d}\zeta=\\&=\int_0^1\int_0^{1-\xi}g\,\boldsymbol{e}_3^T\cdot\frac{\partial^2\boldsymbol{p}}{(\partial\tilde{\boldsymbol{x}}^r)^2}\cdot N\sum_{i=0}^{2}\left[h^{i+1}J_i^0\sum_{l=1}^{\sharp layers}\left(\rho_l\int_{\zeta_{l-1}}^{\zeta_l}\zeta^i\,\mathrm{d}\zeta\right)\right]\mathrm{d}\xi\,\mathrm{d}\eta+\\&+\int_0^1\int_0^{1-\xi}g\,\boldsymbol{e}_3^T\cdot\frac{\partial^2\boldsymbol{n}}{(\partial\tilde{\boldsymbol{x}}^r)^2}\sum_{i=0}^{2}\left[h^{i+2}J_i^0\sum_{l=1}^{\sharp layers}\left(\lambda_l\rho_l\int_{\zeta_{l-1}}^{\zeta_l}\zeta^{i+1}\,\mathrm{d}\zeta\right)\right]\mathrm{d}\xi\,\mathrm{d}\eta\end{aligned} \tag{7.56}$$

$$\begin{aligned}\boldsymbol{H}_{S^0}&=\frac{\partial}{\partial\tilde{\boldsymbol{x}}^r}\iint_{\partial\Omega^0}\frac{\partial\bar{\boldsymbol{x}}^T}{\partial\tilde{\boldsymbol{x}}^r}\cdot\boldsymbol{q}_S^0\,\mathrm{d}S^0=\int_0^1\int_0^{1-\xi}\frac{\partial^2\bar{\boldsymbol{x}}^T}{(\partial\tilde{\boldsymbol{x}}^r)^2}\cdot\boldsymbol{q}_S^0J_0\,\mathrm{d}\xi\,\mathrm{d}\eta=\\&=\int_0^1\int_0^{1-\xi}N^T\cdot\frac{\partial^2\boldsymbol{p}^T}{(\partial\tilde{\boldsymbol{x}}^r)^2}\cdot\boldsymbol{q}_S^0J_0\,\mathrm{d}\xi\,\mathrm{d}\eta\end{aligned} \tag{7.57}$$

$$\begin{aligned}\boldsymbol{H}_S&=\frac{\partial}{\partial\tilde{\boldsymbol{x}}^r}\iint_{\partial\Omega}p\frac{\partial\bar{\boldsymbol{x}}^T}{\partial\tilde{\boldsymbol{x}}^r}\cdot\boldsymbol{n}\,\mathrm{d}S=\\&=\int_0^1\int_0^{1-\xi}p\left(\frac{\partial^2\bar{\boldsymbol{x}}^T}{(\partial\tilde{\boldsymbol{x}}^r)^2}\cdot\boldsymbol{n}+\underbrace{\frac{\partial\bar{\boldsymbol{x}}^T}{\partial\tilde{\boldsymbol{x}}^r}\cdot\frac{\partial\boldsymbol{n}}{\partial\tilde{\boldsymbol{x}}^r}}_{\text{non-symmetric}}\right)J_0\,\mathrm{d}\xi\,\mathrm{d}\eta\end{aligned} \tag{7.58}$$

The corresponding equivalent external nodal loads are:

$$\begin{aligned}\boldsymbol{F}_{V^0}^{ext}&=\int_0^1\int_0^{1-\xi}g\,\boldsymbol{e}_3^T\cdot\frac{\partial\boldsymbol{p}}{\partial\tilde{\boldsymbol{x}}^r}\cdot N\sum_{i=0}^{2}\left[h^{i+1}J_i^0\sum_{l=1}^{\sharp layers}\left(\rho_l\int_{\zeta_{l-1}}^{\zeta_l}\zeta^i\,\mathrm{d}\zeta\right)\right]\mathrm{d}\xi\,\mathrm{d}\eta+\\&+\int_0^1\int_0^{1-\xi}g\,\boldsymbol{e}_3^T\cdot\frac{\partial\boldsymbol{n}}{\partial\tilde{\boldsymbol{x}}^r}\sum_{i=0}^{2}\left[h^{i+2}J_i^0\sum_{l=1}^{\sharp layers}\left(\lambda_l\rho_l\int_{\zeta_{l-1}}^{\zeta_l}\zeta^{i+1}\,\mathrm{d}\zeta\right)\right]\mathrm{d}\xi\,\mathrm{d}\eta\end{aligned} \tag{7.59}$$

$$\boldsymbol{F}_{S^0}^{ext}=\int_0^1\int_0^{1-\xi}(\boldsymbol{q}_S^0)^T\cdot\frac{\partial\boldsymbol{p}}{\partial\tilde{\boldsymbol{x}}^r}\cdot N\,J_0\,\mathrm{d}\xi\,\mathrm{d}\eta \tag{7.60}$$

$$\boldsymbol{F}_S^{ext}=\int_0^1\int_0^{1-\xi}p\,\boldsymbol{n}^T\cdot\frac{\partial\bar{\boldsymbol{x}}}{\partial\tilde{\boldsymbol{x}}^r}J_0\,\mathrm{d}\xi\,\mathrm{d}\eta \tag{7.61}$$

## 7.4 Summary

This chapter presents the explicit expressions to construct the tangent stiffness matrix of the BEST element. Taking advantage of the decomposition of the Green-Lagrange tensor presented in the previous chapter and the Jacobian of the element, the author introduces a through-the-thickness pre-integration of the terms of the stiffness matrix (including the higher order terms). The formulæ are valid also in the case of a multi-layered shell. To the author's knowledge this is a novel contribution of this thesis.

The expressions for some of the possible tangent loads matrices are also presented (self-weight loads, dead loads, and follower pressure loads).

The equations presented in this chapter are complemented —for the sake of completeness— with the expressions needed of all the derivatives in appendix D.

# Chapter 8

# On the integration order of the element

SELDOM A DEVELOPER QUESTIONS the integration order of a finite element. This is because the knowledge of isoparametric elements is quite deep and the integration criteria of the stiffness matrix are clear. Nevertheless, given the specificities of the formulation in the present development it is reasonable to ponder about the integration order required for the element. Let's consider the different options:

- The input information is linear. Linear integration?
- The approximation order of the improved geometry is cubic. Quartic integration?
- The functions stemming from the linearization of the normalization of the normal vectors are rational. What order shall be applied? In order to determine the corresponding integration order we shall develop the Taylor series of the expression of the stiffness matrix and determine how many terms of the series are relevant. But the Taylor series expansions are only local and writing the expansion would be a very complex task. Even if we did, determining which are the relevant terms wouldn't be an easy call.

Therefore, the need arises to determine how many Gauss points are required when performing the numerical integrations over the element. Using too many points will result in an increased computational cost of the computations for the element without increasing the precision. Using too few points can lead to unpredictable results (i.e. loosing the full rank of the stiffness matrix) or simply a loss in precision that makes the development of the new element totally worthless.

The methodology to determine the order of the quadrature has been to identify the different options available and evaluate them using a series of representative cases. The quadratures considered are:

**1 Gauss point:** This quadrature corresponds to a linear integration considering that the information of the shape functions —after deriving them to describe the element's deformation— is barely constant.

**3 Gauss points:** This quadrature corresponds to a quadratic integration. This would be the right choice if the functions that describe the deformation of the element contain linear information. As a result, the integrand would be a quadratic function.

**4 Gauss points:** This quadrature corresponds to a cubic integration. This is a very rare quadrature in triangular finite elements because it's order is not even. Nevertheless, the peculiarities of the present development make it worth considering it in the study. Furthermore, in the case of resulting adequate, it is the quadrature that marginally requires the least number of additional evaluations with respect to the lower order quadratures.

**6 Gauss points:** This quadrature corresponds to a quartic integration. This is the last option to consider because it would imply that the information contained in the element's shape functions is cubic at all effects. As a consequence, the functions describing the deformation would be quadratic and the integrands would be quartic functions.

## 8.1 Bending dominant cases

This section includes 2 cases of structures under such loading that the main deformation energy corresponds to the bending deformation. The first case is that of a simply supported slender beam modeled as a shell. The second is a classic verification example for shell elements: a hemisphere subjected to opposite point loads.

### 8.1.1 Slender beam

Firstly, we show the analysis of a simple slender beam. In linear analysis, this configuration only generates bending stresses. The dimensions and the magnitude of the load are defined in such way that the deflection at the center is 1. $L = 10, b = 1, t = 0.01, E = 2.5 \cdot 10^{11}, \nu = 0.3, q = 160$.

The author does not recall big differences amongst the different quadratures. The order of convergence is $\mathcal{O} \propto h^{1/2}$ in all cases. This result will be further discussed in the Summary in section 8.5.

### 8.1.2 Hemisphere with point loads

The second case consists on the already classical example of a hemispheric shell with an 18° hole at the center. The hemisphere is subjected to two pairs of diametrically opposed loads. The displacement of the points loaded is 0.093 for the following values: $\phi = 20, t = 0.04, E = 6.825 \cdot 10^7, \nu = 0.3, P = 2$.

It appears that using fewer Gauss points improves convergence. However, in all cases the convergence order is $\mathcal{O} \propto h$. Notwithstanding this fact, the author recalls the apparent better precision obtained with a quadrature of a single Gauss point. In fact, the precision achieved with a single Gauss point is an order of magnitude better than that obtained with any other quadrature considered.

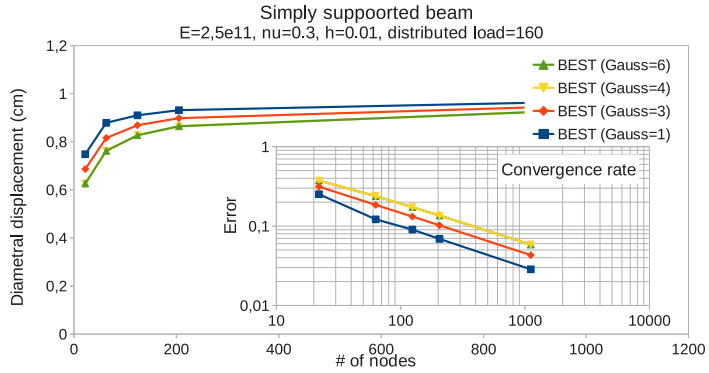


Figure 8.1: Comparison of h-convergence using structured meshes and different numerical quadratures for a simply supported beam.

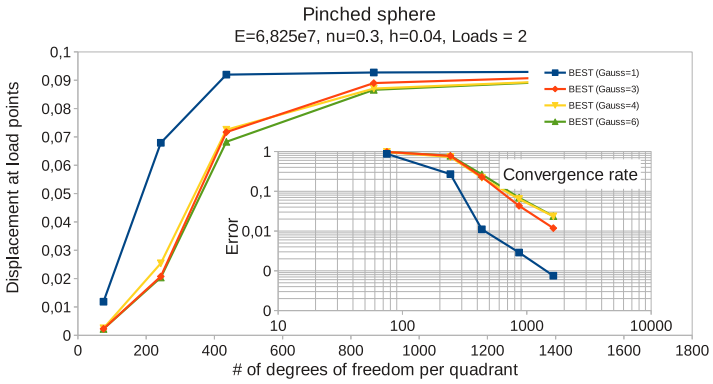


Figure 8.2: Comparison of h-convergence using structured meshes and different numerical quadratures for a pinched hemisphere.

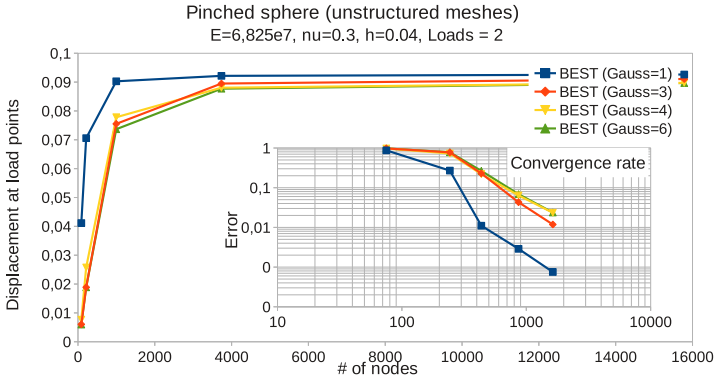


Figure 8.3: Comparison of h-convergence using unstructured meshes and different numerical quadratures for a pinched hemisphere.

## 8.2 Membrane dominant cases

Next we present 2 cases of structures subject to such loading that the main deformation energy corresponds to membrane deformation. The first case is that of a very thin-walled cylinder under internal pressure. The second case is that of a roof in the form of a parabolic cylinder simply supported along its two generatrices and subjected to self-weight loading.

### 8.2.1 Cylinder subject to internal pressure

The motivation for choosing this case stems from the desire to observe the virtues of the BEST element. That is, a case where the description using the cubic Bézier functions for the element's geometry plays an important role in the out-of-plane deformation of the element. For this reason it is important to choose an example with curved geometry yet subject solely to membrane stresses and not to bending stresses. The cylinder is a very well suited geometry to study using structured meshes. In order to avoid activating the bending energy that would experiment the cylinder, its thickness is restricted to an extremely small value. Similarly to the case of the simply supported beam, the parameters of the example have been selected in such way that the radial enlargement is 1. $L = 20, \phi = 10, t = 0.0005, E = 10^8, \nu = 0.3, p = 1000$.

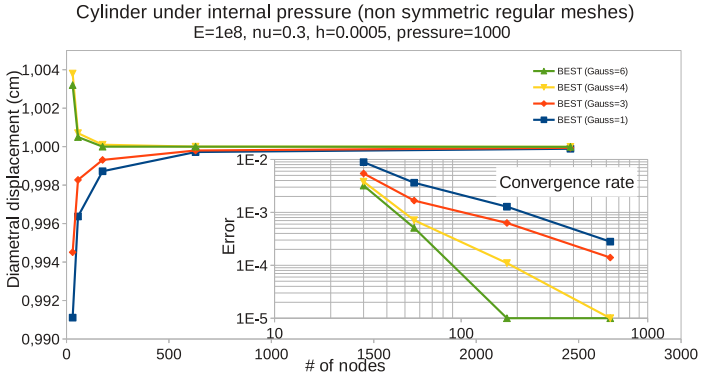


Figure 8.4: Comparison of h-convergence using non-symmetric structured meshes and different numerical quadratures for a thin-walled cylinder.

The observation of the results of this case shows it takes full advantage of the cubic formulation of the BEST element. Using the quartic quadrature of 6 points, corresponding to the theoretical quadrature for an element with cubic shape functions, yields convergence of order $\mathcal{O} \propto h^3$. Using a cubic quadrature of 4 points yields convergence of order $\mathcal{O} \propto h^2$. And using the quadratures quadratic and linear, of 3 and 1 point respectively, yields convergence of order $\mathcal{O} \propto h$.

This is a very important result, as it demonstrates it is possible to achieve cubic convergence out of linear information. The mechanism to accomplish it, unlike other methods based on the construction of macro-

elements, uses the information of the neighboring elements in order to build an element of greater order.

### 8.2.2 Parabolic roof

This case differs slightly from the idealism of the previous case. Now, the roof's self-weight makes the structure experience tractions mainly. However, the real funicular shape of the load shall be a catenary instead of a parabola. Therefore some bending stresses appear, although the main deformation mode is membrane. $L = 50, a = 20, c = 10, t = 0.05, E = 10^8, \nu = 0.0, q = 1000$.

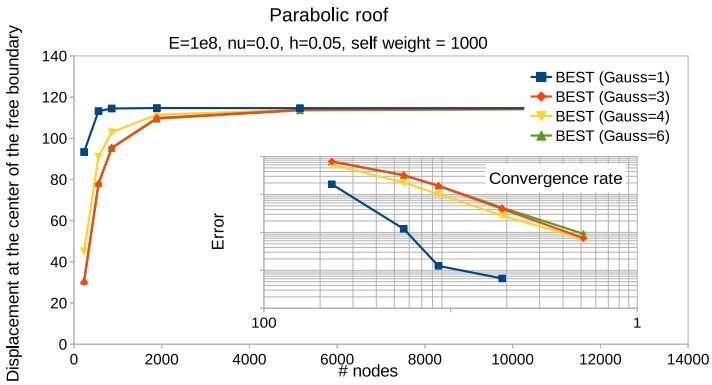


Figure 8.5: Comparison of h-convergence using non-symmetric structured meshes and different numerical quadratures for a parabolic roof.

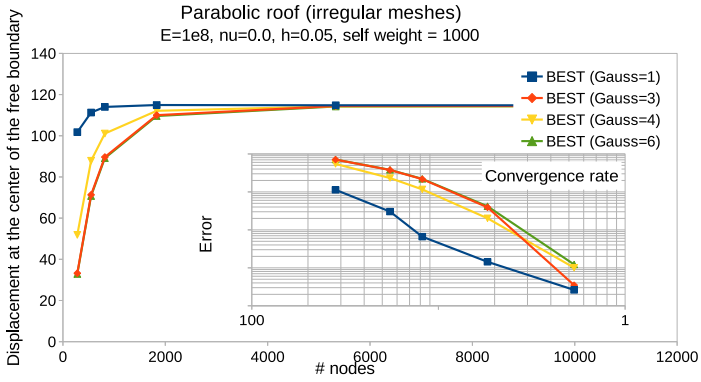


Figure 8.6: Comparison of h-convergence using unstructured meshes and different numerical quadratures for a parabolic roof.

This example shows that when introducing some bending, the excellent convergence properties verified in the previous example are lost, and the quadrature with 1 Gauss point is again the best one. When using structured meshes, the quadrature with 1 Gauss point exhibits convergence of

order $\mathcal{O} \propto h^{5/2}$, while the other quadratures show convergence rates of order $\mathcal{O} \propto h^{3/2}$. In the case of unstructured meshes the convergence properties become reversed and now the quadrature with 1 Gauss point has convergence of order $\mathcal{O} \propto h^2$ while all the other cases improve and now exhibit convergences of order $\mathcal{O} \propto h^{5/2}$. Nevertheless, the quadrature with 1 Gauss point seems to have more precision. The quadrature using 4 Gauss points also obtains notable results with respect to the other quadratures that do not use the triangle's barycenter as an evaluation point in the quadrature. Therefore, it seems as if the barycenter of the triangle has some special property when calculating the bending of the element.

## 8.3 In-plane shear dominant cases

Finally, this section presents 2 cases of structures whose loading makes in-plane shear the main deformation mode. The first case is that of a thick beam modeled with shell elements. The second case is that of a cylinder under uniform torsion.

### 8.3.1 Thick beam

This is the most trivial case to activate the element's in-plane shear. Consists on a cantilevered deep beam subject to a uniform force along its free end. The reference solution is 0.35533.

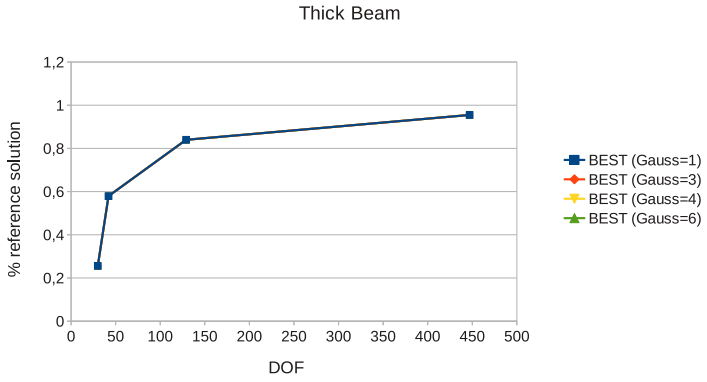


Figure 8.7: Comparison of h-convergence using structured meshes and different numerical quadratures for a thick beam.

In this example the differences between the numerical quadratures aren't significant. Indeed, the results are numerically identic. That's why the different curves of figure 8.7 are overlapped. The convergence is in all cases of order $\mathcal{O} \propto h$. This result is not surprising because the formulation of the BEST element has been designed to take advantage of the cubic Bézier description in the curvature of the element. In a case like this the element behaves in its plane and the cubic description of the Bézier functions doesn't play any role, thus behaving like a vulgar linear element.

### 8.3.2 Cylinder under torsion

This case consists on a cylinder with one base clamped and 2 pairs of tangential forces at the free edge generating a torque. Unlike the case of the cylinder under internal pressure, in this case we set a very thick wall for the cylinder with the objective of activating solely shear deformations and avoid bending the elements.

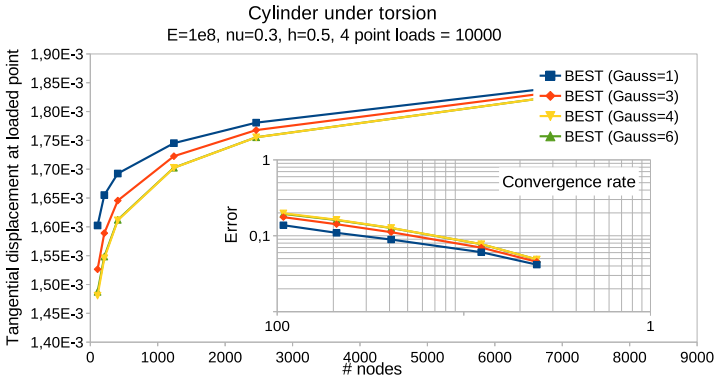


Figure 8.8: Comparison of h-convergence using structured meshes and different numerical quadratures for a cylinder under torsion.

The convergence obtained in this case is very low. All the quadratures achieve a convergence rate of order only $\mathcal{O} \propto h^{1/2}$. It seems again that the quadrature with a single Gauss point has some advantage albeit only marginal with respect to the other quadratures. This result will be further discussed in the Summary in section 8.5.

## 8.4 Effect of the mesh

One of the main goals for designing this new rotation-free thin shell element was to avoid the mesh dependence that the elements developed with the BST technology suffered. It is known that those elements exhibit a clear dependence of the precision of the element on the mesh topology. Thus, in cases of markedly anisotropic meshes, the operator to calculate the curvature of the BST element rapidly looses precision. This is an effect we try to avoid at all costs in the design of the new rotation-free element.

Along the present study on the order of integration we have been able to detect the benefits of a higher order of integration in the influence of the mesh on the results. The author has observed clearly how a reduced order of integration exposes the element to the negative effects of a mesh inadequate to the simulation. On the contrary, when using a quadrature with more Gauss points we can completely cancel out the effect of a mesh that could undermine the result. Next the case of the cylinder under internal pressure is presented.

### 8.4.1 Structured mesh with symmetrical triangles

Generating structured triangle meshes usually becomes a problem in curved surfaces. For example in the case of cylindrical surfaces. Structured triangle meshes are generated based on the corresponding structured quadrangles mesh. For the quadrangles, meshing a cylindrical surface using a structured mesh is a well defined problem and the solution is very satisfactory. But when switching to triangles it doesn't hold. A cylindrical surface has 2 main directions that define it and the quadrangles adapt very well to this space covering it in a Cartesian manner. However the triangles don't fit well in that paradigm, and they should follow a different strategy. Trying to fit triangles using the mesh defined by the quadrangles often results in ugly meshes. In particular, subdividing the quadrangles into symmetric triangles (4 triangles per quadrangle) generates a mesh which does not keep some of the basic properties of the original surface. For example, convexity.

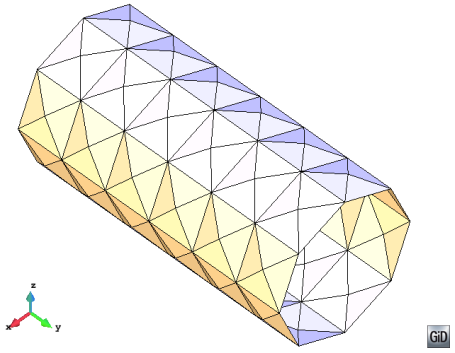


Figure 8.9: Example of a cylinder meshed using a structured mesh of symmetric triangles.

Figure 8.9 shows an example of a structured mesh using symmetric triangles. Few engineers would choose such a mesh for their computations. Both because of the mesh coarseness and because of its quality. The reason for showing this mesh is to illustrate the kind of geometric defect I am arguing.

In figure 8.10 it's easy to see the effect caused by a lower order numerical quadrature when performing the integrals on the results obtained. The main feature to observe is a lack of continuity in the results, exacerbated when using a single Gauss point. Continuity is recovered for the 4 and 6 Gauss points quadratures; cubic and quartic, respectively. We shall recall that a key aspect in the design of the BEST element is precisely the construction of a geometry with greater inter-elemental continuity. Loosing that characteristic because of the numerical quadrature is unacceptable.

### 8.4.2 Structured mesh with non-symmetrical triangles

Non-symmetrical meshes adapt better to the convexity of the surface. For that, every quadrangle is divided into two coplanar triangles. This setup,

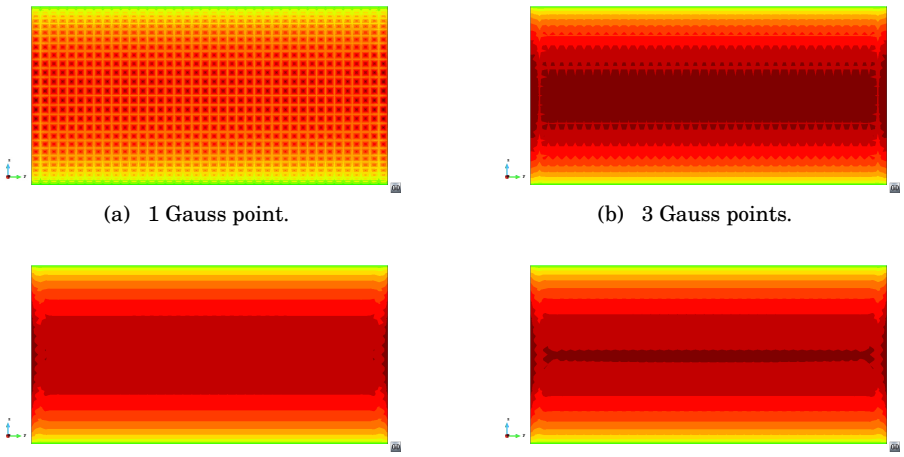

(a) 1 Gauss point. (b) 3 Gauss points.

(c) 4 Gauss points. (d) 6 Gauss points.

Figure 8.10: Qualitative comparison of the results obtained using structured meshes of symmetric triangles and different numerical quadratures for a thin-walled cylinder. Displacements in the x-direction as viewed on the y-z plane.

besides avoiding to increase the number of nodes, takes advantage of the goodness of structured quadrangle meshes. However, it has the disadvantage that unless the mesh is generated with careful attention to details, the result can be a strongly biased mesh. Usually the mesh generator will set all the diagonals that divide the quadrangles in the same orientation. This is what causes the mesh to exhibit a markedly anisotropic behavior that affects the results of the structural analysis. As if the mesh was reinforced in the direction of the diagonals.

Figure 8.11 shows an example of a non-symmetrical structured triangles mesh. Unlike the example shown in figure 8.9 this case maintains the convexity of the geometry, but instead exhibits the diagonals biased as they are all oriented in the same direction.

Once again, figure 8.12 shows clearly the effect produced in the results when using a numerical quadrature of lower order. The mesh effect can be seen very clearly in the results for the cases of low order quadratures. In theory the result should exhibit radial symmetry. Therefore, the isolines of the results should be aligned along the generatrices of the cylinder. The correct orientation of the isolines is recovered for the cases that use quadratures of 4 and 6 Gauss points; cubic and quartic, respectively.

With these two cases we have clearly shown the need to use an adequate integration order to avoid the effect of the mesh on the calculations. At the same time, these results demonstrate qualitatively the good properties of the BEST element to obtain results independent of the mesh topology.

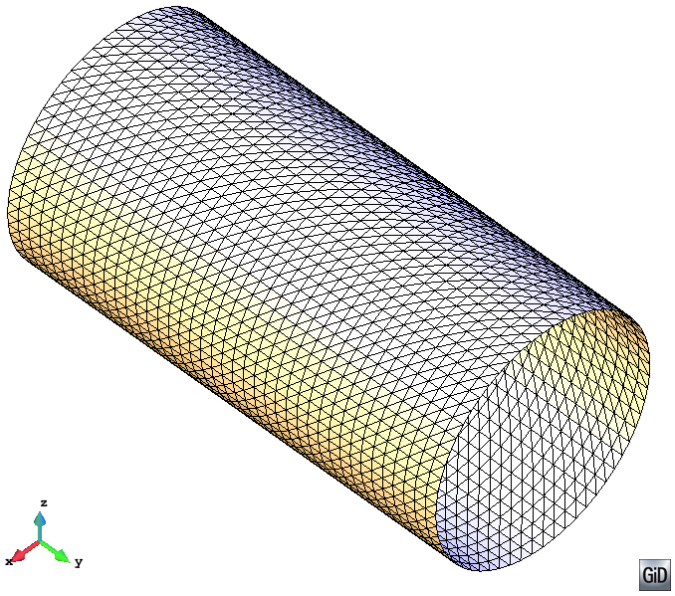


Figure 8.11: Example of a cylinder meshed with a non-symmetrical structured triangles mesh. All the diagonals are oriented in the same direction. This is the mesh used to obtain the results shown in figure 8.12.

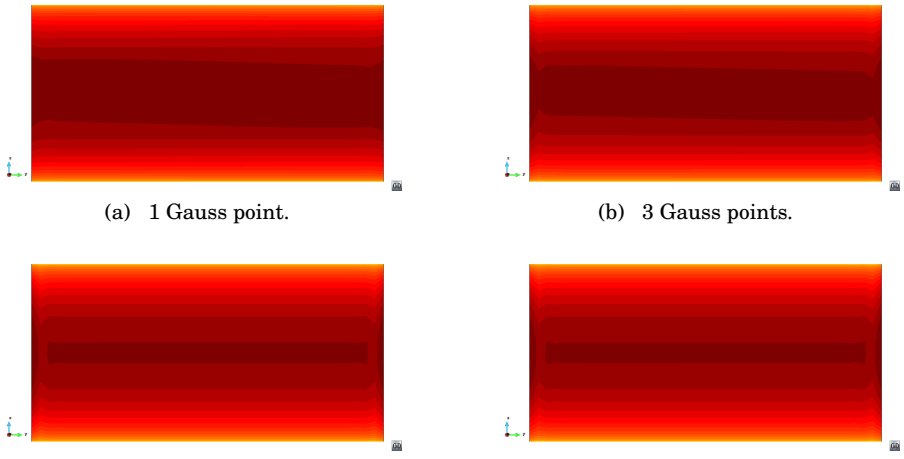

(a) 1 Gauss point.

(b) 3 Gauss points.

(c) 4 Gauss points.

(d) 6 Gauss points.

Figure 8.12: Comparison of the results obtained using different numerical quadratures and non-symmetrical structured triangle meshes for a thin-walled cylinder. Displacements in the x-direction as viewed on the y-z plane. The mesh used is also displayed in figure 8.11 as a reference to indicate the effect of the skewed triangles.

## 8.5 Summary

A number of cases representing different deformation modes have been tested. Each case has been solved in the linear regime using four different quadratures corresponding to different orders of integration: linear, quadratic, cubic and quartic. For the BEST element, full integration requires a quartic order of integration. All the other quadratures tested are therefore instances of reduced quadratures. The deformation modes included in the analysis are the bending mode, the membrane mode and the in-plane shear mode.

In most cases, the results obtained with only one quadrature point are the most accurate. This seems to indicate that reduced integration represents an advantage for the element. The reason for this behavior could be that the BEST element is affected by some sort of locking behavior. Choi et al. [31] assert that "membrane locking only occurs in non-inhibited thin shells" (p. 131), and that it consists in an inadequacy of the finite elements to describe pure bending deformations (i.e. bending of the mid-surface without extensional deformations). The non-inhibited cases tested are the two corresponding to the bending deformation mode: the simply supported beam and the pinched sphere. Actually, the sphere is a non-developable surface and therefore, there is some inhibition caused by the geometry of the shell (not the boundary conditions). It can be observed that the simply supported beam suffers a more severe degradation of the convergence $\mathcal{O} \propto h^{1/2}$. In both cases, however, the reduced integration increases the precision, but it does not affect the order of convergence. The same occurs in the case of the cylinder under torsion. This is consistent with the results reported in [31] where the authors explain that reduced integration does not eliminate membrane locking.

The possible cause for the reduced order of convergence of the BEST element in most cases might be related to another relevant result obtained in section 8.3.1. The thick beam example shows that the BEST element does not show any difference when different quadratures are used in the in-plane shear deformation mode. This result—combined with the result in section 8.2.1 where each quadrature provides the corresponding theoretical order of convergence in the solution—gives an answer to the questions posed at the beginning of the chapter. That is: it is indeed possible to obtain cubic convergence from linear information provided that the adequate geometric construction is built. The information extracted from the neighboring nodes is paramount. But, since the author has not tackled the specific in-plane kinematics of the Bézier-enhanced triangle, the information from the neighboring nodes is not being used adequately. This issue will be studied in detail in chapter 9.

To dispel any doubts on the possible benefits for using reduced integration, the author presents in the last section of the chapter a study on the effects of the mesh when reduced integration is used. As expected, reduced integration causes hourglass modes to appear, or mesh dependence issues to arise. Furthermore, when using full integration, the study shows that the BEST element exhibits an excellent behavior with respect to mesh topology dependence. Therefore, it is highly unadvised to use reduced integration in the BEST element.

# Chapter 9

# Membrane locking of thin shells: a study on how this affects the BEST element and how to solve it

LOOKING AT THE RESULTS OF THE CASES TESTED in the previous chapter, the reader could come to the conclusion that the BEST element suffers from membrane locking. The author agrees with this conclusion, but this is only half the picture. Let's recall the geometric construction of the Bézier-enhanced triangle presented in chapter 5. Particularly item 2 on page 51, where the contour of the triangle is defined by plane curved edges. This decision limits the space of shapes that can be constructed for the Bézier triangle. In particular, it limits the in-plane kinematics of the element. This chapter will review that decision and its consequences. It will also suggest ways to alleviate the poor convergence for those cases where in-plane shear is at play.

## 9.1 On membrane locking of thin shells

Reviewing some relevant works in the literature about the topic of membrane locking in shell elements the author draws two main conclusions. On the one side, Choi et al. [31] affirm that membrane locking only occurs in non-inhibited shells when the element is incapable of deforming under bending without also experimenting membrane deformations of the mid-surface (pure bending deformation). On the other side, both Hakula, Leino and Pitkäranta [51] and Choi et al. [31] conclude that using higher order polynomials reduces the effect of membrane locking in the finite element framework; in particular cubic and higher.

The author has verified that the convergence issues of the BEST element are related to membrane locking. By performing selective reduced integration on a non-inhibited shell structure, the results improve much more when reduced integration is applied to the membrane deformation mode than when reduced integration is applied to the bending deformation mode. This technique is suggested by Oñate in [93, pp. 550–551, 591–593].

Following these results stems that the BEST element should not suffer membrane locking if the full potential of the cubic shape functions is deployed. Precisely, the in-plane cubic kinematic description of the BEST element is limited to linear because of the constraint imposed that the triangle edges shall remain plane curves. This constraint downgrades the cubic description of the cubic Bézier triangle to a linear description of the in-plane kinematics; which determines the membrane deformations of the shell.

Therefore, it is imperative to recover the full cubic description of the element boundaries in order to avoid the locking behavior experimented by the BEST element. The author will suggest some strategies to fulfill this objective. These strategies shall take into account both the kinematics of the shell triangle but also take into account the energy involved in those kinematics in a similar way to the one described in section 5.4.

In order to enrich the in-plane kinematics of the BEST element, it is necessary to allow relative in-plane displacements of the triangle edges. The first idea to describe this kind of kinematics is to emulate the in-plane rotations of the vertices of the triangle. The in-plane rotations of a shell element are commonly referred to as *drilling rotations*. Felippa [39]—for triangles—, and Wisniewski and Turska [140]—for quadrangles— have reported that including the enriched kinematics provided by the drilling rotations improves significantly the precision of the shell elements.

## 9.2 Improving the BEST element kinematics by emulation of drilling rotations

### 9.2.1 Abanico analogy

Figure 9.1: An abanico made in the XIX century. Painted ivory with a Cupid on the frame and with delicate chantilly lace. From the collection donated by Gloria Trueba Gómez in 1997 to the city of Seville and exhibited at the Abanicos' Room of the Reales Alcázares of Seville (Spain).

An abanico is a type of folding hand-fan that was invented in China and introduced in Europe during the XVII century. The author uses this delicate object (see figure 9.1) to illustrate the construction used to emulate the drilling degrees of freedom at the nodes. Since the construction of the BEST element avoids the use of rotation degrees of freedom, the drilling rotations need to be emulated. The author proposes the following analogy: given a node in a mesh, the node shall represent the pivot of the folding hand-fan (abanico), and each of the edges of the mesh converging at that node shall represent the slats of the abanico.

The abanico analogy uses the assumption that—as the abanico opens and folds—the pivot of the abanico experiments the same rotation as the average of the rotations of the individual slats of the abanico. Therefore, it is possible to compute the change in relative orientation of the pivot with respect to each of the slats in the deformed and reference configurations.

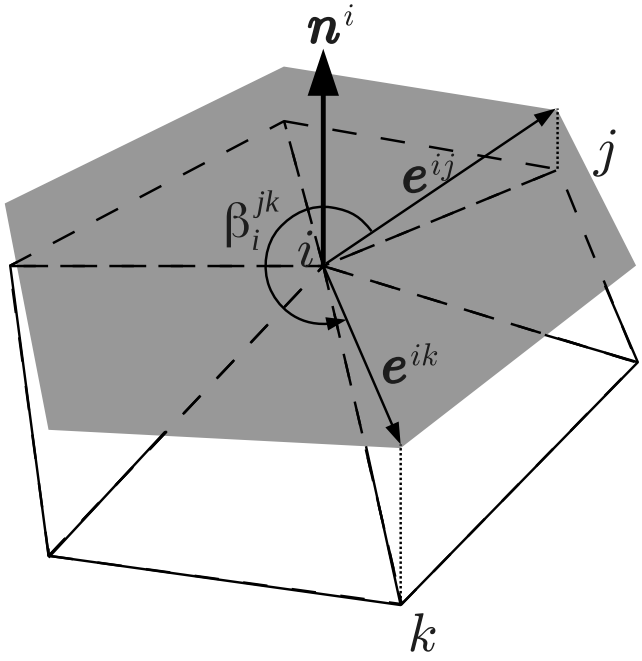


Figure 9.2: Scheme depicting the abanico analogy. For any mesh node $i$, and for any neighboring node $j$, all the $\beta_i^{jk}$ angles are measured for every other neighboring $k$ node. The gray area represents the plane perpendicular to $\boldsymbol{n}^i$ at $i$. And $\boldsymbol{e}^{ij}$ and $\boldsymbol{e}^{ik}$ are the projections of the $i$–$j$ and $i$–$k$ edges onto that plane, respectively.

For every node $i$, and for every pair of neighboring nodes $j$ and $k$, the author defines the angle $\beta_i^{jk}$ (see figure 9.2) which measures the angle formed

between the $i$–$j$ and $i$–$k$ edges, projected on the plane perpendicular to $\boldsymbol{n}^i$.

$$\beta_i^{jk} = \begin{cases} \frac{\pi}{2} & \text{if } \boldsymbol{e}^{ij}\cdot\boldsymbol{e}^{ik} = 0 \wedge (\boldsymbol{e}^{ij}\times\boldsymbol{e}^{ik})\cdot\boldsymbol{n}^i > 0, \\ \frac{3\pi}{2} & \text{if } \boldsymbol{e}^{ij}\cdot\boldsymbol{e}^{ik} = 0 \wedge (\boldsymbol{e}^{ij}\times\boldsymbol{e}^{ik})\cdot\boldsymbol{n}^i < 0, \\ \arctan\left(\frac{|\boldsymbol{e}^{ij}\boldsymbol{e}^{ik}\boldsymbol{n}^i|}{\boldsymbol{e}^{ij}\cdot\boldsymbol{e}^{ik}}\right) & \text{if } \boldsymbol{e}^{ij}\cdot\boldsymbol{e}^{ik} > 0 \wedge (\boldsymbol{e}^{ij}\times\boldsymbol{e}^{ik})\cdot\boldsymbol{n}^i > 0, \\ 2\pi + \arctan\left(\frac{|\boldsymbol{e}^{ij}\boldsymbol{e}^{ik}\boldsymbol{n}^i|}{\boldsymbol{e}^{ij}\cdot\boldsymbol{e}^{ik}}\right) & \text{if } \boldsymbol{e}^{ij}\cdot\boldsymbol{e}^{ik} > 0 \wedge (\boldsymbol{e}^{ij}\times\boldsymbol{e}^{ik})\cdot\boldsymbol{n}^i < 0, \\ \pi + \arctan\left(\frac{|\boldsymbol{e}^{ij}\boldsymbol{e}^{ik}\boldsymbol{n}^i|}{\boldsymbol{e}^{ij}\cdot\boldsymbol{e}^{ik}}\right) & \text{if } \boldsymbol{e}^{ij}\cdot\boldsymbol{e}^{ik} < 0. \end{cases} \tag{9.1}$$

Defined in this way, the angle $\beta_i^{jk}$ is a continuous function with continuous derivatives. The angle $\beta_i^{jk}$ takes values in the interval $(0, 2\pi)$ and is equal to $0$ when $k = j$. The vectors $\boldsymbol{e}^{ij}$ and $\boldsymbol{e}^{ik}$ are defined in figure 9.2 and are computed according to equations (9.2) and (9.3).

$$\boldsymbol{e}^{ij} = (\boldsymbol{I} - \boldsymbol{n}^i \otimes \boldsymbol{n}^{iT})\cdot(\boldsymbol{x}^j - \boldsymbol{x}^i) \tag{9.2}$$

$$\boldsymbol{e}^{ik} = (\boldsymbol{I} - \boldsymbol{n}^i \otimes \boldsymbol{n}^{iT})\cdot(\boldsymbol{x}^k - \boldsymbol{x}^i) \tag{9.3}$$

The abanico analogy above, can be written mathematically as:

$$\alpha^{ij} = \frac{1}{z_i}\sum_{\substack{k=1 \\ k\neq j}}^{z_i} \beta_i^{jk} \tag{9.4}$$

where $\alpha^{ij}$ is the average of the relative angles of the $z_i$ edges (slats) surrounding node $i$ with respect to the edge $i$–$j$. This angle is measured counterclockwise around the normal vector $\boldsymbol{n}^i$.

And by computing the difference between this angle in the reference and deformed configurations, the rotation of the node $i$ with respect to the edge $i$–$j$ is found:

$$\Delta\alpha^{ij} = \alpha^{ij} - \alpha_0^{ij} \tag{9.5}$$

The angle $\Delta\alpha^{ij}$ provides a measure of the drilling rotation of the node.

### 9.2.2 Modified kinematics using the abanico analogy

Using the drilling rotation defined with the help of the abanico analogy the author proposes the following modification of the kinematics of the BEST element. In the construction below, the following assumption is made:

$$\theta^{ij} = \Delta\alpha^{ij} \tag{9.6}$$

The construction used to determine the locations of the contour control points is changed as follows. Still three planes are intersected to find the location of the control point. The planes are the ones displayed in figure 9.3:

1. The plane perpendicular to the normal at the vertex —this is a necessary and sufficient condition to interpolate the normals—. This is the same plane already used in item 1 on page 51.

2. The contour is not anymore a plane curve and we rotate the contour plane defined in item 2 on page 51 in order to impose the drilling rotation on the edge fiber as it approaches the node. In order to maintain $\mathcal{C}^0$ continuity, this has to be a symmetric condition for two adjacent triangles. The selection of the plane is such that one of the directors is the edge of the flat triangle rotated an angle $\theta^{ij}$ and the other director is the normal at the node $\boldsymbol{n}^i$. $\boldsymbol{d}^{ij}$ is the director vector of this plane.

3. And a plane perpendicular to the edge of the flat triangle. the exact location of this plane will be explained in section 9.3. Suffice it to say, that the criterion to position the plane is again based on energy minimization and not on geometric considerations.

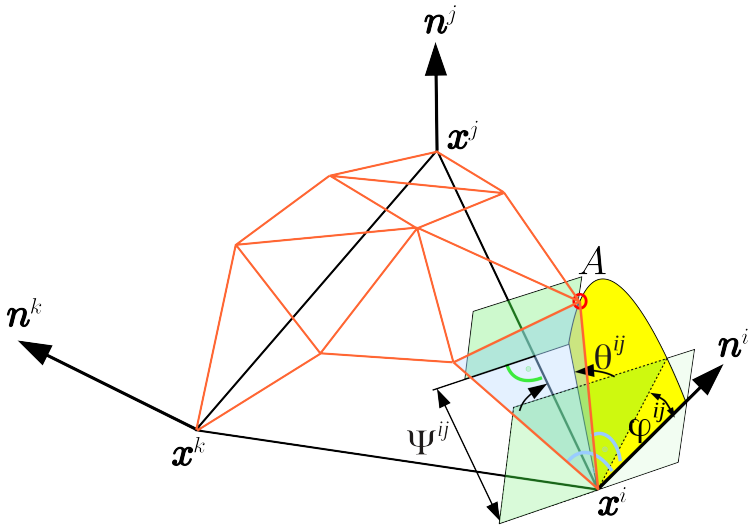


Figure 9.3: Representation of the net of control points (dashed lines) for a cubic Bézier triangle constructed using the nodal positions and normals. This figure differs from figure 5.5 in that the drilling rotations $\theta^{ij}$ are used here. Three planes define the position of a control point $A$ of the contour. The plane that was represented shaded in figure 5.5 is not drawn here for clarity, but remains unchanged. The two dark gray planes are parallel to each other and perpendicular to the $i$–$j$ straight edge. They are placed at a distance $\Psi^{ij}$ which will be determined in section 9.3. The light gray plane has been split and rotated an angle $\theta^{ij}$ about $\boldsymbol{n}^i$ to account for the drilling rotation experimented by the corner node. The angles $\varphi^{ij}$ and $\theta^{ij}$ are not drawn exactly as defined in figures 5.7 and 9.5, respectively.

The mathematical formulas to compute the intersection of these three planes have been already provided in equations (5.15) and (5.16) on page 51.

However, the drilling rotation $\theta^{ij}$ requires to redefine $\boldsymbol{d}^{ij}$.

$$\begin{aligned}\boldsymbol{d}^{ij} =& \boldsymbol{n}^i \times \boldsymbol{R}(\boldsymbol{n}^i, \theta^{ij}) \cdot (\boldsymbol{x}^i - \boldsymbol{x}^j) = \\ =& \boldsymbol{n}^i \times (\boldsymbol{x}^i - \boldsymbol{x}^j) \cdot \cos\theta^{ij} + \boldsymbol{n}^i \times [\boldsymbol{n}^i \times (\boldsymbol{x}^i - \boldsymbol{x}^j)] \cdot \sin\theta^{ij} = \\ =& \boldsymbol{n}^i \times (\boldsymbol{x}^i - \boldsymbol{x}^j) \cdot \cos\theta^{ij} - (\boldsymbol{I} - \boldsymbol{n}^i \otimes \boldsymbol{n}^{iT}) \cdot (\boldsymbol{x}^i - \boldsymbol{x}^j) \cdot \sin\theta^{ij}\end{aligned} \tag{9.7}$$

In the above expression, $\boldsymbol{R}(\boldsymbol{n}^i, \theta^{ij})$ represents the rotation matrix defined by a vector $\boldsymbol{n}^i$ and an angle $\theta^{ij}$. And its expression is obtained using Rodrigues' formula.

The variations in the determination of the contour control points also imply a subtle change on how the central control point shall be obtained. It is still obtained as an average of three candidate points. Since no longer a single plane along the flat edge is used to compute the contour control points, it cannot be used either as an input for computing the candidate central control points (see figure 5.6). In the computation of the candidate central control points, the author proposes to slightly change the plane orthogonal to the plane defined in item 2 on page 51 by another plane which is orthogonal to another plane that also contains $\boldsymbol{n}^{ij}$ and the two intermediate contour control points (see figure 9.4). Notice how the expressions of $\boldsymbol{A}_{\boldsymbol{p}}^{0i}$ and $\boldsymbol{b}_{\boldsymbol{p}}^{0i}$ in equations (5.18) and (5.19) are still correct.

### 9.2.3 This is not an incompatible mode method

Some scholars may see similarities relating this enhancement to the method of incompatible modes [139]. However, this strategy is quite different and totally unrelated [55, 116, 117]. In the case of the incompatible modes method, the authors in the references above try to solve the locking problems stemming from the low order description of the element kinematics by adding specific internal variables to the kinematic description of the element. In the present case, the trick is to unleash the potential of the cubic formulation of the element. So, it is not necessary to add any manufactured kinematic description to the element. The cubic nature of the element already has the inherent capabilities to represent the different deformation modes without causing locking mechanisms. The locking occurs due to the restrictive rules imposed for the geometric construction. These restrictions were so severe because there were no real means (until the emulation of the *drilling* degrees of freedom) to build a meaningful and consistent construction of the element kinematics without the *drilling* degrees of freedom.

## 9.3 Energy minimization for the in-plane shear deformation mode

The introduction of emulated drilling rotations and the corresponding enhancement of the in-plane shear deformation kinematics for the BEST element means that we need to review the definition of $\Psi^{ij}$. Let's recall that $\Psi^{ij}$ was introduced in section 5.4 to determine the precise shape of the Bézier triangle which minimizes the elastic energy of the shell. However,

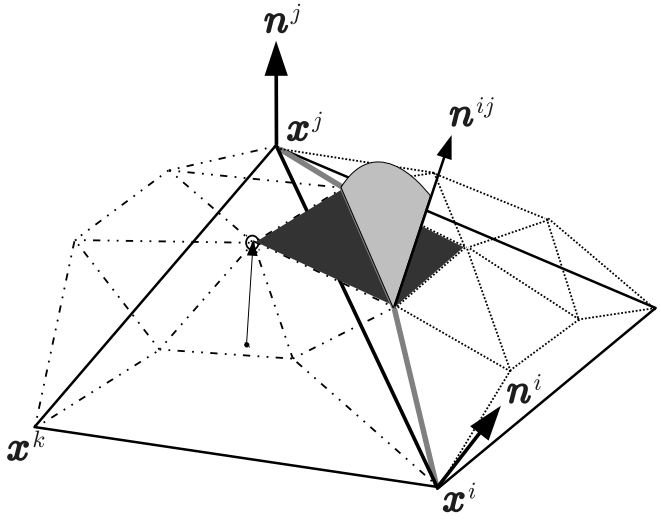


Figure 9.4: Two adjacent Bézier triangles are $\mathcal{G}^1$ continuous if all their adjacent control triangles are co-planar. This condition could be used to enforce $\mathcal{C}^1$ continuity and determine the position of the central control point. The light gray plane contains the average of the two corner normals $\boldsymbol{n}^{ij}$ and passes through the two mid edge control points. The dark gray triangles are orthogonal to the light gray plane. The candidate central control point corresponding to the edge marked with a thick gray line is represented with a circle and is determined intersecting the dark gray plane with the line that passes through the barycenter of the 6 contour control points and is perpendicular to the flat triangle. This construction is similar to the one proposed in figure 5.6, but the present one is more general and can be used with non-flat curved edges.

this energy minimization did not take into account the kinematics associated with the in-plane shear that becomes activated with the use of the drilling rotation.

$\Psi^{ij}$ is the only parameter that does not depend strictly on the geometric considerations of the triangle. Instead, $\Psi^{ij}$ depends on two other geometric parameters—the in-plane shear deformation and the out of plane membrane and bending deformation—but with the objective to minimize the overall elastic energy of the element. In section 5.4 the author obtains an expression of $\Psi^{ij}$ which depends on the value of $\varphi^{ij}$ (see $\Psi^{ij}_{\varphi}$ in equation (5.21)).

Presumably, the value of $\Psi^{ij}$ will depend differently on $\theta^{ij}$ than it does on $\varphi^{ij}$. The author presents next how to obtain this dependency and then how to combine the two kinematic modes and a unique expression of $\Psi^{ij}$ depending on the variables $\varphi^{ij}$ and $\theta^{ij}$.

### 9.3.1 Reduction of the problem

Likewise to the procedure followed in section 5.4.1, the author proposes to analyze a 2D case representative of the problem at hand. In this case, the 2D reduction consists on neglecting the effect that curvature has on the in-plane shear deformation. Therefore, a 2D analysis can be performed considering the full triangle. This simplifies the process and analytic solutions can be obtained.

In [39] Felippa explains the process for determining optimal free parameters of the ANDES template model for isotropic and non-isotropic materials. That process is analogous to the present energy minimization study. Felippa argues that the modes of deformation used in the study were initially the 3 *in-plane bending modes*, but that these are not linearly independent and a fourth *torsion mode* was needed to avoid rank deficiency in the stiffness matrix. The author here proposes to study exclusively the *torsion mode*. The reason behind this decision is simplicity. Considering all the deformation modes implies finding the function for all the six different $\Psi^{\alpha\beta}$ values depending on the six different $\theta^{\alpha\beta}$ angles in the triangle ($\forall\alpha,\beta = 1 \div 3, \alpha \neq \beta$). This is a set of 6 coupled problems in 6 dimensions. Instead, studying exclusively the *torsion mode* allows the author to consider a periodic case and to reduce the set of problems to a single problem in one dimension. This approach implies assuming that the value of each $\Psi^{ij}$ depends only on $\theta^{ij}$ and is uncoupled from the other $\theta^{\alpha\beta}$ values in the triangle.

#### Torsion energy

In order to find an expression of $\Psi^{ij}_{\theta}$ which minimizes the in-plane shear deformation energy, the author has modeled the equations represented by the drawing in figure 9.5 into the Maple® symbolic manipulation software. The analytic solution obtained by Maple® appears very complex at first, but when plotted: it is not (see figure 9.6. The problem reduction stated in section 9.3.1 and depicted in figure 9.5 does not follow the guidelines of the parcel test. That is, the deformation imposed does not correspond to a constant deformation. Instead, the deformation corresponds to a periodic strain state throughout the triangle's surface. The author does not know how to impose a constant in plane shear strain in a triangle using only drilling rotations at the corner nodes. So the author takes this *torsion mode* as the best possible to work with. In fact, in order to verify that only the in-plane shear deformation mode is activated, the author compares the results of the optimized expressions of $\Psi^{ij}_{\theta}$ for three different values of the Poisson coefficient ($\nu = 0, 0.25, 0.5$). The results are plotted in figure 9.6 and they are almost undistinguishable. This verifies that only in-plane shear is at play and the other in-plane axial strains are residual in this problem set.

Taking a close look at figure 9.6, the author notices that the solution exhibits a smooth kink of the plot for values of $\theta \approx \pm\frac{\pi}{10}$. This kink is what makes the analytic expression very complex, and clearly distinguishes two different regimes in the solution. A highly non-linear regime for small values of $\theta$ and an almost linear regime for higher values of $\theta$. For extremely

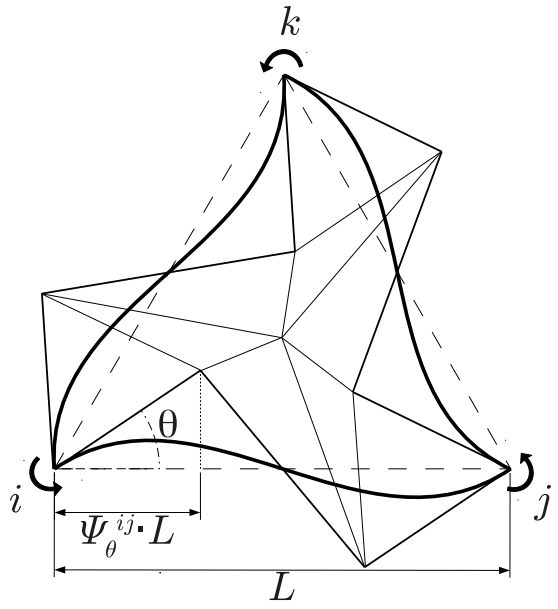


Figure 9.5: Problem reduction to minimize the in-plane shear deformation energy. The author analyzes a flat equilateral triangle subjected to a periodic torsion $\theta$ in all three corner nodes. The dash lines represent the reference configuration, while the thick curved lines represent the deformed configuration. The thin lines represent the control polygon of the deformed configuration.

high values of $\theta$ the author can describe a third regime, but it is so extreme, that it has no real engineering value. It would be possible to adjust the whole curve quite nicely for the full range of values of $\theta$, but doing so with a simple expression means that the kink would be sharp instead of smooth, and continuity of the derivatives would be lost at that point; which is highly undesirable. Therefore, the author decides to settle for an adjustment that captures very well the solution for small values of $\theta$. The reasoning is that in very few cases the deformation will imply values of $\theta$ larger than $\frac{\pi}{10}$. This adjustment is presented in mathematical form in equation (9.9) and plotted in figure 9.6.

$$\Psi_\theta^{ij} = \frac{1}{3}\cos^6\theta \tag{9.8}$$

Using the assumption that this result can be uncoupled for each of the edges of the triangle, we can write the more general expression:

$$\Psi_\theta^{ij}(\theta^{ij}) = \frac{1}{3}\cos^6\theta^{ij} \tag{9.9}$$

## 9.4 Combining the $\Psi_\varphi$ and $\Psi_\theta$ expressions

Both equations (5.21) and (9.9) are used to define the same magnitude in the construction of the control polygon that determines the shape of the

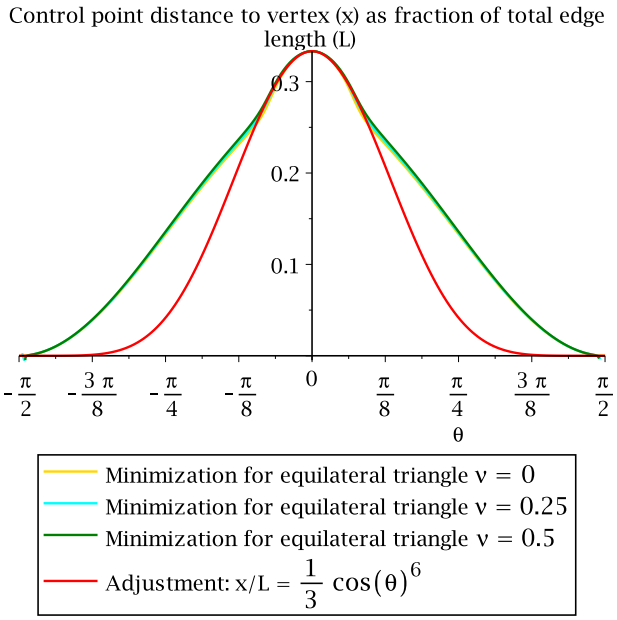


Figure 9.6: Comparison of the minimization solutions for the $\Psi_\theta^{ij}$ values for three different values of the Poisson coefficient $\nu$. The red curve represents an adjustment for small values of $\theta \in [-\frac{\pi}{10}, \frac{\pi}{10}]$.

cubic Bézier triangle. Since these two expressions are not coincident, the author needs to find a way to merge them together into a single expression $\Psi^{ij}(\varphi^{ij}, \theta^{ij})$. The good news is that for $\varphi^{ij} = 0$ and $\theta^{ij} = 0$ the two functions have the same value and even the same derivative. Taking a look at figure 9.7 the reader can observe that the two functions diverge significantly as the variables increase their value. Therefore the merging proposal shall take into account how to take this fact into account.

The most simple proposal is to use a weighted average of the two seed expressions. The weighting factor shall depend on the main variable for each expression. It makes sense that the function whose variable exhibits a bigger value also has more influence on the overall function that defines the merged expression. But how much influence? Well, this is an easy one to answer. Since the $\Psi$ functions are defined with the aim of minimizing the deformation energy of the triangle, the resulting merged function should maintain this objective intact. In this sense, in general, the author assumes that the deformation energy varies quadratically with the kinematic variables. So the square of the variables should be a good weighting factor. For a very quick verification the author has compared on one hand how the total deformation energy of the *torsion mode* defined in section 9.3 and using the expression in equation (9.9) varies with respect the variable $\theta$, and on the other hand a simple quadratic expression of $\theta$, and I can say it matches pretty well. The result in figure 9.8 also serves to verify that the solution obtained for an equilateral triangle is not too far off in the

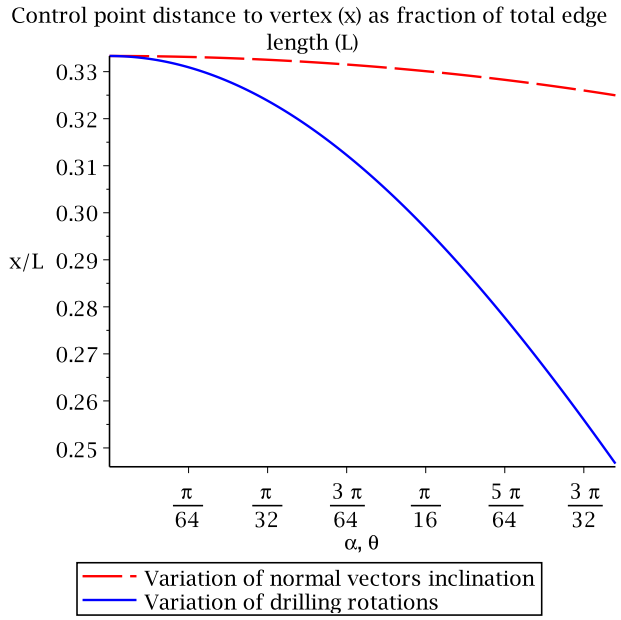


Figure 9.7: Comparison of the minimization functions $\Psi_\varphi^{ij}$ (dashed) and $\Psi_\theta^{ij}$ (continuous) in the range of the variables $\varphi^{ij}, \theta^{ij} \in [0, \frac{\pi}{10}]$.

case of a rectangle triangle.

As a conclusion to all these thoughts, the author defines the following function that combines the expressions of equations (5.21) and (9.9) into one:

$$\Psi^{ij} = \Psi^{ij}(\varphi^{ij}, \theta^{ij}) = \frac{{\varphi^{ij}}^2 \cdot \Psi_\varphi^{ij} + {\theta^{ij}}^2 \cdot \Psi_\theta^{ij}}{{\varphi^{ij}}^2 + {\theta^{ij}}^2} \tag{9.10}$$

Notice that the above expression has an indetermination when

$${\varphi^{ij}}^2 + {\theta^{ij}}^2 \to 0 \tag{9.11}$$

### 9.4.1 Solution of the indeterminate limit

This indetermination can be worked out using the following change of variable:

$$\varphi^{ij} = \rho \cos\omega \tag{9.12}$$

$$\theta^{ij} = \rho \sin\omega \tag{9.13}$$

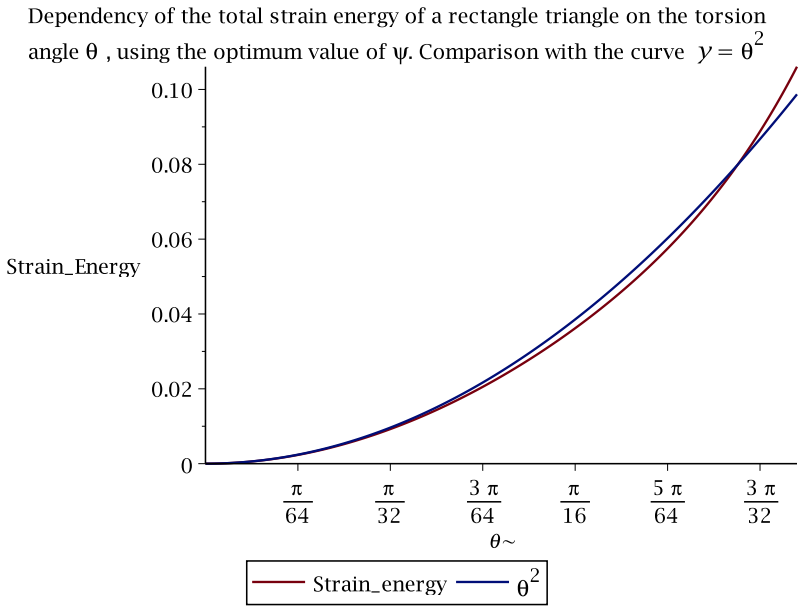


Figure 9.8: Comparison of the variation of the total strain energy with the drilling rotation angle to verify that it follows a quadratic variation. The example is performed with a rectangle triangle subjected to an in-plane shear deformation in torsion mode as defined in figure 9.5 (red line), and a simple quadratic function (blue line).

then

$$\varphi^{ij\,2} + \theta^{ij\,2} \to 0 \Leftrightarrow \varphi^{ij} \to 0 \wedge \theta^{ij} \to 0 \Leftrightarrow \rho^2 \to 0 \Leftrightarrow \rho \to 0 \tag{9.14}$$

$$\Psi^{ij} = \cos^2\omega \cdot \Psi^{ij}_{\varphi} + \sin^2\omega \cdot \Psi^{ij}_{\theta} \tag{9.15}$$

$$\lim_{\rho^2 \to 0} \Psi^{ij} = \lim_{\substack{\varphi^{ij} \to 0 \\ \theta^{ij} \to 0}} \Psi^{ij} = \cos^2\omega \cdot \frac{1}{3} + \sin^2\omega \cdot \frac{1}{3} = \frac{1}{3} \tag{9.16}$$

Now we can rewrite equation (9.10) pointing out the solution of the indetermination.

$$\Psi^{ij} = \Psi^{ij}(\varphi^{ij}, \theta^{ij}) = \begin{cases} \dfrac{\varphi^{ij\,2} \cdot \Psi^{ij}_{\varphi} + \theta^{ij\,2} \cdot \Psi^{ij}_{\theta}}{\varphi^{ij\,2} + \theta^{ij\,2}} & \text{if } \varphi^{ij\,2} + \theta^{ij\,2} \neq 0, \\ \dfrac{1}{3} & \text{if } \varphi^{ij\,2} + \theta^{ij\,2} = 0. \end{cases} \tag{9.17}$$

It is also important to point out that the value of $\varphi^{ij}$ needs to be com-

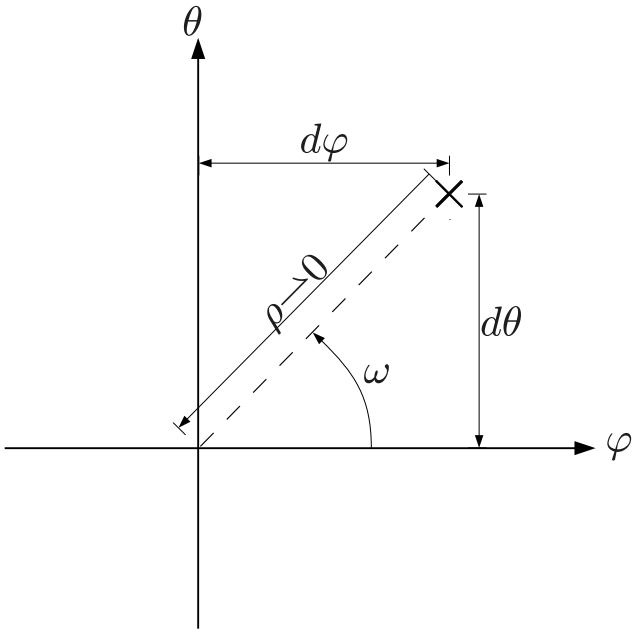


Figure 9.9: Geometric interpretation of the change of variables applied in equations (9.12) and (9.13) at the limit when $\rho^2 \to 0$.

puted as[1]

$$\varphi^{ij} = 2 \cdot \arctan\left(\frac{\|\|\boldsymbol{x}^i - \boldsymbol{x}^j\|\boldsymbol{n}^i - \|\boldsymbol{n}^i\|(\boldsymbol{x}^i - \boldsymbol{x}^j)\|}{\|\|\boldsymbol{x}^i - \boldsymbol{x}^j\|\boldsymbol{n}^i + \|\boldsymbol{n}^i\|(\boldsymbol{x}^i - \boldsymbol{x}^j)\|}\right) - \frac{\pi}{2} \tag{9.18}$$

**First derivative**

The solution of the indetermination in the case of the first derivative can be obtained quite straightforwardly using the same change of variables indicated in equations (9.12) and (9.13).

$$\frac{\partial \Psi^{ij}}{\partial \tilde{\boldsymbol{x}}^r} = \frac{\partial \Psi^{ij}}{\partial x^h_{(v)}} = 2 \sin\omega \cdot \cos\omega \cdot \frac{\partial \omega}{\partial x^h_{(v)}}(\Psi_\theta - \Psi_\varphi) + \cos^2\omega \frac{\partial \Psi_\varphi}{\partial x_{(v)}} + \sin^2\omega \frac{\partial \Psi_\theta}{\partial x_{(v)}} \tag{9.19}$$

[1]Equation (9.18) always delivers a correct value of $\varphi^{ij} \in [0, \pi]$. And as reported by Kahan in [61, 62] this formula is much more accurate than the other trigonometric formulæ. Indeed, the author has traced back the cause of the numerical loss of accuracy in the calculation of some examples to an inadecuate definition of $\varphi^{ij}$ using other trigonometric formulæ.

$$\begin{aligned}\lim_{\substack{\varphi^{ij}\to 0\\ \theta^{ij}\to 0}} \frac{\partial \Psi^{ij}}{\partial x^h_{(v)}} =& 2\sin\omega\cdot\cos\omega\cdot\frac{\partial\omega}{\partial x^h_{(v)}}\cdot 0+\cos^2\omega\left.\frac{\partial\Psi_\varphi}{\partial x_{(v)}}\right|_{\varphi^{ij}=0}+\sin^2\omega\left.\frac{\partial\Psi_\theta}{\partial x_{(v)}}\right|_{\theta^{ij}=0}=\\ &=\cos^2\omega\left.\frac{\partial\Psi_\varphi}{\partial\varphi^{ij}}\right|_{\varphi^{ij}=0}\frac{\partial\varphi^{ij}}{\partial x_{(v)}}+\sin^2\omega\left.\frac{\partial\Psi_\theta}{\partial\theta^{ij}}\right|_{\theta^{ij}=0}\frac{\partial\theta^{ij}}{\partial x_{(v)}}=\\ &=\cos^2\omega\cdot 0\cdot\frac{\partial\varphi^{ij}}{\partial x_{(v)}}+\sin^2\omega\cdot 0\cdot\frac{\partial\theta^{ij}}{\partial x_{(v)}}=0\end{aligned} \tag{9.20}$$

We can then write:

$$\frac{\partial\Psi^{ij}}{\partial\tilde{\boldsymbol{x}}^r}=\frac{\partial\Psi^{ij}}{\partial x^h_{(v)}}=\begin{cases}\dfrac{1}{{\varphi^{ij}}^2+{\theta^{ij}}^2}\left\{\dfrac{1}{3}\left[\left(4\varphi^{ij}\dfrac{\cos\varphi^{ij}}{1+\cos\varphi^{ij}}-\right.\right.\right.\\ \left.-2{\varphi^{ij}}^2\dfrac{\sin\varphi^{ij}}{(1+\cos\varphi^{ij})^2}\right)\dfrac{\partial\varphi^{ij}}{\partial x^h_{(v)}}+\\ \left.+(2\theta^{ij}\cos^6\theta^{ij}-\right. & \text{if } {\varphi^{ij}}^2+{\theta^{ij}}^2\neq 0,\\ \left.-6{\theta^{ij}}^2\cos^5\theta^{ij}\sin\theta^{ij})\dfrac{\partial\theta^{ij}}{\partial x^h_{(v)}}\right]-\\ \left.-2\Psi^{ij}\left(\varphi^{ij}\dfrac{\partial\varphi^{ij}}{\partial x^h_{(v)}}+\theta^{ij}\dfrac{\partial\theta^{ij}}{\partial x^h_{(v)}}\right)\right\}\\ 0 & \text{if } {\varphi^{ij}}^2+{\theta^{ij}}^2=0.\end{cases} \tag{9.21}$$

The expressions for $\dfrac{\partial\varphi^{ij}}{\partial x^h_{(v)}}$ and $\dfrac{\partial\theta^{ij}}{\partial x^h_{(v)}}$ can be found in appendix D.

**Second derivative**

Following the same process and using the change of variables specified in equations (9.12) and (9.13), the second derivative of equation (9.10) can be written as:

$$\begin{aligned}\frac{\partial^2\Psi^{ij}}{\partial x^h_{(v)}\partial x^s_{(w)}}=&\cos^2\omega\frac{\partial^2\Psi_\varphi}{\partial x^h_{(v)}\partial x^s_{(w)}}+\sin^2\omega\frac{\partial^2\Psi_\theta}{\partial x^h_{(v)}\partial x^s_{(w)}}+\\ &+2\sin\omega\cdot\cos\omega\left[\frac{\partial\omega}{\partial x^h_{(v)}}\left(\frac{\partial\Psi_\theta}{\partial x^s_{(w)}}-\frac{\partial\Psi_\varphi}{\partial x^s_{(w)}}\right)+\frac{\partial\omega}{\partial x^s_{(w)}}\left(\frac{\partial\Psi_\theta}{\partial x^h_{(v)}}-\frac{\partial\Psi_\varphi}{\partial x^h_{(v)}}\right)\right]+\\ &+2\left[(\cos^2\omega-\sin^2\omega)\frac{\partial\omega}{\partial x^h_{(v)}}\frac{\partial\omega}{\partial x^s_{(w)}}+\sin\omega\cdot\cos\omega\frac{\partial^2\omega}{\partial x^h_{(v)}\partial x^s_{(w)}}\right](\Psi_\theta-\Psi_\varphi)\end{aligned} \tag{9.22}$$

$$\lim_{\substack{\varphi^{ij}\to 0\\ \theta^{ij}\to 0}}\frac{\partial^2\Psi^{ij}}{\partial x^h_{(v)}\partial x^s_{(w)}}=\lim_{\substack{\varphi^{ij}\to 0\\ \theta^{ij}\to 0}}\cos^2\omega\frac{\partial^2\Psi_\varphi}{\partial x^h_{(v)}\partial x^s_{(w)}}+\lim_{\substack{\varphi^{ij}\to 0\\ \theta^{ij}\to 0}}\sin^2\omega\frac{\partial^2\Psi_\theta}{\partial x^h_{(v)}\partial x^s_{(w)}} \tag{9.23}$$

The author concludes that, in light of equation (9.23), the second derivative does not have a solution to the indetermination when $\rho^2\to 0$. This is so because the second derivatives for $\Psi^{ij}_\varphi$ and $\Psi^{ij}_\theta$ are different at the indetermination point. And as a consequence the second derivative of $\Psi^{ij}(\varphi^{ij},\theta^{ij})$ depends on the direction ($\omega$) considered.

In order to find a workaround, let's remind us the need for having this second derivative. The second derivative is required by the Newton-Raphson algorithm to solve the non-linear system of equations (equation (6.76)). The second derivative appears because the geometric non-linearities already use first derivatives of the kinematic expressions. Therefore, the second derivative is used by the Newton-Raphson algorithm to make an approximation of the solution in the iterative process. Then, the expression needed to overcome the indetermination at the point $\rho^2 \to 0$ shall preserve the equilibrium if the equilibrium is reached at that point; and should push the approximation out of the indetermination point if that is not the solution. Once the approximation is out of the indetermination, full convergence properties of the Newton-Raphson algorithm are recovered.

Let's take a look at figure 9.9. using this construction we can establish that:

$$\lim_{\substack{\varphi^{ij}\to 0\\ \theta^{ij}\to 0}} \cos^2\omega = \frac{\mathrm{d}{\varphi^{ij}}^2}{\mathrm{d}{\varphi^{ij}}^2 + \mathrm{d}{\theta^{ij}}^2} \tag{9.24}$$

$$\lim_{\substack{\varphi^{ij}\to 0\\ \theta^{ij}\to 0}} \sin^2\omega = \frac{\mathrm{d}{\theta^{ij}}^2}{\mathrm{d}{\varphi^{ij}}^2 + \mathrm{d}{\theta^{ij}}^2} \tag{9.25}$$

On the other hand, since we are in the context of deriving with respect to $\partial x^h_{(v)}$ and $\partial x^s_{(w)}$: these are the only two variables that affect $\mathrm{d}\varphi^{ij}$ and $\mathrm{d}\theta^{ij}$. Therefore, in this context and only in this context:

$$\mathrm{d}\varphi^{ij} = \frac{\partial\varphi^{ij}}{\partial x^h_{(v)}}\,\mathrm{d}x^h_{(v)} + \frac{\partial\varphi^{ij}}{\partial x^s_{(w)}}\,\mathrm{d}x^s_{(w)} \tag{9.26}$$

$$\mathrm{d}\theta^{ij} = \frac{\partial\theta^{ij}}{\partial x^h_{(v)}}\,\mathrm{d}x^h_{(v)} + \frac{\partial\theta^{ij}}{\partial x^s_{(w)}}\,\mathrm{d}x^s_{(w)} \tag{9.27}$$

It is very tempting to impose the condition

$$\mathrm{d}x^h_{(v)} = \mathrm{d}x^s_{(w)} \tag{9.28}$$

However, this is an arbitrary condition that does not respond to any mathematical reality. The author decides to impose it nevertheless because it allows to obtain a determinate expression of equation (9.23). Applying equation (9.28) and substituting equations (9.26) and (9.27) into equations (9.24) and (9.25), the author now rewrites the latter:

$$\lim_{\substack{\varphi^{ij}\to 0\\ \theta^{ij}\to 0}} \cos^2\omega = \frac{\left(\dfrac{\partial\varphi^{ij}}{\partial x^h_{(v)}} + \dfrac{\partial\varphi^{ij}}{\partial x^s_{(w)}}\right)^2}{\left(\dfrac{\partial\varphi^{ij}}{\partial x^h_{(v)}} + \dfrac{\partial\varphi^{ij}}{\partial x^s_{(w)}}\right)^2 + \left(\dfrac{\partial\theta^{ij}}{\partial x^h_{(v)}} + \dfrac{\partial\theta^{ij}}{\partial x^s_{(w)}}\right)^2} \tag{9.29}$$

$$\lim_{\substack{\varphi^{ij}\to 0\\ \theta^{ij}\to 0}} \sin^2\omega = \frac{\left(\dfrac{\partial\theta^{ij}}{\partial x^h_{(v)}} + \dfrac{\partial\theta^{ij}}{\partial x^s_{(w)}}\right)^2}{\left(\dfrac{\partial\varphi^{ij}}{\partial x^h_{(v)}} + \dfrac{\partial\varphi^{ij}}{\partial x^s_{(w)}}\right)^2 + \left(\dfrac{\partial\theta^{ij}}{\partial x^h_{(v)}} + \dfrac{\partial\theta^{ij}}{\partial x^s_{(w)}}\right)^2} \tag{9.30}$$

and finally obtains (under all the previous conditions)

$$\lim_{\substack{\varphi^{ij}\to 0\\ \theta^{ij}\to 0}} \frac{\partial^2\Psi^{ij}}{\partial x^h_{(v)}\partial x^s_{(w)}} = -\frac{1}{6}\frac{\left(\frac{\partial\varphi^{ij}}{\partial x^h_{(v)}}+\frac{\partial\varphi^{ij}}{\partial x^s_{(w)}}\right)^2 \frac{\partial\varphi^{ij}}{\partial x^h_{(v)}}\cdot\frac{\partial\varphi^{ij}}{\partial x^s_{(w)}}}{\left(\frac{\partial\varphi^{ij}}{\partial x^h_{(v)}}+\frac{\partial\varphi^{ij}}{\partial x^s_{(w)}}\right)^2+\left(\frac{\partial\theta^{ij}}{\partial x^h_{(v)}}+\frac{\partial\theta^{ij}}{\partial x^s_{(w)}}\right)^2} - \\ -2\frac{\left(\frac{\partial\theta^{ij}}{\partial x^h_{(v)}}+\frac{\partial\theta^{ij}}{\partial x^s_{(w)}}\right)^2 \frac{\partial\theta^{ij}}{\partial x^h_{(v)}}\cdot\frac{\partial\theta^{ij}}{\partial x^s_{(w)}}}{\left(\frac{\partial\varphi^{ij}}{\partial x^h_{(v)}}+\frac{\partial\varphi^{ij}}{\partial x^s_{(w)}}\right)^2+\left(\frac{\partial\theta^{ij}}{\partial x^h_{(v)}}+\frac{\partial\theta^{ij}}{\partial x^s_{(w)}}\right)^2} \tag{9.31}$$

For the more general case—away from the indetermination—the expression without change of variables is:

$$\begin{aligned}\frac{\partial^2\Psi^{ij}}{\partial x^h_{(v)}\partial x^s_{(w)}} &= \frac{1}{{\varphi^{ij}}^2+{\theta^{ij}}^2}\left\{\frac{1}{3}\left[\frac{-2{\varphi^{ij}}^2}{(1+\cos\varphi^{ij})^2}\left(\sin\varphi^{ij}\frac{\partial^2\varphi^{ij}}{\partial x^h_{(v)}\partial x^s_{(w)}}+\right.\right.\right.\\
&+(2-\cos\varphi^{ij})\frac{\partial\varphi^{ij}}{\partial x^h_{(v)}}\frac{\partial\varphi^{ij}}{\partial x^s_{(w)}}\Big) - \frac{8\varphi^{ij}\sin\varphi^{ij}}{(1+\cos\varphi^{ij})^2}\frac{\partial\varphi^{ij}}{\partial x^h_{(v)}}\frac{\partial\varphi^{ij}}{\partial x^s_{(w)}}+\\
&+\frac{4\cos\varphi^{ij}}{1+\cos\varphi^{ij}}\left(\frac{\partial\varphi^{ij}}{\partial x^h_{(v)}}\frac{\partial\varphi^{ij}}{\partial x^s_{(w)}}+\varphi^{ij}\frac{\partial^2\varphi^{ij}}{\partial x^h_{(v)}\partial x^s_{(w)}}\right)+2\cos^4\theta^{ij}(\cos^2\theta^{ij}-\\
&-12\theta^{ij}\cos\theta^{ij}\sin\theta^{ij}+15{\theta^{ij}}^2\sin^2\theta^{ij}-3{\theta^{ij}}^2\cos^2\theta^{ij})\frac{\partial\theta^{ij}}{\partial x^h_{(v)}}\frac{\partial\theta^{ij}}{\partial x^s_{(w)}}+\\
&\left.+2\cos^5\theta^{ij}(\theta^{ij}\cos\theta^{ij}-3{\theta^{ij}}^2\sin\theta^{ij})\frac{\partial^2\theta^{ij}}{\partial x^h_{(v)}\partial x^s_{(w)}}\right]-\\
&-2\frac{\partial\Psi^{ij}}{\partial x^h_{(v)}}\left(\varphi^{ij}\frac{\partial\varphi^{ij}}{\partial x^s_{(w)}}+\theta^{ij}\frac{\partial\theta^{ij}}{\partial x^s_{(w)}}\right)-2\frac{\partial\Psi^{ij}}{\partial x^s_{(w)}}\left(\varphi^{ij}\frac{\partial\varphi^{ij}}{\partial x^h_{(v)}}+\theta^{ij}\frac{\partial\theta^{ij}}{\partial x^h_{(v)}}\right)-\\
&-2\Psi^{ij}\left(\frac{\partial\varphi^{ij}}{\partial x^h_{(v)}}\frac{\partial\varphi^{ij}}{\partial x^s_{(w)}}+\varphi^{ij}\frac{\partial^2\varphi^{ij}}{\partial x^h_{(v)}\partial x^s_{(w)}}+\frac{\partial\theta^{ij}}{\partial x^h_{(v)}}\frac{\partial\theta^{ij}}{\partial x^s_{(w)}}+\theta^{ij}\frac{\partial^2\theta^{ij}}{\partial x^h_{(v)}\partial x^s_{(w)}}\right)\Bigg\}\end{aligned} \tag{9.32}$$

The expressions for $\frac{\partial^2\varphi^{ij}}{\partial x^h_{(v)}\partial x^s_{(w)}}$ and $\frac{\partial^2\theta^{ij}}{\partial x^h_{(v)}\partial x^s_{(w)}}$ can be found in appendix D.

## 9.5 Fine-tuning the kinematics associated to the drilling rotations

The author reports that using the enhancement enabled by the drilling degrees of freedom as detailed above produces a significant improvement in the precision of the BEST element. This can be observed in the example of the thick beam (see figure 9.10 which includes also another solution with a definition of symmetric drilling rotations that will be introduced in section 9.5.1). This example has been selected to test the improvements brought by the emulated drilling rotations because it is the one that best characterizes the in-plane shear locking behavior of the element.

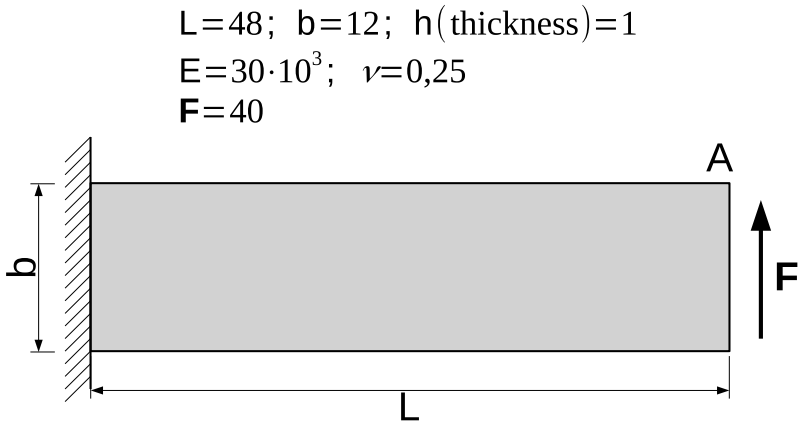


(a) Geometry and properties of the problem.

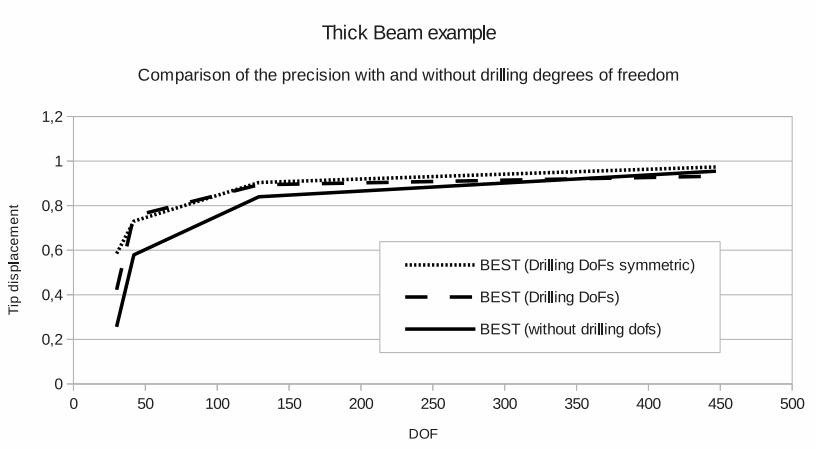


(b) Displacement of the free tip of the beam. Results normalised using as reference solution 0,35533.

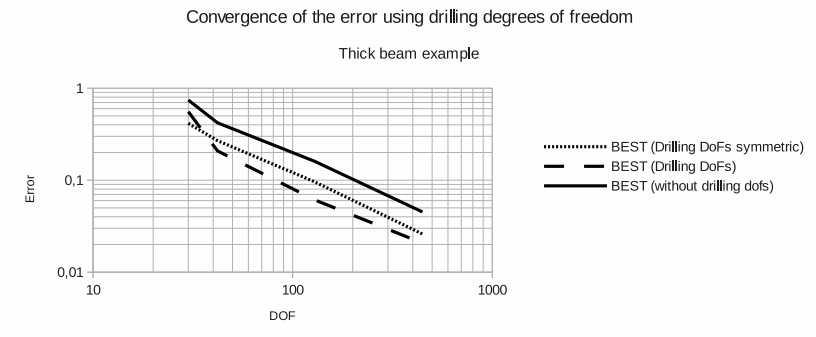


(c) Error convergence with different meshes.

Figure 9.10: Study of the effect of including drilling rotations on the thick beam example. The results are scaled with respect to the reference solution published in [82]. The continuous line corresponds to the solution when no drilling rotations are used and the boundaries are constrained to remain flat. The discontinuous line corresponds to the solution when drilling rotations are used and the formula presented in equation (9.6) is applied. The pointed line corresponds to the solution when drilling rotations are used and the formula presented in equation (9.33) is applied.

### 9.5.1 A temporary fix

Despite the apparent improvement in the precision of the element for coarse meshes, there is something wrong in the new formulation: the element does not converge to the right result. It seems that the element is too stiff. The author suspects that the kinematics associated to the drilling rotations are not well adjusted mesh-wise. Let's analyze a simple example.

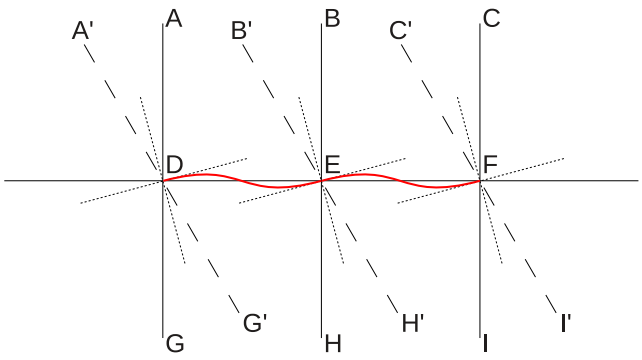


Figure 9.11: Geometric interpretation of the definition of the drilling rotation provided by equation (9.6) and how it affects the actual deformation of the edges D-E-F in the mesh.

Let's consider a Cartesian mesh (for the sake of simplicity we will only consider the edges) subjected to a constant in-plane shear deformation (see figure 9.11). The dashed lines represent the orientation of the straight edges in the deformed configuration as the A, B, C, G, H and I points shift position to their A', B', C', G', H', and I' counterparts. According to the theory of continuum mechanics we know that the actual position of the edges in the deformed configuration is the one marked by the dashed lines. However, because of the emulation of the drilling rotations of the nodes given by the abanico analogy and because of how we have applied them to the rotation of the edges at the node by virtue of equation (9.6), the orientation of the edges at the nodes is the one described by the short pointed lines. Indeed! By applying the relative rotation of the node with respect to the edge back to each edge, we recover the original relative angle of each of the edges with respect to the node, but at a rotated orientation! Of course, by doing this but forcing the edges to preserve their relative angles at the reference configuration, the deformed edges become so crooked that they take deformation energy in excess.

After realizing this mistake, the author sought a quick fix and proposes to change the definition of $\theta^{ij}$.

$$\theta^{ij} = \Delta\alpha^{ij} - \Delta\alpha^{ji} = -\theta^{ji} \tag{9.33}$$

Figure 9.12 provides an interpretation of the effect of this new definition. It clearly improves the behavior in the sense that the deformed edges do not take as much deformation energy. In fact, using equation (9.33) the BEST element converges to the right result. However, it still does so at

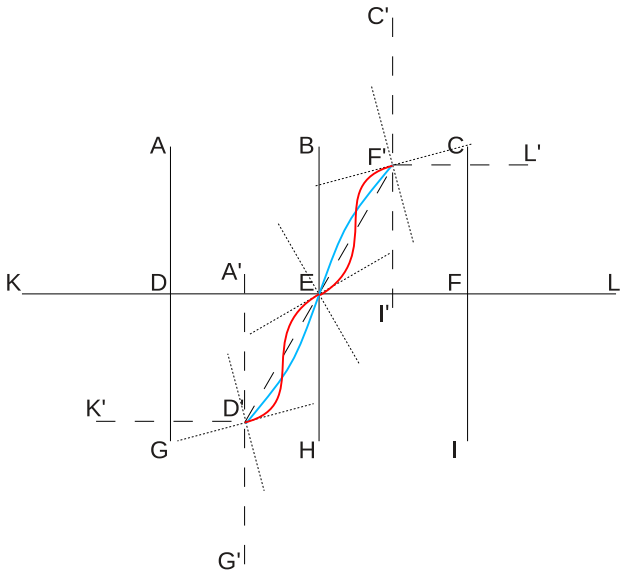


Figure 9.12: Geometric interpretation of the definition of the drilling rotation provided initially by equation (9.6) in red, compared to the effect caused by the new definition of equation (9.33) in blue.

the same mere linear rate of convergence reported earlier. This has many reasons. Firstly, because the new definition of $\theta^{ij}$ no longer uses local information. Instead, it is using a larger set of information without using it to have better precision. Secondly, because by using a symmetric definition of $\theta^{ij}$ and $\theta^{ji}$ a degree of freedom is lost in the kinematic description of the in-plane shear of the BEST element. So this represents a step backwards with respect everything discussed in this chapter.

For all the above reasons, the author also proposes another possible value for $\theta^{ij}$.

$$\theta^{ij} = 0 \tag{9.34}$$

This value is proposed considering that it can be as good as any other arbitrary value of $\theta$. But with the caveat that unlike the developments presented in this thesis previous to introducing the drilling rotations, now the kinematics of the element have been changed and therefore, even with a value of the drilling rotations set to zero, the boundaries of the element are no longer restricted to remain in a flat curve. Therefore there is interest in knowing how this change affects the BEST element.

### 9.5.2 The real deal

After the analysis included above, the author realizes that the formula in equation (9.6) is incomplete. The net effect of equation (9.6) is to apply a solid rigid rotation to all the edges converging on the node $i$, but preserving the relative angles of the reference configuration. Notwithstanding, the

element should represent the deformed configuration wholly. Being able to capture the solid rigid rotation of the node is a good accomplishment and it's what the abanico analogy was all about (see section 9.2.1). But in order to really take advantage of the advanced kinematics brought in by the drilling rotations, it is absolutely necessary to add on top of the solid rigid rotation, the in-plane shear deformation; which is what the BEST element really needs.

The drilling rotation shall be composed of two terms: one corresponding to the solid rigid rotation of the node and another one corresponding to the in-plane shear deformation of the element.

$$\theta^{ij} = \underbrace{\Delta\alpha^{ij}}_{\text{solid rigid rotation}} + \underbrace{\gamma^{ij}}_{\text{in-plane shear}} \tag{9.35}$$

The difficulty now lies in that $\gamma^{ij}$ shall be determined consistently for all the edges converging at the node. The data available, which corresponds to the deformation of each of the neighboring elements, does not need to correspond to a unique value of the local shear deformation at the node. The idea is therefore to use the data provided by the neighboring nodes and approximate the in-plane shear deformation that occurs at the node. This characterization shall then serve to impose the correct direction of the edges' tangents at node $i$ so that the in-plane shear deformation is compliant and consistent. Or put in other words: this construction shall enforce continuity at the nodes of the in-plane shear deformation. The following paragraphs attempt to provide a systematic way to characterize the local in-plane shear deformation at the node based on the information provided by the surrounding nodes. That is, finding a good approximation to a local value, based on global information. By proceeding this way, we will also satisfy the Patch Test. Because in the case of a constant deformation of the mesh, there will be no difference between the local deformation at the node and the deformation obtained by averaging the information gathered from the nodes surrounding the node of interest.

Let's consider the plane defined in figure 9.2 and perpendicular to the normal vector at the node ($\boldsymbol{n}^i$). This is the plane used in figure 9.13. The author is interested in characterizing the shear deformation that happens on that plane. That is, at the tangent plane to the surface at $i$. Or in other words: in the limit when the area considered degenerates into the material point $\boldsymbol{x}^i$ (see figure 9.13).

The formula that determines the relative angle in the deformed configuration between two given fibers defined at the reference configuration is:

$$\cos\beta_i^{jk} = \frac{\dfrac{\breve{\boldsymbol{e}}^{ijT}}{\|\breve{\boldsymbol{e}}^{ij}\|}\cdot(\boldsymbol{I}+2\breve{\boldsymbol{E}})\cdot\dfrac{\breve{\boldsymbol{e}}^{ik}}{\|\breve{\boldsymbol{e}}^{ik}\|}}{\sqrt{1+2\dfrac{\breve{\boldsymbol{e}}^{ijT}}{\|\breve{\boldsymbol{e}}^{ij}\|}\cdot\breve{\boldsymbol{E}}\cdot\dfrac{\breve{\boldsymbol{e}}^{ij}}{\|\breve{\boldsymbol{e}}^{ij}\|}}\cdot\sqrt{1+2\dfrac{\breve{\boldsymbol{e}}^{ikT}}{\|\breve{\boldsymbol{e}}^{ik}\|}\cdot\breve{\boldsymbol{E}}\cdot\dfrac{\breve{\boldsymbol{e}}^{ik}}{\|\breve{\boldsymbol{e}}^{ik}\|}}} \tag{9.36}$$

Where we maintain the notation provided in figures 9.2 and 9.13. The vectors $\breve{e}^{ij}$ and $\breve{e}^{ik}$ correspond to the $\boldsymbol{e}^{ij}$ and $\boldsymbol{e}^{ik}$ vectors after being rotated an angle $\Delta\alpha^{ij}$ and $\Delta\alpha^{ik}$, respectively. After this rotation, the vectors recover

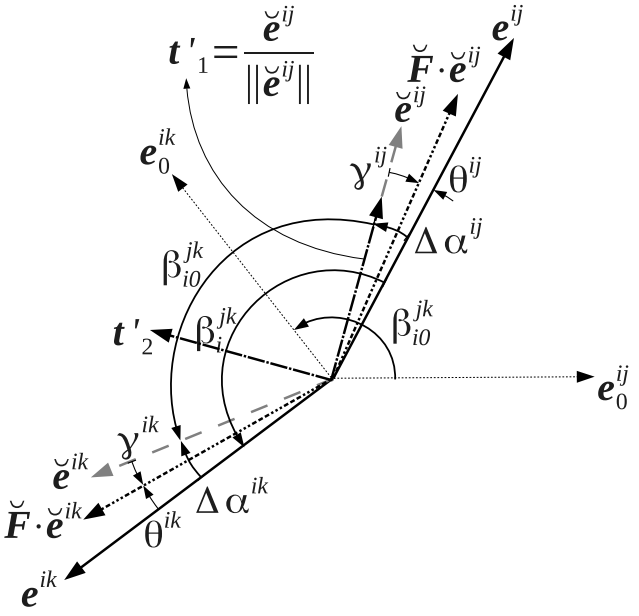


Figure 9.13: Scheme depicting the process to find the value of $\theta^{ij}$ using equation (9.35). The vectors $\boldsymbol{e}_0^{ij}$ and $\boldsymbol{e}_0^{ik}$ are not really in the plane of the figure, but they are represented anyway to indicate that their angle $\beta_{i0}^{jk}$ is the same as the angle between $\breve{\boldsymbol{e}}^{ij}$ and $\breve{\boldsymbol{e}}^{ik}$.

the same relative angles as those of the reference configuration. $\breve{\boldsymbol{E}}$ is a Green-Lagrange strain tensor, but differs from the tensors defined in section 4.3 and chapter 6 in that this tensor is defined only in two dimensions and serves only to characterize the shear deformation at the node. Now, by confining the tensors to the two dimensions of the plane and defining a local reference frame $\breve{\boldsymbol{T}}$ centered at $\boldsymbol{x}^i$ and with the direction of the first versor coincident with $\breve{\boldsymbol{e}}^{ij}$, we can rewrite equation (9.36) as:

$$\cos\beta_i^{jk} = \frac{\begin{pmatrix}1\\0\end{pmatrix}^T \cdot (\boldsymbol{I} + 2\breve{\boldsymbol{E}}_{[\breve{\boldsymbol{T}}]}) \cdot \begin{pmatrix}\cos\beta_{i0}^{jk}\\ \sin\beta_{i0}^{jk}\end{pmatrix}}{\sqrt{1 + 2\begin{pmatrix}1\\0\end{pmatrix}^T \cdot \breve{\boldsymbol{E}}_{[\breve{\boldsymbol{T}}]} \cdot \begin{pmatrix}1\\0\end{pmatrix}} \cdot \sqrt{1 + 2\begin{pmatrix}\cos\beta_{i0}^{jk}\\ \sin\beta_{i0}^{jk}\end{pmatrix}^T \cdot \breve{\boldsymbol{E}}_{[\breve{\boldsymbol{T}}]} \cdot \begin{pmatrix}\cos\beta_{i0}^{jk}\\ \sin\beta_{i0}^{jk}\end{pmatrix}}} \tag{9.37}$$

Taking into account that we only care about the in-plane shear deformation produced between the reference and current configurations, it is safe to say that the tensor $\breve{\boldsymbol{E}}$ is a deviatoric tensor and has the following general expression:

$$\breve{\boldsymbol{E}}_{[\breve{\boldsymbol{T}}]} = \underbrace{\breve{\boldsymbol{E}}^h_{[\breve{\boldsymbol{T}}]}}_{\text{hydrostatic}} + \underbrace{\breve{\boldsymbol{E}}^d_{[\breve{\boldsymbol{T}}]}}_{\text{deviatoric}} = \breve{\boldsymbol{E}}^d_{[\breve{\boldsymbol{T}}]} = \begin{bmatrix} E_d^i & \gamma^i/2 \\ \gamma^i/2 & -E_d^i \end{bmatrix} \tag{9.38}$$

The $(\cdot)^i$ superindices serve to emphasize the message that the $\breve{\boldsymbol{E}}$ tensor is defined and has meaning only at the node $i$. The reference frame $\breve{\boldsymbol{T}}$ is defined in figure 9.13 by the orthonormal vectors $\boldsymbol{t}'_1$ and $\boldsymbol{t}'_2$.

Substituting equation (9.38) into equation (9.37) and rearranging terms we obtain the following non-linear equation:

$$\begin{pmatrix} 2\cos\beta_{i0}^{jk} & \sin\beta_{i0}^{jk} \end{pmatrix} \cdot \begin{pmatrix} E_d^i \\ \gamma^i \end{pmatrix} = -\cos\beta_{i0}^{jk} + \\ + \cos\beta_i^{jk}\sqrt{1+2E_d^i}\sqrt{1+2E_d^i\cdot\cos 2\beta_{i0}^{jk}+\gamma^i\cdot\sin 2\beta_{i0}^{jk}} \quad (9.39)$$

where $E_d^i$ and $\gamma^i$ are the unknowns.

A system of equations can be built with every instance of equation (9.39) for each edge $i$–$k$ different than $i$–$j$. A number of cases can be considered:

- In the case when there is only one triangle having node $i$ as a vertex, the system of equations will have only one equation and cannot be solved. In this case the author chooses to let the edge's tangents at the node follow the direction dictated by the mesh. And the value of $\theta^{ij}$ in equation (9.35) is set to zero. So that node will not have any emulated drilling rotation.

- In the case when there are two edges other than $i$–$j$ converging at $i$, the system of equations will have exactly two equations and can be solved in an ordinary way.

- In the case when there are three or more edges other than $i$–$j$, the system of equations will be over-determined. In this case, a least squares solution can be worked out.

Assuming solved the system of equations—and $\breve{\boldsymbol{E}}$ obtained—, there is still another necessary step in order to obtain the value of $\gamma^{ij}$ in equation (9.35). The Green-Lagrange deformation tensor provides information about the relative position of material points in the current configuration based on their relative position in the reference configuration. But does not provide any information about the relative position of a material point in the current configuration with respect to its position in the reference configuration. The tensor that provides that information is the tensor gradient of deformation $\breve{\boldsymbol{F}}$.

$$\boldsymbol{I} + 2\breve{\boldsymbol{E}}_{[\breve{\boldsymbol{T}}]} = \breve{\boldsymbol{F}}^T_{[\breve{\boldsymbol{T}}]} \cdot \breve{\boldsymbol{F}}_{[\breve{\boldsymbol{T}}]} \quad (9.40)$$

In the general 2D case, $\breve{\boldsymbol{F}}$ has 4 independent components, so it is not possible to obtain them from this equation because this is the equation of a symmetric tensor and therefore 2 components are linearly dependent (identical). But we can take advantage of the fact that we have the information on the solid rigid rotation provided by the abanico analogy, and benefit from the polar decomposition of the deformation gradient tensor:

$$\breve{\boldsymbol{F}}_{[\breve{\boldsymbol{T}}]} = \underbrace{\boldsymbol{R}}_{\text{rotation}} \cdot \underbrace{\boldsymbol{U}}_{\text{deformation}} \quad (9.41)$$

where $\boldsymbol{R}$ is an orthogonal tensor and $\boldsymbol{U}$ is a symmetric tensor. Substituting equation (9.41) into equation (9.40) the following is obtained:

$$\boldsymbol{I} + 2\breve{\boldsymbol{E}}_{[\breve{\boldsymbol{T}}]} = \boldsymbol{U}^T \cdot \boldsymbol{R}^T \cdot \boldsymbol{R} \cdot \boldsymbol{U} = \boldsymbol{U} \cdot \boldsymbol{U} = \boldsymbol{U}^2 \tag{9.42}$$

The first thing that equation (9.42) teaches us is that the deformation described by $\breve{\boldsymbol{E}}$ is independent of solid rigid rotations. Therefore it can be interpreted that the value of $\breve{\boldsymbol{E}}$ is obtained based on the relative angles of the edges converging on $i$ in the reference configuration ($\beta_{i0}^{jk}$), or the same relative angles after being rotated by the solid rigid rotation of the node and evaluated using the abanico analogy (see figure 9.13). The author chooses the latter. Therefore, the author assumes that there is no rigid body rotation after the relative orientations of the edges in the reference configuration are recovered using the abanico analogy. And writes:

$$\breve{\boldsymbol{F}}_{[\breve{\boldsymbol{T}}]} = \boldsymbol{R} \cdot \boldsymbol{U} = \boldsymbol{I} \cdot \boldsymbol{U} = \boldsymbol{U} = \sqrt{\boldsymbol{I} + 2\breve{\boldsymbol{E}}_{[\breve{\boldsymbol{T}}]}} \tag{9.43}$$

Finally, $\gamma^{ij}$ can be computed using the following development:

$$\mathrm{d}\boldsymbol{x}_{[\breve{\boldsymbol{T}}]} = \breve{\boldsymbol{F}}_{[\breve{\boldsymbol{T}}]} \cdot \mathrm{d}\boldsymbol{X}_{[\breve{\boldsymbol{T}}]} \tag{9.44}$$

$$\mathrm{d}s \cdot \begin{pmatrix} \cos(\beta_{i0}^{jk} + \gamma^{ik}) \\ \sin(\beta_{i0}^{jk} + \gamma^{ik}) \end{pmatrix} = \mathrm{d}S \cdot \breve{\boldsymbol{F}}_{[\breve{\boldsymbol{T}}]} \cdot \begin{pmatrix} \cos\beta_{i0}^{jk} \\ \sin\beta_{i0}^{jk} \end{pmatrix} \tag{9.45}$$

$$\gamma^{ik} = \arctan\left( \frac{\dfrac{F_{12}\cos\beta_{i0}^{jk} + F_{22}\sin\beta_{i0}^{jk}}{F_{11}\cos\beta_{i0}^{jk} + F_{12}\sin\beta_{i0}^{jk}} - \tan\beta_{i0}^{jk}}{1 + \tan\beta_{i0}^{jk}\dfrac{F_{12}\cos\beta_{i0}^{jk} + F_{22}\sin\beta_{i0}^{jk}}{F_{11}\cos\beta_{i0}^{jk} + F_{12}\sin\beta_{i0}^{jk}}} \right) \tag{9.46}$$

and in particular, when $k = j$

$$\gamma^{ij} = \arctan\left(\frac{F_{12}}{F_{11}}\right) \tag{9.47}$$

## 9.6 Summary

The topic of membrane locking in thin shells has been discussed. The author presents solid arguments existing in the bibliography to support the idea that a fully cubic BEST element should not suffer from membrane locking. However, it does because not all the potential of the cubic description of the BEST element is unleashed. in order to fix it, the author proposes to emulate the concept of drilling degrees of freedom and therefore provide the information needed to complete the geometric construction of the cubic triangle.

The geometric construction of the element taking into account the corner drilling rotations again brings about the issue of energy minimization. The author solves the problem by uncoupling the problem and reducing it to a 2D periodic *torsion mode*. The function that minimizes the energy for the in-plane shear deformation differs from the function that also minimizes the energy for the bending and out-of-plane membrane deformation

reported in section 5.4. This issue is solved by constructing a weighted average function. The indetermination of this weighted average function is also presented and solved for the primitive and its derivatives.

Finally, the author reports a problem in the definition of the corner drilling rotation based on the rotations of the neighboring edges. The initial definition results in overly crooked elements, and thus an excessively stiff response of the shell. In order to correct this issue a simple fix is presented, although represents a step backwards and makes all the effort of little advantage.

It is necessary a more thorough theoretic work on the definition of the corner drilling rotations based on the rotations of the neighboring triangles. The author presents an idea focused on sound continuum mechanics concepts about the deformation at a point. In particular, the author proposes that the solution should enforce the continuity of the in-plane shear deformation between elements at the nodes. This in-plane shear is characterized uniquely for each node but means that the in-plane shear angle depends on the orientation of the fibers in the tangent plane. This idea has not been implemented numerically. Numerical results cannot be reported to verify the validity and goodness of the idea.

# Chapter 10

# How to apply Dirichlet boundary conditions on rotations and their application to kinking and branching configurations

AS HAS BEEN DISCUSSED in section 4.1.1, rotation-free elements have inherent difficulties in imposing boundary conditions over the rotations because they don't have rotational degrees of freedom associated. The author has considered different alternatives like using Lagrange multipliers, the penalty method or even applying the boundary condition in other weak form using Nitsche's method. But none of these options are of the author's liking because they have uninteresting algorithmic or stability implications.

Somewhat surprisingly, the application of the Dirichlet boundary conditions on rotations is straightforward for the BEST element. This chapter will explain how and why. The original idea in the BEST element is to impose the rotation boundary conditions not on displacements but on the normals... because they are explicitly defined! By doing this, the shape functions of the element are indeed modified in order to satisfy the boundary conditions. And this has the advantages that the size of the system matrix does not increase, there is no need to deal with esoteric coefficients and furthermore: the symmetric and positive definite character of the matrix is conserved.

This chapter is organized assigning each section to a specific boundary condition or combination of them. Section 10.1 presents the case where all the out-of-plane rotations are inhibited. This case is presented first because of its pedagogic value. Next, section 10.2 explains the boundary condition which inhibits the in-plane rotations. It is presented as a continuous simple support along the boundary because it is completely equivalent.

Sections 10.3 and 10.4 present the decomposition of the boundary condition presented in section 10.1 according to the local axes at the boundary. That is: whether the rotations are inhibited in the direction perpendicular

to the boundary, or in the direction parallel to the boundary. As in section 10.2, the boundary condition which inhibits out-of-plane rotations in the direction parallel to the boundary is presented as a continuous simple support along the boundary because it is completely equivalent.

In all cases, the strategy used to constrain the rotations is focused on the construction process of the element's geometry. That is, when computing the location of the Bézier control points of the element, instead of using the information provided by the neighboring elements to compute the normal direction, the fixed normal will be used. And the corresponding equation will be identified and swapped by a new one that applies the specific boundary condition. Note that the normal direction must not be directly imposed. Instead, its rotations are to be set. This is an important caveat, as doing otherwise would certainly generate undesired deformations and introduce unwanted deformation energy with respect to the reference configuration.

A boundary condition of particular interest to the finite element analyst is the symmetry boundary condition. This is a condition that does not correspond to a physical reality. But its effect is very real and moreover, it is useful. Because it allows the finite element analyst to significantly reduce the computational cost of a simulation where this condition can be applied. Section 10.5 explains how to obtain this particular boundary condition combining the conditions presented in sections 10.2 and 10.3.

Then, the chapter takes a turn and proceeds explaining how to solve the more advanced configurations involving internal hinges or kinks in the shell. These are detailed in sections 10.6 and 10.7.

Finally, the author provides guidance into how to evolve to the more complex configurations involving the convergence of three or more shells using combinations of the boundary conditions already explained. This is presented in section 10.8.

## 10.1 Fully clamped boundary condition

This is the easiest condition and will be presented first for pedagogic purposes. Fully clamped means that nothing moves. This means that all three displacements and rotations are fixed. Let's talk about the rotations as the process for the displacements is standard in the literature.

That the rotations are fixed is equivalent to the following statement:

$$\boldsymbol{n}^i = \boldsymbol{\mathcal{N}}^i \qquad \forall\, t > t_0 \tag{10.1}$$

Equation (10.1) substitutes equation (5.3) for those nodes having the condition. As a result, equations (D.28) and (D.29) are substituted by equations (10.2) and (10.3), respectively for those nodes having the fully clamped condition.

$$\frac{\partial \boldsymbol{n}^i}{\partial \tilde{\boldsymbol{x}}} = \boldsymbol{0} \tag{10.2}$$

$$\frac{\partial^2 \boldsymbol{n}^i}{(\partial \tilde{\boldsymbol{x}})^2} = \boldsymbol{0} \tag{10.3}$$

The reader shall not be confused by this expression. The interpretation of the above derivatives is not a free movement of the normal direction at the node independent of the nodal displacements. This is prevented by equation (10.1). No, instead equations (10.2) and (10.3) are implicitly and subtly modifying the derivatives of the pseudo-deformation tensor $\boldsymbol{B}$ and $\frac{\partial \boldsymbol{B}}{\partial \bar{\boldsymbol{x}}}$ in a way that provides the necessary information to the stiffness matrix to account for the particular way the element will deform maintaining the normal direction $\boldsymbol{n}^i$ still.

Notice that this condition also results as a combination of the conditions described in sections 10.3 and 10.4 (see figure 10.1).

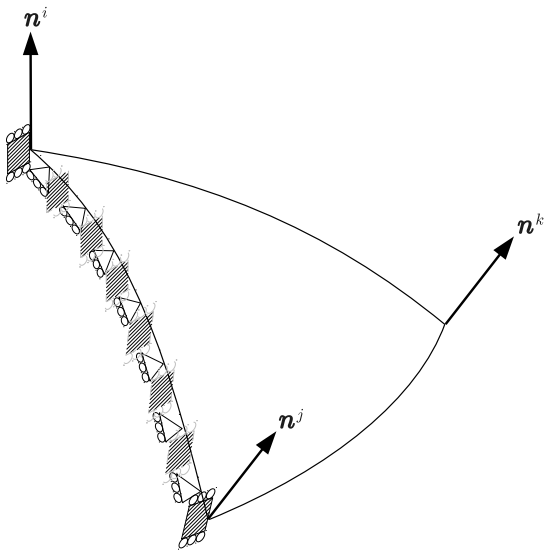


Figure 10.1: Figure showing the meaning of a fully clamped boundary condition as a combination of two different conditions. See figures 10.3 and 10.4.

## 10.2 Continuous simply supported shell in the tangent plane direction

A simple support would usually be applied directly to the displacement degrees of freedom. However, in order to properly apply a continuously supported boundary condition, attention to the rotations must be given as well. In this sense, if the edge of a triangle spanning nodes $i$ and $j$ is set to have a simply supported boundary condition in the tangent plane (see figure 10.2), this means that the drilling rotations associated to the $i$–$j$ edge will be zero.

$$\theta^{ij} = \theta^{ji} = 0 \tag{10.4}$$

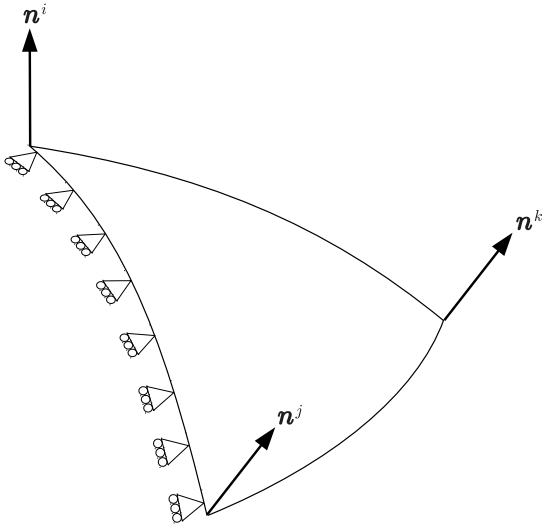


Figure 10.2: Figure showing the meaning of the boundary condition of a continuous simply supported shell edge in the tangent plane direction.

And therefore equation (9.7) becomes:

$$\boldsymbol{d}^{ij} = \boldsymbol{\mathcal{N}}^i \times (\boldsymbol{X}^i - \boldsymbol{X}^j) \tag{10.5}$$

$$\boldsymbol{d}^{ji} = \boldsymbol{\mathcal{N}}^j \times (\boldsymbol{X}^j - \boldsymbol{X}^i) \tag{10.6}$$

for each segment affected by the condition. And consequently the following also applies, substituting equations (D.42) and (D.43).

$$\frac{\partial \boldsymbol{d}^{ij}}{\partial \tilde{\boldsymbol{x}}} = \boldsymbol{0} \tag{10.7}$$

$$\frac{\partial^2 \boldsymbol{d}^{ij}}{(\partial \tilde{\boldsymbol{x}})^2} = \boldsymbol{0} \tag{10.8}$$

## 10.3 Boundary clamped in the perpendicular direction

Similarly to the case presented in section 10.1, in this case a condition is established on the normal $\boldsymbol{n}^i$. The key is to define the unit vector representing the direction about which the rotation of $\boldsymbol{n}^i$ is not constrained. Let's name that vector $\boldsymbol{t}_\perp$ (see figure 10.3). Then, the following condition must be satisfied:

$$\boldsymbol{n}^i \cdot \boldsymbol{t}_\perp = \boldsymbol{\mathcal{N}}^i \cdot \boldsymbol{t}_\perp \tag{10.9}$$

In order to satisfy this condition, equation (5.3) is modified in the fol-

lowing way:

$$\boldsymbol{n}^i = \sqrt{1-(\boldsymbol{\mathcal{N}}^i\cdot\boldsymbol{t}_\perp)^2}\cdot\frac{(\boldsymbol{I}-\boldsymbol{t}_\perp\otimes\boldsymbol{t}_\perp)\cdot\sum\limits_{k=1}^{r_i}w^k_{\alpha/A_\circ}\cdot\hat{\boldsymbol{y}}^k}{\left\|(\boldsymbol{I}-\boldsymbol{t}_\perp\otimes\boldsymbol{t}_\perp)\cdot\sum\limits_{k=1}^{r_i}w^k_{\alpha/A_\circ}\cdot\hat{\boldsymbol{y}}^k\right\|}+(\boldsymbol{\mathcal{N}}^i\cdot\boldsymbol{t}_\perp)\cdot\boldsymbol{t}_\perp \tag{10.10}$$

For the general case it is necessary to explicitly define the direction of $\boldsymbol{t}_\perp$ by the user. Notice that this directly allows to specify a clamped condition allowing rotation about an axis not necessarily contained in the tangent plane of the shell.

Deriving equation (10.10) we obtain:

$$\frac{\partial\boldsymbol{n}^i}{\partial\tilde{\boldsymbol{x}}^r}=\frac{\sqrt{1-(\boldsymbol{\mathcal{N}}^i\cdot\boldsymbol{t}_\perp)^2}\cdot(\boldsymbol{I}-\boldsymbol{t}_\perp\cdot\boldsymbol{t}_\perp{}^T)}{\left\|(\boldsymbol{I}-\boldsymbol{t}_\perp\cdot\boldsymbol{t}_\perp{}^T)\cdot\sum\limits_{k=1}^{r_i}w^k_{\alpha/A_\circ}\hat{\boldsymbol{y}}^k\right\|}\cdot\left\{\sum_{k=1}^{r_i}\frac{\partial}{\partial\tilde{\boldsymbol{x}}^r}\left(w^k_{\alpha/A_\circ}\hat{\boldsymbol{y}}^k\right)-\right.$$
$$\left.-\frac{\left(\sum\limits_{k=1}^{r_i}w^k_{\alpha/A_\circ}\hat{\boldsymbol{y}}^k\right)^T\cdot(\boldsymbol{I}-\boldsymbol{t}_\perp\cdot\boldsymbol{t}_\perp{}^T)\cdot\sum\limits_{k=1}^{r_i}\frac{\partial}{\partial\tilde{\boldsymbol{x}}^r}\left(w^k_{\alpha/A_\circ}\hat{\boldsymbol{y}}^k\right)}{\left\|(\boldsymbol{I}-\boldsymbol{t}_\perp\cdot\boldsymbol{t}_\perp{}^T)\cdot\sum\limits_{k=1}^{r_i}w^k_{\alpha/A_\circ}\hat{\boldsymbol{y}}^k\right\|^2}\cdot\sum_{k=1}^{r_i}w^k_{\alpha/A_\circ}\hat{\boldsymbol{y}}^k\right\} \tag{10.11}$$

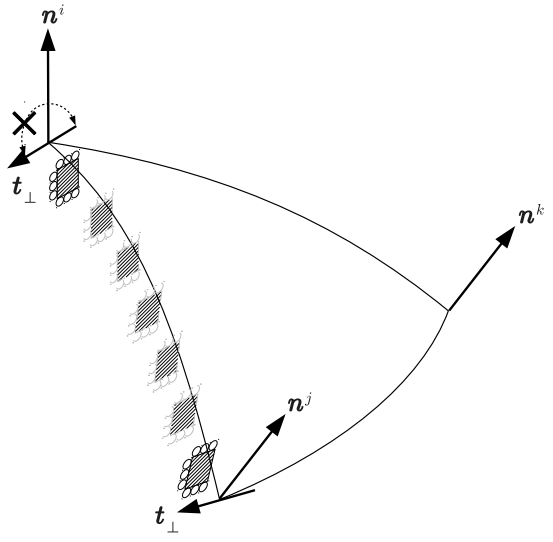


Figure 10.3: Figure showing the meaning of the boundary clamped in the perpendicular direction. A graphical interpretation of the meaning of equation (10.9) is also presented. That is, the vector $\boldsymbol{n}^i$ can rotate only about the vector $\boldsymbol{t}_\perp$. However, even if this condition is met at the two nodes bounding an edge, it cannot be enforced along all the edge. Doing so would require imposing conditions on the triangle's central control point.

and

$$\frac{\partial^2 \boldsymbol{n}^i}{\partial x^h_{(v)} \partial x^s_{(w)}} = \frac{\sqrt{1-\left(\boldsymbol{\mathcal{N}}^i \cdot \boldsymbol{t}_\perp\right)^2} \cdot \left(\boldsymbol{I} - \boldsymbol{t}_\perp \cdot \boldsymbol{t}_\perp{}^T\right)}{\left\| \left(\boldsymbol{I} - \boldsymbol{t}_\perp \cdot \boldsymbol{t}_\perp{}^T\right) \cdot \sum\limits_{k=1}^{r_i} w^k_{\alpha/A_\circ} \hat{\boldsymbol{y}}^k \right\|} \cdot \left\{ \sum_{k=1}^{r_i} \frac{\partial^2 \left( w^k_{\alpha/A_\circ} \hat{\boldsymbol{y}}^k \right)}{\partial x^h_{(v)} \partial x^s_{(w)}} + \right.$$

$$+ 3 \frac{\left( \sum\limits_{k=1}^{r_i} w^k_{\alpha/A_\circ} \hat{\boldsymbol{y}}^k \right)^T \cdot \left(\boldsymbol{I} - \boldsymbol{t}_\perp \cdot \boldsymbol{t}_\perp{}^T\right) \cdot \sum\limits_{k=1}^{r_i} \frac{\partial}{\partial x^h_{(v)}} \left( w^k_{\alpha/A_\circ} \hat{\boldsymbol{y}}^k \right)}{\left\| \left(\boldsymbol{I} - \boldsymbol{t}_\perp \cdot \boldsymbol{t}_\perp{}^T\right) \cdot \sum\limits_{k=1}^{r_i} w^k_{\alpha/A_\circ} \hat{\boldsymbol{y}}^k \right\|^2} \cdot$$

$$\cdot \frac{\left( \sum\limits_{k=1}^{r_i} w^k_{\alpha/A_\circ} \hat{\boldsymbol{y}}^k \right)^T \cdot \left(\boldsymbol{I} - \boldsymbol{t}_\perp \cdot \boldsymbol{t}_\perp{}^T\right) \cdot \sum\limits_{k=1}^{r_i} \frac{\partial}{\partial x^s_{(w)}} \left( w^k_{\alpha/A_\circ} \hat{\boldsymbol{y}}^k \right)}{\left\| \left(\boldsymbol{I} - \boldsymbol{t}_\perp \cdot \boldsymbol{t}_\perp{}^T\right) \cdot \sum\limits_{k=1}^{r_i} w^k_{\alpha/A_\circ} \hat{\boldsymbol{y}}^k \right\|^2} \cdot \sum_{k=1}^{r_i} w^k_{\alpha/A_\circ} \hat{\boldsymbol{y}}^k -$$

$$- \frac{\left( \sum\limits_{k=1}^{r_i} w^k_{\alpha/A_\circ} \hat{\boldsymbol{y}}^k \right)^T \cdot \left(\boldsymbol{I} - \boldsymbol{t}_\perp \cdot \boldsymbol{t}_\perp{}^T\right) \cdot \sum\limits_{k=1}^{r_i} \frac{\partial}{\partial x^h_{(v)}} \left( w^k_{\alpha/A_\circ} \hat{\boldsymbol{y}}^k \right)}{\left\| \left(\boldsymbol{I} - \boldsymbol{t}_\perp \cdot \boldsymbol{t}_\perp{}^T\right) \cdot \sum\limits_{k=1}^{r_i} w^k_{\alpha/A_\circ} \hat{\boldsymbol{y}}^k \right\|^2} \cdot \sum_{k=1}^{r_i} \frac{\partial}{\partial x^s_{(w)}} \left( w^k_{\alpha/A_\circ} \hat{\boldsymbol{y}}^k \right) -$$

$$- \frac{\left( \sum\limits_{k=1}^{r_i} w^k_{\alpha/A_\circ} \hat{\boldsymbol{y}}^k \right)^T \cdot \left(\boldsymbol{I} - \boldsymbol{t}_\perp \cdot \boldsymbol{t}_\perp{}^T\right) \cdot \sum\limits_{k=1}^{r_i} \frac{\partial}{\partial x^s_{(w)}} \left( w^k_{\alpha/A_\circ} \hat{\boldsymbol{y}}^k \right)}{\left\| \left(\boldsymbol{I} - \boldsymbol{t}_\perp \cdot \boldsymbol{t}_\perp{}^T\right) \cdot \sum\limits_{k=1}^{r_i} w^k_{\alpha/A_\circ} \hat{\boldsymbol{y}}^k \right\|^2} \cdot \sum_{k=1}^{r_i} \frac{\partial}{\partial x^h_{(v)}} \left( w^k_{\alpha/A_\circ} \hat{\boldsymbol{y}}^k \right) -$$

$$- \left[ \frac{\left( \sum\limits_{k=1}^{r_i} \frac{\partial}{\partial x^h_{(v)}} w^k_{\alpha/A_\circ} \hat{\boldsymbol{y}}^k \right)^T \cdot \left(\boldsymbol{I} - \boldsymbol{t}_\perp \cdot \boldsymbol{t}_\perp{}^T\right) \cdot \sum\limits_{k=1}^{r_i} \frac{\partial}{\partial x^s_{(w)}} \left( w^k_{\alpha/A_\circ} \hat{\boldsymbol{y}}^k \right)}{\left\| \left(\boldsymbol{I} - \boldsymbol{t}_\perp \cdot \boldsymbol{t}_\perp{}^T\right) \cdot \sum\limits_{k=1}^{r_i} w^k_{\alpha/A_\circ} \hat{\boldsymbol{y}}^k \right\|^2} + \right.$$

$$\left. \left. + \frac{\left( \sum\limits_{k=1}^{r_i} w^k_{\alpha/A_\circ} \hat{\boldsymbol{y}}^k \right)^T \cdot \left(\boldsymbol{I} - \boldsymbol{t}_\perp \cdot \boldsymbol{t}_\perp{}^T\right) \cdot \sum\limits_{k=1}^{r_i} \frac{\partial^2 \left( w^k_{\alpha/A_\circ} \hat{\boldsymbol{y}}^k \right)}{\partial x^h_{(v)} \partial x^s_{(w)}}}{\left\| \left(\boldsymbol{I} - \boldsymbol{t}_\perp \cdot \boldsymbol{t}_\perp{}^T\right) \cdot \sum\limits_{k=1}^{r_i} w^k_{\alpha/A_\circ} \hat{\boldsymbol{y}}^k \right\|^2} \right] \cdot \sum_{k=1}^{r_i} w^k_{\alpha/A_\circ} \hat{\boldsymbol{y}}^k \right\} \tag{10.12}$$

which substitute equations (D.28) and (D.29), respectively.

## 10.4 Continuous simply supported shell in the normal direction

If the edge of a triangle containing node $i$ is set to have a simply supported boundary condition in the normal direction, this means that the curvature parallel to the boundary is constrained. This condition is imposed by defining a unit vector parallel to the boundary. Let's name that vector $\boldsymbol{t}_\parallel$ (see

figure 10.4). Then, the following condition must be satisfied:

$$\boldsymbol{n}^i \cdot \boldsymbol{t}_{\|} = \boldsymbol{\mathcal{N}}^i \cdot \boldsymbol{t}_{\|} \tag{10.13}$$

Which translates into the following variation of equation (5.3):

$$\boldsymbol{n}^i = \sqrt{1 - (\boldsymbol{\mathcal{N}}^i \cdot \boldsymbol{t}_{\|})^2} \cdot \frac{(\boldsymbol{I} - \boldsymbol{t}_{\|} \cdot \boldsymbol{t}_{\|}{}^T) \cdot \sum_{k=1}^{r_i} w^k_{\alpha/A_\circ} \cdot \hat{\boldsymbol{y}}^k}{\left\| (\boldsymbol{I} - \boldsymbol{t}_{\|} \cdot \boldsymbol{t}_{\|}{}^T) \cdot \sum_{k=1}^{r_i} w^k_{\alpha/A_\circ} \cdot \hat{\boldsymbol{y}}^k \right\|} + (\boldsymbol{\mathcal{N}}^i \cdot \boldsymbol{t}_{\|}) \cdot \boldsymbol{t}_{\|} \tag{10.14}$$

For the general case it is necessary to explicitly define the direction of $\boldsymbol{t}_{\|}$ by the user. In particular, it must be defined by the pre-processor, as the direction tangent to the boundary at the node cannot be obtained from the mesh and needs to be provided by the actual geometry of the shell.

Deriving equation (10.14) we obtain the following expressions to substitute equations (D.28) and (D.29):

$$\frac{\partial \boldsymbol{n}^i}{\partial \tilde{\boldsymbol{x}}^r} = \frac{\sqrt{1 - \left(\boldsymbol{\mathcal{N}}^i \cdot \boldsymbol{t}_{\|}\right)^2} \cdot (\boldsymbol{I} - \boldsymbol{t}_{\|} \cdot \boldsymbol{t}_{\|}{}^T)}{\left\| (\boldsymbol{I} - \boldsymbol{t}_{\|} \cdot \boldsymbol{t}_{\|}{}^T) \cdot \sum_{k=1}^{r_i} w^k_{\alpha/A_\circ} \hat{\boldsymbol{y}}^k \right\|} \cdot \left\{ \sum_{k=1}^{r_i} \frac{\partial}{\partial \tilde{\boldsymbol{x}}^r} \left( w^k_{\alpha/A_\circ} \hat{\boldsymbol{y}}^k \right) - \right.$$

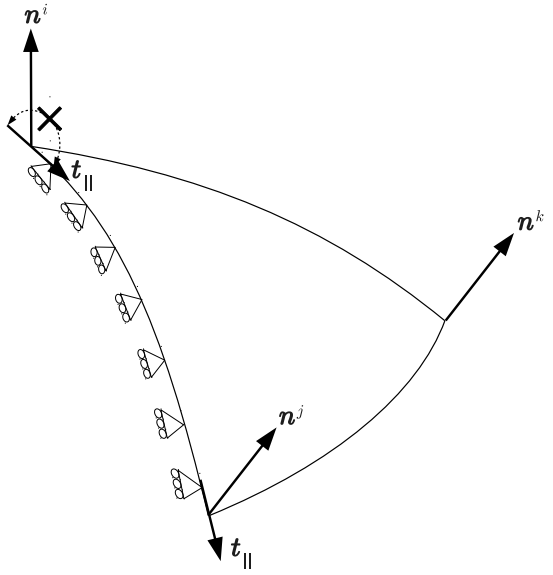


Figure 10.4: Figure showing the meaning of the boundary condition of a continuous simply supported shell edge in the direction normal to the tangent plane. A graphical interpretation of the meaning of equation (10.13) is also presented. That is, the vector $\boldsymbol{n}^i$ can rotate only about the vector $\boldsymbol{t}_{\|}$. When this condition is met at the two nodes bounding an edge, then it is satisfied along all the edge.

$$-\frac{\left(\sum_{k=1}^{r_i} w^k_{\alpha/A_\circ}\hat{\boldsymbol{y}}^k\right)^T\cdot(\boldsymbol{I}-\boldsymbol{t}_\parallel\cdot\boldsymbol{t}_\parallel{}^T)\cdot\sum_{k=1}^{r_i}\frac{\partial}{\partial\tilde{\boldsymbol{x}}^r}\left(w^k_{\alpha/A_\circ}\hat{\boldsymbol{y}}^k\right)}{\left\|(\boldsymbol{I}-\boldsymbol{t}_\parallel\cdot\boldsymbol{t}_\parallel{}^T)\cdot\sum_{k=1}^{r_i} w^k_{\alpha/A_\circ}\hat{\boldsymbol{y}}^k\right\|^2}\cdot\sum_{k=1}^{r_i} w^k_{\alpha/A_\circ}\hat{\boldsymbol{y}}^k\Bigg\} \tag{10.15}$$

and

$$\begin{aligned}\frac{\partial^2\boldsymbol{n}^i}{\partial x^h_{(v)}\partial x^s_{(w)}} = \frac{\sqrt{1-\left(\boldsymbol{\mathcal{N}}^i\cdot\boldsymbol{t}_\parallel\right)^2}\cdot(\boldsymbol{I}-\boldsymbol{t}_\parallel\cdot\boldsymbol{t}_\parallel{}^T)}{\left\|(\boldsymbol{I}-\boldsymbol{t}_\parallel\cdot\boldsymbol{t}_\parallel{}^T)\cdot\sum_{k=1}^{r_i} w^k_{\alpha/A_\circ}\hat{\boldsymbol{y}}^k\right\|}\cdot\Bigg\{\sum_{k=1}^{r_i}\frac{\partial^2\left(w^k_{\alpha/A_\circ}\hat{\boldsymbol{y}}^k\right)}{\partial x^h_{(v)}\partial x^s_{(w)}}+\\ +3\frac{\left(\sum_{k=1}^{r_i} w^k_{\alpha/A_\circ}\hat{\boldsymbol{y}}^k\right)^T\cdot(\boldsymbol{I}-\boldsymbol{t}_\parallel\cdot\boldsymbol{t}_\parallel{}^T)\cdot\sum_{k=1}^{r_i}\frac{\partial}{\partial x^h_{(v)}}\left(w^k_{\alpha/A_\circ}\hat{\boldsymbol{y}}^k\right)}{\left\|(\boldsymbol{I}-\boldsymbol{t}_\parallel\cdot\boldsymbol{t}_\parallel{}^T)\cdot\sum_{k=1}^{r_i} w^k_{\alpha/A_\circ}\hat{\boldsymbol{y}}^k\right\|^2}\cdot\\ \cdot\frac{\left(\sum_{k=1}^{r_i} w^k_{\alpha/A_\circ}\hat{\boldsymbol{y}}^k\right)^T\cdot(\boldsymbol{I}-\boldsymbol{t}_\parallel\cdot\boldsymbol{t}_\parallel{}^T)\cdot\sum_{k=1}^{r_i}\frac{\partial}{\partial x^s_{(w)}}\left(w^k_{\alpha/A_\circ}\hat{\boldsymbol{y}}^k\right)}{\left\|(\boldsymbol{I}-\boldsymbol{t}_\parallel\cdot\boldsymbol{t}_\parallel{}^T)\cdot\sum_{k=1}^{r_i} w^k_{\alpha/A_\circ}\hat{\boldsymbol{y}}^k\right\|^2}\cdot\sum_{k=1}^{r_i} w^k_{\alpha/A_\circ}\hat{\boldsymbol{y}}^k-\\ -\frac{\left(\sum_{k=1}^{r_i} w^k_{\alpha/A_\circ}\hat{\boldsymbol{y}}^k\right)^T\cdot(\boldsymbol{I}-\boldsymbol{t}_\parallel\cdot\boldsymbol{t}_\parallel{}^T)\cdot\sum_{k=1}^{r_i}\frac{\partial}{\partial x^h_{(v)}}\left(w^k_{\alpha/A_\circ}\hat{\boldsymbol{y}}^k\right)}{\left\|(\boldsymbol{I}-\boldsymbol{t}_\parallel\cdot\boldsymbol{t}_\parallel{}^T)\cdot\sum_{k=1}^{r_i} w^k_{\alpha/A_\circ}\hat{\boldsymbol{y}}^k\right\|^2}\cdot\sum_{k=1}^{r_i}\frac{\partial}{\partial x^s_{(w)}}\left(w^k_{\alpha/A_\circ}\hat{\boldsymbol{y}}^k\right)-\\ -\frac{\left(\sum_{k=1}^{r_i} w^k_{\alpha/A_\circ}\hat{\boldsymbol{y}}^k\right)^T\cdot(\boldsymbol{I}-\boldsymbol{t}_\parallel\cdot\boldsymbol{t}_\parallel{}^T)\cdot\sum_{k=1}^{r_i}\frac{\partial}{\partial x^s_{(w)}}\left(w^k_{\alpha/A_\circ}\hat{\boldsymbol{y}}^k\right)}{\left\|(\boldsymbol{I}-\boldsymbol{t}_\parallel\cdot\boldsymbol{t}_\parallel{}^T)\cdot\sum_{k=1}^{r_i} w^k_{\alpha/A_\circ}\hat{\boldsymbol{y}}^k\right\|^2}\cdot\sum_{k=1}^{r_i}\frac{\partial}{\partial x^h_{(v)}}\left(w^k_{\alpha/A_\circ}\hat{\boldsymbol{y}}^k\right)-\\ -\Bigg[\frac{\left(\sum_{k=1}^{r_i}\frac{\partial}{\partial x^h_{(v)}}w^k_{\alpha/A_\circ}\hat{\boldsymbol{y}}^k\right)^T\cdot(\boldsymbol{I}-\boldsymbol{t}_\parallel\cdot\boldsymbol{t}_\parallel{}^T)\cdot\sum_{k=1}^{r_i}\frac{\partial}{\partial x^s_{(w)}}\left(w^k_{\alpha/A_\circ}\hat{\boldsymbol{y}}^k\right)}{\left\|(\boldsymbol{I}-\boldsymbol{t}_\parallel\cdot\boldsymbol{t}_\parallel{}^T)\cdot\sum_{k=1}^{r_i} w^k_{\alpha/A_\circ}\hat{\boldsymbol{y}}^k\right\|^2}+\\ +\frac{\left(\sum_{k=1}^{r_i} w^k_{\alpha/A_\circ}\hat{\boldsymbol{y}}^k\right)^T\cdot(\boldsymbol{I}-\boldsymbol{t}_\parallel\cdot\boldsymbol{t}_\parallel{}^T)\cdot\sum_{k=1}^{r_i}\frac{\partial^2\left(w^k_{\alpha/A_\circ}\hat{\boldsymbol{y}}^k\right)}{\partial x^h_{(v)}\partial x^s_{(w)}}}{\left\|(\boldsymbol{I}-\boldsymbol{t}_\parallel\cdot\boldsymbol{t}_\parallel{}^T)\cdot\sum_{k=1}^{r_i} w^k_{\alpha/A_\circ}\hat{\boldsymbol{y}}^k\right\|^2}\Bigg]\cdot\sum_{k=1}^{r_i} w^k_{\alpha/A_\circ}\hat{\boldsymbol{y}}^k\Bigg\}\end{aligned} \tag{10.16}$$

## 10.5 Symmetry boundary condition

This condition is obtained combining the conditions described in sections 10.2 and 10.3 (see figure 10.5). In this case, the direction of $\boldsymbol{t}_\perp$ corresponds to

the director vector of the plane of symmetry.

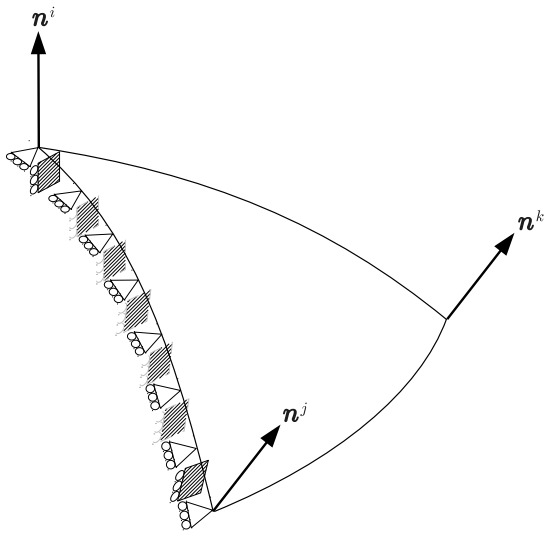


Figure 10.5: Figure representing the conditions that configure a symmetry boundary condition.

## 10.6 Hinge

With this case the author starts the cases where the shell presents two distinct areas that do not present continuity in the normal direction. This can be because the shell is folded, or hinged, or branched. The case of the hinge is treated first for pedagogic purposes.

Whenever a region of the shell presents discontinuity in the normal direction, the modeler using the BEST finite element shall instruct the pre-processor to identify the surface entities at each side of the discontinuity line. This can be established as a special boundary condition. Doing so allows the computer program to compute two different normal directions for one same node located on the discontinuity line: one for each surface entity (see figure 10.6). By discriminating the elements, the computation of the normals for one surface entity is independent of the elements at the other side of the hinge, which allows the two sides to have the free rotation intended by the hinge. For notation purposes, let's label the magnitudes relative to the surface entity on the same side of the discontinuity line as the element being considered using a bullet and a vertical line ($\bullet|$) as a subscript. The magnitudes relative to the surface entity on the opposite side of the discontinuity line to the element being considered will be identified

using a vertical line and a circle ($|\circ$) as subscript.

$$\boldsymbol{n}^i_{\bullet|} = \frac{\sum_{k=1}^{r_i}{}_{\bullet|}\, w^k_{\alpha/A_\circ}\hat{\boldsymbol{y}}^k}{\left\| \sum_{k=1}^{r_i}{}_{\bullet|}\, w^k_{\alpha/A_\circ}\hat{\boldsymbol{y}}^k \right\|} \tag{10.17}$$

$$\boldsymbol{n}^i_{|\circ} = \frac{\sum_{k=1}^{r_i}{}_{|\circ}\, w^k_{\alpha/A_\circ}\hat{\boldsymbol{y}}^k}{\left\| \sum_{k=1}^{r_i}{}_{|\circ}\, w^k_{\alpha/A_\circ}\hat{\boldsymbol{y}}^k \right\|} \tag{10.18}$$

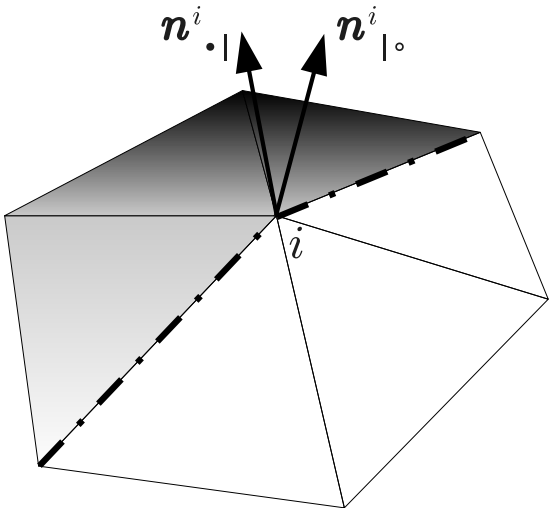


Figure 10.6: Whenever two surface entities meet at an angle, their normals shall be distinguished at the nodes along the discontinuity line. Here the dark surface has the normal vector $\boldsymbol{n}^i_{\bullet|}$ at $i$. And the light surface has the normal vector $\boldsymbol{n}^i_{|\circ}$ at $i$.

A hinge causes the two regions at each side of the hinge to have only $\mathcal{C}^0$ continuity at the boundary defined by the hinge line. In order to enforce $\mathcal{C}^0$ continuity it is necessary not only to share the corner nodes, but also that the boundary control points along the hinge are coincident. So far, the construction of the BEST elements accomplishes this, as long as the normal vectors at the nodes are coincident for all the elements sharing the node. As soon as the normals become dissociated along a hinge line, the geometry of the intersection between the two elements at each surface entity becomes indeterminate. As a result, the author suggests the following approach.

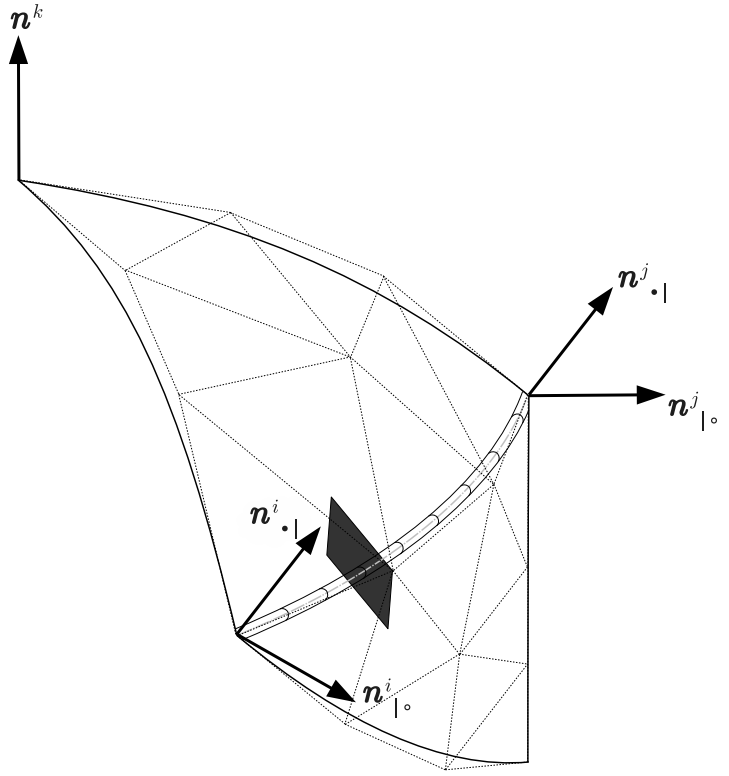


Figure 10.7: Representation of two curved elements meeting at a hinge line. The geometry of the intersection is determined by intersecting the planes perpendicular to $\boldsymbol{n}^i_{\bullet|}$ (horizontal stripes) and $\boldsymbol{n}^i_{|\circ}$ (vertical stripes), respectively. Finally, the precise location of the intermediate control points along the hinge line is determined by the intersection of an additional plane (shaded dark gray), which is located at the distance specified by the parameter $\Psi$ (equation (10.20)).

The intersection line between the two elements needs to be computed (see figure 10.7). The location of the control points along the hinge determines the tangent direction of the hinge at the nodes. The tangent direction of the intersection between two surfaces can be computed as the intersection of the two surfaces' tangent planes. Once the hinge's tangent line has been obtained, the distance at which the control points shall be located needs to be determined. This distance will be different for the two connecting triangles because they are no longer co-planar. Therefore the author proposes averaging the values of $\Psi(\varphi, \theta)$ obtained for the triangles at each side of the hinge line.

Using all the above, the contour control points of an element having one side at a hinge are determined intersecting the following three planes:

1. The plane perpendicular to the normal at the vertex ($\boldsymbol{n}^i = \boldsymbol{n}^i_{\bullet|}$).

2. The plane perpendicular to the other normal at the vertex ($\boldsymbol{n}^i_{|\circ}$).

3. The plane perpendicular to the edge of the flat triangle considered. The exact location of this plane will be defined by the magnitude $\Psi^{ij}$.

The mathematical expression of these three planes and their intersection is presented in equation (10.19):

$$\begin{bmatrix} {\boldsymbol{n}^i_{\bullet|}}^T \\ {\boldsymbol{n}^i_{|\circ}}^T \\ (\boldsymbol{x}^i - \boldsymbol{x}^j)^T \end{bmatrix} \cdot \boldsymbol{p}^{ij} = \begin{bmatrix} {\boldsymbol{n}^i_{\bullet|}}^T \cdot \boldsymbol{x}^i \\ {\boldsymbol{n}^i_{|\circ}}^T \cdot \boldsymbol{x}^i \\ (\boldsymbol{x}^i - \boldsymbol{x}^j)^T \cdot \left[(1-\Psi^{ij})\boldsymbol{x}^i + \Psi^{ij}\boldsymbol{x}^j\right] \end{bmatrix} \tag{10.19}$$

It's obvious to say that when $\boldsymbol{n}^i_{\bullet|}$ and $\boldsymbol{n}^i_{|\circ}$ are coincident, then this system is indeterminate. But this would most probably be a result of a design error, since there is no point in setting a hinge in a shell only to result in a perfectly $\mathcal{G}^1$ continuous shape. The virtue of the hinge is that it allows the two sides to be at an angle and therefore increases the axial carrying load without overloading the bending capacity of the shell. If the two sides are $\mathcal{G}^1$ continuous, it means that there wouldn't be a significant bending moment across the hinge line and therefore the hinge is totally unnecessary. Furthermore, a structural designer will use a hinge wherever large point loads are likely to appear in the transverse direction of the shell midsurface, and would otherwise cause a very large and local bending moment. In order to better resist these loads, the structural designer will shape the shell parts at an angle to the load direction in order to better resist the loads with the phenomenal axial carrying capacity of the shell. Usually, the hinge will result in smaller bending moments in the shell. If however the displacements are an issue of concern, the structural designer will instead dispose a kink in the shell that will form an even stiffer structure. This configuration will be covered in section 10.7.

Using the definition of equation (9.17), the value of $\Psi^{ij}$ is redefined for the hinged sides of an element in the following way:

$$\Psi^{ij} = \frac{\Psi(\varphi^{ij}_{\bullet|}, \theta^{ij}_{\bullet|}) + \Psi(\varphi^{ij}_{|\circ}, \theta^{ij}_{|\circ})}{2} \tag{10.20}$$

and where $\varphi^{ij}_{\bullet|}$ and $\varphi^{ij}_{|\circ}$ are defined by extension of equation (9.18)

$$\varphi^{ij}_{\bullet|} = \arcsin \frac{\boldsymbol{n}^i_{\bullet|} \cdot (\boldsymbol{x}^i - \boldsymbol{x}^j)}{\|\boldsymbol{x}^i - \boldsymbol{x}^j\|} \tag{10.21}$$

$$\varphi^{ij}_{|\circ} = \arcsin \frac{\boldsymbol{n}^i_{|\circ} \cdot (\boldsymbol{x}^i - \boldsymbol{x}^j)}{\|\boldsymbol{x}^i - \boldsymbol{x}^j\|} \tag{10.22}$$

$$\theta^{ij}_{\bullet|} = \arcsin \frac{\sin\varphi^{ij}_{\bullet|} \cdot (\boldsymbol{n}^i_{\bullet|} \cdot \boldsymbol{n}^i_{|\circ}) - \sin\varphi^{ij}_{|\circ}}{\cos\varphi^{ij}_{\bullet|} \cdot \|(\boldsymbol{I} - \boldsymbol{n}^i_{\bullet|} \otimes \boldsymbol{n}^{iT}_{\bullet|}) \cdot \boldsymbol{n}^i_{|\circ}\|} \tag{10.23}$$

$$\theta^{ij}_{|\circ} = \arcsin \frac{\sin\varphi^{ij}_{|\circ} \cdot (\boldsymbol{n}^i_{|\circ} \cdot \boldsymbol{n}^i_{\bullet|}) - \sin\varphi^{ij}_{\bullet|}}{\cos\varphi^{ij}_{|\circ} \cdot \|(\boldsymbol{I} - \boldsymbol{n}^i_{|\circ} \otimes \boldsymbol{n}^{iT}_{|\circ}) \cdot \boldsymbol{n}^i_{\bullet|}\|} \tag{10.24}$$

Note that the above definitions of $\theta^{ij}_{\bullet|}$ and $\theta^{ij}_{|\circ}$ serve the only purpose of computing $\Psi^{ij}$ and they have no direct effect on the determination of the

geometry of the element edge. Therefore, we do not care about the actual sign of $\theta^{ij}_{\bullet|}$ and $\theta^{ij}_{|\circ}$ because the function $\Psi^{ij}(\varphi^{ij}, \theta^{ij})$ is an even function with respect to both variables.

Note also that dissociating the normals along the hinge line for each surface entity implies that the sets of nodes used to compute $\boldsymbol{n}^i_{\bullet|}$ and $\boldsymbol{n}^i_{|\circ}$ are each a subset of all the nodes that would form the patch around the node in the absence of the hinge line (see equations (10.17) and (10.18)). But because the two magnitudes are used in the formulas, all the nodes in the patch are needed in order to compute the stiffness matrix of the element; regardless of whether they belong to a different surface entity.

The equations (5.16), (7.25) and (7.26) are used changing the expressions for $\boldsymbol{A}^{ij}_{\boldsymbol{p}}$ and $\boldsymbol{b}^{ij}_{\boldsymbol{p}}$ according to equation (10.19). The derivatives of these expressions as well as the derivatives of equation (10.23) can be found in appendix D.

## 10.7 Kinked shell

The term kink is synonymous of fold or bend and implies a sharp corner of an otherwise smooth geometry. When a shell presents a kink, the finite element analyst can no longer assume $\mathcal{G}^1$ continuity; unless a very refined mesh is used. For these cases it is common to assume that the angle between the normal vectors at the edge of the elements on each side of the fold remains constant throughout the deformation process [42]. This assumption is consistent with maintaining the continuity of the shell's transverse fibers at the kink.

$\mathcal{C}^0$ continuity is achieved using the same approach used for hinges in section 10.6. The location of the control points along the boundary of the elements at both sides of the kink is determined by solving the intersection of the two neighboring elements at each side of the kink or mesh set. However, in this case, unlike in section 10.6, the relative angle of the normals is constrained and must be kept constant throughout the deformation.

The author proposes to apply the same approach already explored in section 9.2.1 to maintain a rigid angle at the kink. The abanico analogy showed that by imposing a rotation equal to the average of the relative rotations of the remaining vectors, a rigid rotation of all the vectors is recovered (see section 9.5.1).

The normal vector $\boldsymbol{n}^i$ is obtained by conveniently rotating the average of the normals of the surrounding triangles on the same side of the kink line ($\boldsymbol{n}^i_{\bullet|}$). In order to maintain the relative angle of $\boldsymbol{n}^i$ with respect to the other normal at the node $\overset{\star}{\boldsymbol{n}}{}^i$ (see figure 10.8), the latter is also obtained by conveniently rotating the normal computed as an average of the normals of the surrounding triangles on the opposite side of the kink line ($\boldsymbol{n}^i_{|\circ}$). The normals $\boldsymbol{n}^i_{\bullet|}$ and $\boldsymbol{n}^i_{|\circ}$ have been defined in equations (10.17) and (10.18).

First, let's define the relative angle between the two normals as

$$\tau^{ij}_{\bullet|\circ} = \begin{cases} +\arccos(\boldsymbol{n}^i_{\bullet|} \cdot \boldsymbol{n}^i_{|\circ}) & \text{if } (\boldsymbol{n}^i_{\bullet|} \times \boldsymbol{n}^i_{|\circ}) \cdot (\boldsymbol{x}^i - \boldsymbol{x}^j) > 0, \\ -\arccos(\boldsymbol{n}^i_{\bullet|} \cdot \boldsymbol{n}^i_{|\circ}) & \text{if } (\boldsymbol{n}^i_{\bullet|} \times \boldsymbol{n}^i_{|\circ}) \cdot (\boldsymbol{x}^i - \boldsymbol{x}^j) < 0. \end{cases} \tag{10.25}$$

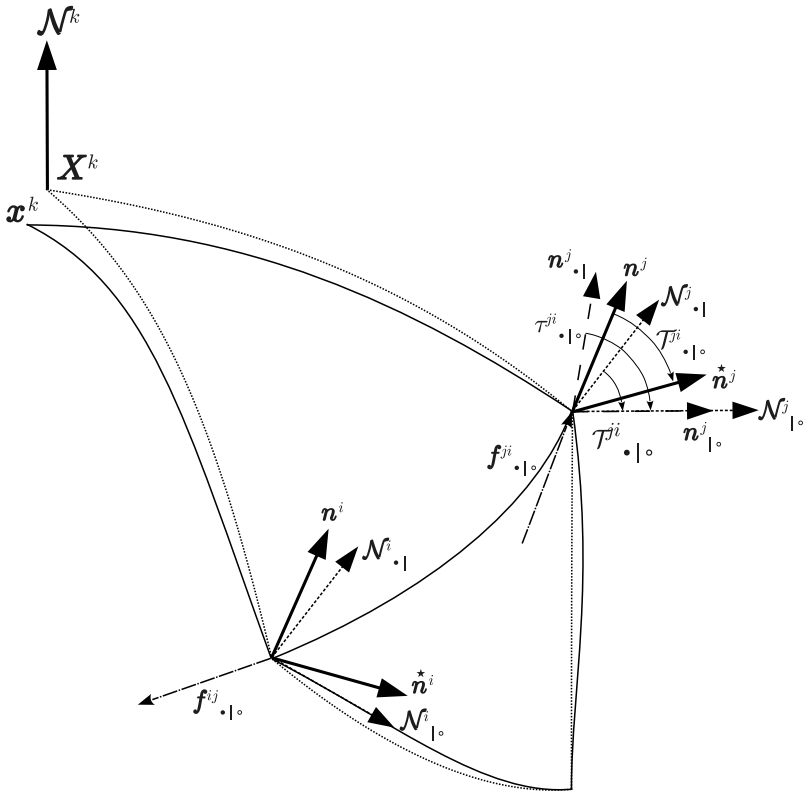


Figure 10.8: Representation of two curved elements meeting at a kink. In this case the reference configuration is represented (doted lines). This is used to explain that the relative angles between the two surfaces converging at the kink are maintained in the deformed configuration. The normal vector at each side of the fold line is obtained by conveniently rotating the normals of the adjacent elements ($\boldsymbol{n}^j_{\bullet|}$ and $\boldsymbol{n}^j_{|\circ}$) until the relative angle between the normals at each side of the kink line ($\mathcal{T}^j_{\bullet|\circ}$) is recovered. The geometry of the intersection is determined following the procedure depicted in figure 10.7.

It's straightforward to infer that

$$\tau^{ij}_{\circ|\bullet} = -\tau^{ij}_{\bullet|\circ} \tag{10.26}$$

The author defines an associated unit rotation vector aligned with the tangent of the kink line or fold ($\hat{\boldsymbol{f}}^{ij}$).

$$\hat{\boldsymbol{f}}^{ij} = \begin{cases} +\dfrac{\boldsymbol{n}^i_{\bullet|} \times \boldsymbol{n}^i_{|\circ}}{\|\boldsymbol{n}^i_{\bullet|} \times \boldsymbol{n}^i_{|\circ}\|} & \text{if } (\boldsymbol{n}^i_{\bullet|} \times \boldsymbol{n}^i_{|\circ}) \cdot (\boldsymbol{x}^i - \boldsymbol{x}^j) > 0, \\ -\dfrac{\boldsymbol{n}^i_{\bullet|} \times \boldsymbol{n}^i_{|\circ}}{\|\boldsymbol{n}^i_{\bullet|} \times \boldsymbol{n}^i_{|\circ}\|} & \text{if } (\boldsymbol{n}^i_{\bullet|} \times \boldsymbol{n}^i_{|\circ}) \cdot (\boldsymbol{x}^i - \boldsymbol{x}^j) < 0. \end{cases} \tag{10.27}$$

Note that the functions defining $\tau^{ij}_{\bullet|\circ}$ and $\hat{\boldsymbol{f}}^{ij}$ are not defined when

$$(\boldsymbol{n}^i_{\bullet|} \times \boldsymbol{n}^i_{|\circ}) \cdot (\boldsymbol{x}^i - \boldsymbol{x}^j) = 0$$

This should not be a problem because this only happens if:

- $\boldsymbol{n}^i_{\bullet|}$, $\boldsymbol{n}^i_{|\circ}$ and $(\boldsymbol{x}^i - \boldsymbol{x}^j)$ are co-planar (impossible); or
- if $\boldsymbol{n}^i_{\bullet|}$ and $\boldsymbol{n}^i_{|\circ}$ are parallel, which is contradictory with the definition of kink.

Finally equation (5.3) is modified and the normal vector is corrected applying the Rodrigues' formula and the abanico analogy. Also the normal of the other surface entity is corrected in order to determine the intersection between the two surface entities.

$$\boldsymbol{n}^i = \boldsymbol{R}\left(\hat{\boldsymbol{f}}^{ij}, \frac{\tau^{ij}_{\bullet|\circ} - \mathcal{T}^{ij}_{\bullet|\circ}}{2}\right) \cdot \boldsymbol{n}^i_{\bullet|} \tag{10.28}$$

$$\overset{\star}{\boldsymbol{n}}{}^i = \boldsymbol{R}\left(\hat{\boldsymbol{f}}^{ij}, \frac{\tau^{ij}_{\circ|\bullet} - \mathcal{T}^{ij}_{\circ|\bullet}}{2}\right) \cdot \boldsymbol{n}^i_{|\circ} = \boldsymbol{R}^T\left(\hat{\boldsymbol{f}}^{ij}, \frac{\tau^{ij}_{\bullet|\circ} - \mathcal{T}^{ij}_{\bullet|\circ}}{2}\right) \cdot \boldsymbol{n}^i_{|\circ} \tag{10.29}$$

$\mathcal{T}^{ij}_{\bullet|\circ}$ corresponds to the value of $\tau^{ij}_{\bullet|\circ}$ in the reference configuration.

Equation (10.19) holds for determining the geometry of the intersection of the kink because the intersection of the planes perpendicular to $\boldsymbol{n}^i$ and $\overset{\star}{\boldsymbol{n}}{}^i$ is the same as the intersection of the planes perpendicular to $\boldsymbol{n}^i_{\bullet|}$ and $\boldsymbol{n}^i_{|\circ}$. The only thing that changes is the value of $\Psi^{ij}$.

$$\Psi^{ij} = \frac{\Psi(\varphi^{ij}, \theta^{ij}) + \Psi(\overset{\star}{\varphi}{}^{ij}, \overset{\star}{\theta}{}^{ij})}{2} \tag{10.30}$$

and where $\varphi^{ij}$ was defined in equation (9.18), and $\overset{\star}{\varphi}{}^{ij}$ is defined by extension

$$\overset{\star}{\varphi}{}^{ij} = \arcsin \frac{\overset{\star}{\boldsymbol{n}}{}^i \cdot (\boldsymbol{x}^i - \boldsymbol{x}^j)}{\|\boldsymbol{x}^i - \boldsymbol{x}^j\|} \tag{10.31}$$

$$\theta^{ij} = \arcsin \frac{\sin\varphi^{ij} \cdot (\boldsymbol{n}^i \cdot \overset{\star}{\boldsymbol{n}}{}^i) - \sin\overset{\star}{\varphi}{}^{ij}}{\cos\varphi^{ij} \cdot \|(\boldsymbol{I} - \boldsymbol{n}^i \otimes \boldsymbol{n}^{iT}) \cdot \overset{\star}{\boldsymbol{n}}{}^i\|} \tag{10.32}$$

$$\overset{\star}{\theta}{}^{ij} = \arcsin \frac{\sin\overset{\star}{\varphi}{}^{ij} \cdot (\overset{\star}{\boldsymbol{n}}{}^i \cdot \boldsymbol{n}^i) - \sin\varphi^{ij}}{\cos\overset{\star}{\varphi}{}^{ij} \cdot \|(\boldsymbol{I} - \overset{\star}{\boldsymbol{n}}{}^i \otimes \overset{\star}{\boldsymbol{n}}{}^{iT}) \cdot \boldsymbol{n}^i\|} \tag{10.33}$$

## 10.8 Branching configurations

In the previous two sections the author has presented general approaches to solve hinges and kinks in shells. The approach presented takes advantage that only two different surfaces converge at each interface. Thanks to this, the tangent direction of the intersection of both surfaces is easily determined. When the number of converging surfaces grows to three or more, the determination of the intersection tangent is not unique, in general.

One possible approach to this scenario could be to compute an average intersection tangent. But the author is rather inclined to combine different boundary conditions. In this case, for the third and onward incoming surfaces to a kink or a hinge, an additional boundary condition should be applied. That would be a boundary condition equivalent to a continuous simply supported shell (both in the tangent and normal directions). Review sections 10.2 and 10.4.

## 10.9 Summary

In the BEST element, only the application of Dirichlet boundary conditions on the displacements of discrete points is straightforward.

For the application of Dirichlet boundary conditions on displacements of lines it does not suffice fixing the value of the displacement degrees of freedom of the corner nodes. The displacement of the control points at the boundary also needs to be fixed. And for that, the user needs to impose conditions either on the direction of the normal $n$ at the nodes of the boundary or on the drilling rotations $\theta$ of the edges on the boundary.

Likewise, the application of Dirichlet boundary conditions on the rotations of discrete points or lines also requires to impose conditions either on the direction of the normal $n$ at the nodes or on the drilling rotations $\theta$ of the edges on the line.

In doing this, the shape functions of the element are indeed modified to satisfy the boundary conditions. The advantages of this method are that the system matrix does not increase in size (as could have been if we were to impose additional constrains on the relation amongst the free variables and then applying the penalty method), and that there is no need to deal with esoteric coefficients. But more importantly the symmetric and positive definite character of the matrix is conserved.

The simplicity of applying those conditions on internal variables of the BEST element is a clear advantage with respect to other rotation-free shell elements that require the use of additional nodes to apply Dirichlet boundary conditions on the rotations of the element [100, 142].

However, in order to implement these boundary conditions in the overall workflow, the pre-processor has to share the information about the conditions on lines with the solver. In this thesis, the author has used the GiD pre- and post-processor to run the examples. The solver has been programmed using the RamSeries solver framework for the Tdyn solver suite of multi-physics problems. The *problemtype* definition for the RamSeries solver framework in GiD does not provide by default the information set on the line boundaries to the edges of the mesh. It transfers the information of the conditions of lines to the nodes on those lines. Therefore, it would be required to adapt the RamSeries *problemtype* to the requirements of the element. This thesis stops short of doing that adaptation. And all the numeric examples are run without the correct application of the boundary conditions on lines.

The ease of the BEST element to apply Dirichlet boundary conditions on the rotations is equivalent to that of other a rotation-free shell ele-

ments, and satisfies one of the main design goals set out for the element in section 2.2.

# Chapter 11

# Numerical examples

THIS CHAPTER PRESENTS A SERIES OF BENCHMARK TESTS using the BEST element developed in the present thesis. A series of tests have been performed on the element to evaluate its performance and also to find out the goodness of the two possible values of $\theta^{ij}$ proposed in section 9.5.1. The tests have been selected to evaluate the specific performance of the BEST element under the different deformation modes of a shell: membrane shear, membrane extension, and bending. Finally, the shell obstacle course is used to compare the performance of the BEST element with respect to other shell elements in the literature.

## 11.1 In-plane shear oriented examples

### 11.1.1 Thick beam

This example consists on a cantilever thick beam subject to a point load at its tip. The purpose of this test is to confirm whether the in-plane shear mode is preventing the element from achieving fast convergence. The author had the intuition that shear deformation, which had not been dealt with specifically, was responsible for the slow convergence of the element to the solution of the different problems. The reference solution for the displacement of the tip, as reported in [82], is 0,35533. Both translation degrees of freedom are restrained at the root nodes. The properties of the example are shown in figure 11.1. And the calculation meshes used are shown in figure 11.2. This problem has already been used to evaluate the improvement of the BEST element when drilling degrees of freedom are added to the kinematics of the element. But further comments are deserved than those provided in chapter 9.

This example tests the plane defromation properties of the shell element. This includes the membrane stretch kinematics and in-plane shear kinematics. But the bending mechanism is non-existent because the out-of-plane displacements are restrained. This is a very well suited example to evaluate the improvements brought in by the drilling degrees of freedom in shell and plane deformation elements.

The reader can observe that the BEST element with symmetric drilling degrees of freedom achieves similar precision to that obtained with other

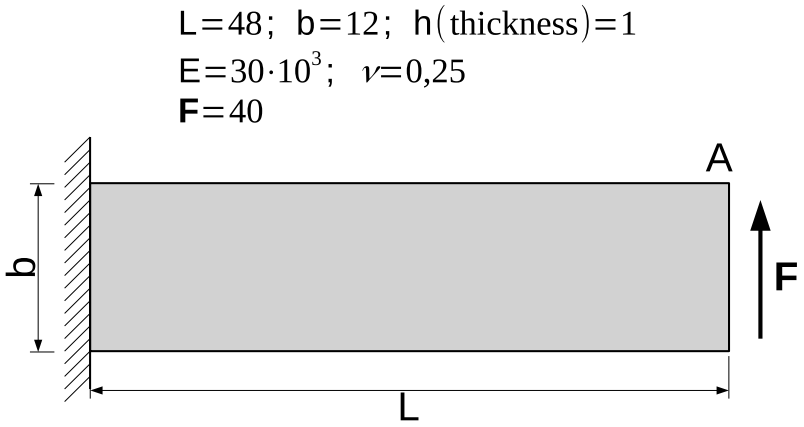


(a) Geometry and conditions of the problem.

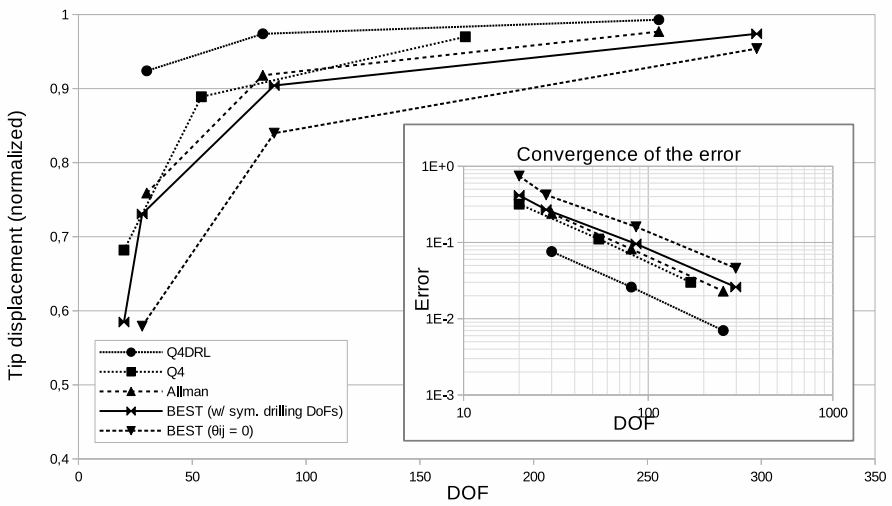


(b) Vertical displacement and its error of the free tip of the beam. Results normalised using as reference solution 0,35533.

Figure 11.1: Thick beam. Comparison of results with other elements from the literature. The data from other elements is obtained from [82].

elements in the literature. Although there are elements with signifficantly better precision.

Unlike the next example of the cylinder under torsion, in this example the configuration of the element setting the angle $\theta^{ij} = 0$ does not improve the results over what had been presented in figure 8.7 on page 94. Indeed, the results are identical because in this problem with a flat geometry, the modification on the computation of the control points introduced in section 9.2.2 (see figures 5.5 and 9.3 on page 52 and on page 105) does not produce any difference in the computation of the control points and their kinematics if $\theta^{ij}$ is set to 0.

Nevertheless, in all the cases the error converges linearly. Therefore,

if the improvement suggested in section 9.5.2 were to be be successful and the element achieved the full cubic convergence enabled by the potential of the cubic nature of the description of its kinematics, then the BEST element would prove to be a superior element to the other elements in the literature with similar characteristics.

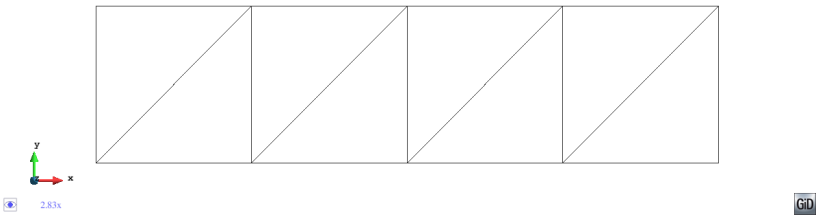

(a) Mesh with 20 degrees of freedom.

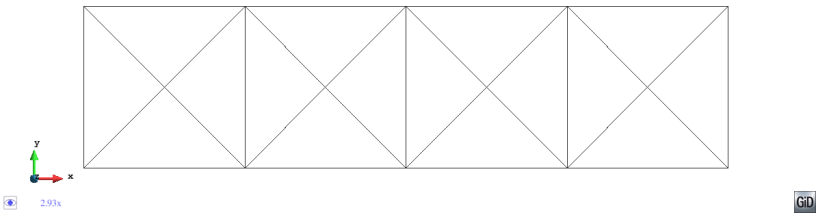

(b) Mesh with 28 degrees of freedom.

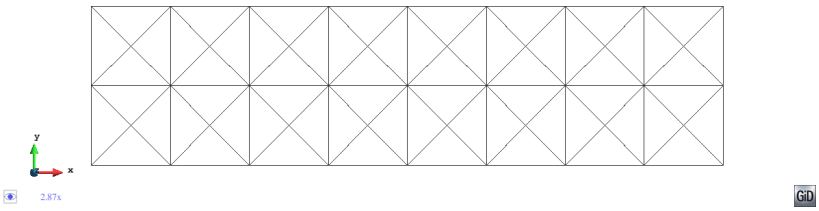

(c) Mesh with 86 degrees of freedom.

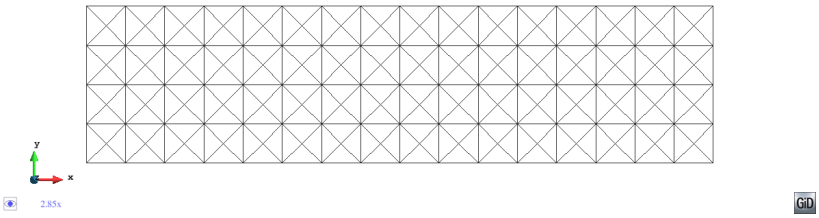

(d) Mesh with 298 degrees of freedom.

Figure 11.2: Calculation meshes used for the thick cantilever beam example.

### 11.1.2 Torsion of tube

This example consists on a cylindrical shell subject to pure torsion. In this case the torque is applied using 4 point loads on one of its bases, while the other base is fixed (see figure 11.3). This example was devised by the author to test the the BEST element subject to in-plane shear and complement the results obtained in the "thick beam" example. In the thick beam example the geometry is flat and therefore the BEST elements do not have any curvature. In this example, the deformation remains strictly as in-plane shear, but in this case the geometry of the BEST elements is curved, therefore the advantages of the kinematics implemented in section 9.2.2 (see figures 5.5 and 9.3 on page 52 and on page 105) may have an effect. So this simple example using Saint-Venant's theory for pure torsion of hollow tubes is used. In order to prevent an excessive effect of the localised loads, a thick wall is used in this example. And the reference measurements are taken in the midle of the cylinder to stay away from those local deformations caused by the point loads.

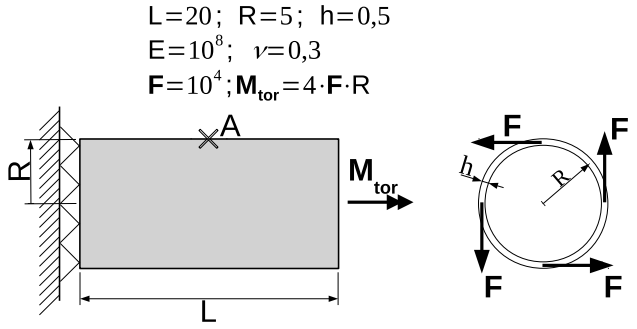


Figure 11.3: Geometry and conditions of the problem. Elevation and lateral view.

Under Saint-Venant's hypotheses, which are valid for a straight cylinder under uniform torque, the rate of angular torsion is constant along the length of the tube and there is no warping of the cross-sections of the cílinder. This allows to find a very simple solution to the problem.

$$\alpha = \frac{M_{tor} \cdot l}{G \cdot I_0} \tag{11.1}$$

Where $\alpha$ is the total rotation of the tube from end to end, $M_{tor}$ is the torque applied, $l$ is the distance from the fixed base of the cylinder to the measurement point, and $I_0$ is the polar moment of the tube's section. For a thin walled tube the polar moment of inertia can be calculated as

$$I_0 = 2 \cdot \pi \cdot R^3 \cdot h \tag{11.2}$$

where $h$ is the wall thickness. Then, the tangential displacement of the measurement point is equal to the angle $\alpha$ times the radius. Under these assumptions, the displacement of a point A in the middle of the cylinder should be $6,621 \cdot 10^{-4}$. But instead, the numerical solution for the average of the mid section seems to converge towards a value of $6,6046 \cdot 10^{-4}$, which

is within a $0,5\%$ margin of error. Certainly the localized application of the torque load leads to localized deformations which in turn leaves less deformation energy available to the torsion mechanism.

The first thing to notice when looking at the results in figure 11.4 is that for the averaged measurement of the tangential displacement of the mid section of the tube, the solutions obtained using a value of $\theta^{ij} = -\theta^{ji}$ equation (9.33), differ from the solutions obtained using a value of $\theta^{ij} = 0$ equation (9.34). More so: while with $\theta^{ij} = 0$ the solution converges rapidly, with $\theta^{ij} = -\theta^{ji}$ the convergence is much slower. The second thing to notice is that for the tangential displacement of point A, and when using $\theta^{ij} = -\theta^{ji}$, the structured and unstructured meshes yield different results, whereas when using $\theta^{ij} = 0$ the results with structured and unstructured meshes converge to the same value. This leads the author to suspect about the validity of the results obtained with $\theta^{ij} = -\theta^{ji}$, which is a very arbitrary condition. The results obtained with $\theta^{ij} = 0$ converge to a value of $6.566 \cdot 10^{-4}$ for the tangential displacement of point A.

Figure 11.5 shows an unstructured mesh using 1268 nodes and the corresponding converged results. The results are as expected. Half of the cylinder exhibits the effects of the localised loads. This can be observed in the displacements in the direction of the cylinder's axis, which although they are restricted to vey low values (of the order of $10^{-5}$), they pinpoint clearly the position of the point loads that provide the torque. The other half of the cylinder does not exhibit any displacement in the direction of the axis. This is consistent with the theory. The displacements in the X and Z directions are conjugate of each other, as they represent the two directions in the cross section of the cylinder. They also reflect the position of the point loads. It is best then to analyze the modulus of the displacement in order to evaluate the results in the cross section of the cylinder, because we have already determined that the displacement in the axial direction is 0. Taking a look at the modulus of the displacements we can conclude that the tangential displacement varies linearly along the first half of the cylinder, which is also consistent with the theory.

But the most interesting detail to notice is that, contrary to what could be expected, the convergence obtained in this example with $\theta^{ij} = 0$ is noticeably faster than what was achieved in section 8.3.1 on page 94. In order to introduce the drilling rotations, the construction of the BEST element has been changed (see section 9.2.2). This result is a definitive proof that the improved kinematics of the BEST element to emulate drilling rotations, which unleash the cubic nature of the element for the in-plane shear deformations, are a step in the right direction. Even with the drilling rotations locked —with $\theta^{ij} = 0$—, when the element has curvature, the boundary of the element is no longer confined to a flat curve, and instead is allowed to warp. Even without fully unleashing the potential that the drilling rotations provide, just this slight modification represents a great improvement for the accuracy of the element. Remains to test whether the proposed value by the author for $\theta^{ij}$ as a sum of the rigid body rotation and the rotation caused by the in-plane shear (see equation (9.35) on page 120), can yield even better convergence properties.

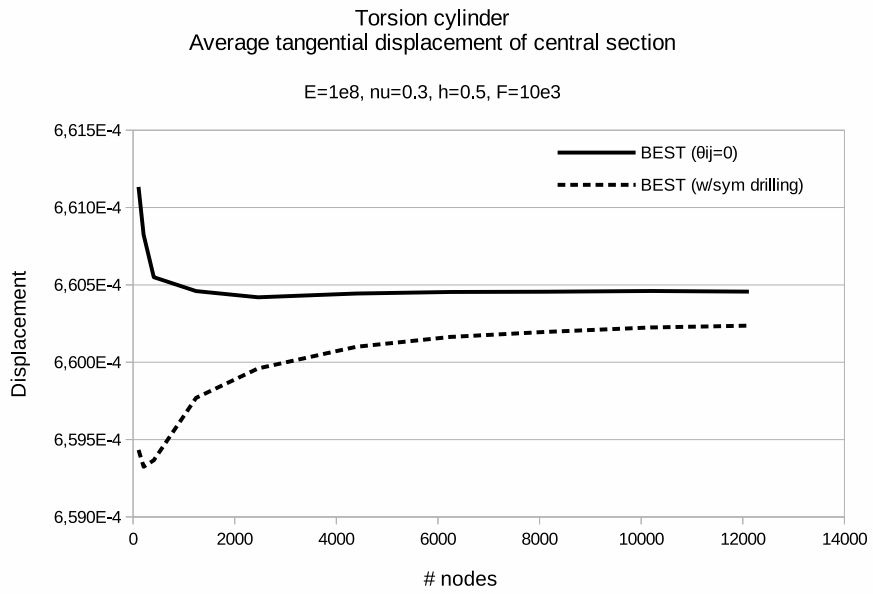


(a) Average tangential displacement of the central section of the cylinder. The average of a quarter of the section is computed. Results obtained using structured meshes.

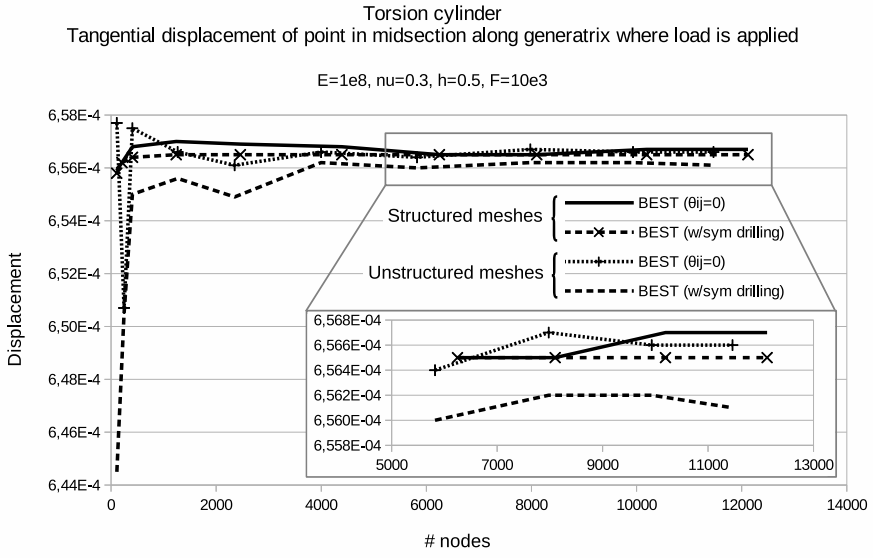


(b) Tangential displacement of point A (along the same generatrix of a loaded point). Results obtained using structured and unstructured meshes.

Figure 11.4: Torsion of tube. Comparison of results with 2 different values for $\theta^{ij}$: using a symmetric definition of $\theta^{ij}$ according to equation (9.33), or setting $\theta^{ij} = 0$.

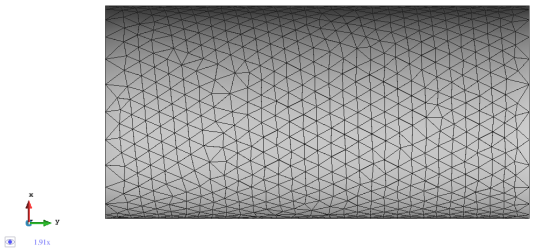

(a) Unstructured mesh with 1268 nodes.

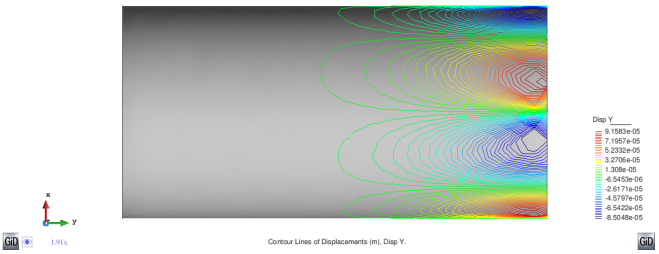


(b) Displacements in the axial direction of the cylinder.

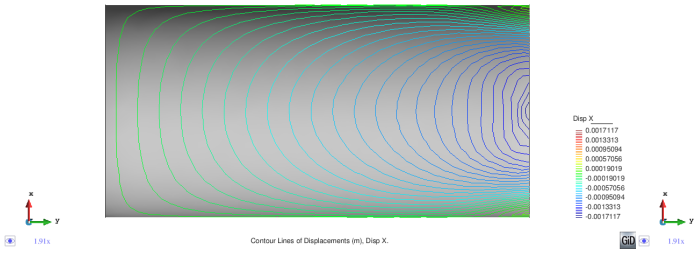


(c) Displacements in the X direction.

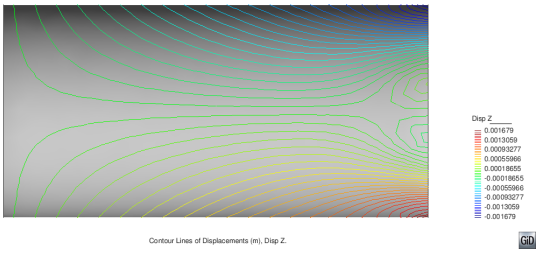


(d) Displacements in the Z direction.

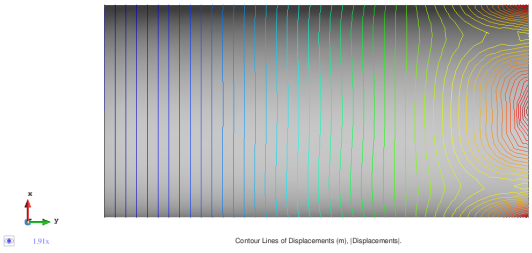


(e) Modulus of displacements.

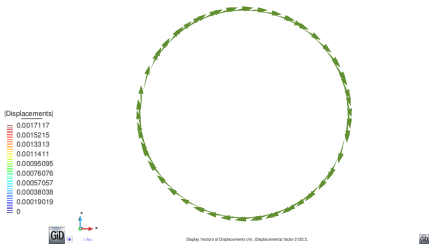


(f) Tangential displacements of the cross section at point A.

Figure 11.5: Torsion of tube. Results obtained using an unstructured mesh with 1268 nodes. These results correspond to a value of $\theta^{ij} = 0$.

## 11.2 Membrane oriented tests

### 11.2.1 Cylinder under internal pressure

This test was selected by the author in section 8.2.1 to determine whether using full quartic integration for the BEST element was worth it. Indeed, figure 8.4 made the case for using full quartic integration for the BEST element. In the present chapter, the author runs the test again after applying the changes described in chapter 9.

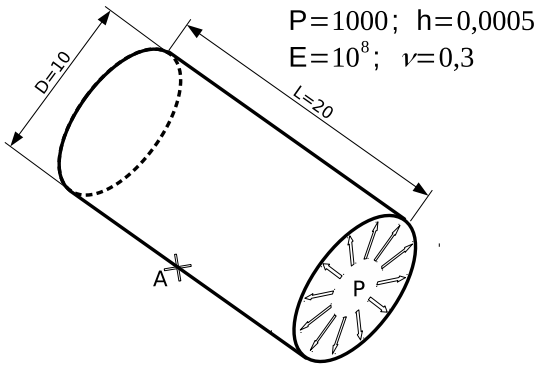


(a) Geometry and properties of the problem.

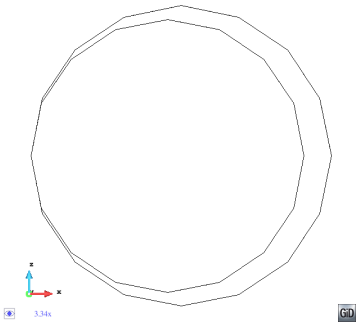

(b) Original and deformed mesh for a mesh with 16 divisions around the perimeter and 10 divisions along the length of the cylinder.

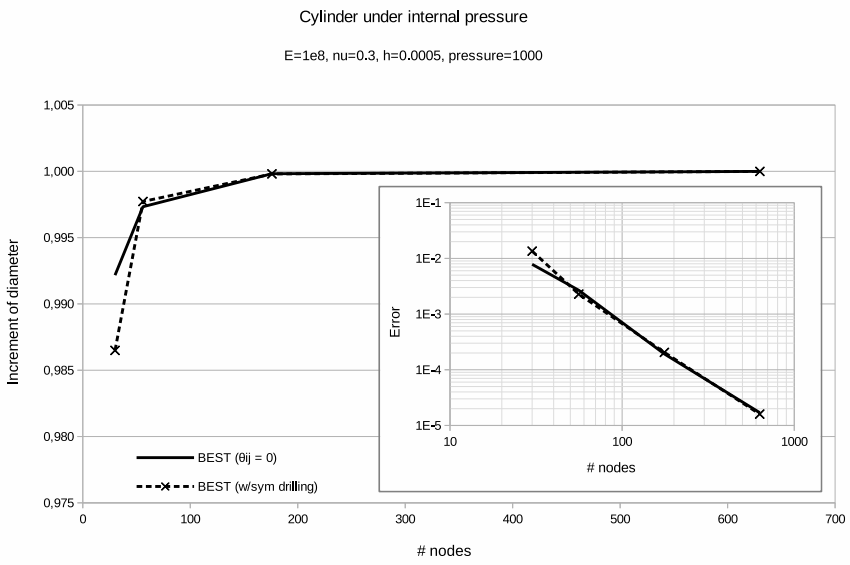


(c) Diameter variation at point A. Results obtained using structured biased meshes.

Figure 11.6: Cylinder under internal pressure. Results obtained for two possible definitions of the drilling rotations: $\theta^{ij} = 0$ and $\theta^{ij} = -\theta^{ji}$. The reference solution for the variation of the diameter is 1.

Figure 11.6c shows that results computed using both values of $\theta^{ij}$ converge very quickly, although only quadratic convergence is obtained and not cubic. It appears that for the kinematics defined in section 9.2.2, neither $\theta^{ij} = 0$ nor $\theta^{ij} = -\theta^{ji}$ are good enough to ensure optimal convergence. Nevertheless, both values do converge to the correct value and do so at a quadratic rate of convergence. Figure 11.7 shows no spurious effects of the mesh.

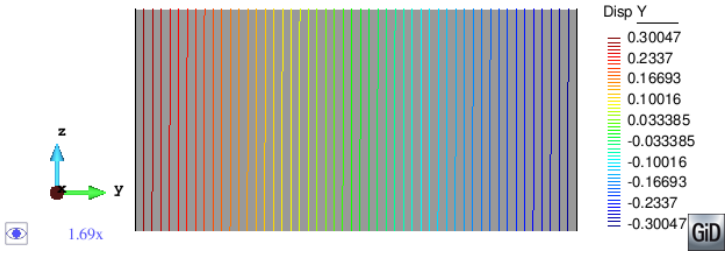


Figure 11.7: Transverse shrinkage due to the Poisson modulus. The reference value of the displacement at the edges is 0.3. Result obtained using a mesh with 16 divisions around the perimeter and 10 divisions along the lengh.

### 11.2.2 Parabolic roof

This example was also used in chapter 8, section 8.2.2 to test the membrane capabilities of the BEST element. This test takes inspiration from the roof structure of the Dulles International Airport. Other buildings that have also used a similar roof typology are shown in figure 11.9.

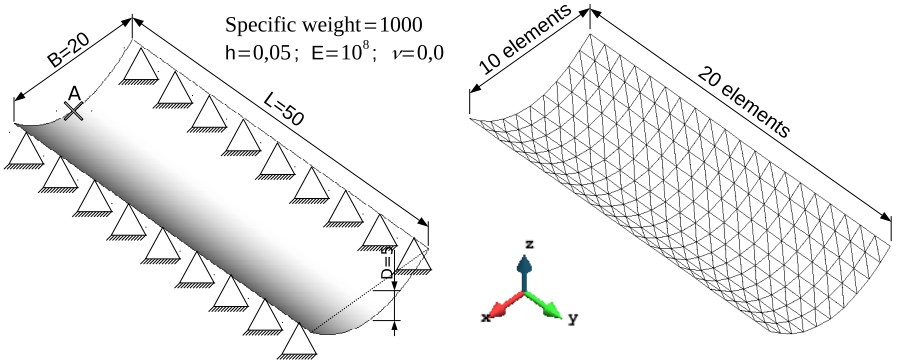


Figure 11.8: Parabolic roof problem. (a) Geometry and material properties of the problem. (b) Sample structured mesh with biased triangles. Mesh with 231 nodes and 400 elements.

The parabolic roof example aproaches the geometry of the catenary. But is not equal. Therefore, under self-weight load it will develop some

(a) The roof of the Dulles International Airport was designed by Eero Saarinen as a catenary.

(b) The roof of the Caracas hipodrome was designed by Arthur Froehlich as a series of catenaries.

(c) The canopy of the Bellvitge gas station (Barcelona) was also designed as a series of catenaries.

(d) The canopy of the Portuguese pavilion for the Expo'98 in Lisbon is a spectacular catenary conceived by Alvaro Siza Vieira and designed by Cecil Balmond.

Figure 11.9: The example of the parabolic roof is inspired in catenary roofs built around the world. The parabolic shape is the funicular of a uniform distributed load. While the catenary shape is the funicular of the self-weight load.

bending stresses (just as the cylinder under internal pressure does due to the decrease in curvature when the radius increases). The deformation of the roof will approach the catenary. The shape of a catenary is shallower at the trough and steeper at the abutments than the parabola. Therefore, the shell will rise at the trough and descend at the flanks to approach the catenary (see figure 11.10). We will measure how much the shell elevates at the center of the free edge.

The problem has been solved using both structured and structured meshes. The full model has been meshed. In the case of the structured meshes, non-symmetric meshes have been used (see figure 11.8b).

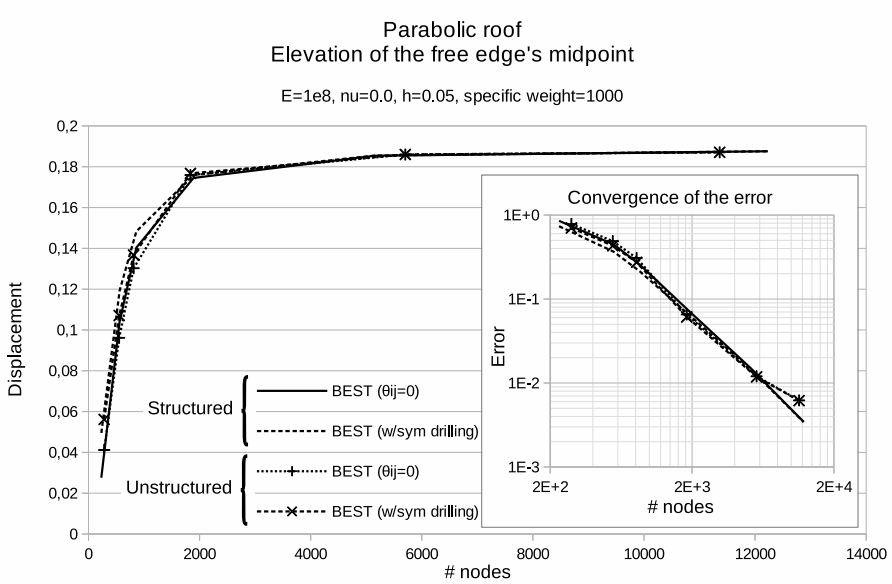


(a) Elevation of the free edge's midpoint. Averaged values of the two free edges. Convergence of the error.

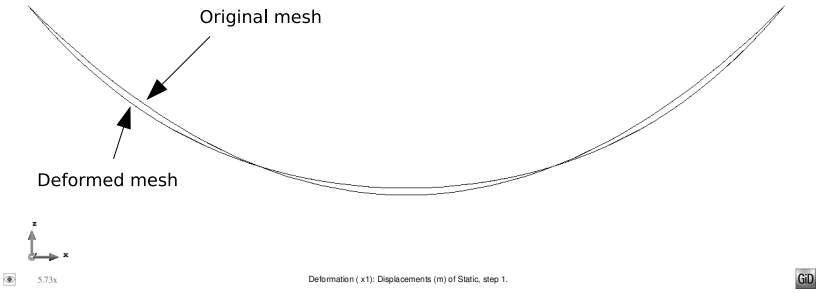


(b) Lateral view of the parabolic roof. Comparison of the reference mesh and the deformed mesh. Solution obtained with a structured mesh of 10000 elements and 5151 nodes.

Figure 11.10: Results of the parabolic roof example.

Figure 11.10 shows the convergence of the different meshes with the two different settings of $\theta^{ij}$. In all cases the convergence is similar and the results converge quadratically with the number of nodes in the mesh. Refinement has been analogous in the two main directions of the mesh. A converged solution has been obtained using an extra-refined mesh in the direction of the parabola (with 160 divisions in the direction of the parabola and 150 divisions length-wise), and a value of 0,1882 has been used as a reference elevation at A.

The effects of the biased mesh can be seen in the y-displacements field, see figure 11.11. As the displacements along the y-axis direction ought to be 0, plotting the field of displacements in the direction of the y-axis reveals the magnitude of the effect that the biased mesh has on the numeric results. As figure 11.11 shows, the effect of mesh bias is some orders of magnitude smaller than the displacement values in the z- or x-axis. And its value diminishes as the mesh is refined. Therefore, we can conclude that the BEST element is safe from the effects of mesh bias.

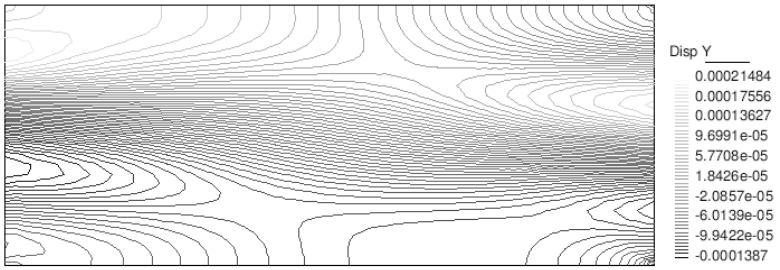


(a) Mesh with 3600 elements and 1891 nodes.

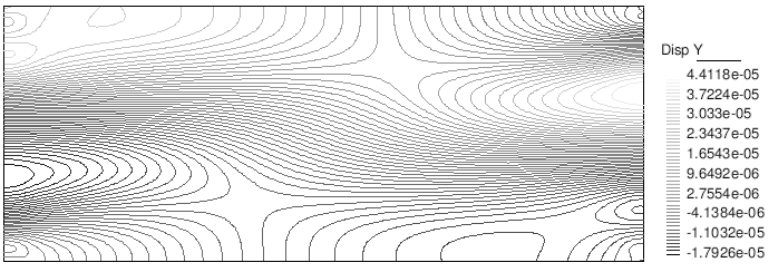


(b) Mesh with 24000 elements and 12231 nodes.

Figure 11.11: Effects of mesh bias on the results. As the mesh is refined the effect of the mesh bias diminishes. Displacements in the direction of the supported edges of the parabolic roof example.

## 11.3 Bending oriented tests

Shells have the property of resisting deformations through sheer membrane rigidity. That's what confers them their unique advantage. In order

to evaluate the bending properties of the BEST element, the author proposes using examples with a flat geometry.

In the linear regime, the BEST element cannot activate its membrane rigidity if the geometry is flat and the loads are exclusively oriented perpendicular to the shell's surface. Under these circumstances, the shell acts as a plate because in the reference configuration the shell has no curvature to transfer the loads to the membrane load bearing mechanisms. However, as the shell deforms due to bending, the current configuration presents curvature and the membrane load bearing mechanisms are activated.

The author takes advantage of this property in order to evaluate the bending accuracy of the BEST element with 2 simple examples.

### 11.3.1 Slender beam

This example consists on a rectangular plate simply supported in the two far sides, acting as a simply supported flat beam. The plate has a uniform load. See figure 11.12.

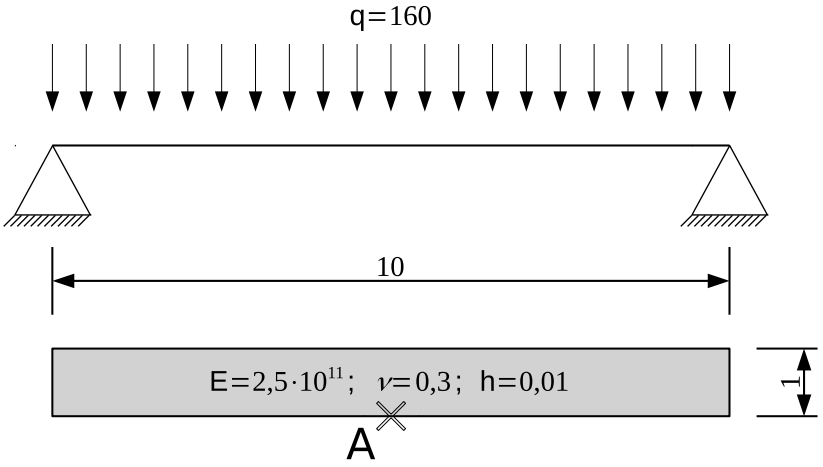


Figure 11.12: Geometry, boundary conditions and property materials for the slender beam problem. Both short edges of the plate are simlpy supported. Plan and elevation.

Under linear analysis, this problem degenerates to a plate. The shell does not develop membrane strains because under linear analysis the loads perpendicular to the midsurface of the shell cause only displacements also perpendicular to the midsurface of the shell. And because of that orthogonality, the tensor that relates the membrane deformations to the nodal coordinates ($\boldsymbol{B}_m$) is also orthogonal to the nodal displacements ($\Delta\tilde{\boldsymbol{x}}^r$), and the multiplication $\Delta\tilde{\boldsymbol{x}}^r \cdot \boldsymbol{B}_m = 0$. That's why linear analysis is only valid for small deflections.

The author has used 2 series of structured meshes to analyze this problem. A set of symmetrically divided quadrangles and another set of unsymmmetrically divided quadrangles have been used for the computations (see figure 11.13).

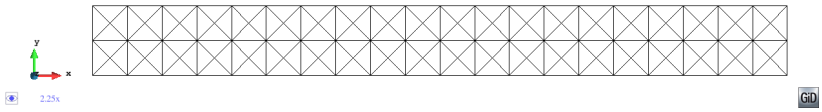

(a) Symmetric mesh. Quadrangles divided symmetrically.

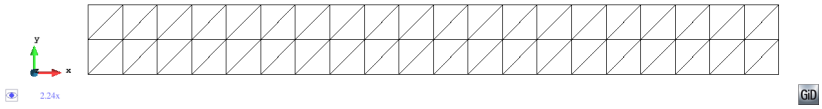

(b) Unsymmetric/biased mesh. Quadrangles divided assymetrically.

Figure 11.13: Samples of meshes for the slender beam problem. Top: example for the series of symmetric meshes. Bottom: example for the series of unsymmetric/biased meshes.

### Linear analysis

The problem is set so that large deflections develop. Actually, the analytical solution —as a beam— for the midpoint deflection in this particular case is $w_{max} = 1 \Rightarrow \frac{w_{max}}{L} = \frac{1}{10}$. This is a value well beyond what is considered small deflections ($\frac{w}{L} \approx \frac{1}{1000} \vee w < h$). Nevertheless, we carry on with the linear analysis to continue the characterization of the BEST element.

The most striking result when looking at figure 11.14 is that the symmetric and unsymmetric meshes converge to different results. And the other obvious result is that both settings with $\theta^{ij} = 0$ and $\theta^{ij} = -\theta^{ji}$ are identical (only the results with $\theta^{ij} = 0$ are presented). The second observation stems from the fact previously explained that $\boldsymbol{B}_m \perp \Delta\tilde{\boldsymbol{x}}^r$. Therefore, the value of $\theta^{ij}$ —which for a flat geometry only affects $\boldsymbol{B}_m$— is irrelevant. Let's discuss into more detail the first observation.

In this case, the convergence deteriorates signifficantly. The author argues that the cause for this phenomenon, which occurs in a flat geometry of the shell —but not when the shell has curvature— is in the definition of $\Psi^{ij}_{\varphi}$. We shall recall that the definition of $\Psi^{ij}_{\varphi}$ in equation (5.21) on page 57 obeys to a very strong hypothesis: that of assuming that the curve described by the edge of the triangle is a flat curve and also that this curve is a circular arch with symmetric angles with respect to the flat triangle at the vertices. This determines a function $\Psi^{ij}_{\varphi}(\varphi)$ which has a derivative equal to 0 when the geometry of the shell is flat ($\varphi = 0$) See figure 9.7 on page 111. This derivative equal to 0 makes the element overly stiff in this particular example.

Furthermore, in this flat geometry the element becomes overly sensitive to mesh anisotropy. For the symmetric series of meshes, the author has created meshes with divisions of an equal size for the two main directions of the beam; with 2 exceptions. In one case, the author has divided the width in 8 divisions while dividing the length in 96 divisions. This makes divisions with a size ratio of $1.2 : 1$ for the two main directions of the mesh; and the result doesn't fit in the convergence curve. Instead, in a mesh with fewer nodes (8 divisions across and 80 divisions length-wise) the result is much more accurate and also fits better in the convergence graph.

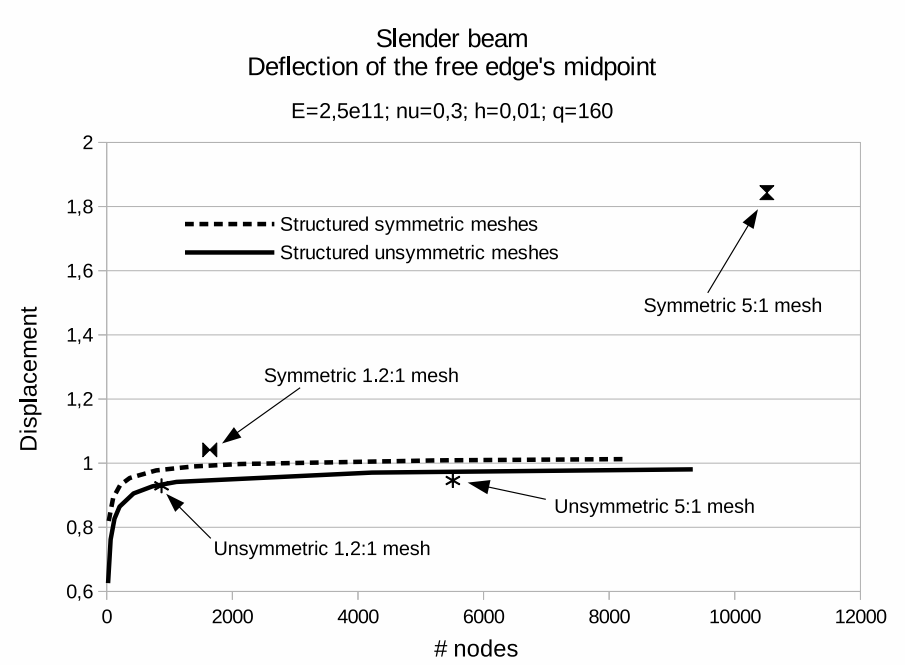


Figure 11.14: Convergence of the deflection of the free edge's midpoint. Series of results of the linear problem obtained with regular meshes of 1:1 sized cells (continuous and discontinuous lines); both symmetrically and unsymmetrically divided (see figure 11.13). Individual results for meshes of different size ratios are also plotted (see figure 11.15 for an example of a mesh with a 5:1 size ratio of the cells symmetrically divided).

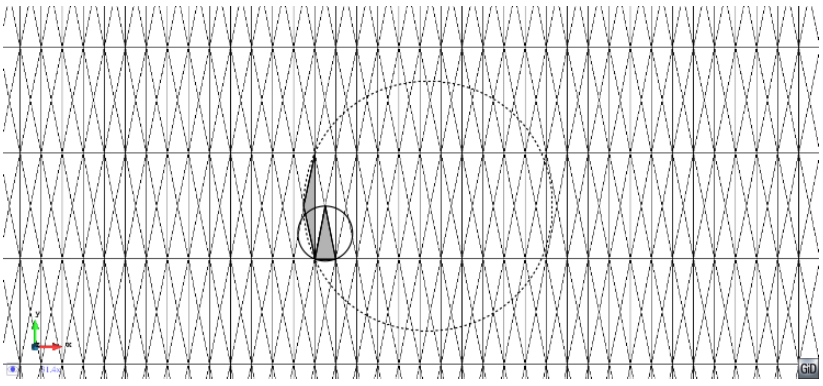

Figure 11.15: Detail of an anisotropic mesh using symmetric divisions. Divisions with a size ratio of $5:1$. The resulting triangles have circumscribed circles of very different sizes. The larger circle has a radius 4.5 times that of the smaller circle; and an area 20 times larger.

Using a larger size ratio only exacerbates the problem (see figure 11.14).

The reason for this behavior stems from the definition of the normal vector at the nodes. The normal vector at the nodes is defined assuming that the mesh approximates a quadric surface; and that each of the triangles in the mesh represents a section of that quadric surface (see [129]). This assumption determines the weights that ultimately define the direction of the normal at the node. In the case of the flat surface, there is no doubt about which is the normal vector. But the problem lies in its derivative as the midsurface of the shell deforms. The relative shapes and sizes of the triangles surrounding the node determine the behavior of the derivative of the normal. There is no geometric information to characterize the normal derivative because the surface has no curvature. Therefore, the characterization of the normal derivative depends only on the mesh topology. Then, if the relative sizes and shapes of the triangles surrounding the nodes of the flat surface are uneven, most probably the information on the normal derivatives will behave oddly. This is for example the case for an extra-refined mesh in the length-wise direction; with 500 elements length-wise and only 10 elements across. So the triangles have a ratio of $5:1$ for the two main directions of the mesh (see figure 11.15). With a symmetrically divided mesh, the differences between the triangles are very pronounced and the result is completely wrong in magnitude. However, with a biased mesh, the triangles are all equal (all equally skewed). And in this case the result is much closer to the correct one (although overstiff).

For these two reasons —which also cause the mismatch of the convergence of the two mesh sets— the author concludes that the BEST element isn't suitable for linear analysis of plate problems. And that in those cases it has to be used always in the non-linear regime in order to overcome the shortcomings described above. Those two shortcomings are corrected once the geometry has some curvature, which is the defining characteristic of shells and what the BEST element has been designed for.

Therefore, it becomes important to perform a non-linear analysis of shells under large-displacements assumptions in order to accurately characterize the exact elastic response of the shell to the loading applied.

**Non-linear analysis**

When switching to the non-linear analysis, we are turning this problem, which was conceived as a bending dominated problem, into a membrane dominated problem. Because, now, as the supported edges of the plate are restricted from moving toward each other, the shell will undergo important axial stresses which not only will dwarf the bending stresses of the shell, but which will also reduce the bending moments in the shell.

Timoshenko and Woinowsky-Krieger [127] present the analytical solution for the general problem of a rectangular plate simply supported on two oposite sides and with an uniform load. The analytical solution is $3,0000 \cdot 10^{-2}$. The difference with respect to the numerical results may be due to the fact that the analytical solution is for a strip of the plate sufficiently separated from the free edges of the plate. And not only this problem is too narrow to have any point sufficiently separated from the free edges, but in addition, the numerical result is measured at the edge.

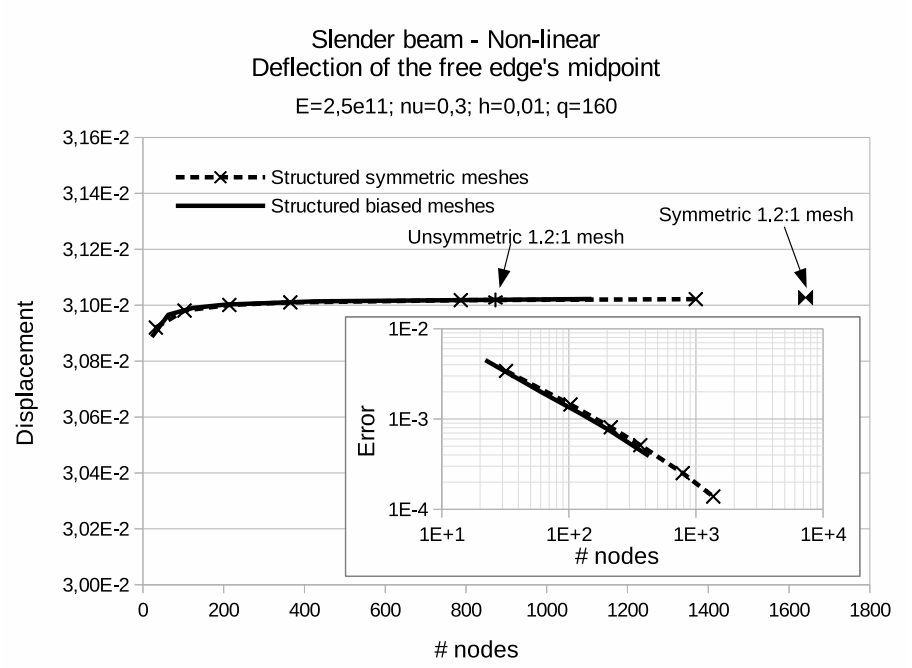


Figure 11.16: Convergence of the deflection of the free edge's midpoint. Series of results of the non-linear problem obtained with regular meshes of 1:1 sized cells; both symmetrically and unsymmetricaly divided (see figure 11.13). Only the formulation with $\theta^{ij} = 0$ converges to a result. Defining $\theta^{ij} = -\theta^{ji}$ does not yield convergence.

Nevertheless, the numerical result is sufficiently close to the analytical result to accept that the numerical result is correct.

But the most relevant result of all is that in trying to solve the non-linear problem, the author has faced the same problem reported earlier in this thesis in section 5.4. When trying to solve the non-linear problem following the Newton-Raphson method and having defined $\theta^{ij} = -\theta^{ji}$, the program cannot reach convergence. When the residual seems to be reducing, all of a sudden it jumps in value again. The cause of the problem now and then is very similar. In [132], the problem was the definition of the kinematic parameter $\Psi$ as fixed. The author concluded that the space of solutions created by the way the Bézier triangle was being constructed, did not include the solution to the non-linear problem. With the present result we may reach the same conclusion. Either way, what causes this issue is that the problem is not well posed.

Notwithstanding the previous negative result, the author reports excellent convergence for the non-linear problem using the formula in equation (9.34). That is: $\theta^{ij} = 0$. As explained in section 9.5.1, this is just a temporary fix. And a more rich and comprehensive definition of $\theta^{ij}$ is desirable in order to continue improving the BEST element. The author has proposed a framework to find that comprehensive definition of $\theta^{ij}$ in section 9.5.2. An in depth discussion will ensue in chapter 12.

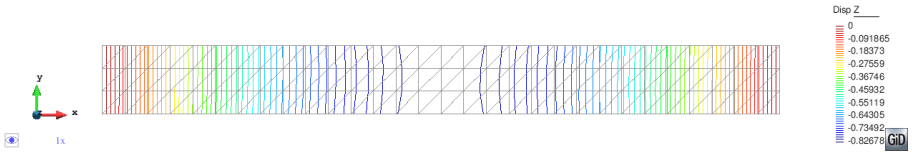


(a) Linear solution. The effect of the biased mesh can be noticed if paying close attention to the curved isolines.

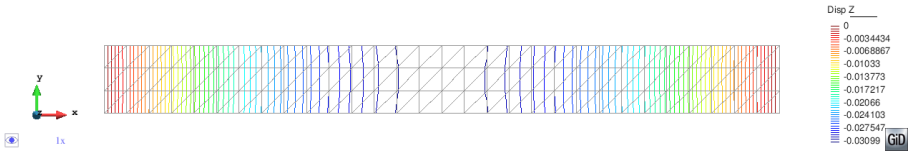


(b) Non-linear solution. The effect of the biased mesh is completely eliminated.

Figure 11.17: Comparison of the effect of the biased meshes on the result of the displacements in the Z-direction. Results obtained with a mesh of 124 nodes.

Be as it may, the BEST element shows linear convergence for the non-linear problem. Also important is the fact that convergence is reached with much coarser meshes than for the linear problem. The issue of the different converging values for the two different sets of meshes (symmetric and biased) is completely alleviated (see figure 11.16). The slight effect of the biased meshes on the results is mostly vanished (see figure 11.17). The only issue that remains is the effect of the meshes with uneven element sizes for the two main directions. Albeit even that problem has been signifficantly reduced when solving the problem in the non-linear regime.

### 11.3.2 Circular plate

This is also a classic problem that has the same characteristics as the slender beam problem above. However, in this case, because of the axisymmetric symmetry we can use a different mesh topology. And evaluate the performance of the BEST element in these conditions.

#### Linear analysis

The analytical solution for the linear analysis of a circular plates under uniform load is provided by Timoshenko and Woinowsky-Krieger [127] and by Ventsel and Krauthammer [135]. The maximum deflection at its center is calculated with the following simple formula:

$$w_{max} = \frac{3qR^4(1-\nu^2)}{16Eh^3}\left(\frac{5+\nu}{1+\nu}\right) \tag{11.3}$$

In the case defined in figure 11.18 the value for the maximum deflection at the center is $8,28125 \cdot 10^-2$.

The results show that the convergence graph crosses the result. This produces a peculiar pattern in the error graph. The error graph in figure 11.20 shows two distinctive branches. Because the convergence graph

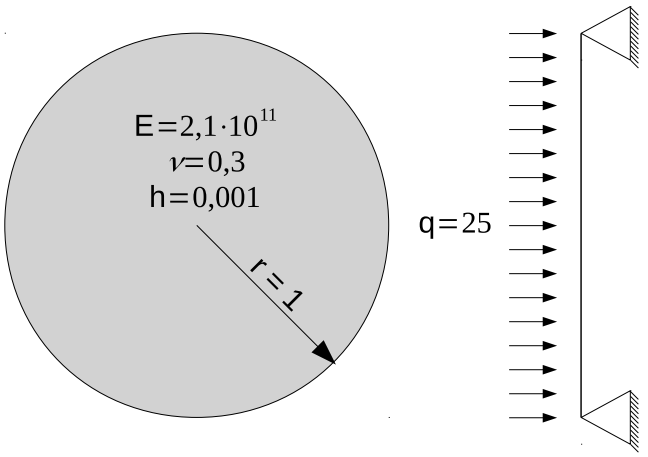


Figure 11.18: Geometry, boundary conditions and material properties of the circular plate problem. Plan and cross section.

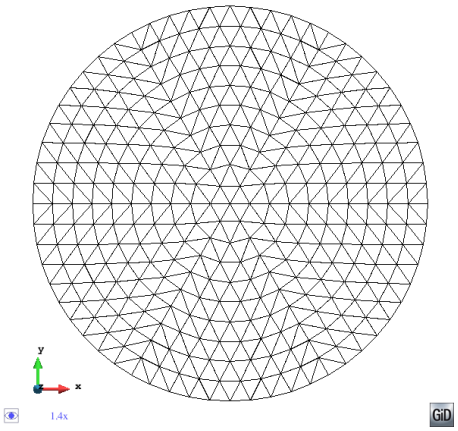


Figure 11.19: Sample mesh of the circular plate problem with 10 divisions in the radial direction.

crosses the exact result, only the later part of the error graph can be interpreted. Convergence in this problem is very slow. The cause of this apparently poor performance is that the author has not implemented in the program the boundary conditions for continuous supports described in chapter 10. Particularly the continuous simply supported shell in the tangent plane direction condition (see section 10.2) and the continuous simply supported shell in the normal direction condition (see section 10.4). Both conditions are needed to adequately model this problem. Without them, the continuous support of the boundary is only modeled discretely at the vertices of the triangles. So convergence to the right solution occurs much slower than it should because the model needs that many more nodes at the boundary.

Another cause for the poor convergence performance of the BEST el-

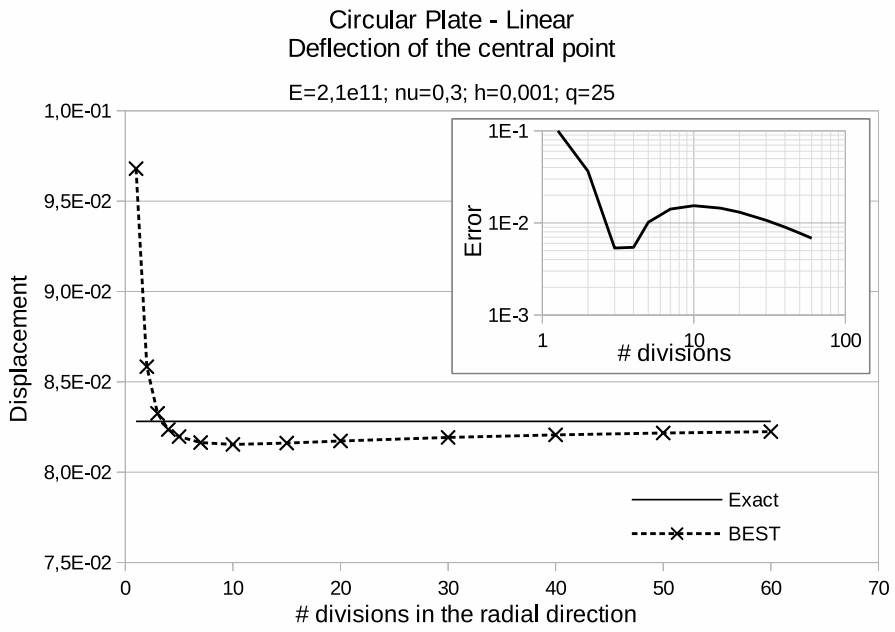


Figure 11.20: Convergence of the deflection of the central point in the circular plate problem. Linear solution. Results obtained with regular meshes (see figure 11.19).

ement in this problem has already been discussed in section 11.3.1 and consists on the role played by the definition of the $\Psi_\varphi$ function and its derivative equal to 0 when $\varphi = 0$.

### Non-linear analysis

Let's swtich again the problem into the non-linear regime. Again, when doing so we are turning this problem, which was conceived as a bending dominated problem, into a membrane dominated problem.

Timoshenko and Woinowsky-Krieger [127] present the analytical solution for the general problem of a circular plate simply supported under uniform load for the particular case of $\nu = 0.3$. They also provide a series of graphics for the case of $\nu = 0.25$.

This case is aproaching the very thin shell problem. And therefore is prone to membrane locking. As should have been expected, membrane locking occurs in this problem. It did not happen for the linear analysis, because shell elements do not lock when solving plate problems[1] (Choi, Palma, Sanchez-Palencia and Vilariño [31]). However, this example shows the problem caused by not having found a comprehensive solution for the drilling rotations. Fixing the value of $\theta^{ij}$ to 0 limits the degree of the polynomial expression of the in-plane kinematics of the element. Choi et al. prove in [31, p. 139] that representing the in-plane kinematics of the shell

[1]Shell elements don't lock when solving plate problems because under linear analysis they do not develop membrane stresses. See section 11.3.1.

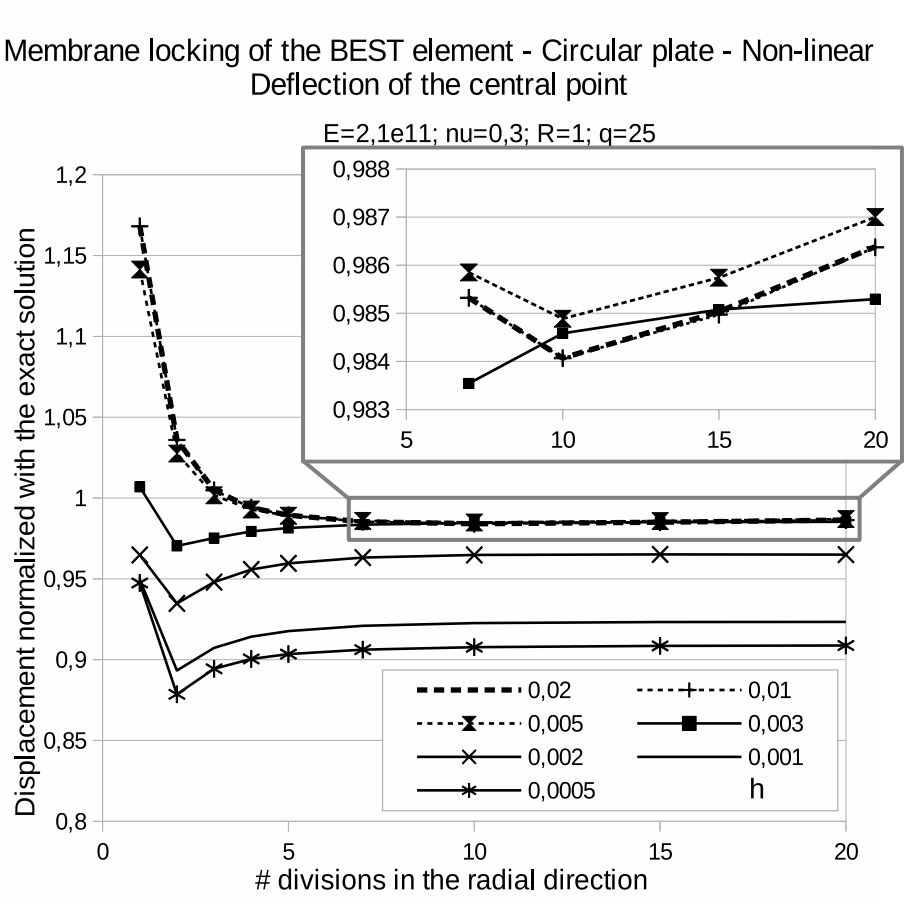


Figure 11.21: Evolution of the convergence of the BEST element as the thickness decreases. Example of a simply supported circular plate. Non-linear solution. Results obtained with regular meshes (see figure 11.19).

element with polynomials of lower order than the order used to represent the out-of-plane kinematics of the element leads inevitably to membrane locking. While Hakula, Leino and Pitkäranta demonstrate that even for finite elements with the same finite element representation in all the components of the displacement field [51, p. 161], locking may still occur then the polynomial degree of such representation is low (1 or 2). Hakula et al. also demonstrate numerically that for such elements using polynomial expressions of degree 3 and higher, the elements should not show signifficant locking problems.

In figure 11.21 the author presents the evolution of the convergence curves as the ratio thickness/radius becomes smaller and smaller. We can observe how the numerical solution using the BEST element progressively diverges from the exact solution. Even the pattern of the convergence curves changes at a given point, when it becomes apparent that even in

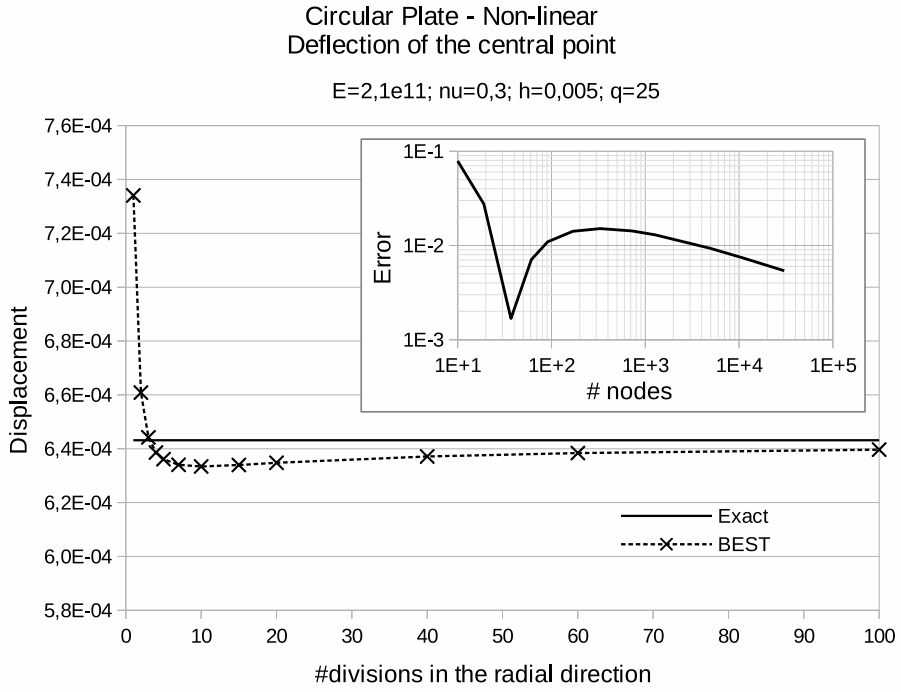


Figure 11.22: Convergence of the deflection of the central point in the circular plate problem. Non-linear solution. Results obtained with very refined regular meshes (see figure 11.19). Particular case for h=0.005.

the limit of the size of the elements approaching 0 the numerical solution will not reach convergence to the exact solution.

For the case of h=0.005, the author presents in figure 11.22 an extended convergence curve that shows how as the mesh becomes very refined it converges to the correct result, albeit very slowly.

## 11.4 Shell Obstacle Course

Next, I present the comparison of the performance of the BEST element with other elements in the literature using three well known test examples. These three examples are commonly refered to as the *shell obstacle course* [10] because "together they are a very discriminating set of problems".

After having tested the BEST element with the previous set of examples, the author has reached the conclusion that the variation of the formulation using $\theta^{ij} = -\theta^{ji}$ according to equation (9.33) does not offer any advantage performance-wise nor precision-wise with respect to the basic solution $\theta^{ij} = 0$ proposed in equation (9.34). Furthermore, it has been demonstrated that using equation (9.33) does not produce convergence in non-linear problems, and therefore it leads to a non-well-posed problem; while equation (9.34) does yield convergence for non-linear problems. Be-

casue all of this, the tests of the shell obstacle course will be presented using only $\theta^{ij} = 0$.

The comparison will be presented against a wide range of shell elements to have an accurate view of how does the BEST element rank with respect other elements. For comparison with another family of rotation-free finite elements I have chosen the BST/enhanced basic shell triangle (EBST) family by Oñate, Zárate and Flores [95]. For comparison with other elements with rotations, I have taken the linear triangle S3 from ABAQUS [1] and a quadratic element family: the T6/T6H elements implemented in ANSYS [4]. Also the versions of the EBST shell element with rotational degrees of freedom called EBST+ and EBST+1 [145] are included in the comparison. Finally, also the quadrangular elements MITC9 [6], Q8H [54] and S4 (and its reduced integration version S4R) also from ABAQUS are included.

The results published in [68] have been used to benchmark the BEST element with respect to the following elements: Q8H, MITC9, T6, T6H, S3, S4 and S4R. The author expresses his gratitude to professor Laulusa for gratiously providing his published results in tabulated form. For the BST/EBST/EBST+/EBST+1 family of elements, the results for comparison are taken from [95, 145]

### 11.4.1 Scordelis-Lo Roof

This problem consists on a cylindrical roof under a uniform pressure load. The roof is simply supported on rigid diafragms on both ends (the diafragms are rigid in their plane but flexible out of plane). The structure is loaded with a uniform dead weight $q = 90$.

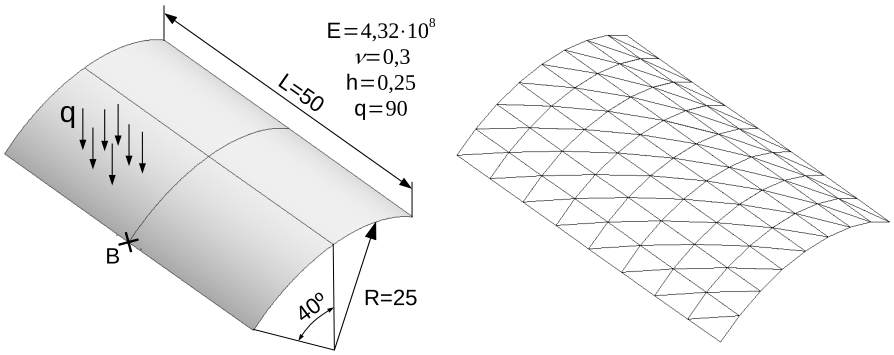


Figure 11.23: Scordelis-Lo problem. (a) Geometric definition and material properties. (b) Mesh used for the computations. A structured mesh is used with biased triangles. The full domain is computed.

The results presented are all normalized and the unit of comparison of the meshes is the total number of degrees of freedom used for $\frac{1}{4}$ of the geometry.

Figure 11.24 presents a comparison of the performance between a series of shell elements. This problem exemplifies the virtues of shells to

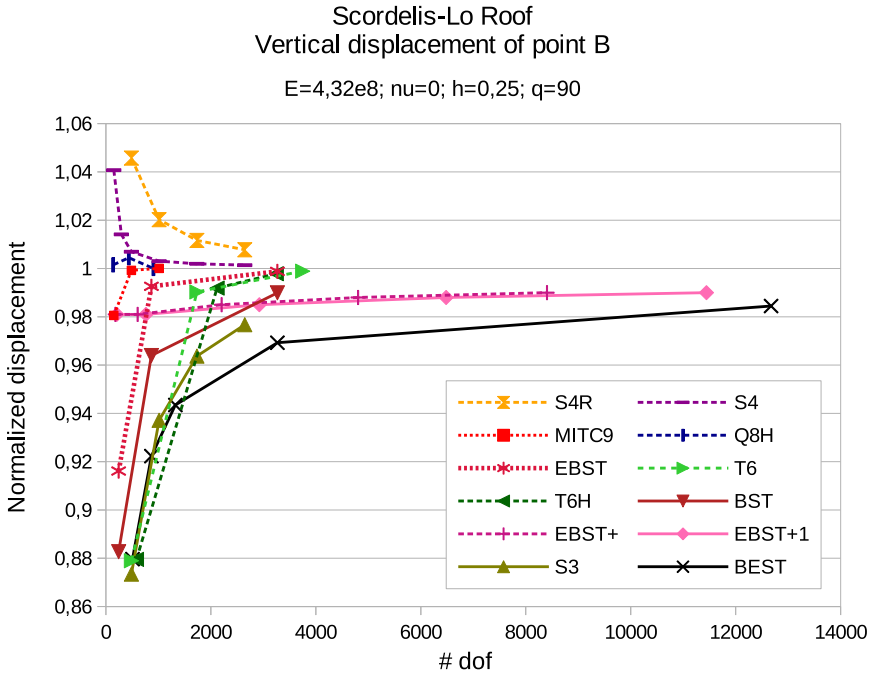


Figure 11.24: Comparison of the convergence between different shell elements for the Scordelis-Lo problem. The reference solution is taken as 0.3024.

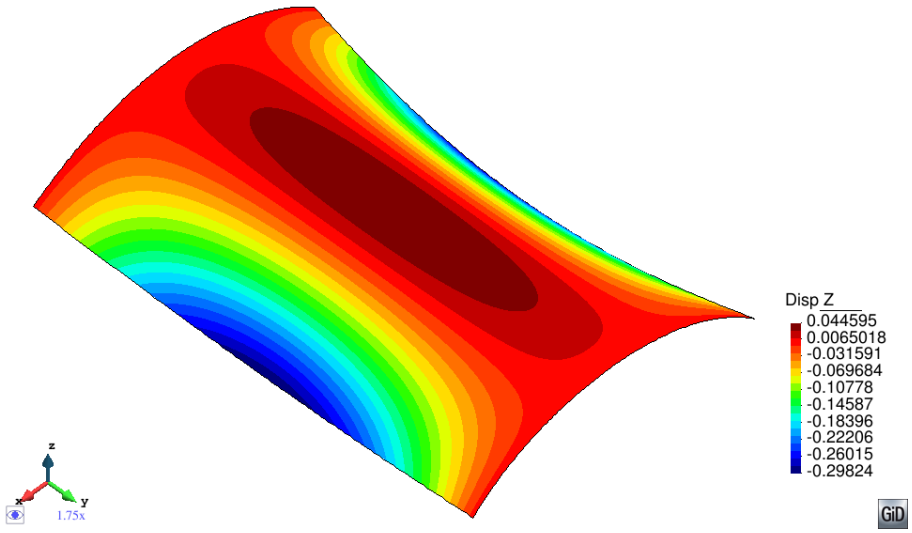


Figure 11.25: Field of vertical displacements of the Scordelis-Lo roof problem. Results obtained using a mesh with 64 divisions for half the span and half the arch. Representation of the deformation of the structure magnified x10.

resist loads through form and membrane stresses. Therefore, in this example the roof undergoes all sorts of membrane deformations while minimizing bending. In the words of Belytschko et al. [10, p. 239]: "A substantial part of the strain energy is membrane strain energy". This implies also the presence of in-plane membrane shear in the shell; just as in the case of the circular plate problem. And they further predict: "[...] inadequacies in membrane stress accuracy will severely inhibit convergence." We already know that the BEST element lacks accuracy to represent in-plane shear strains and as a result its performance is clearly subpar when compared with all the other elements. Nevertheless, the author has also reported the reason for this defect (see section 11.3.2) and the belief that it can be very much alleviated (see chapter 9). Figure 11.25 displays the deformed structure magnified.

### 11.4.2 Pinched Cylinder

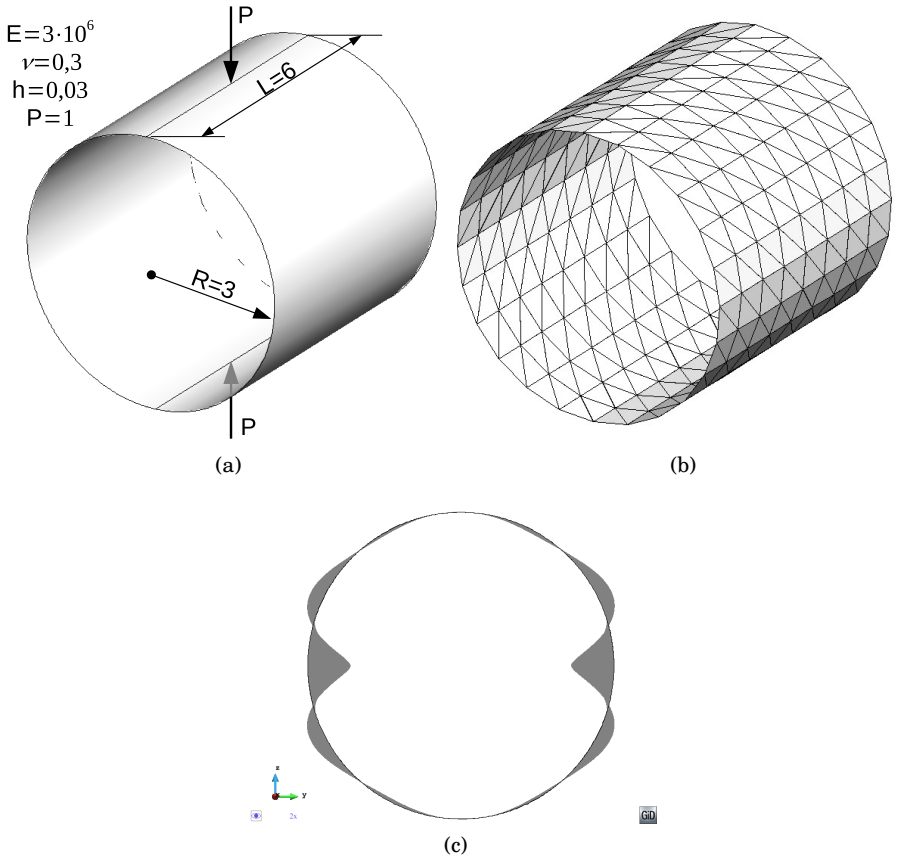


Figure 11.26: Pinched cylinder problem. (a) Geometric definition and material properties. (b) Mesh used for the computations. A structured mesh is used with biased triangles. The full domain is computed. (c) Axial view of the deformation of the cylinder. Magnification factor: x500.

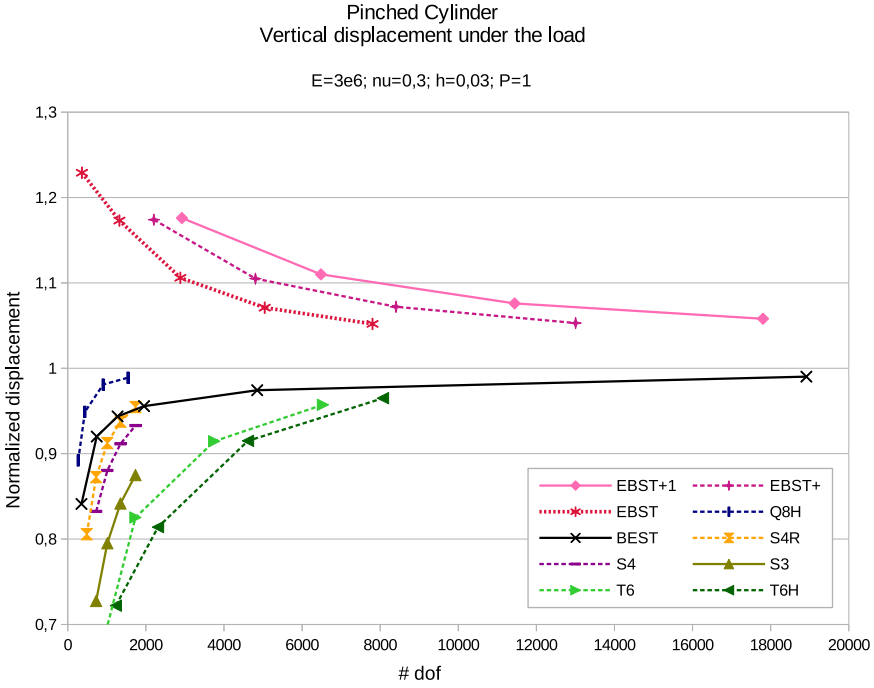


Figure 11.27: Comparison of the convergence between different shell elements for the pinched cylinder problem. The reference solution is taken as 0.0018249.

This example consists on a cylinder subjected to two diametrically opposed puntual loads, see figure 11.26. The ends of the cylinder are simply supported on rigid diafragms (the diafragms are rigid in their plane but flexible out of plane). It is (according to Belytschko et al. [10, p. 239]) "one of the most severe tests for both inextensional bending modes and complex membrane states". However, this statement is challenged by Chapelle and Bathe [22] who state that in this problem "pure bending is inhibited". Therefore it does not test the elements for inextensional bending modes to the degree claimed by Belytschko et al. The author agrees with Chapelle and Bathe. As we will see in section 11.4.3, the hemispherical shell problem really poses a problem to those elements which are not able to reproduce inextensional bending modes.

The results of the Pinched Cylinder in figure 11.27 show the excellent behavior of the BEST element. It clearly outperforms the EBST family of elements (with and without rotations). It also outperforms all the other triangular elements in the set; both linear and quadratic (S3, T6 and T6H). It is on par with the quadrilateral elements S4 and S4R. The only elements in the set that perform better than the BEST element in this problem are the MITC9 and the Q8H elements. Nevertheless, the author believes that if the in-plane shear problems of the BEST element are solved, there is still room for improvement even for this excellent result.

Figure 11.26c and figure 11.28 display the deformed structure magni-

fied.

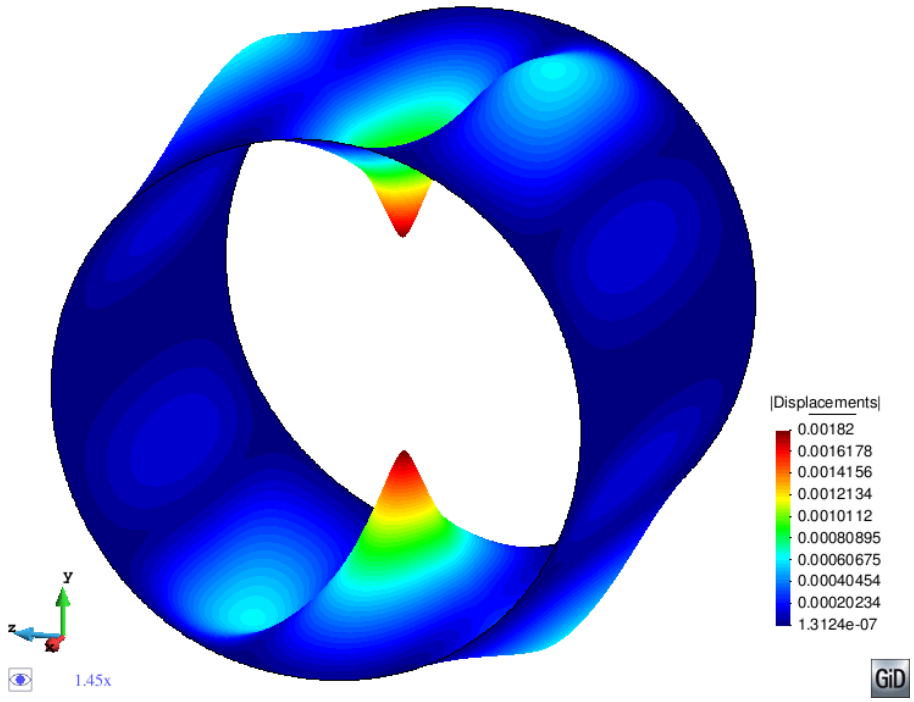


Figure 11.28: Field of displacements (modulus) of the pinched cylinder problem. Results obtained using a mesh with 96 divisions for a quarter of the circumference and 64 divisions for half the length of the cylinder. Representation of the deformation of the structure magnified x1000.

### 11.4.3 Pinched Sphere / Hemispherical Shell

The pinched sphere example (also called hemispherical shell) is also a classic benchmark example for shell elements. It consists on a hemispherical shell truncated at the top according to an 18º hole. The shell is subject to diametral opposed forces on the 2 main axis. One pair of forces pulls the shell while the other pair of forces pinches the shell. This is an example of what Chapelle and Bathe [22] call non-hinhibited bending. Therefore, the problem is bending dominated and as Belytschko et al. report: “it exhibits almost no membrane strains”. Although, as Chapelle and Bathe point out, the geometry of the problem is very sensitive to the boundary conditions and could very easily become an inhibited bending problem. We shall expect the BEST element to have difficulties solving this problem.

As expected, figure 11.30 shows the issues of the BEST element with inextensional bending modes. The EBST family of elements performs better than the BEST element, although not by much. The author is surprised about the results reported by Laulusa et al. [68] for the S4 and S4R elements. Being all of them linear elements, it is remarkable that in this problem so prone to membrane locking they outperform other higher order

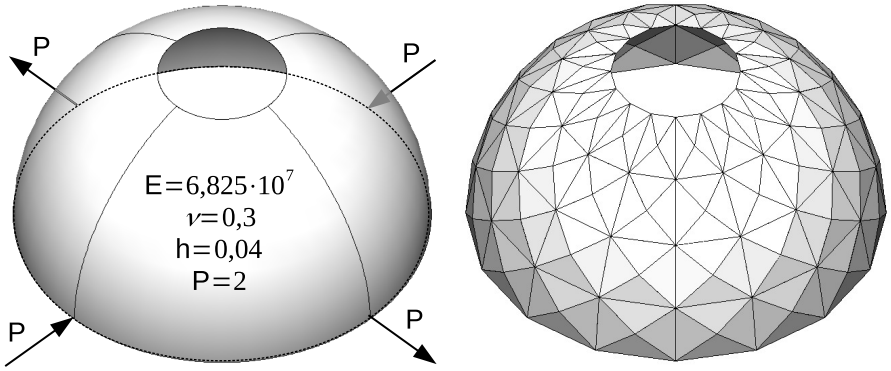


Figure 11.29: Pinched sphere problem. (a) Geometric definition and material properties. (b) Mesh used for the computations. A structured mesh is used with symmetric triangles. The full domain is computed.

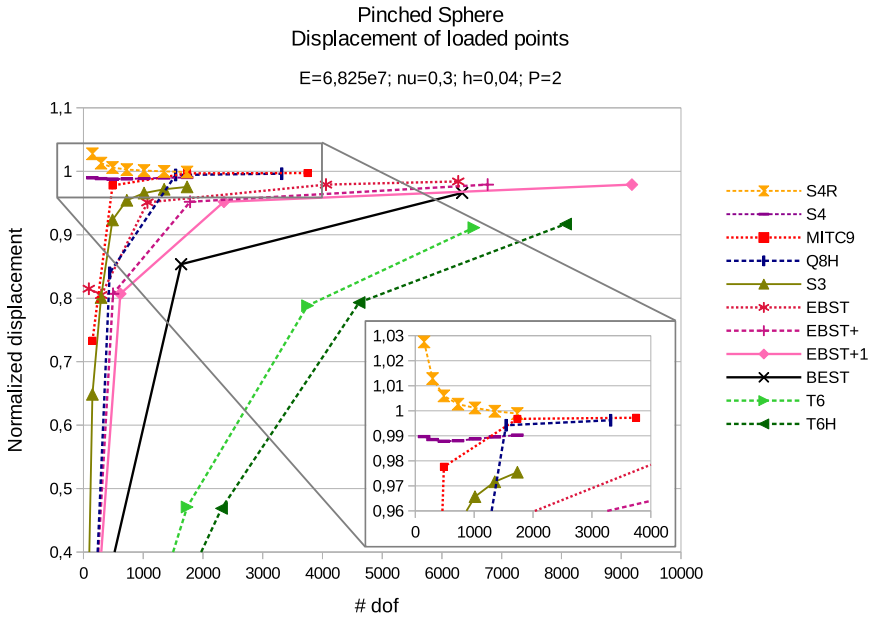


Figure 11.30: Comparison of the convergence between different shell elements for the hemispherical shell problem. The reference solution is taken as 0.094.

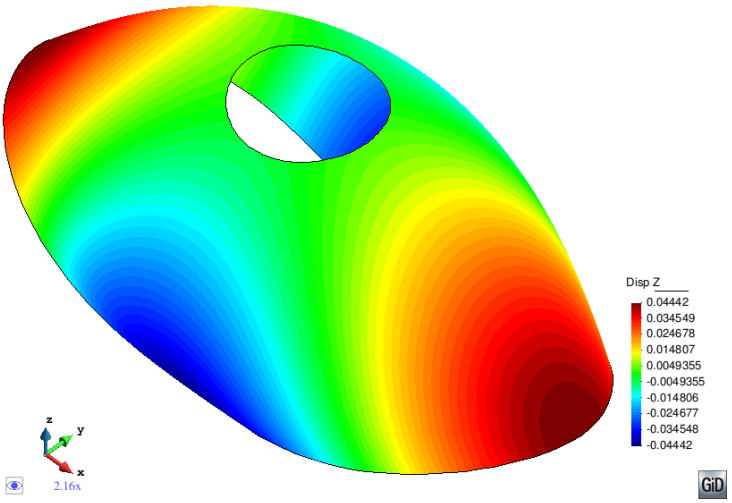


Figure 11.31: Field of vertical displacements of the hemispherical shell problem. Results obtained using a mesh with 32 divisions for a quarter of the equator and for each meridian. Deformations magnification factor x50.

elements such as the MITC9 and the Q8H; and the triangular S3 is not far behind. In the opinion of the author, the result obtained by Laulusa et al. in [68, Fig. 12] contradicts the results obtained by Hakula et al. in [51]. Figure 11.31 displays the contour fill for the vertical displacements field of the shell.

## 11.5 Summary

Four sets of tests have been presented. The first three sets have tested the BEST element convergence properties for the 3 different deformation modes of a shell: in-plane shear, axial strain (membrane) and bending. Also, for these first three sets, the two different formulæ for the value of the drilling rotations —equations (9.33) and (9.34)— have been tested.

The results obtained for the thick beam problem (section 11.1.1) demonstrate the benefits of enriching the kinematics of the element through the value of $\theta^{ij}$. However the improvement is minimal because the value assigned in equation (9.33) is not a sufficiently good approximation.

On the other hand, the results obtained for the torsion of a tube give a first hint at the problems that the equation (9.33) might introduce that surpass the advantages. This first hint is a lack of consistency in the results between structured and unstructured meshes.

With respect to the membrane oriented tests, there is almost no difference between the results obtained by the use of equation (9.33) or equation (9.34). And in both problems, the cylinder under internal pressure, and the parabolic roof, the convergence is better than linear. There has been a loss of convergence speed in the problem of the cylinder under internal pressure with respect to the results already reported in section 8.2.1.

The difference between the two results can only be caused by the changes in the construction of the element to enable the $\theta$ drilling rotations (see the differences between figures 5.5 and 9.3). So, cubic convergence has been lost for this problem, but if a correct value of $\theta$ is found, it should be recoverable.

Finally, in order to test the bending deformation mode of the BEST element, the author uses two plate examples: a rectangular plate configured as a slender beam and a circular plate. These examples are chosen because mathematically, in the linear case, the shell elements do not develop membrane strains. Therefore the analyst can focus exclusively on the bending mode response of the element. However, since there is no membrane strain and the geometry is flat, this means that there is no difference in the results between the use of equation (9.33) or equation (9.34). Nevertheless, a wealth of information is extracted from these two examples.

The first interesting result is that for the slender beam problem, discretizing the domain with biased meshes or with symmetrically divided meshes, yields different results —although very close to the correct result. This result leads the author to conclude that the BEST element isn't well suited for plate problems, because it needs the information provided by the curvature of the surfaces. The curvature of the surface embeds information onto the mesh to determine not just the direction of the normals, but also their derivatives when the surface deforms. With zero initial curvature, the mesh has zero initial information from the surface on how the normals will change as the surface deforms. And therefore that information becomes mesh-dependant. Since the plate doesn't have initial curvature, the computation becomes overly sensitive to the mesh discretization.

The author demonstrates these statements by turning the problem into geometrically non-linear. In this non-linear configuration the BEST element recovers the consistency between the sets of meshes (biased triangles and symetrically divided triangles). But the author also discovers that using the equation (9.33) for $\theta^{ij}$, the BEST element does not converge in the non-linear solving alogrithm. The author reports that the behavior is similar to the one already reported in section 5.4 —fixing the value of $\Psi = \frac{1}{3}$ made it impossible to obtain convergence in the non-linear Newton-Raphson algorithm—. This result is conclusive to discard the use of equation (9.33) in the construction of the BEST element; as it produces an ill-posed problem. On the contrary, using equation (9.34) the BEST element converges optimally in the Newton-Raphson algorithm.

The circular plate problem provides another opportunity to further characterize the BEST element. While for the linear problem the BEST element converges to the correct result (albeit very slowly), when turning it into geometrically non-linear the author found that the BEST element wasn't converging to the correct result. This result was shocking at first. Certainly, the mechanisms of the linear and the non-linear problems are different. While for the linear problem the response is only in bending mode, for the non-linear problem the response is mostly in membrane mode. But an error of over 7% was completely unexpected. The portion of the deformation energy absorbed by the membrane mode becomes larger as the thickness becomes small. This fact led the author to test the same problem in the non-linear regime for different thicknesses, finding a very

enlightening result. Figure 11.21 shows how the BEST element progressively becomes locked as the thickness of the plate becomes smaller. This result is consistent with the explanation published by Choi et al. [31].

The last set of problems is the *shell obstacle course*. In this set of problems the most remarcable result is obtained for the pinched cylinder problem. For the pinched cylinder problem, the BEST element exhibits excellent performance, proving to be superior to all the other elements used for comparison except for the more sophisticated MITC9 and Q8H elements which are quadratic quadrangular elements with rotation degrees of freedom. For the Scordelis-Lo roof problem and the hemispherical shell problem the results obtained are consistent with the results already discussed for the slender beam, the circular plate and the thick beam tests. The advantage of using examples that test the specific deformation modes of the element is that it allows to better identify the defects of the element. Whereas the advantages of using the examples in the *shell obstacle course* is that it provides a consistent base to compare against other elements in the literature.

# Chapter 12

# Future work and further research

ANY RESEARCH WORK departs from one or many starting points and makes developments based on that basis; and in most cases without reaching a closed result. Usually research efforts serve rather to open windows than to close doors, and I believe that this thesis is a good example. I am sincerely satisfied with my work, but I can't refrain from expressing some annoyance because there is still job to do. The exercise of starting a research work, exploring the knowledge, *pursuing the endless frontier* (borrowing the words from Chuck Vest [136]); is an intrinsically bold and ambitious endeavor. As a consequence, as it usually happens, the author did not measure with precision the effort required to achieve the initial objectives; because it is impossible to evaluate the difficulty of solving the challenges and overturn the adversities that such a discovery endeavor entails.

This chapter lists those aspects of the research that are affected because eventually we all have to call it a day in order to move on. The thesis includes considerations of varying degree to shine some light on the paths that are left to explore. There is even two full chapters of the thesis devoted to expose clearly the opinion and recommendation of the author to improve the results reached by the thesis.

# *Futuros trabajos y propuestas de mejora*

TODO TRABAJO DE INVESTIGACIÓN *toma uno o varios puntos de partida y realiza unos desarrollos a partir de ellos; en la inmensa mayoría de casos sin llegar a un resultado acabado. Normalmente los trabajos de investigación sirven más para abrir puertas que para cerrarlas, y creo que esta tesis es un ejemplo de ello. Estoy sinceramente satisfecho con el trabajo que he hecho, pero no puedo dejar de manifestar una cierto desasosiego por aquello que queda por hacer. El ejercicio de emprender un trabajo de investigación, de exploración del conocimiento, de* perseguir la frontera inalcanzable *(en palabras de Chuck Vest [136]); es un ejercicio inherentemente atrevido y ambicioso. Es natural por consiguiente que el autor no midiera con precisión el esfuerzo requerido para cumplir los objetivos iniciales planteados, porque era imposible medir la dificultad de resolver los desafíos y sortear los obstáculos que se encontrarían en ese ejercicio de descubrimiento.*

*Este capítulo enumera de manera sucinta aquellos aspectos de la tesis que por motivos varios se han quedado en el tintero. La tesis incluye reflexiones de distinta profundidad sobre la manera de abordar los caminos que quedan por transitar. Incluso dos capítulos enteros de la tesis están dedicados a detallar la resolución que el autor propone a estos retos. Sirvan pues los contenidos de este capítulo para exponer de manera clara cual es la opinión y la recomendación del autor para mejorar los resultados alcanzados en esta tesis.*

## 12.1 Optimize the programming

The BEST element presented in this thesis has been programmed and implemented in a computer code. The implementation done by the author makes an abuse of the tensors of many dimensions (up to 5 dimensions) for the storage of variables. The code also makes an abuse of nested loops in order to process all those variables. In reality most of the components of these tensors are zero. This abuse of tensors and nested loops generates a great inefficiency in the element's system matrix build routine. Therefore, the current implementation of the code does many superfluous operations and is using a lot of unneeded memory.

It is necessary, indeed, to improve the implementation of the programming code of the BEST element by optimizing and using specialized libraries for the manipulation of tensors of many dimensions which are essentially sparse and the corresponding algorithms to operate with them. Without that optimization it is pointless to analyze the computational efficiency of the BEST element in detail.

## *Optimizar la programación*

*El código que ha programado el autor para implementar el elemento BEST desarrollado en esta tesis hace un abuso de los tensores de varias dimensiones (hasta 5 dimensiones) para el almacenamiento de variables. Asimismo también abusa de los bucles anidados para procesar todas esas variables. En realidad muchos de los componentes de esos tensores son cero. Ese abuso de tensores y de bucles anidados causa una gran ineficiencia en la rutina de construcción de la matriz del sistema del elemento. Puesto que con la implementación actual del código se están realizando muchas operaciones superfluas y se está usando espacio de memoria de manera innecesaria.*

*Una evidente y necesaria mejora de la implementación del código del elemento BEST sería la optimización y uso de librerías especializadas para la manipulación de tensores de múltiples dimensiones eminentemente sparse y los correspondientes algoritmos para operar con ellos. Sin dicha optimización no es ni siquiera planteable un análisis en profundidad de la eficiencia computacional del elemento BEST.*

## 12.2 Nodal vs elemental assembly: edge-based assembly?

In [96] Oñate and Zárate make a point for using vertex-based rotation-free shell elements (BSN). In their case, the precision improvement of the vertex-based formulation over the element-based formulation stems from the increased number of connectivities achieved by the vertex-based formulation.

The BEST element performs most of the calculations using the nodes as the reference to access the information. So much so, that for each calculation the information can be structured and contained associated to the node instead of the element. Therefore it is appropriate to consider whether programming the element using nodal assembly could be faster and more efficient than using an elemental assembly algorithm. In a nodal assembly program there are lots of possibilities to reduce repeated operations that happen in elemental assembly because the variables associated to each node are recomputed once and

## *Ensamblaje nodal vs ensamblaje elemental: ¿ensamblaje por aristas?*

*En [96] Oñate y Zárate introducen la consideración de usar elementos de lámina sin rotaciones basados en los vértices (BSN). En su caso, la mejora de la precisión de la formulación basada en los vértices (sobre la formulación basada en los elementos) se debe al mayor número de conectividades logrado por la formulación basada en los vértices.*

*El elemento BEST realiza casi la totalidad de las operaciones tomando como referencia los nodos. De tal manera que en cada operación se puede estructurar la información conteniéndola en el nodo en lugar de en el elemento. Por consiguiente es oportuno plantear si una programación del elemento ensamblando por nodos puede ser más rápida y eficiente que una programación ensamblando por elementos. En la programación ensamblando por nodos hay muchas posibilidades de reducir la repetición de operaciones que en el ensamblaje por elementos se producen dado que las variables asociadas a cada nodo son recalculadas una y otra vez por todos los elementos que lo comparten.*

again by all the elements that share that node.

The only values of the element requiring the simultaneous information from the 3 nodes of the element are those related to the central control point of the element. Since the information to compute the central control point requires information from the three edges, an edge-based formulation can be considered worth studying. In fact, different authors have performed adaptations of shell finite elements into an edge-based smoothed formulations recently [30, 69, 101].

## 12.3 Solve the membrane locking

Chapter 9 has shown that the BEST element suffers membrane locking because of the way it has been kinematically built. This problem has also been reproduced with more severity in the example of the circular plate (see section 11.3.2). Such locking inhibits the element from converging cubically wherever there may be any in-plane shear deformation, and instead exhibits only linear convergence —or worse—. It is highly desirable to fix this behavior, as that would conclusively justify the strategy developed in this thesis. Nevertheless, the results obtained, albeit partial, confirm that the strategy developed is correct; although an evolution is highly desirable. The author has also set forth in chapter 9 the existing defect in the element's kinematic construction which causes that locking behavior. And has come up with an idea to solve this issue liberating the so called *drilling* degrees of freedom. The BEST element allows to emulate the effect of these *drilling* degrees of freedom, that's why it isn't necessary to include them in the description of the element. What the element needs is to modify the kinematics of its construction to be able to accurately reproduce their effects.

The author has successfully shown how to unleash the kinematics of the *drilling rotations* in the element. And in doing so he shows that the element improves its convergence properties. However, the results only display a marginal improvement, because the implementation still does not translate the kinematics of the *drilling rotations* into a precise description of the deformation of the element. The author has implemented in the computer code a very basic description of the de-

*Los únicos datos del elemento que requieren de la información simultánea de los 3 nodos del elemento son los relativos al cálculo del punto de control central del elemento. Como la información para calcular el punto de control central toma como punto de partida la información de las tres aristas, podría ser ventajoso estudiar una formulación basada en las aristas. De hecho, recientemente varios autores han desarrollado adaptaciones de elementos finitos de lámina a formulaciones basadas en las aristas aplicando técnicas de suavizado [30, 69, 101].*

## *Resolver el bloqueo por membrana*

*Como se ha mostrado en el capítulo 9 el elemento BEST tal y como se ha definido cinemáticamente padece de bloqueo por membrana. Este problema también se ha demostrado con más severidad en el ejemplo de la placa circular (véase el apartado 11.3.2). Dicho bloqueo impide que el elemento pueda converger cúbicamente en aquellos casos en los que exista deformación por cortante en el plano del elemento en alguna medida, y en su lugar sólo exhibe convergencia lineal —o peor—. Es altamente deseable poder corregir este comportamiento, pues ello terminaría de justificar la estrategia desarrollada en esta tesis. No obstante, se han alcanzado resultados parciales que corroboran que la estrategia desarrollada es acertada; si bien es muy deseable una evolución. El autor ha señalado en el capítulo 9 el defecto en la construcción de la cinemática del elemento que causa este bloqueo. Y ha propuesto resolver ese defecto liberando los llamados grados de libertad de* taladro*. El elemento BEST permite emular el efecto de estos grados de libertad de* taladro*, y por ello no es preciso añadirlos a la descripción del elemento. Lo que se precisa es adaptar la cinemática de la construcción del elemento para que éste pueda reproducir su efecto.*

*El autor ha demostrado con éxito la manera de liberar la cinemática de las* rotaciones de taladro *en el elemento. Y con ello muestra la mejora que experimenta la convergencia el elemento. Si bien, los resultados sólo muestran una mejora marginal, pues aún es necesario traducir la cinemática de las* rotaciones de taladro *en una descripción de la deformación del elemento precisa. La descripción que se ha implementado en el código programado por el autor es todavía muy primitiva. Por ello se propone mejorar la descripción de la deformación del elemento asociada a la cinemática de*

formation, and lacks sophistication. The author proposes to improve the description of the deformation of the element associated to the kinematics of the *drilling rotations*. This description of the deformation shall be consistent with the continuum mechanics theories in order to avoid adding an artificial stiffness to the element of any kind; which is the cause for the membrane locking behavior in our case.

In section 9.5.2 the author sets forth a framework that leads to a precise description of the deformation based on the *drilling rotations* kinematics. That framework establishes that the element's edge kinematics shall account for a solid rigid rotation and a rotation associated to the in-plane shear deformation. And on the other side, it explains that the deformation gradient tensor associated to the tangent plane at the vertex —where the *drilling rotations* are conceptualized— is also decomposed into a (solid rigid) rotation tensor and a shear deformation tensor (in-plane). And therefore proposes to relate the *drilling rotations* kinematics to the description of the deformation, by deriving the corresponding formulæ. However, the full development of those formulæ and the implications on the rest of the element's kinematics is an adaptation left to be done in a future work.

## 12.4 Implement Dirichlet boundary conditions

The BEST element presented in this thesis has been programmed and implemented in a computer code. The implementation done by the author lacks the complementary routines to apply the Dirichlet boundary conditions on the models. In order to extend the use of the BEST element to a wide range of academic and engineering problems it is necessary to implement these boundary conditions (see chapter 10). Nevertheless, the examples shown in this thesis allow to reach sufficiently founded conclusions regarding the developments of the thesis.

Indeed, the conclusions of this thesis clearly express the need to improve the performance of the BEST element with respect to the membrane locking phenomenon. In the opinion of the author, it is worthless evaluating the BEST element

*las* rotaciones de taladro. *Esta descripción de la deformación debería ser consistente con los postulados de la mecánica del continuo para evitar introducir en el elemento algún tipo de rigidez artificiosa, que es lo que en definitiva está activando el bloqueo por membrana del elemento.*

*En el apartado 9.5.2 el autor avanza un marco de trabajo que debe permitir esa descripción precisa de la deformación a partir de la cinemática de las* rotaciones de taladro. *Dicho marco de trabajo establece que la cinemática del elemento debe contemplar que para cada arista del elemento, la* rotación de taladro *se descompone en un giro de sólido rígido y un giro de deformación de cortante en el plano. Y por otro lado se explica como el tensor gradiente de la deformación asociado al plano tangente en el vértice —donde se conceptualizan las* rotaciones de taladro— *también se descompone a su vez en una componente de rotación (de sólido rígido) y otra de deformación de cortante (en el plano). Y se propone una manera de relacionar la cinemática de las* rotaciones de taladro *con la descripción de la deformación, derivando las correspondientes fórmulas. No obstante, el desarrollo completo de dichas fórmulas y la adecuación del resto de la cinemática del elemento a lo que estas fórmulas implican es un trabajo que queda para el futuro.*

## *Implementar las condiciones de contorno de Dirichlet*

*El código que ha programado el autor para implementar el elemento BEST desarrollado en esta tesis no incluye las rutinas necesarias para aplicar las condiciones de contorno de Dirichlet en los modelos. Si bien la implementación de dichas condiciones de contorno (véase el capítulo 10) es necesaria para poder extender el uso del elemento BEST a una amplia casuística de problemas académicos e ingenieriles, los ejemplos expuestos en esta tesis permiten alcanzar conclusiones suficientemente fundamentadas en relación a los desarrollos de la tesis.*

*De hecho, las conclusiones de esta tesis indican claramente la necesidad de mejorar el rendimiento del elemento BEST frente al fenómeno de bloqueo por membrana. Es la opinión del autor que carece de interés evaluar el elemento BEST frente a un conjunto de ejemplos más amplio que los presentados en esta*

using a broader set of examples than those presented in this thesis without previously improving the behavior of the BEST element to prevent membrane locking. Nonetheless, it is highly desirable to include in the code of the program that implements the BEST element the feature to apply those boundary conditions described in chapter 10 in order to benchmark the BEST element capabilities thoroughly and compare them to other existing formulations in the literature and using a wider variety of benchmarking examples commonly used.

## 12.5 Develop adequate representation techniques for the BEST element

The development of this research would have benefited from having a graphical representation system of the element's Bézier-enhanced geometry. The only such representation included in this thesis is in figure 5.10c. And it was generated after programming the elements of that mesh one by one on a Maple sheet. Lacking the means to visualize the resulting Bézier constructions has been a handicap in diagnosing the problems encountered.

It is thus highly advisable —in any further development to improve the BEST element— to arrange a geometric representation system which enables the visualization of the resulting Bézier geometric reconstruction.

Such work would yield an additional advantage when post-processing the results. As the results could then be plotted on the geometric representation of the Bézier-enhanced elements. Currently the results are being represented on the original mesh of linear triangles. This implies an obvious loss of resolution of the results actually computed, which are of cubic nature.

## 12.6 Try a different curvature operator

During the research work to find an optimal operator to approximate the normal direction at the nodes of the mesh (see section 5.1 [129]), an interesting reference on the approximation of curvatures in triangle meshes arose [48]. That paper evaluates the relative precision and compu-

*tesis sin previamente mejorar el elemento BEST frente al fenómeno de bloqueo por membrana. Dicho esto, es altamente deseable la inclusión en el código del programa que implementa el elemento BEST la posibilidad de aplicar las condiciones de contorno que se detallan en el capítulo 10 para entonces evaluar en toda su extensión las capacidades del elemento BEST y comparar sus virtudes y defectos con otras formulaciones existentes en la literatura usando una variedad más completa de los ejemplos académicos normalmente utilizados comúnmente.*

## *Desarrollar técnicas de representación adecuadas para el elemento BEST*

*Hubiera sido muy deseable para el desarrollo del trabajo de esta tesis haber dispuesto de un sistema de representación gráfica de la geometría del elemento de Bézier reconstruido. La única representación incluida en esta tesis se encuentra en la figura 5.10c y se generó programando los elementos de esa malla uno a uno en una hoja de cálculo de Maple. Sin la posibilidad de visualizar la construcción geométrica de Bézier resultante, ha sido muy complicado para el autor diagnosticar los problemas que se iba encontrando.*

*Es por lo tanto altamente recomendable que —en futuros desarrollos orientados a mejorar el elemento BEST— se cuente con un sistema de representación de la geometría que permita visualizar los resultados de la reconstrucción geométrica de Bézier.*

*Este desarrollo tendría un efecto añadido beneficioso para el post-proceso de los resultados. Ya que actualmente los resultados se están representando sobre la malla original de triángulos lineales. Esto supone una evidente pérdida de resolución de los resultados realmente obtenidos, que tienen carácter cúbico.*

## *Probar con un operador de la curvatura distinto*

*Durante los trabajos de obtención de un operador óptimo para aproximar la dirección de la normal en los nodos de la malla (ver apartado 5.1 [129]), apareció una referencia interesante sobre la aproximación de curvaturas en mallas de triángulos [48]. En dicho artículo se evalúa la relativa precisión y coste compu-*

tational cost of different approximation methods of triangle meshes' curvature. This is a fundamental operator in shell analysis, and has been a central aspect of the development of the present thesis. Gatzke and Grimm distinguish 3 different families of operators:

- methods that interpolate a surface to the nodes of the mesh,
- discrete methods (which attempt to obtain partial metrics related to the curvature based on different hypotheses), and
- methods of estimation of the curvature tensor.

The paper includes methods that use the nodes of the first ring of neighboring nodes, the second ring and up to the third ring of neighboring nodes.

This thesis hasn't explored the possibility of finding the metric of the curvature of the element based on any of these methods. It is very appealing to analyze the convenience of using any of these methods and compare both their precision and their computational cost with those of the finite element developed in this thesis. Nevertheless, the author makes some aprioristic considerations. The methods based on the interpolation of surfaces of increasing polynomial order suffer from various defects. Amongst them, their sensibility to mesh distortions caused by the ill-conditioning of the system matrix that needs to be solved in order to obtain the coefficients of the interpolating surface. As a result, the computational cost of solving that matrix is affected if iterative methods are used. Discrete methods are the most efficient from the point of view of their computational cost, but they give unusable results for shell analysis, because they do not provide the complete information of the curvature tensor; which would cause a significant loss of precision in the calculation of the element. The methods that estimate the curvature tensor offer some practical interest. Although the results provided by Gatzke and Grimm aren't promising on what relates to their sensibility to mesh regularity. As element robustness with respect to mesh distortion and irregularity was an aspect specifically sought by this thesis development, this is a research topic that has not been explored.

*tacional de diversos métodos de aproximación de la curvatura de mallas de triángulos. Este es un operador fundamental en el cálculo de láminas y ha sido un aspecto central del desarrollo de esta tesis. De acuerdo con Gatzke y Grimm, se pueden distinguir 3 familias de operadores:*

- *métodos de interpolación de superficies a los nodos de la malla,*
- *métodos discretos (que pretenden obtener métricas parciales relacionadas con la curvatura a partir de distintas hipótesis), y*
- *métodos de estimación del tensor de curvatura.*

*En el artículo se consideran métodos que usan los nodos del primer anillo de vecinos, del segundo anillo de vecinos o incluso de hasta el tercer anillo de vecinos.*

*En esta tesis no se ha explorado la posibilidad de obtener la métrica de la curvatura en el elemento a partir de cualquiera de estos métodos. Puede resultar interesante analizar la idoneidad del uso de cualquiera de estos métodos y comparar tanto su precisión y coste computacional con la precisión y coste computacional del método de cálculo de la curvatura del elemento desarrollado en esta tesis. En cualquier caso, se pueden hacer algunas consideraciones apriorísticas. Los métodos basados en la interpolación de superficies de creciente orden polinómico padecen de varios defectos. Entre ellos, la sensibilidad a las distorsiones de malla debido al mal condicionamiento de la matriz del sistema que es preciso resolver para obtener las coeficientes de la superficie interpolante y por consiguiente también el elevado coste computacional de la resolución de esa matriz por métodos iterativos. Los métodos discretos son los más eficientes desde el punto de vista computacional, pero ofrecen resultados poco útiles para el cálculo de láminas porque no ofrecen la información completa del tensor de curvatura; lo que conduciría a una pérdida significativa de precisión en el cálculo del elemento. Los métodos de estimación del tensor de curvatura son los que pueden ofrecer algún interés práctico. Aunque los resultados de Gatzke y Grimm no son muy halagüeños en lo que se refiere a la sensibilidad de estos métodos respecto de la regularidad de la malla. Dado que la robustez del elemento desarrollado con respecto a la irregularidad de la malla era un aspecto que se buscaba explícitamente en esta tesis, esta es una línea de investigación que no se ha explorado.*

It could be of some interest to explore the possibility of developing a rotation-free thin shell finite element based on the use of a curvature approximation operator at the nodes of the mesh, and evaluate whether it entails any computational advantage. A comparative study on the precision in the calculation of the curvature between the methods based on operators as those cited in the paper [48] and the method developed in the present thesis ought to be done. However, from the author's standpoint, the level of specialization achieved in the present thesis should provide an edge regarding the precision/computational cost relationship. The method used in this thesis uses 1 ring of neighboring nodes (for every node of the triangle). As a result, it should be more efficient than the methods that use 2 rings of neighboring nodes. And the specialization of the treatment of data should provide better results than the methods using 2 or even a third ring of neighbors. But dispelling these guesses could be an interesting exercise.

*Podría resultar interesante explorar la posibilidad de desarrollar un elemento finito de lámina delgada sin rotaciones a partir del uso de un operador de aproximación de la curvatura en los nodos de la malla y evaluar si ello implica ventajas computacionales. En ese sentido se tendría que realizar un estudio comparativo sobre la precisión en el cálculo de la curvatura entre los métodos basados en operadores como los indicados en el artículo citado [48] y el método desarrollado en la presente tesis. Aunque desde el punto de vista del autor, la especialización del método desarrollado en la presente tesis debería implicar una ventaja en cuanto a la relación precisión / coste computacional. El método desarrollado en la presente tesis usa un anillo de vecinos (para cada nodo del triángulo). Por consiguiente debería ser más eficiente computacionalmente que los métodos que usan 2 anillos de vecinos. Y la especialización del tratamiento de los datos debería dar resultados mejores que los métodos que usan 2 o incluso hasta el tercer anillo de vecinos. Pero sería interesante dilucidar todas estas conjeturas.*

## 12.7 What about composite and layered shells?

## *¿Cómo se resuelven las láminas de materiales compuestos y laminadas?*

One of the requirements of the new element was the possibility to solve for composite and layered shells. However, it has been decided not to include this development in the scope of this thesis. Certainly the use of a rotation-free element affects the possibilities of simulating a composite structure. In his book [93] Oñate explains in detail the reasons why composite beams/shells even if slender, need to account for shear deformations. Without the rotation degrees of freedom it is harder to reproduce the Reissner-Mindlin hypotheses, which are better suited to account for shear deformations than the Kirchhoff-Love hypotheses. Nevertheless, for the case of layered shells, there are other theories like the *refined zig-zag* theory which can solve this issue [124, 126], or *hierarchical split of the displacements* method which has been applied successfully but has not yet been extended to geometrically nonlinear problems [87]. Despite the fact that this thesis' scope doesn't include finally the consideration for composite and layered shells, this re-

*Uno de los requisitos para el nuevo elemento era la posibilidad de resolver láminas de materiales compuestos y laminadas. Sin embargo, se ha optado por no incluir este desarrollo en la tesis. Ciertamente el uso de un elemento sin rotaciones afecta las posibilidades de simular una estructura de materiales compuestos. En este libro [93] Oñate explica en detalle las razones por las que incluso las vigas y láminas de materiales compuestos delgadas necesitan contemplar las deformaciones de cortante. Sin los grados de libertad sin rotaciones es más complicado reproducir las hipótesis de Reissner-Mindlin, que son más indicadas para tener en cuenta las deformaciones de cortante que las hipótesis de Kirchhoff-Love. No obstante, para el caso de láminas laminadas existen otras teorías como la del* zig-zag refinado *que permite resolver este aspecto [124, 126], o el método del* desacoplamiento jerárquico de los desplazamientos *que ha sido aplicado exitosamente aunque no se ha extendido todavía a problemas geométricamente no-lineales [87]. A pesar de que finalmente el alcance de la tesis no incluye la consideración de láminas de materiales compuestas y lami-*

quirement has been taken into account so that it doesn't hamper future efforts to implement this capability. The reason is explained below.

***Continuum-based* formulation**

The concern for addressing the issue of composite and layered shells is one of the reasons to opt for a *continuum-based* approach (also called *degenerated solid* approach) instead of a shell theory approach. Besides providing a sound mathematical foundation to the formulation, the continuum-based model defines the stress and strain state of each material point in the shell with precision. This is because, it handles with ease all the high order terms. Instead, in a resultant based shell element, or in a shell theory model, usually the high order terms are more difficult to deal with —particularly in the non-linear regime— and are often dropped.

Additionally, it is the view of the author, that for engineering purposes, in the case of layered shells made of anisotropic materials it is much more interesting to provide the analyst with information on the stress and strain states of each material layer, rather than providing him with generalized (integrated through the thickness) measures of strains and stresses. Even more so, when in the non-linear regime, the higher order terms might become relevant and their corresponding generalized measures (called bi-moments) don't have an easy interpretation to the engineer [13]. Furthermore, if required, these generalized measures can be computed as a post-process.

*nadas, se ha tenido en cuenta este requisito para que no obstaculice futuros desarrollos para implementar esta capacidad. La razón se explica a continuación.*

***Formulación basada en el continuo***

*La preocupación por abordar el asunto de las láminas hechas de materiales compuestos y laminadas es uno de los motivos para escoger una formulación* basada en el continuo *(también llamada formulación de* sólido degenerado*) en vez de un planteamiento basado en la teoría de láminas. Otro motivo muy importante para la esta elección es la firme base matemática que proporciona la formulación* basada en el continuo *y que define el estado de tensión y deformación en cada punto material de la lámina con precisión. Esto es gracias a que maneja con naturalidad todos los términos de alto orden. En cambio, en un elemento de lámina basado en resultantes de esfuerzos, o en un modelo de teoría de láminas, normalmente los términos de alto orden son más complicados de manipular— particularmente en el régimen no-lineal—y a menudo se obvian.*

*Por otro lado, es la opinión del autor que para propósitos ingenieriles, en el caso de láminas laminadas formadas por materiales anisótropos es mucho más adecuado proveer al calculista la información de los estados de tensión y deformación de cada capa de material; en lugar de proveer al calculista los esfuerzos generalizados (integrados en el espesor) de tensiones y deformaciones. Por añadidura, en el régimen no-lineal los términos de alto orden pueden resultan relevantes y sus correspondientes métricas generalizadas (llamadas bi-momentos) no tienen una interpretación sencilla para el ingeniero [13]. Finalmente, si es preciso, estas métricas generalizadas se pueden calcular como un post-proceso.*

## 12.8 Practical applications

## *Aplicaciones prácticas*

In view of all the items included previously in this chapter, and taking into account the motivation set forth in chapter 1, it appears clear that I fell short of the expectations coveted initially. And particularly on what relates the justification for the selection of the objective of this thesis; explained in section 2.3:

"Firstly, because there's a need to analyze sails as shells under non-linear assumptions of large strains/displacements. And secondly, be-

*A la vista de todos los puntos incluidos previamente en este capítulo, y teniendo en cuenta la motivación expuesta en el capítulo 1, resulta evidente que me he quedado lejos de las metas ambicionadas inicialmente. Y particularmente en lo que respecta a la justificación de la selección del objetivo de esta tesis; explicada en el apartado 2.3:*

*"En primer lugar, por la necesidad de analizar las velas como láminas en condiciones de no-linealidad y asumiendo grandes deformaciones/desplazamientos.*

cause the use of this technology can subsequently be used broadly in the structural analysis of the sailboat."

In this thesis I haven't been able to perform a sail's practical analysis. Nor have I applied the BEST element to the general analysis of a sailboat's structure. In order to put the BEST element into practice, the challenges set forth in sections 12.1 to 12.7 ought to be solved. Once these milestones are accomplished, the BEST element shall be applied to the practical case of a sailboat analysis.

In order to do it, first the BEST element has to be coupled with a CFD code. This should be relatively simple since, as I have explained in section 10.9, the BEST element has been integrated in the RamSeries program; which in turn belongs to the Tdyn suite. Tdyn is an excellent multiphysics solvers suite that has sorted out fluid-structure interaction and includes a top notch CFD solver (as credited by the reference [28]).

And secondly a set of tests have to be defined to validate the BEST element. Id est, for the analysis of a sail, a benchmark case ought to be chosen including:

1. the geometric definition of the sail's design,
2. the boundary and wind flow conditions for the analysis, and
3. the geometric definition of the deformed *flying* shape;

in order to compare the results of the BEST element analysis with those of the experiment. And for the analysis of a sailboat, another benchmark case ought to be chosen including:

1. the geometric definition of the boat's design,
2. the experiment's conditions, and
3. the experiment's results.

In all likelihood, in order to adequately reproduce the sail's benchmark, it will be necessary to combine the BEST element with other structural cable and beam elements, as well as adding to the program the capability to prestress appropriately the shell structure.

*Y en segundo lugar, porque el uso de esta tecnología se puede aplicar posteriormente al análisis general de la estructura del barco de vela."*

*En esta tesis no he llegado a realizar un caso práctico de análisis de una vela. Y tampoco he aplicado el elemento BEST al análisis general de la estructura de un barco de vela. Para poder poner en práctica el elemento BEST, es necesario resolver los retos planteados en los apartados 12.1 a 12.7. Una vez se hayan cumplido esos hitos, es preciso aplicar el elemento BEST al cálculo práctico de un barco de vela.*

*Para ello, en primer lugar será preciso hacer que el elemento BEST esté acoplado con un código de resolución de fluidos. Esto debería ser relativamente sencillo pues, como ya se ha explicado en el apartado 10.9, el elemento BEST se ha integrado en el programa RamSeries que a su vez pertenece a la suite Tdyn. Tdyn es una excelente suite de* solvers *multifísica que ya tiene bien resuelta la interacción fluido-estructura e incluye un solver de dinámica de fluidos de la máxima solvencia (como lo pone de manifiesto la referencia [28]).*

*Y en segundo lugar habrá que definir una serie de tests de validación del funcionamiento del elemento BEST. Es decir, para el análisis de una vela hay que elegir un caso de* benchmark *que incluya:*

1. *la definición geométrica del diseño de una vela,*
2. *las condiciones de contorno y de flujo de viento en las que se analiza, y*
3. *la definición geométrica de su forma deformada* en vuelo*;*

*para así comparar los resultados del análisis del elemento BEST con los del ensayo. Y para el análisis de un barco de vela, hay que elegir un caso de* benchmark *que incluya:*

1. *la definición geométrica del diseño del barco,*
2. *las condiciones de ensayo, y*
3. *los resultados del ensayo.*

*Con toda probabilidad, para poder reproducir adecuadamente el* benchmark *de una vela, será necesario combinar el elemento BEST con otros elementos estructurales de biga y de cables, así como añadir la capacidad al programa de pretensar convenientemente la estructura de la lámina.*

# Chapter 13

# Conclusions

THE WORK PRESENTED IN THIS THESIS has implied a learning path. After the lessons learned I would most certainly do things differently if I were to redo them again. And that's precisely the purpose of the research work in a doctorate. A doctorate consists on generating new knowledge and finding new discoveries, but not only. It is also a path for learning (and re-learning) pre-existing knowledge. I will try to reflect on the following lines what are the most notable aspects of that learning path and signal the main contributions of this thesis.

## 13.1 Contributions

### 13.1.1 A new thin shell finite element

There are lots of shell finite elements in the subject's literature. To review them all is a task for the very few. That's why it is important to underscore the references cited in the last paragraph of section 3.1 and the references therein which, albeit they do not encompass all the different elements that exist, they represent a genuine effort to include comprehensively the ensemble of the developments on shell finite elements. This diversity of shell elements showcases the inherent difficulty of finding an overall solution to the problem. The BEST element doesn't achieve it either, but constitutes another element in the family of shell finite elements and, in particular, in the family of rotation-free thin shell finite elements, solving some of their shortcomings.

# *Conclusiones*

LA ELABORACIÓN DE ESTA TESIS *ha supuesto un camino de aprendizaje. Seguramente con todo lo aprendido haría muchas cosas de manera distinta si tuviera que volver a hacerlas. Pero precisamente en eso consiste también el trabajo de investigación de un doctorado. Un doctorado no consiste únicamente en descubrir o en generar nuevo conocimiento, que también. Además es un camino de aprendizaje (y reaprendizaje) de conocimiento ya existente. He tratado y trataré de reflejar en las siguientes líneas en qué ha consistido ese aprendizaje en sus aspectos más destacables así como señalar cuáles son las aportaciones de esta tesis.*

## *Aportaciones*

### *Un nuevo elemento finito de lámina delgada*

*Existen muchos elementos finitos de lámina en la literatura de la materia. Es una tarea al alcance de muy pocas personas el revisarlos todos. Por ello es preciso destacar las referencias citadas en el último párrafo del apartado 3.1 y las referencias contenidas en ellos, que aunque no los revisan absolutamente todos, sí hacen un esfuerzo por abarcar de manera exhaustiva el conjunto de trabajos para desarrollar elementos finitos de lámina. Esta diversidad de elementos pone de manifiesto la dificultad de alcanzar una solución que cierre el problema. El elemento BEST tampoco lo consigue, pero representa un nuevo elemento en la familia de los elementos finitos de lámina, y en particular en la de los elementos finitos de lámina delgada sin rotaciones que resuelve algunas de sus deficiencias.*

*El elemento BEST trata de resolver el problema de*

The BEST element tackles the problem of rotation-free shell elements' precision dependency with respect to mesh distortion. Gärdsback and Tibert explain in [49] that those rotation-free shell elements which compute curvature as a 2D tensor, achieve better consistency in their accuracy with respect to irregular meshes than rotation-free shell elements which consider the curvature of the surface as a superposition of unidimensional curvatures. Accordingly, the BEST element adopts the approach of defining the curvature as a 2D tensor (see equation (4.6) where this approach is clearly shown; and equation (6.65) where the pseudo-deformation associated to bending is represented in Voigt notation taking advantage of the symmetry of the tensor).

There is another aspect that improves the precision of the rotation-free shell elements, regarding the computation of curvature, with respect to the mesh used. Oñate and Zárate explain in [96] that the BSN element achieves better accuracy than the BST element. The difference between the nodal implementation (BSN) and the elemental implementation (BST) consists in using all the connectivities surrounding each node for the former, or just the adjacent triangles for the latter. Cirak, Ortiz et al. [24–26] propose the subdivision surfaces paradigm to also take advantage of all the connectivities of the nodes of the triangle situated in a regular patch. Likewise, the BEST element takes advantage of all the nodes' connectivities in each triangle of the mesh (see figure 4.2). In order to avoid the restriction of having to use regular meshes of triangles, the BEST element performs an intermediate step calculating the normal vectors at the nodes, and thus condensing the information of the triangles surrounding each node.

BEST is therefore a new rotation-free thin shell finite element developed as a continuum-based finite element, which uses a *total Lagrangian* formulation for the resolution of the non-linear problem. The BEST element solves correctly thin shell problems under the Kirchhoff-Love hypothesis, although it suffers from membrane locking, which becomes more severe as the shell becomes thinner (see chapter 11). The name of the BEST element is obtained as the acronym of *Bézier-Enhanced Shell Triangle*.

*la dependencia de la precisión de los elementos de lámina sin rotaciones con respecto a la distorsión de la malla. En [49] Gärdsback y Tibert explican que los elementos de lámina sin rotaciones que calculan la curvatura como un tensor 2D obtienen mayor robustez respecto a mallas irregulares que los elementos de lámina sin rotaciones que contemplan la curvatura de la superficie como una superposición de curvaturas unidimensionales. En este sentido, el elemento BEST adopta el planteamiento de definir la curvatura como un tensor 2D (véase la ecuación* (4.6) *donde se muestra claramente este planteamiento; y la ecuación* (6.65) *donde se describe la pseudo-deformación asociada a la flexión en notación de Voigt aprovechando la simetría del tensor).*

*Además, existe otro aspecto que mejora la precisión de los elementos de lámina sin rotaciones, en lo que respecta al cálculo de la curvatura, en relación con la malla usada. En [96] Oñate y Zárate explican que el elemento BSN alcanza mejor precisión que el elemento BST. La diferencia entre la implementación nodal (BSN) y la implementación elemental (BST) consiste en usar todas las conectividades alrededor de cada nodo en el primer caso, o solamente los triángulos adyacentes en el segundo caso. Cirak, Ortiz et al. [24-26] proponen el paradigma de las superficies subdivididas mediante el que también aprovechan todas las conectividades de los nodos del triángulo situado en una parcela regular. El elemento BEST hace lo propio, y también aprovecha todas las conectividades de los nodos de cada triángulo de la malla (ver la figura 4.2). Para evitar la restricción de usar mallas regulares de triángulos, en el elemento BEST se realiza el paso intermedio de calcular los vectores normales en los nodos, condensando así la información de los triángulos que rodean cada nodo.*

*Por lo tanto, BEST es un nuevo elemento finito de lámina delgada sin rotaciones desarrollado como un elemento basado en el continuo, y que utiliza una formulación* Lagrangiana total *para la resolución del problema no-lineal. El elemento BEST resuelve correctamente problemas de lámina delgada bajo las hipótesis de Kirchhoff-Love, aunque adolece de bloqueo por membrana que se acentúa a medida que la lámina se hace más y más delgada (ver capítulo 11). El nombre del elemento BEST resulta del acrónimo de* lámina triangular mejorada con Bézier *(en inglés).*

### 13.1.2 Optimal estimation of the surface normal from a faceted mesh

A key development aspect of the BEST element is the precise approximation of the surface normals at the nodes. Being an intermediate step in the calculations, I was particularly worried about carrying errors on to the construction of the element. Therefore, I wanted to make sure I could minimize the error incurred in the estimation of the surface normal at the node, when condensing the information of the triangles surrounding each node.

For this reason I have created a framework to reinterpret each triangle's normal vector meaning, in a mesh of triangles. In this framework I have considered that a quadric is a second order approximation to a smooth surface. And that the triangles of the mesh represent planar sections of that quadric surface. Therefore, each triangle's normal vector represents a normal vector of the surface to the same extent as the section of the quadric represented by the triangle represents the point of interest in the surface. Along with Estruch and García-Espinosa, in [129] I have developed this framework and I have justified the use of different metrics as averaging weights of the triangles' normal vectors, for the estimation of the surface's normal direction at each node of the mesh.

Ubach, Estruch and García-Espinosa performed a comprehensive statistical comparison of different weighting factors including other weights previously used in the literature. The conclusion of that work is that the inverse of the area of the circumscribed circle to the triangle and the internal angle of the triangle at the node considered should be used as weighting factor (see equations (5.2) and (5.3) in section 5.1). This result is an original contribution of the cited paper, but it is also an integral part of this thesis' research. Using this new weighting factor, we reduce by about 10% the root mean square error in the estimation of normals of randomly generated surfaces with respect to the previous best weighting factor found in the literature and proposed by Max [77] (see [129, Table I]).

### *Estimación óptima de la normal a una superficie a partir de una malla de triángulos*

*Un aspecto clave del desarrollo del elemento BEST es la estimación precisa de las normales a la superficie en los nodos. Al ser un paso intermedio del cálculo, me preocupaba especialmente que cualquier imprecisión se propagase a la subsiguiente construcción del elemento. Por consiguiente, he querido asegurarme de minimizar el error incurrido al condensar la información de los triángulos que rodean cada nodo, para estimar el vector normal a la superficie en el nodo.*

*Por ese motivo he desarrollado un marco teórico para reinterpretar el significado de los vectores normales de cada triángulo de una malla de triángulos. En este marco teórico, he considerado que una cuádrica es una aproximación de segundo orden a una superficie suave. Y que los triángulos de la malla representan secciones planas de dicha superficie cuádrica. Por consiguiente, el vector normal de cada triángulo de la malla es representativo de un vector normal a la superficie, en la medida que la sección representada por el triángulo es representativa del punto de la superficie que se quiere aproximar. Junto con Estruch y García-Espinosa, en [129] he desarrollado dicho marco teórico y he justificado el uso de distintas medidas para ponderar las normales de los triángulos de la malla, para estimar la dirección de la normal en cada nodo de la malla.*

*Ubach, Estruch y García-Espinosa realizaron una comparación estadística exhaustiva de distintos factores de ponderación, incluyendo otros usados previamente en la literatura. La conclusión de dicho trabajo conduce a usar como factor de ponderación para calcular una media de los vectores normales de los triángulos: el inverso del área de la circunferencia circunscrita al triángulo y el ángulo interno del triángulo en el nodo considerado (ver ecuaciones* (5.2) *y* (5.3) *en el apartado 5.1). Este resultado es una aportación original del artículo citado, pero forma parte integral del trabajo de investigación de esta tesis. Usando este nuevo factor de ponderación, se reduce en aproximadamente un 10 % el error medio cuadrático cometido en la estimación de las normales de superficies generadas aleatoriamente, respecto del mejor factor de ponderación usado previamente en la literatura y propuesto por Max [77] (ver [129, Tabla I]).*

### 13.1.3 New paradigm to reconstruct a cubic shell element using the neighboring elements

The BEST element takes advantage of the surface's geometric information provided by the triangles around each of the mesh nodes. With this information it builds cubic geometries starting from a mesh of flat triangles. To accomplish it, approximated surface normals are computed at each node of the triangle using the information of the neighboring triangles. The computation of the normal vectors at the nodes doesn't depend on the number of triangles surrounding each node of the mesh. Unlike the subdivision surfaces paradigm by Cirak, Ortiz et al., the BEST element is independent from the mesh topology.

Using the information of the normal vectors at the nodes, I have developed a new paradigm consisting on reconstructing the geometry of a cubic triangular element exploiting the properties of cubic B-spline functions (cubic Bézier triangle). This way, I build a conforming shell finite element which overcomes the unsatisfactory result presented in section 4.3. This approach is an original contribution of this thesis.

The construction of the cubic Bézier triangle requires fixing 30 parameters. Therefore it needs to apply 30 independent conditions. 15 of these conditions are given directly by the positions of the 3 vertices of the triangle and the orientations of the normal vectors at the 3 vertices (see figure 5.5). These 15 conditions ensure that the triangles maintain $\mathcal{C}^1$ continuity at the vertices.

6 of the remaining 15 conditions are obtained using criteria of internal energy minimization of the element. I have deduced these internal energy minimization criteria of the element by solving reduced problems on the geometric construction of the Bézier triangle (see the sections 5.4, 9.3 and 9.4).

In order to avoid the definition of an ill-conditioned system of equations (or even incompatible) for finding the position of the element's central control point, I have opted for a solution of the 3 coordinates of the central control point by averaging three approximate estimations; see the equations (5.17) to (5.19). Each of these three approximated estimations is defined by extending the concepts of minimization of the deformation

### *Nuevo paradigma de reconstrucción de un elemento cúbico usando la información de los elementos vecinos*

*El elemento BEST aprovecha la información sobre la geometría de la superficie facilitada por los triángulos que rodean cada uno de los triángulos de la malla. Con esta información genera geometrías cúbicas a partir de una malla de triángulos planos. Para conseguirlo, se calcula una aproximación del vector normal a la superficie en cada uno de los nodos del triángulo a partir de la información de los triángulos que rodean cada nodo. El cálculo de los vectores normales en los nodos no depende del número de triángulos que rodean cada nodo de la malla. De esta manera el elemento BEST es independiente de la topología de la malla, a diferencia del paradigma de las superficies subdivididas desarrollado por Cirak, Ortiz et al.*

*A partir de la información de los vectores normales en los nodos he desarrollado un nuevo paradigma que consiste en reconstruir la geometría de un elemento triangular cúbico usando funciones cúbicas B-spline (triángulo cúbico de Bézier). De esta manera construyo un elemento finito de lámina que es conforme y que sortea el resultado insatisfactorio presentado en el apartado 4.3. Este planteamiento es una contribución original de la presente tesis.*

*La construcción del triángulo cúbico de Bézier requiere determinar 30 parámetros. Para ello es necesario aplicar 30 condiciones independientes. 15 de estas condiciones se deducen de manera directa de la posición de los 3 vértices del triángulo y de las orientaciones de los vectores normales en los 3 vértices (ver la figura 5.5). Con estas 15 condiciones se asegura que los triángulos mantienen continuidad $\mathcal{C}^1$ en los vértices.*

*De las otras 15 condiciones que quedan por imponer, 6 de ellas las obtengo a partir de criterios de minimización de la energía interna de deformación del elemento. Estos criterios de minimización de la energía interna del elemento los deduzco a base de solucionar problemas reducidos de la construcción geométrica del triángulo de Bézier (ver los apartados 5.4, 9.3 y 9.4).*

*Para evitar el planteamiento de un sistema de ecuaciones mal condicionado (o incluso incompatible) en la determinación del punto de control central del elemento, he optado por una solución de las 3 coordenadas del punto de control central promediando tres estimaciones aproximadas; ver las ecuaciones* (5.17)

energy by taking the barycenter of the six intermediate control points as a reference, and using the goal of approaching $\mathcal{C}^1$ continuity across the elements along the edges (see figure 5.6).

The 6 remaining conditions are obtained from the drilling rotations for each of the edges that converge on each node (see section 9.2). The results obtained in this thesis finally lead to establish the value of the drilling rotation as 0 in equation (9.34). But I propose as future work the modification of the element to establish drilling rotations different than 0 based on the description of the in-plane shear deformation —on the plane tangent to the surface at each node— consistently with the theory of deformation of the continuum (see section 9.5.2).

Built in this manner, the only variables of the BEST element are the vertices positions (9 variables). And it solves internally the remaining parameters corresponding to the geometric definition (21 parameters). 13 of these parameters are determined based on geometric considerations, strictly speaking: 6 out of the normal orientations at the vertices, 6 out of the drilling rotations at the vertices and 1 out of the central control point elevation with respect to the barycenter. Whereas the other 8 parameters are determined based on mechanic energy minimization considerations: 6 $\Psi$ values and the 2 coordinates which define the position of the barycenter. In order to fix the values of these 21 internal parameters, each BEST element needs to solve 9 systems of linear equations of rank 3.

Taking all this into account, the BEST element can also be understood as a reduced order cubic shell element; for which the 30 variables of the cubic element have been condensed into just 9. This represents a new paradigm in which the model is not order-reduced as a whole, but through the order-reduction of each of the model's elements.

### 13.1.4 Successful element construction based on energy minimization principles

An original aspect of this thesis consists on the geometric definition of the cubic Bézier triangle

*a* (5.19). *Cada una de las tres estimaciones aproximadas está definida también extendiendo los conceptos de minimización de la energía de deformación tomando como referencia el baricentro de los seis puntos de control intermedios del perímetro, y partiendo del objetivo de que los elementos aproximen la continuidad $\mathcal{C}^1$ a lo largo de las aristas (ver la figura 5.6).*

*Las 6 condiciones restantes las obtengo de las rotaciones de taladro para cada una de las aristas que convergen en cada nodo (ver el apartado 9.2). Los resultados obtenidos en esta tesis finalmente establecen el valor de las rotaciones de taladro en 0 en la ecuación* (9.34)*. Pero propongo para un trabajo futuro la modificación del elemento para poder establecer rotaciones de taladro distintas de 0 basadas en la descripción de la deformación de cortante en el plano —según el plano tangente a la superficie en cada nodo— de manera consistente con la teoría de la deformación del continuo (véase el apartado 9.5.2).*

*El elemento BEST construido de esta manera mantiene únicamente como incógnitas las posiciones de los vértices (9 variables). Y resuelve internamente los parámetros correspondientes al resto de la definición geométrica (21 parámetros). 13 de estos parámetros quedan determinados en base a consideraciones estrictamente geométricas: 6 de las orientaciones de las normales en los vértices, 6 de las rotaciones de taladro en los vértices y 1 de la elevación del punto de control central respecto del baricentro. Mientras que los 8 parámetros restantes se determinan a partir de consideraciones de minimización de la energía mecánica del elemento: 6 valores de $\Psi$ y las 2 coordenadas que definen la posición del baricentro. La determinación de estos 21 parámetros internos del elemento implica la resolución de 9 sistemas de ecuaciones lineales de rango 3 para cada elemento BEST.*

*Por todo ello también se puede reinterpretar el elemento BEST como un elemento de lámina cúbico de orden reducido, en el que se han condensado las 30 variables del elemento cúbico en únicamente 9. Esto representa un nuevo paradigma en el que no se reduce el orden del modelo en su conjunto sino a través de la reducción de cada uno de los elementos del modelo.*

### *Reconstrucción exitosa del elemento basada en principios de minimización de la energía*

*Un aspecto original de esta tesis consiste en la definición geométrica del triángulo cúbico de Bézier, com-*

combining, geometric information from the mesh and energy minimization considerations. I drew the conclusion that it is necessary to introduce energy considerations in the geometric construction of the element when I tried to solve examples in the non-linear regime. Before that, faced with the under-determination of the 30 necessary parameters to define the element's geometry, I felt compelled to make some arbitrary but plausible choices. The most determining of them was assuming that the value of the $\Psi$ parameter was equal to $\frac{1}{3}$ (see section 5.4). When I realized that if I used this fixed value for $\Psi$, the element was not well-posed —and reaching this conclusion by pondering on an internal energy disequilibrium— I became convinced that I would find the solution to the ill-posedness of the element by introducing energy minimization considerations in the element's geometric construction.

These energy minimization aspects are focused on the parametrization of the Bézier cubic triangle's surface construction. This way I establish a relationship between the parametric definition of the Bézier triangle's surface —which is governed by the position of the control points— and the element's internal deformation energy. Since the resolution of a mechanic problem using the finite element method, implies in essence the resolution of an energy minimization problem with respect to the problem's variables; and since in the paradigm of the BEST element, the internal control points' positions do not belong to the set of the problem's variables, then: the determination of the control points' positions was being put aside from the resolution of the overall mechanic energy minimization problem. Therefore, I have defined a set of reduced problems in order to determine the value of the element's internal parameters depending on energy considerations and which are sufficiently representative and general in order to avoid the need to solve their values globally; not even for the element as a whole. More specifically, I have defined 3 different reduced problems for the 3 different shell deformation modes:

1. Reduced problem for the bending deformation, or curvature variation (see the section titled Bending energy on page 57).
2. Reduced problem for the membrane defor-

*binando información geométrica de la malla y consideraciones de minimización de la energía. Llegué a la conclusión de que era necesario introducir consideraciones de índole energética en la construcción geométrica del elemento, al intentar resolver ejemplos en régimen no-lineal. Previamente, ante la infradeterminación de los 30 parámetros necesarios para definir la geometría del elemento, me vi impulsado a tomar decisiones arbitrarias pero plausibles. La más determinante inicialmente fue suponer que el valor del parámetro $\Psi$ era igual a $\frac{1}{3}$ (ver el apartado 5.4). Al comprobar que con este valor fijo de $\Psi$, el elemento resultaba mal planteado —y al llegar a esta conclusión por un razonamiento de desequilibrio de la energía interna— decidí que la solución al mal planteamiento del elemento la tenía que obtener introduciendo aspectos de minimización de la energía en la construcción geométrica del elemento.*

*Estos aspectos de minimización de la energía se concretan en este caso en la parametrización de la construcción de la superficie del triángulo cúbico de Bézier. De modo que establezco una relación entre la definición paramétrica de la superficie del triángulo de Bézier —que depende de la posición de los puntos de control— y la energía interna de deformación del elemento. Como al resolver un problema mecánico por el método de los elementos finitos, en el fondo estoy resolviendo un problema de minimización de la energía con respecto a las variables del problema; y como en el paradigma del elemento BEST las posiciones de los puntos de control interiores del triángulo no forman parte de las variables del problema: la determinación de las posiciones de los puntos de control estaba quedando al margen de la solución del problema de minimización de la energía mecánica de todo el modelo. Por consiguiente he desarrollado un conjunto de problemas reducidos para poder determinar el valor de los parámetros internos del elemento que dependen de consideraciones energéticas y que son lo suficientemente representativos y generales para no tener que resolver sus valores de manera global; ni siquiera a nivel de todo el elemento. Concretamente he planteado 3 problemas reducidos para los 3 modos de deformación de la lámina:*

1. *Problema reducido de la deformación de flexión, o variación de la curvatura (ver el apartado Bending energy en la página 57).*
2. *Problema reducido de la deformación de membrana, o extensión en el plano (ver el apartado*

mation, or in-plane extension (see the section titled Axial (membrane) energy on page 59).

3. Reduced problem for the in-plane shear deformation, or drilling rotation (see the section titled Energy minimization for the in-plane shear deformation mode on page 106).

The solution to the first reduced problem yields a result that approximates very well the solution of the second reduced problem (see figure 5.9). However, the third reduced problem yields a different result from the first two (see figure 9.7). I have solved the disagreement between the two solutions by averaging them with weights following equation (9.10).

The second and third reduced problems include implicitly the hypothesis of linear elastic material (see equation (5.25) and figure 9.8). The third reduced problem also includes implicitly the hypothesis of isotropic material (see figure 9.5). Moreover, the weighted average between the solutions of the first and third reduced problems also implies the hypothesis of linear elastic material. It's easy to change the weighting factor in equation (9.10) for non-linear materials. In the case of anisotropic and/or non-linear materials it would be advisable to check whether the hypothesis on the elastic properties of the material, introduced implicitly, affect too negatively the results.

By implementing the solutions of these reduced problems, I have successfully applied the BEST element to the analysis of thin shells in linear and geometrically non-linear regimes using an implicit method (see figure 11.22).

### 13.1.5 Cubic convergence using linear information

I had serious doubts about the element's order of convergence because the approach to develop the BEST element is non-orthodox (see chapter 8). And this cause of concern was certainly justified, because there are cases in which convergence is not even linear (specially when the element suffers from membrane locking), but there are also cases where convergence is linear (see figure 11.1b), other cases in which the convergence is quadratic (see figures 11.6c and 11.10a),

*Axial (membrane) energy en la página 59).*

3. *Problema reducido de la deformación de cortante en el plano, o rotación de taladro (ver el apartado Energy minimization for the in-plane shear deformation mode en la página 106).*

*La solución del primer problema reducido genera un resultado muy aproximado al de la solución del segundo problema reducido (ver la figura 5.9). En cambio la solución del tercer problema reducido genera un resultado distinto a los dos primeros (ver la figura 9.7). He resuelto la discrepancia entre ambas soluciones realizando una media ponderada de las dos soluciones según la ecuación* (9.10)*.*

*El segundo y tercer problema reducidos contienen de manera implícita la hipótesis de que el material es elástico lineal (ver ecuación* (5.25) *y figura 9.8). Adicionalmente, el tercer problema reducido también incluye de manera implícita la hipótesis de material isótropo (ver la figura 9.5). Y además, la ponderación entre las soluciones del primero y tercer problemas reducidos también contiene de manera implícita la hipótesis de que el material es elástico lineal. Es fácil cambiar la ponderación de la ecuación* (9.10) *para materiales no-lineales. Sería conveniente comprobar si las hipótesis incluidas de manera implícita sobre las propiedades elásticas del material, influyen de manera excesivamente negativa para el caso de materiales anisótropos y/o no-lineales.*

*Con la implementación de las soluciones a estos problemas reducidos, he conseguido aplicar con éxito el elemento BEST al cálculo de láminas delgadas en régimen lineal y geométricamente no-lineal con un método implícito (ver la figura 11.22).*

### *Convergencia cúbica usando información lineal*

*Al adoptar un enfoque no ortodoxo para el desarrollo del elemento BEST, tenía serias dudas sobre el orden de convergencia del elemento (ver el capítulo 8). Y esta preocupación estaba ciertamente justificada, ya que hay casos en los que ni siquiera se obtiene convergencia lineal (especialmente cuando el elemento sufre por bloqueo de membrana), pero también hay casos en los que se obtiene convergencia lineal (ver la figura 11.1b), otros en los que se obtiene convergencia cuadrática (ver las figuras 11.6c y 11.10a), e incluso he*

and I have even obtained a result with cubic convergence (see figure 8.4).

This last result shows that the BEST element has the potential to achieve cubic convergence. But at the same time, the fact that this order of convergence depends on the value given to the drilling rotations, and that with the value finally used in this particular case (Cylinder under internal pressure) I have only achieved quadratic convergence, casts doubts on the possibility of reproducing this result for a wide range of problems.

I have also demonstrated that for in-plane shear dominated problems, the formulation used in this thesis only achieves linear convergence.

This thesis does not tackle the issue of the computational cost-benefit analysis of the BEST element compared to other classical elements. That is, whether the precision improvement provided by a quadratic or cubic order of convergence, compensates the extra cost added by the resolution of the systems of linear equations of rank 3 for the element's cubic geometric reconstruction. Besides, the cost-benefit analysis should also take into account that the resolution of the global system of equations is not equivalent to that of a linear element —despite the total number of variables is equivalent to that of a linear element—. In the BEST element, the global system's bandwidth is larger than those of other linear rotation-free shell elements; because, as I have said earlier, more connectivities from neighboring elements are used.

Be as it may, I have demonstrated numerically for different problems, that the BEST element achieves a better-than-linear order of convergence (quadratic or cubic). This is a very relevant result, because it means a potential advantage of the paradigm developed in this thesis.

*obtenido un resultado con convergencia cúbica (ver la figura 8.4).*

*Este último resultado demuestra que el elemento BEST tiene potencial para alcanzar convergencia cúbica. Pero al mismo tiempo, el hecho de que este orden de convergencia dependa del valor de las rotaciones de taladro, y que con el valor adoptado finalmente en este caso concreto solo se haya conseguido convergencia cuadrática hace que existan dudas sobre la posibilidad de reproducir de manera consistente este resultado para un amplio rango de problemas.*

*También se ha demostrado que para problemas dominados por la deformación de cortante en el plano, la formulación utilizada en esta tesis solo alcanza convergencia lineal.*

*En esta tesis no se ha abordado el análisis de coste-beneficio computacional del elemento BEST respecto a elementos clásicos. Es decir, si el coste añadido que supone la resolución de los sistemas lineales de ecuaciones de rango 3 para la reconstrucción de la geometría cúbica del elemento BEST, queda compensado por la mejora de precisión que representa una convergencia de orden cuadrático o cúbico. Por otro lado, también se tendría que tener en cuenta que el coste de resolución del sistema de ecuaciones global no es equivalente al de un elemento lineal —aunque el número total de variables sí sea equivalente al de un elemento lineal— ya que en el elemento BEST el ancho de banda del sistema global está ampliado con respecto a otros elementos de lámina sin rotaciones lineales, dado que como he explicado anteriormente, se usan más conectividades de elementos vecinos.*

*Sea como fuere, se ha demostrado numéricamente que para distintos problemas el elemento BEST alcanza un orden de convergencia más-que-lineal (cuadrático o cúbico). Este es un resultado muy relevante, porque representa una ventaja potencial del paradigma desarrollado en esta tesis.*

### 13.1.6 Efficient and geometrically accurate through-the-thickness pre-integration

### *Preintegración en el espesor eficiente y con precisión geométrica*

This is without doubt the most difficult conclusion to write down. It strikes me that Stanley proposed the through-the-thickness pre-integration for continuum-based shell elements using an *Updated Lagrangian* formulation, to reduce the computational cost in the building of the shell elements, back in 1985; and since then, this solution has not been yet applied for a *Total La-*

*Esta es seguramente la conclusión más difícil de redactar. Me resulta sorprendente que en 1985 Stanley propusiera la preintegración en el espesor para elementos de lámina basados en el continuo con formulación* Lagrangiana actualizada*, para economizar el coste computacional de la construcción de los elementos de lámina; y que desde entonces no se haya aplicado esta misma solución para una formulación*

*grangian* formulation. Citing Stanley [120, REMARK 3.4]: "It appears [to him] that harsher assumptions would be required to achieve the same thickness-decoupling effect with a *Total Lagrange* description (. . . ) due to the explicit non-linearity thereby engendered."

Actually, the problem doesn't lie in the non-linearity associated with a *Total Lagrangian* formulation, but in the simplifications that Stanley [120, p. 34] and many other scholars [9, pp. 545–549] apply, in the *Updated Lagrangian* formulation, when they linearize the rotation-associated displacements of the fiber perpendicular to the shell's midsurface. Because, on the one hand, using identical hypothesis —on what relates to the thickness decoupling— to those used by Stanley, I have also accomplished the thickness decoupling result; including all the higher order terms of the deformation description. And, on the other hand, the *Updated Lagrangian* and *Total Lagrangian* formulations are equivalent. Different scholars that use the *Updated Lagrangian* formulation for non-linear problems, prefer it because by updating the configuration at each time-step or load-step of the non-linear resolution process, the error incurred by discarding the higher order terms of the linearization of the equations is limited. Whereas in the *Total Lagrangian* formulation this error would add-up; particularly the one associated to large rotations.

Therefore, I am stricken by not having found in all the bibliography reviewed (which is broader than the cited bibliography) any references of the thickness decoupling and through-the-thickness pre-integration of the description of the deformation and Jacobian expressions without applying further simplifications, for shell elements with *Total Lagrangian* formulation. This thickness decoupling and through-the-thickness pre-integration are also a novelty for thin shell rotation-free elements.

Stanley [120] already described how the continuum-based shell elements benefited from the advantages associated with this thickness decoupling and through-the-thickness pre-integration. The through-the-thickness pre-integration grants to make the technology of continuum-based shell elements competitive in cost with the resultant-based shell elements or the elements based on shell theories; while keep-

Lagrangiana total. *Como dice el propio Stanley [120, REMARK 3.4]: a su entender "serían necesarias hipótesis más severas [que las que Stanley utiliza] para lograr el mismo efecto de desacoplamiento en el espesor con una descripción* Lagrangiana total *(. . . ) debido a la no-linealidad explícita que se engendraría."*

*En realidad el problema no subyace en la no-linealidad que conlleva la formulación* Lagrangiana total*, sino en las simplificaciones que Stanley [120, p. 34] y numerosos otros autores [9, pp. 545–549] aplican en la formulación* Lagrangiana actualizada *al linealizar los desplazamientos asociados a las rotaciones de la fibra perpendicular a la superficie media de la lámina. Ya que, por un lado, con hipótesis idénticas —a efectos del desacoplamiento en el espesor— a las que usa Stanley, yo también he logrado el efecto de desacoplamiento en el espesor; incluyendo todos los términos de alto orden de la descripción de la deformación. Y por el otro lado las formulaciones* Lagrangiana actualizada *y* Lagrangiana total *son equivalentes. Los distintos autores que usan la formulación* Lagrangiana actualizada *para problemas no-lineales la prefieren porque al actualizar la configuración en cada paso de tiempo o incremento de carga de la resolución del problema no-lineal, se limita el error que se comete al descartar los términos de alto orden que se desprecian al linealizar las ecuaciones. Mientras que en la formulación* Lagrangiana total *ese error se acumularía; en particular el relacionado con las grandes rotaciones.*

*Así pues, estoy sorprendido de no haber encontrado referencias en la bibliografía revisada (que es más extensa que la citada) del desacoplamiento y pre-integración en el espesor de los términos de la descripción de la deformación y del jacobiano sin aplicar simplificaciones adicionales para elementos de lámina con formulación* Lagrangiana total*. Este desacoplamiento y pre-integración en el espesor también son una novedad para los elementos de lámina delgada sin rotaciones.*

*Stanley [120] ya describía las ventajas que conllevan este desacoplamiento y pre-integración en el espesor para los elementos de lámina basados en el continuo. Y es que lo que permite esta preintegración en el espesor, es hacer que la tecnología de elementos de lámina basados en el continuo sea equivalente en coste a los elementos basados en resultantes o en teorías de lámina; al tiempo que se conserva toda la potencia conceptual y formal de los elementos basados en el continuo. Sin embargo, en la formulación* Lagrangiana ac-

ing all the conceptual and formal power of the continuum-based shell elements. However, in the *Updated Lagrangian* formulation there is still the need to reevaluate the through-the-thickness integrals at each time-step or load-step, that is: for each configuration update. Whereas in the *Total Lagrangian* formulation, the through-the-thickness integrals are evaluated just once: at the reference configuration. The cost of the through-the-thickness integrals after decoupling the thickness terms is relatively cheap. There are just 14 scalar integrals to perform for each Gauss point. Therefore the difference in computational cost between the *Total Lagrangian* and the *Updated Lagrangian* formulations can be evaluated for each time-step or load-step. Anyway, the conceptual advantage is significant.

In the development of the present thesis I have decomposed the pseudo-deformation tensor —$g$— and the matrix of change of coordinates from local of the material to parametric of the element —$\boldsymbol{A}$ in tensor notation and $\boldsymbol{Q}$ in Voigt notation— (a concept similar to the *shifter* used by other scholars but not exactly equal), into three components depending on the exponent {0,1,2} affecting the thickness coordinate $\zeta$ present in the numerator of the equations (6.48), (6.59) and (6.63) on pages 71–73. The deformation tensor has been decomposed into the: membrane, bending and non-linear terms. The matrix of change of coordinates has been decomposed into the constant and linear terms —for $\boldsymbol{A}$— and into the: constant, linear and quadratic terms —for $\boldsymbol{Q}$. This way, the equations (7.3) and (7.4) on page 78 are transformed into the expressions of equations (7.32) and (7.33) and equations (7.34) and (7.35) on page 83; where the thickness integrals are turned into the scalar integrals shown in equations (7.36) to (7.47) on pages 83–84.

To sum up this section, I conclude that it is possible to perform a decomposition of the description of the deformation terms and the matrices of change of coordinates, that grants an efficient and geometrically accurate through-the-thickness pre-integration. This conclusion is equivalent to that provided by Stanley [120]. However, unlike Stanley, in this case I have been able to apply this through-the-thickness pre-integration for a *Total Lagrangian* formulation. The development of a rotation-free shell tualizada *todavía es preciso reevaluar las integrales en el espesor en cada paso de tiempo o incremento de carga, es decir: en cada actualización de la configuración; mientras que para la formulación* Lagrangiana total *sólo es necesario evaluar las integrales en el espesor una sola vez: para la configuración de referencia. Es verdad que tal y como se ha explicado en la página 85, las integrales en el espesor se han reducido a 14 integrales distintas para cada punto de Gauss, con lo que su coste computacional no es significativo. Por consiguiente, se puede evaluar el incremento de coste computacional entre las formulaciones* Lagrangiana total *y* Lagrangiana actualizada *para cada paso de tiempo o paso de carga. En cualquier caso, el avance conceptual es notable.*

*En el desarrollo realizado se han descompuesto el tensor de pseudo-deformaciones —$g$— y la matriz de cambio de coordenadas de locales del material a paramétricas del elemento —$\boldsymbol{A}$ en notación tensorial y $\boldsymbol{Q}$ en notación de Voigt— (un concepto parecido al de* shifter *que se usa en la bibliografía pero que no es exactamente el mismo), en tres componentes en función del exponente {0,1,2} que afecta a la coordenada del espesor $\zeta$ presente en el numerador de las ecuaciones* (6.48)*,* (6.59) *y* (6.63) *en las páginas 71-73. En el caso del tensor de deformaciones, éste se ha descompuesto en la componente de membrana, de flexión y de los términos no-lineales. En el caso de la matriz de cambio de coordenadas, ésta se ha descompuesto en los términos constante en el espesor y lineal —para $\boldsymbol{A}$— y en los términos constante, lineal y cuadrático —para $\boldsymbol{Q}$. Con ello se consigue transformar las ecuaciones* (7.3) *y* (7.4) *en la página 78 en las expresiones de las ecuaciones* (7.32) *y* (7.33) *y las ecuaciones* (7.34) *y* (7.35) *en la página 83; donde las integrales en el espesor quedan condensadas en integrales de valores escalares en las expresiones de las ecuaciones* (7.36) *a* (7.47) *en las páginas 83-84.*

*Así pues, en este apartado concluyo que es posible realizar una descomposición de los términos de la descripción de la deformación y de las matrices de cambio de coordenadas que permite pre-integrar en el espesor del elemento de manera eficiente y geométricamente precisa. Esta conclusión es equivalente a la de Stanley [120]. Sin embargo, a diferencia de Stanley, en este caso he logrado aplicar esta pre-integración en el espesor para una formulación* Lagrangiana total*. El haber desarrollado un elemento de lámina sin rotaciones es un factor que sin duda ha contribuido a este resultado al no tener que tratar con la complejidad de*

element has certainly contributed to this result, by not having to deal with the complexity of the large rotations in the framework of a *Total Lagrangian* formulation.

## 13.2 Lessons learned

### 13.2.1 The quantum nature of research work

I have done this research thesis in parallel to other professional assignments. While many ordinary work tasks can be distributed linearly and interrupted almost whenever desired; on what concerns research, this practice is counterproductive. I reached this conclusion relatively early. And this is why I concentrated my efforts to work on the thesis during the summers (and specially during the months of August) in order to attain progresses. Because pursuing the knowledge frontier and pushing beyond it, requires a detailed understanding of the shadowy areas that remain away from the established knowledge lights. Transiting through these shadowy areas needs careful consideration from many points of view. This requires a very intense abstraction exercise that has to be sustained, until the problem at hand is fully comprehended. Interrupting this abstraction effort for long periods of time forces the researcher to retreat back to square one when the research work is resumed. That's the reason why I speak about the quantum nature of research work. A quantum work threshold is required in order to reach new knowledge grounds. The combination of smaller efforts that, taken individually, do not reach that quantum work threshold, will not lead to the achievement of the knowledge grounds being pursued; even if all of them combined exceeds largely that quantum threshold value.

### 13.2.2 I stand up for libraries

As I wrote at the introduction of this chapter: there's a lot of learning in a doctoral work. But this learning isn't necessarily ordered. There's a lot of self-learning. The researcher must find answers as he or she asks questions. The main source of knowledge to find those answers is the

*las grandes rotaciones en el marco de una formulación* Lagrangiana total.

## *Lecciones aprendidas*

### *La naturaleza cuántica del trabajo de investigación*

*He realizado el trabajo de investigación para esta tesis en paralelo a otros desempeños profesionales. Si bien el trabajo ordinario se puede linealizar e interrumpir prácticamente a voluntad en multitud de desempeños, en lo que concierne a la investigación, esto es contraproducente. Llegué a esta conclusión relativamente temprano. Y por ello concentré mis esfuerzos para trabajar en la tesis durante los meses de verano (y especialmente los meses de agosto) para conseguir avances. Porque franquear la frontera del conocimiento y empujarla más allá, requiere una comprensión detallada de las zonas de penumbra que no tienen la iluminación de los focos del conocimiento establecido. El tránsito por estas zonas de penumbra se necesita hacer desde multitud de puntos de vista, teniendo en cuenta multitud de consideraciones. Esto requiere un esfuerzo de abstracción muy intenso y que se tiene que mantener hasta que se alcanza la comprensión del problema que se está abordando en cada caso. La interrupción de dicho esfuerzo de abstracción por periodos de tiempo prolongados obliga inevitablemente a que el investigador regrese a la casilla de salida cuando retoma el trabajo de investigación. Por este motivo hablo de la naturaleza cuántica del trabajo de investigación. Para alcanzar nuevos niveles de conocimiento se requieren umbrales cuánticos de esfuerzo. La combinación de esfuerzos que individualmente no alcancen el umbral cuántico de esfuerzo necesario no conducirán a alcanzar el nivel de conocimiento perseguido; incluso si la suma de todos ellos supera con creces el valor de umbral cuántico.*

### *Rompo una lanza a favor de las bibliotecas*

*Como decía en la introducción de este capítulo: en el trabajo de doctorado hay mucho de aprendizaje. Pero este aprendizaje no es ordenado. Hay mucho de autoaprendizaje. El investigador o la investigadora tiene que encontrar respuestas a medida que se formula preguntas. Y la principal fuente para encontrar di-*

published scientific production.

The university libraries facilitate the mechanisms to search and access the published scientific production. And in doing so, they become an invaluable instrument for researchers; equally essential as a pen, paper or a computer. The advent of information technologies and the subscriptions that university libraries pay to scientific journal aggregators: facilitates the work of researchers, shortens the times to consult bibliographic references on the spot, and also reduce the interaction of the researcher with the physical infrastructure of the library. But there are still many resources which can only be consulted at the libraries' buildings and there are papers which can only be obtained by requesting them specifically. These circumstances require the library staff to intervene.

A substantial part of this thesis' research work takes place in the time frame of the economic crisis that unfolded in the year 2008. Universities haven't come out unscathed from this economic crisis, and have applied several budget cuts. One of such decisions made by the Polytechnic University of Catalonia has been to close the libraries during the summer vacations period. The decision made by the Polytechnic University of Catalonia to close its libraries during the summer vacations period has an impact on its own scientific output, because a non-academic period does not imply necessarily a non-working period; particularly for research. The opposite is true: the non-academic periods are the most productive for research. And to sustain this statement I refer to section 13.2.1. I have found myself in many occasions in need of consulting a given resource, that I haven't been able to request until the libraries reopened. This circumstance made me lose a window of opportunity to take full advantage of of that quantum work threshold I could invest during those months of August.

It's paramount, for a university that aspires to generate scientific output, to preserve its libraries open all year round. This is a statement of principles that no economic crisis should undermine. Because accepting without a protest the shutdown of libraries, is accepting the mutation of the very nature and mission of the Polytechnic University of Catalonia.

This thesis has largely benefited from the

*chas respuestas es la producción científica publicada.*

*Las bibliotecas universitarias que facilitan los mecanismos de búsqueda y acceso a la producción científica publicada, son un instrumento valiosísimo para los investigadores; e igual de imprescindible que el papel, el lápiz o el ordenador. Las tecnologías de la información y la suscripción que pagan las bibliotecas universitarias a los agregadores de revistas científicas: hacen posible el trabajo del investigador, acortan los tiempos necesarios para consultar referencias bibliográficas* al vuelo *y reducen también la interacción del investigador con la infraestructura física de la biblioteca. Pero todavía hay recursos que sólo se pueden consultar en los edificios de las bibliotecas y hay artículos que sólo se pueden obtener solicitándolos expresamente; cosa que requiere la intervención de personal de la biblioteca.*

*Buena parte del trabajo de investigación de esta tesis se enmarca en el marco temporal de la crisis económica que estalló en el año 2008. Las universidades no han quedado indemnes de esta crisis económica y han aplicado una serie de ajustes en sus presupuestos. Una de las decisiones que ha tomado la Universitat Politècnica de Catalunya ha sido el cierre de las bibliotecas durante el periodo no lectivo de verano. La decisión de la Universitat Politècnica de Catalunya de cerrar sus bibliotecas durante los periodos no-lectivos de verano es una decisión con impacto sobre la producción científica de la propia universidad. Porque un periodo no-lectivo no implica que sea no hábil para la investigación. Lo contrario en cambio es cierto: los periodos no-lectivos en la universidad son los más productivos para la investigación. Y para sostener esta afirmación me remito al apartado 13.2.1. Me he encontrado en más de una ocasión con la necesidad de consultar un recurso que no he podido solicitar hasta la reapertura de la biblioteca. Perdiendo así una ventana de oportunidad para aprovechar al máximo ese umbral de esfuerzo cuántico de que disponía durante el mes de agosto.*

*Es fundamental que una universidad que aspira a generar producción científica mantenga abiertas sus bibliotecas durante todo el año. Ello es una declaración de principios que ninguna crisis económica puede perturbar. Porque aceptar sin rechistar el cierre de las bibliotecas, es aceptar la mutación de la naturaleza misma y razón de ser de la Universitat Politècnica de Catalunya.*

*Esta tesis se ha beneficiado en gran medida de los trabajos de muchos otros científicos que han publica-*

work of many other scientists that have published their results. And it would have been impossible to achieve the results included in this thesis, along with the clear and concise explanations within, without the possibility for the author to consult the references cited in the bibliography. Nevertheless, not all the references included in this thesis have been obtained using the libraries' services. Some of them have been downloaded from the internet. And I haven't been able to check at all a few of the references included; but they are included because of the relevance of the contribution they provide, and whose results have perpetuated over time to the credit of their authors. Therefore, it is necessary to continue strengthening the libraries' resources to guarantee the access to published knowledge by the research community.

*do su trabajo. Y hubiera sido imposible alcanzar los resultados que aquí se incluyen, junto con sus explicaciones claras y concisas, sin que el autor hubiera podido consultar las referencias que se indican. Aún así, no todas las referencias incluidas en esta tesis se han obtenido por la vía de la biblioteca. Algunas las he descargado de internet. Y algunas de las referencias incluidas ni siquiera las he podido consultar. Pero están referenciadas por la relevancia de la contribución que contenían esas publicaciones y cuyos resultados se han perpetuado a lo largo del tiempo para acreditar a los autores. Así pues, es necesario seguir reforzando los recursos de las bibliotecas para asegurar el acceso al conocimiento publicado por parte de la comunidad científica.*

### 13.2.3 Goals vs Objectives

### *Metas vs Objetivos*

The third profound lesson learned in this thesis is that goals and objectives shall not be confused. That is, the objectives stated in chapter 2 must be understood as goals. The goals shall serve to keep in mind which is the direction in which I want to progress, and why. But the objectives are measurable advances in the path towards those goals. In this sense, my thesis advisor proposed me in a clear way the objective for a thesis (my thesis): "can you improve the performance of the EBST [41] element?"

I have mixed the objective stated by my thesis advisor with my motivations. And this has led me to lose the focus on the objective. This has also been the result of having perceived some overoptimism regarding my research abilities. This distraction between goals and objectives (also induced by the burdens of research projects that finance research) has somewhat distracted me from my endeavor to achieve the objective.

If I had more firmly held the focus of my research work towards achieving the objective, I would have probably noticed earlier the need to take notice of the membrane locking issues in shell elements. This is an aspect of the shell finite elements technology I ignored in my engineering training. But I should have become aware of this issue towards the beginning rather than towards the end of the learning process. Indeed, as re-

*El tercer aprendizaje de calado de esta tesis es que no se deben confundir las metas con los objetivos. Es decir, los objetivos expresados en el capítulo 2 deben entenderse en realidad como metas. Las metas deben servir para no perder de vista la dirección en la que se quiere avanzar y porqué. Pero los objetivos son avances medibles en el camino hacia esas metas. En este sentido, mi director de tesis me planteó de manera muy nítida el objetivo para una tesis (mi tesis): "a ver si consigues mejorar el rendimiento del elemento EBST [41]".*

*Yo he combinado el objetivo que me marcaba mi director de tesis con mis motivaciones. Y ello me ha llevado a perder el enfoque del objetivo. Ello también ha sido fruto de haber percibido un posible exceso de optimismo respecto de mis capacidades como investigador. Esa distracción entre metas y objetivos (también inducida por las necesidades de los proyectos de investigación que financian la actividad investigadora) ha hecho que no haya orientado suficientemente el trabajo hacia la consecución del objetivo.*

*De haber mantenido con más firmeza la orientación de la labor de investigación hacia la consecución del objetivo, seguramente me habría percatado más rápidamente de la necesidad de prestar atención a los problemas de bloqueo por membrana de los elementos de lámina. Este era un aspecto de la tecnología de elementos finitos de lámina que desconocía en mi formación como ingeniero. Pero que en mi recorrido*

flected by section 3.2.2, in the review of the state of the art I did not pay sufficient attention to the issue of membrane locking. And therefore I was not sufficiently on guard against this type of problems presented in continuum-based shell finite elements which, however, the references cited in this thesis comment on. As Bischoff, Wall, Bletzinger and Ramm explain in [12, p. 123]: "Although literature in finite element technology in general is extremely rich, the problem of membrane locking has enjoyed less attention than, for instance, transverse shear locking in plates and shells.", it should have served me as a clear warning and I should have taken adequate measures early on.

### 13.2.4 Non-linearity is a lifeline, not a hurdle

Dealing with the issue of non-linearity may be perceived as an added complexity when developing a new structural finite element. However, the benefits obtained by solving the non-linear problem, require little additional work from the point of view of equation writing and programming.

In my particular case, testing how the element worked in the non-linear regime, allowed me to detect problems caused by the hypothesis used in the formulation. Despite these hypothesis may not raise suspicions beforehand, putting them to the test using a non-linear example, allows sorting out quickly whether the hypothesis applied lead to a well-posed problem or, on the contrary, the problem is actually not well-posed and therefore does not respond to the physical reality being modeled.

For this very reason, any researcher intending to develop a new structural finite element, should quickly put the new formulation to the test against a non-linear problem in order to check the validity of the approach.

I have benefited twice from this trait of the non-linear setting. And in both occasions I have regretted not having performed the test earlier on. Hence, we must view non-linear tests as a lifeline to avoid making serious mistakes in our development's hypothesis; not as an additional hurdle.

*durante el doctorado debería haber adquirido hacia el principio y no hacia el final. De hecho, como lo demuestra el apartado 3.2.2, en la revisión del estado del arte no presté suficiente atención a la cuestión del bloqueo por membrana. Y por consiguiente no estaba prevenido frente a este tipo de problemas en los elementos finitos basados en la teoría del continuo que sin embargo las referencias que incluyo en esta tesis comentan. Como explican Bischoff, Wall, Bletzinger y Ramm en [12, p. 123]: "Aunque la literatura en tecnología de elementos finitos es en general muy rica, el problema del bloqueo por membrana ha recibido menos atención que, por ejemplo, el problema del bloqueo por cortante en placas y láminas.", me debiera haber servido de advertencia y yo debía haber tomado las debidas precauciones desde un primer momento.*

### *La no-linealidad es una tabla de salvación,* no un obstáculo

*En el desarrollo de un nuevo elemento finito estructural, se puede percibir el tratamiento del problema de la no-linealidad como una dificultad añadida. Sin embargo, el trabajo añadido que conlleva resolver el problema no-lineal desde el punto de vista de formulación y programación es muy pequeño en comparación a los beneficios que aporta.*

*En mi caso, la realización de pruebas sobre el funcionamiento del elemento en régimen no-lineal me ha permitido detectar problemas con las hipótesis aplicadas en la formulación. Pese a ser hipótesis que de antemano no despierten sospechas, el ponerlas a prueba con un ejemplo no-lineal permite detectar enseguida si las hipótesis que se están aplicando conducen a un problema bien planteado o si por el contrario el problema que resulta está mal planteado y por consiguiente no responde a la realidad física que se quiere modelar.*

*Por este motivo, cualquier investigador que pretenda desarrollar un nuevo elemento finito estructural, debería tener cierta prisa por someter la nueva formulación al test de un problema no-lineal para verificar la bondad del planteamiento.*

*Yo me he beneficiado en 2 ocasiones de esta virtud del planteamiento no-lineal. Y en ambas ocasiones me he arrepentido de no haber hecho la prueba antes. Así pues, debemos ver las pruebas no-lineales como una tabla de salvación para evitar cometer errores de bulto con las hipótesis de nuestros desarrollos; no como un obstáculo añadido.*

# Appendix A

# The use of numerical methods in sailboat design

# *El cálculo por métodos numéricos en el mundo de los veleros*

IN ORDER TO DISCUSS THE USE of numerical methods in sailboats design it is compulsory to refer to the practices of the sailing sport where competitivity is maximum and therefore the best and latest advances are required in order to obtain those tiny bits of extra speed and turn them into the winning competitive advantage. The competition which reflects that spirit the best and beyond any doubt is the *America's Cup*. While the competition has become the testing laboratory for new and wonderful technologies, once their validity has been verified they are applied once and again beyond the competitive setting if there is an economic chance.

For example, the superyacht market is growing despite the economic crises [66] partly because technology enables making ever larger sails without increasing their weight in such a way that it would become impossible to move them onboard (despite cranes are needed often). This is possible because of the use of advanced composite materials. But also because of the numerical tools and programs that compute their stresses and optimize every gram of material used.

We find another example in the competitions with sailboats that, given their size and overall budget, can hardly count on the resources required to benefit from those developments. I am refering to the dinghies that take

PARA TRATAR EL USO *de los métodos numéricos en el mundo de los veleros es preciso referirse a los ámbitos de la práctica del deporte de la vela, donde la competitividad es máxima y por lo tanto se requieren los mejores y últimos avances para obtener esas décimas extras de velocidad que se conviertan en una ventaja competitiva definitiva. La competición que refleja este espíritu a la perfección y como ninguna otra es la* Copa del América. *Pero si bien la competición ha sido el laboratorio de ensayos para el desarrollo de nuevas y maravillosas tecnologías; éstas, una vez comprobada su validez no se quedan en el ámbito de la competición y son aplicadas una y otra vez siempre que haya oportunidad económica para ello.*

*Por ejemplo, el mercado de superyates está creciendo aún a pesar de la crisis económica [66] en parte gracias a que la tecnología permite fabricar velas cada vez más grandes sin que ello repercuta en un peso de las velas tan desmesurado que sea imposible moverlas a bordo (aunque a menudo se necesitan grúas para ello). Esto es posible por la utilización de avanzados materiales compuestos, pero también a las herramientas numéricas que calculan sus tensiones para así poder realmente optimizar el uso del material.*

*Otro ejemplo se encuentra en las competiciones de barcos que por su tamaño difícilmente dispondrían de suficiente presupuesto para justificar semejantes desarrollos. Estamos hablando de los barcos de vela ligera que regularmente participan en*

part on the summer Olympic Games. In these regattas the competition is so close that some teams use the most advanced technologies to accelerate the learning curve and pull ahead of their competitors and themselves. So far, the use of technology for accelerated learning is limited [74], but the use of numerical methods to accelerate the learning curve is certainly in the path to the future.

## A.1 The America's Cup as a sports and technological pinnacle

The America's Cup hardly needs any introduction. I will simply make the compulsory remark that it is the oldest continuously awarded trophy in international sport. A winning strike of 132 years by the United States only increases the legend of this competition. It increases its prestige because it was precisely a technological advance what permited *Australia II* to take the cup from the americans in 1983. It was thanks to a revolutionary keel design concept by Van Oossanen. Indeed, as Oossanen himself explains in the paper by Spurr [119], numerical methods and CFD simulation played a vital role in the development of the design of the Australia II. They used a simulation program created for airplane wings at the National Aerospace Laboratory in Amsterdam that allowed calculating the viscous resistance and was modified by Joop Slooff to include the wave making resistance effect. This is a decisive moment in sailing history; a sport historically dominated by tradition and folklore.

The americans realized the need to apply cutting edge technology if they were to recover the America's Cup (and part of the pride lost with it). And that's how it went. In the next edition in 1987 *Stars & Stripes* achieved winning back the cup after an unprecedented research and development effort [113].

The prior history of the America's Cup has little importance regarding numerical methods. But the more recent history talks by itself. The efforts the United States made for the 1987 campaign were sustained and increased

*los Juegos Olímpicos de verano. En estas regatas la competencia es tan igualada que algunos equipos recurren a las técnicas más avanzadas para poder adquirir conocimientos de manera acelerada y así superar a sus contrincantes y a sí mismos. Por ahora el uso de la tecnología para el aprendizaje acelerado es todavía limitado [74], pero ciertamente el uso de métodos numéricos para continuar el aprendizaje está en el camino hacia el futuro.*

## *La Copa del América como referente tecnológico y deportivo*

*Apenas hace falta presentar la Copa del América. Simplemente haré la obligada reseña recordando que es la competición deportiva más antigua de cuantas se continúan celebrando. La leyenda engendrada tras una racha de victorias de 132 años por Estados Unidos ensalza aún más si cabe el prestigio de esta competición. Lo ensalza porque fue precisamente un adelanto tecnológico el que permitió al* Australia II *arrebatar la copa a los norteamericanos en 1983 gracias a un revolucionario concepto en el diseño de la quilla realizado por Van Oossanen. De hecho, tal y como explica Van Oossanen en el artículo de Spurr [119], los métodos numéricos y la simulación CFD jugaron un papel muy importante en el desarrollo del diseño de la quilla del Australia II. Se utilizó un programa de simulación para alas de avión del Laboratorio Nacional Aeroespacial de Amsterdam que permitía calcular la resistencia viscosa y que fue modificado por Joop Slooff para incluir los efectos de la resistencia por formación de olas. Este fue un momento decisivo en la historia de la vela; un deporte dominado históricamente por la tradición y las costumbres.*

*Los norteamericanos se dieron cuenta de la necesidad de aplicar la tecnología más puntera si pretendían recuperar la Copa del América (y con ella parte del orgullo perdido). Y así fue, en la siguiente edición de 1987 el* Stars & Stripes *logró recuperar la copa tras un esfuerzo en investigación y desarrollo sin precedentes [113].*

*La historia anterior de la Copa del América tiene poca importancia en cuanto a su relación con los métodos numéricos. Sin embargo la historia más reciente habla por sí sola. El esfuerzo realizado por Estados Unidos en la campaña de 1987 lo mantuvieron y lo incrementaron si cabe defendiendo con éxito la*

defending successfully the cup in 1992[1] with *America*[3].

But the other nations had already noticed the possibility of winning a trophy with the prestige and history of the America's Cup by investing in technology. And thus, again in 1995 the americans werre defeated. This time the winner was *Black Magic* from New Zealand. This team was awash with talent[2], but also demonstrated that thanks to investing in technology they could achieve a competitive level enabling them to succeed.

While until then the technological advances had focused mainly in the reduction of the resistance to the hull advance through the water, the newzealanders caught their rivals by surprise when they set off an ambitious research and development program in sails; that is, the power source of the boats.[3] The study of sails entails some added challenges to that of the study of of hull dynamics in the water. While an aspect of the hulls in the water problem —not found in the study of sails— is the variation they cause to the free surface when they move, the hulls are generally considered as rigid and the water flow around them has a main and uniform direction. Instead, the sails change their shape provided their extreme slenderness. And the air flow around them changes in velocity and dominant direction with height because of the atmospheric boundary layer and its vectorial combination

[1]I am intentionally ommitting the 1988 regatta where many technological advances were applied, particularly brought from aeronautics, but the development time was far too short to allow any substantial advance and of prolonged effect.

[2]Two of the key team members of that newzealander syndicate: Russell Coutts and Brad Butterworth, have won in all the America's Cup editions in which they have taken part of since that regatta of 1995 until they faced off (then only one could win). In the 2010 regatta *BMW Oracle* with Russell Coutts defeated *Alinghi* with Brad Butterworth.

[3]Notice the change in the different tactics for increasing the boat speed. While the blunt of the developments had remained previously on minimizing the hull resistance and that of its appendages through the water, now the effort included maximizing the power and efficiency that could be obtained from the sails.

*copa en 1992*[1] *con* America[3].

*Pero el resto de naciones ya habían tomado buena nota de que la inversión en tecnología les podía valer la conquista de un trofeo con la historia y el prestigio de la Copa del América. Así, de nuevo en 1995 los norteamericanos fueron derrotados, esta vez por* Black Magic *de Nueva Zelanda. Este equipo rebosaba talento deportivo*[2]*, pero demostró asimismo que gracias a la inversión en tecnología se podía estar a un nivel competitivo que permitía aspirar a todo.*

*Si hasta ese momento los desarrollos y avances tecnológicos se habían centrado principalmente en la reducción de la resistencia al avance del casco a través del agua, los neozelandeses cogieron por sorpresa a sus rivales al poner en práctica un ambicioso programa de investigación y desarrollo en velas; es decir, la propulsión de los barcos.*[3] *El estudio de las velas entraña algunas dificultades añadidas al estudio de la dinámica de los cascos en el agua. Si bien una componente del problema de los cascos en el agua —que no encontramos en el estudio de las velas— es la alteración que estos producen en la superficie libre al moverse, los cascos se consideran en general como rígidos y que el flujo de agua a su rededor tiene una dirección dominante uniforme. Sin embargo las velas cambian de forma debido a su extrema esbeltez y el flujo de aire a su rededor varia en celeridad y en dirección dominante con la altura debido al efecto de la capa límite atmosférica y a su combinación vectorial con la velocidad de avance del velero.*[4] *El programa de investigación y desa-*

[1]En este pasaje obvio intencionadamente la regata celebrada en 1988, pues si bien se aplicaron numerosos avances tecnológicos sobretodo importados desde el campo de la aeronáutica, los tiempos de desarrollo fueron excesivamente cortos para permitir un avance sustancial y de efecto prolongado.

[2]Dos de los miembros clave de aquél equipo neozelandés: Russell Coutts y Brad Butterworth, han vencido en todas las ediciones de la Copa del América en las que han participado desde aquella regata de 1995 hasta que se enfrentaron (sólo uno podia ganar). En aquella regata de 2010 el *BMW Oracle* con Russell Coutts venció al *Alinghi* con Brad Butterworth.

[3]Nótese el contraste entre los enfoques adoptados para mejorar la velocidad de los barcos. Si previamente el peso de los desarrollos había recaído principalmente en minimizar el freno que supone el avance del casco y sus apéndices a través del agua, ahora se incluía además maximizar la potencia y la eficiencia que se podía obtener de la propulsión de las velas.

[4]Es lo que se comúnmente se conoce como efecto *twist*. Es precisamente este efecto, combinado con las dificultades de los ensayos a escala en túnel de viento en el estudio de las velas, que llevó al desarrollo del llamado *Sailing Dynamometer* [60] en 1988 por un estudiante de J. Milgram en MIT.

with the sailboat's forward speed.[4] The research and development program of the New Zealand team for sails design focused on various aspects. Burns Fallow [36] explains that the new technology developed by North Sails with the 3DL sails [7] opened the design space for the sail designers. Also, these new sails needed new structural analysis tools. That's why North Sails assigned Michael Richelsen (one of its employees) to develop a software program called MemBrain $^{TM}$[5]. At the same time and provided the greater importance of the downwind courses for the 1995 edition of the America's Cup with respect to the previous editions the team from New Zealand, in collaboration with North Sails New Zealand and the University of Auckland, decided to build a *twisted* flow wind tunnel. This wind tunnel [40] —it still remains a world reference in its class— permited the team of New Zealand to pull ahead of their competitors in the knowledge of how these sails work. The combination of this knowledge, the effort made to exploit as much as possible the advantages offered by the 3DL sails, and the new calculation tools *Black Magic* won the 1995 regatta with a blowing 5–0 in front of a powerless *Young America* crewed by the crew of *Stars & Stripes*.

New Zealand held the cup for another edition until in 2003 technology again helped another nation win the America's Cup. Switzerland, being a landlocked country, doesn't have a nautical tradition. Nevertheless, its *Alinghi* sindicate did count with great talent onboard. By that time, numerical methods were already

*rrollo para el diseño de velas en el equipo de Nueva Zelanda se centró en varios aspectos. Tal y como comenta Burns Fallow en [36], la nueva tecnología desarrollada por North Sails con las velas 3DL [7] abría el campo de juego para los diseñadores de velas. Asimismo, este tipo de velas requería de nuevas herramientas de análisis estructural. Es por ello que North Sails encargó a Michael Richelsen (uno de sus empleados) el desarrollo de un programa de cálculo llamado MemBrain$^{TM}$[5]. Al mismo tiempo, y dada la mayor importancia que tenían los rumbos de empopada en la edición de la Copa del América de 1995 con respecto a ediciones anteriores, el equipo de Nueva Zelanda, en colaboración con North Sails Nueva Zelanda y la Universidad de Auckland, decidió construir un túnel de viento de flujo* retorcido. *Este túnel de viento [40] —que todavía es una referencia mundial en su clase— permitió al equipo de Nueva Zelanda avanzar a sus competidores en el conocimiento y funcionamiento de las velas. Combinando este conocimiento con el esfuerzo realizado para aprovechar al máximo las capacidades ofrecidas por las velas 3DL y las nuevas herramientas de cálculo,* Black Magic *ganó la regata de 1995 por un contundente 5–0 ante un impotente* Young America *tripulado por la tripulación del* Stars & Stripes.

*No fue hasta dos ediciones posteriores, en 2003, cuando nuevamente la tecnología (respaldada por supuesto por un gran talento a bordo de la embarcación) permitió en este caso a una nación sin apenas tradición náutica, como es Suiza, conquistar la Copa del América con el sindicato* Alinghi. *Para entonces los métodos numéricos ya habían cobrado gran aceptación como herramienta de diseño en un entorno tan exigente y los suizos demostraron gran habilidad en utilizarla en sus estudios para el diseño de unas máquinas que se demostraron netamente superiores a las de sus contrincantes tanto en 2003 como en 2007[3]. En su artículo de 2005, Parolini y Quar-*

[4] This is what is commonly known as the *twist* effect. Precisely this effect, combined with the complication of conducting scale tests in wind tunnel to study sail shapes, is what encouraged the development of the *Sailing Dynamometer* [60] in 1988 by a pupil of J. Milgram at MIT.

[5] Despite an exhaustive bibliographic research I haven't found any reference with the detailed functioning of the Membrain$^{TM}$ program. However, I do know, through a number of interviews with North Sails designers (Mickey Ickert and Sandro Benini, although not with Michael Richelsen hihmself) that the MemBrain program is a finite element program which uses a membrane model to calculate the strains and stresses of the sails. The program performs a static analysis of the sails; despite modeling them as membranes (see the discussion in section 1.4). As I can't provide documental evidences of the working of MemBrain, I consider it state of practice and not state of the art.

[5] A pesar de una exhaustiva búsqueda bibliográfica no he encontrado ninguna referencia específica detallando el funcionamiento del programa MemBrain$^{TM}$. Sin embargo sí conozco, mediante numerosas entrevistas con diseñadores de North Sails (aunque no con el propio Michael Richelsen) que el programa MemBrain es un programa de elementos finitos que utiliza un modelo de membranas para calcular los esfuerzos y las deformaciones de las velas. El modelo analiza las velas de manera estacionaria aun a pesar de modelarlas como membranas (véase la discusión en el apartado 1.4). Al no existir evidencias documentales acerca del funcionamiento de MemBrain, lo consideraremos como estado de la práctica y no como estado del arte.

widely accepted as a design tool in such a demanding environment. The swiss showed their ability in using it to design a two boat program that proved to be superior to their rivals' both in 2003 and in 2007[3]. In their 2005 paper, Parolini and Quarteroni [98] explain some of the numerical tools used in the design and analysis of the Alinghi syndicate boats. Watching this evolution it becomes clear that reduced and full scale tow tank tests have given way to numerical methods and computer simulations.

So then, which have been the technological advances in numerical analysis that have occured in the more recent editions of the America's Cup? I'll describe them succintly below.

**The computer revolution**
If there had not occured signifficant advances in the application of numerical methods to the sailing industry in general and high performance in particular before it's mainly because of the very high computational cost of the numerical tools or simply the lack of resources to make the computations before the 1980's. It's somewhat awkward to use terms like *computational cost* nowadays that a smartphone weighing less than 200 grams and costing around $100 has the same computer power as a supercomputer 30 years ago which occupied an entire room and costed several thousand $. That's the main reason why numerical methods still lacked validation and the scientific community relied heavily on laboratory tests in order to make their designs and technological advances. Take for example the paper by Jerome Milgram [79] on the different technologies developed and applied in the design of the boats of the *America*$^3$ syndicate. Within that paper and the ensuing discussion Milgram explains the controversy still existing in 1992!!! between numerical and experimental tools.

**VPPs**
Amongst Milgram's contributions in the referenced paper there is the pivotal role of velocity prediction programs or VPPs in that epoch (and still today). VPPs are simple computer programs that solve the equilibrium equations in some of the degrees of freedom in space of

*teroni [98] detallan parte del abanico de herramientas numéricas utilizadas para el análisis y el diseño de los barcos del sindicato Alinghi. Queda claro, a la vista de esta evolución, que los ensayos a escala en canal y a escala real han dejado paso a los métodos numéricos y las simulaciones por ordenador.*

*Así pues, ¿cuáles son los desarrollos tecnológicos de análisis numérico que han tenido lugar en las ediciones recientes de la Copa del América? Los enumero a continuación de manera muy resumida.*

***La revolución computacional***
*El principal motivo por el que previamente no se habían producido avances significativos en materia de métodos numéricos aplicados al mundo de la vela en general, y en particular a la máxima competición, es el altísimo coste computacional que tenían los métodos numéricos o directamente la inexistencia de recursos para realizar los cálculos con anterioridad a la década de 1980. Resulta extraño hablar en estos términos de* coste computacional *en la actualidad en que un teléfono móvil que pesa apenas 200 gramos y cuesta alrededor de $100 tiene la misma capacidad computacional que un superordenador de hace 30 años, ocupaba una sala entera y costaba unos cuantos miles de $. Por este mismo motivo, los métodos numéricos estaban todavía poco validados y la comunidad científica todavía se apoyaba principalmente en ensayos de laboratorio para realizar sus diseños y avances tecnológicos. Valga como referencia el artículo [79] de Jerome Milgram en el que describe las diversas tecnologías desarrolladas y aplicadas en el diseño de los barcos del sindicato* America$^3$. *En dicho artículo y en la discusión que lo sucede, Milgram explica la controvertida relación existente todavía en 1992!!! entre las técnicas numéricas y las experimentales.*

***Los VPP***
*Una de las aportaciones de Milgram en el artículo mencionado es el papel central que adoptaron en aquella época (y todavía hasta hoy) los programas de predicción de velocidad o VPP (en sus siglas en inglés). Los VPP son sencillos programas de ordenador que resuelven las ecuaciones de equilibrio de fuerzas en algunos de los ejes del espacio para un velero. Sostengo que son sencillos porque resuelven pequeños sistemas de ecuaciones —en algunos casos hasta 6 ecuaciones—. Los VPP entrañan un cierto grado de dificultad debido a que las ecuaciones son*

a sailboat. I make the statement that these programs are simple because they solve small systems of equations —at most 6 equations—. VPPs entail some degree of difficulty because the equations are non-linear and the terms used to fill the different components of the forces are in many cases semi-empirical, and this might cause some inconsistencies, which in turn leads to lack of convergence or an excess of solutions in the design space [79].[6] According to Milgram, VPPs facilitated working out different designs and evauate which performed better and which performed worse. However, the key for a good VPP is still the estimation of the forces —and their different components— acting on a boat. This is a science still under development today.

**Advances in fluid mechanics**

Today's technologies are superior to those available 20 years ago. The advances have been possible largely thanks to the improvement of the computational capabilities and the accessibility thereof. Besides, numerical techniques have also improved signifficantly. It suffices taking a look at the results published by CIMNE researchers; some of their tools were used in the development of the boats of the Alinghi syndicate [28]. I will just cite a compilatory reference of the intense activity of CIMNE scientists[7] in the field of CFD [97]. It is also convenient citing recent results published by Julio Garcia in the topic of validation of CFD tools comparing with tow tank test results of boat hulls [47]. While the advances achieved by scientists in the last decade are notable, it is appropriate saying that the teams competing in the America's Cup have progressively used more and more those commercial tools that bring to the market the most advanced techniques while maintaining the robustness required to avoid compromising the short development times of the boats' development. Let's use two references to

[6] A detailed explanation of VPP programs can be found in the paper [90] by Van Oossanen. A review of its usage along with an estimation of the forces acting on a sailboat can be found in the paper [59] by DeBord et al.

[7] Professor Idelsohn alternated his dedication between CIMNE and CIMEC in Santa Fe, Argentina.

*no-lineales y los términos que sirven para alimentar las distintas componentes de las fuerzas son en muchos casos semi-empíricas, por lo que puede llegar a producirse alguna inconsistencia, lo que conduce a veces a una ausencia de convergencia o a un exceso de soluciones en el espacio de diseño [79].*[6] *Según explica Milgram, los VPP permitían barajar con rapidez varios diseños y evaluar cuáles eran mejores y cuáles peores. Sin embargo, la clave para un buen VPP sigue siendo la evaluación de las fuerzas —y sus distintas componentes— que actúan sobre una embarcación y esa es una ciencia que sigue avanzando en la actualidad.*

***Avances en mecánica de fluidos***

*Las herramientas disponibles hoy en día superan en gran medida las capacidades de las disponibles hace 20 años. En gran medida los avances han sido posibles por el incremento de la capacidad computacional y la accesibilidad a la misma. Pero por el otro lado, las técnicas numéricas también han experimentado mejoras significativas. Baste ver los resultados publicados por científicos de CIMNE; algunas de cuyas herramientas se utilizaron en el desarrollo de los barcos del sindicato Alinghi [28]. En este sentido nos limitamos a citar un documento recopilatorio de la intensa actividad de los científicos de CIMNE*[7] *en el ámbito del CFD [97]. También es pertinente citar los recientes resultados publicados por Julio García en materia de validación de los métodos numéricos CFD frente a resultados experimentales en canales de ensayo para cascos de embarcaciones [47]. Si bien los avances realizados por los científicos son muy notables en la última década, es pertinente comentar que los equipos que compiten en la Copa del América se han decantado progresivamente por el uso de herramientas comerciales que aportan al mercado las técnicas más avanzadas posible pero manteniendo la robustez necesaria para no comprometer los tiempos de desarrollo necesarios para el diseño de las embarcaciones. Ilustraremos esta afirmación con dos referencias. Si en 2001 Jones y Korpus [58] reportaban el uso por primera vez en la Copa del América de un*

[6] Para una explicación detallada acerca del funcionamiento de los programas VPP véase el artículo [90] de Van Oossanen. Para una revisión de su utilización conjuntamente con las distintas técnicas de estimación de las fuerzas que actúan en un barco de vela, véase el artículo de DeBord et al. [59].

[7] El profesor Idelsohn alterna su dedicación a CIMNE y al CIMEC en Santa Fe, Argentina.

further discuss this idea. While in 2001 Jones and Korpus [58] documented the use for the first time in the America's Cup of a RANS[8] model for CFD calculations, Viola et al. [137] report that in 2003 there were still few teams using these simulations, and that in 2007 almost all of them did. And they did so using a commercial software like Fluent, unlike the FANS code that in the year 2000 had a marked experimental character.

**Sails simulation in upwind and downwind courses**

The development of the MemBrain program by North Sails opened the door to ensuing developments to improve the performance analysis of sails. The practical monopoly of North Sails in the America's Cup facilitates that all of these developments happened either within North Sails or in collaboration with other research universities. First, the developments aimed at the simulation of the rigs upwind. This is because the earliest available and mature CFD techology was the simulation of potential flow using the panel method.[9] Also, in the 1990s several fluid-structure interaction techniques emerged. Although they have improved, these techniques were already useful to designers. In [106] Razenbach (from the Quantum Sail Design Group) and Xu describe the simulation procedure using these techniques for upwind courses. North Sails has promoted a so called *Virtual Wind Tunnel*, which is nothing else than coupling MemBrain with *Fluent* using the tool *GAMBIT*[10] in order to analyze sails performance downwind [53].

**Structural analysis**

Adoption of numerical methods in the America's Cup occurred earlier applied to the struc-

[8]Reynolds-Averaged Navier-Stokes

[9]The tool developed by Michael Richelsen for North Sails is called Flow$^{TM}$. Likewise MemBrain, I haven't obtained references describing the way Flow works, but through interviews with North Sails' designers I have confirmed that it is a software program that solves the potential flow equation using a panel method. Therefore, as with MemBrain, in lacking written evidence on the functioning of Flow, it can't be considered state of the art and I will consider it state of practice.

[10]ANSYS has changed the tool GAMBIT by the product *Design Modeler*.

*modelo RANS*[8] *para cálculos CFD; Viola et al. [137] informan que en 2003 todavía eran pocos los equipos que utilizaron este tipo de simulaciones, y que en 2007 casi todos los equipos lo hacían. Y lo hicieron utilizando software comercial como Fluent, a diferencia del código FANS que en el año 2000 tenía un carácter marcadamente más experimental.*

***Simulación de velas en rumbos de ceñida y portantes***

*El desarrollo del programa MemBrain por parte de North Sails abrió la puerta a subsiguientes desarrollos para mejorar el análisis del rendimiento de las velas. La situación práctica de monopolio de North Sails propicia que todos estos desarrollos se hayan desarrollado o bien en el seno de North Sails o bien en colaboración con otras entidades de investigación universitarias. Los primeros desarrollos tuvieron por objetivo la simulación de las velas y sus arboladuras en rumbos de ceñida. Esto es debido a que la tecnología CFD madura y disponible para ello fue en primer lugar la de simulación de flujo potencial.*[9] *Asimismo, en la década de 1990 surgieron múltiples técnicas de interacción fluido-estructura. Aunque se han ido mejorando, estas técnicas ya permitían obtener resultados muy útiles para los diseñadores. En [106] Razenbach (del Grupo de Diseño de Velas Quantum) y Xu explican el proceso de simulación combinando estas técnicas para rumbos de ceñida. North Sails ha promovido el desarrollo de lo que han denominado como* Túnel de Viento Virtual*, que no es más que el acoplamiento de MemBrain con* Fluent *facilitado por la herramienta* GAMBIT[10] *para poder analizar el rendimiento de las velas en rumbos portantes [53].*

***Cálculos estructurales***

*La adopción de los métodos numéricos en la Copa del América tuvo lugar antes en el campo del cálculo*

[8]Reynolds-Averaged Navier-Stokes

[9]La herramienta desarrollada por Michael Richelsen para North Sails recibe el nombre de Flow$^{TM}$. Igual a como ocurre con el programa MemBrain, no he conseguido obtener referencias que describan el funcionamiento de Flow, aunque mediante entrevistas con diseñadores de North Sails he podido confirmar que se trata de un software que resuelve las ecuaciones de flujo potencial utilizando un método de paneles. De modo similar a como sucede con MemBrain, al no existir evidencia documentada sobre el funcionamiento de Flow, no se puede considerar estado del arte y lo consideraremos estado de la práctica.

[10]ANSYS ha sustituido la herramienta GAMBIT por el producto *Design Modeler*.

tural calculation of the hulls of the boats than any other aspect commented before (CFD calculation of hulls and sails, or structural analysis of sails). This phenomenon happened along the transition towards the use of fiber reinforced plastics in the construction of the America's Cup boats. For that, the manufacturing and calculation methods stemming from the aeronatical industry were used [52, 75]. For an in depth review on structural calculation methods used in sailboats the author reccomends the material published by the 17$^{th}$ International Ship and Offshore Structures Congress [115]. This document describes with great deal of detail the state of the art regarding the manufacturing and analysis techniques of: hulls, masts and appendages of sailboats. Nevertheless, even though according to that report it might seem that the methods to calculate and analyze sailboat's structures are well established, it's surprising realize that the high performance boats designed to race around the world in regattas such as the *Volvo Ocean Race*[11] keep suffering catastrophic failures [14, 32, 83, 84]. Indeed, one of the common facts of the winning boats in the top competitions is their reliability in competition [76]. That is, the lack of breakages forcing them to retire from the race. This phenomenon is not exclusive of sailing. It happens in any discipline. That's why it is so important the capability to analyze the structural response of high performance sailboats. Making them light is an ever increasing need to make them fast, but it works directly against their reliability. Finding the optimal compromise in design is fundamental. CIMNE researchers have also made significant contributions in this field [88, 89, 105] that could improve the analysis of composite materials structures used in the construction of sailboats.

[11]Even though this section uses the America's Cup as the main reference in the development of sailing sport, on what relates structural analysis another competition takes precedence. This is because the structural integrity of the boats is fundamental when the competitors find themselves thousands of miles away of any other external help when racing around the world.

*estructural de los cascos de las embarcaciones que en el resto de áreas comentadas anteriormente (cálculo CFD de casco y velas, y análisis estructural de velas). Este fenómeno tuvo lugar de manera paralela a la incorporación del uso de los plásticos reforzados con fibras en la fabricación de los barcos en la Copa América. En este caso se adoptaron tanto los métodos de fabricación como de cálculo utilizados en la industria aeronáutica [52, 75]. Para una revisión exhaustiva sobre métodos de cálculo estructurales en veleros, es recomendable el material publicado por el 17º International Ship and Offshore Structures Congress [115]. En este documento se detalla de manera exhaustiva el estado del arte relativo a las técnicas de fabricación y de análisis de: cascos, mástiles y apéndices de barcos de vela. Sin embargo, a pesar de que a la vista de este informe parece que los métodos de análisis y cálculo de las estructuras de los veleros están muy consolidadas, sorprende comprobar que los barcos de competición diseñados para dar la vuelta al mundo como en la* Volvo Ocean Race[11] *siguen sufriendo fallos catastróficos [14, 32, 83, 84]. De hecho, una de las características comunes de los barcos vencedores en las máximas competiciones es su fiabilidad en competición [76]. Es decir, la ausencia de roturas que les obliguen a retirarse de la competición. Este es un fenómeno que no es exclusivo del deporte de la vela, sino que está presente en cualquier deporte. Por ello, cobra máxima importancia la capacidad de analizar estructuralmente la respuesta de los barcos de vela de competición, pues aligerarlos es una necesidad imperiosa para hacerlos veloces; pero obra directamente en contra de la fiabilidad. Encontrar el punto óptimo de dimensionamiento es fundamental. Científicos de CIMNE también han realizado aportaciones relevantes [88, 89, 105] que podrían permitir mejorar los cálculos de las estructuras de materiales compuestos que se utilizan en la construcción de los barcos de vela.*

[11]Aunque esta sección utiliza la Copa del América como referente fundamental del desarrollo en el deporte de la vela, en este apartado referente al cálculo estructural cobra mayor importancia otra competición como referente principal. Esto es debido a que la fiabilidad estructural de los barcos es primordial cuando los competidores se encuentran a miles de kilómetros de cualquier fuente de ayuda externa mientras navegan alrededor del mundo.

## A.2 Summary

It's very telling in light of the review performed in the present chapter that the concepts used nowadays for the analysis on the performance of a sail boat (VPP programs, decomposition of the water resistance to a sailboat into different components, analysis of sails as membranes, stationary simulations, etc.) are the same that were proposed more than 20 years ago. This is just the evidence of the burden of heritage and the importance it exerts on the natural process of humans to acquire new knowledge. But once this understanding has been achieved, it would constitute an enormous mistake to consider that the big problem is the sum of the different components into which the mind has broken down the problem and built artificially. In reality the big problem has the added complexity of understanding how all the little components interact.

The problem of analyzing a sailboat is not an exception, as Milgram points out [80, pp. 618–619]. This author stands firmly on that statement and radicalizes it, if that's possible, extrapolating it beyond the field of hydrodynamics and the hull. The goal of this point of view is to effectively take into account the interaction between all the boat parts and the external forces: both aerodynamic and hydrodynamic. The final result of this point of view would provide us with the possibility of analyzing the whole boat as a structure integrated in its environment and stop assuming that the hull is a rigid solid in transit through the water and the waves, or that the spars and the sails have a stationary position while the boat sails.

## *Sumario*

*Resulta muy reveladora la revisión realizada y ver que los conceptos con los que se trabaja actualmente en materia de análisis del rendimiento de un velero (programas VPP, descomposición de la resistencia al avance de un buque en distintas componentes, análisis de las velas como membranas, simulaciones estacionarias, etc.) son los mismos que ya se proponían hace más de 20 años. Esto no es más que una muestra del peso que tiene la herencia y de la importancia que tiene para el conocimiento humano el dividir los problemas grandes en partes más pequeñas. Forma parte del proceso natural del ser humano para adquirir conocimiento, el dividir un problema grande en problemas más pequeños para poder comprender mejor su complejidad. Pero una vez alcanzada esa comprensión sería un error considerar que el problema grande es la suma de las pequeñas componentes que la mente ha construido artificialmente. En realidad el problema grande tiene una complejidad añadida que es cómo todas esas componentes interaccionan entre sí.*

*El problema del estudio y análisis de un barco de vela no es una excepción y así lo apunta Milgram en [80, pp. 618–619]. Esta tesis se posiciona firmemente sobre esta afirmación y la radicaliza, si cabe, extrapolándola más allá del campo hidrodinámico que afecta al casco de la embarcación. El objetivo de este enfoque es considerar de manera efectiva la interacción de todas las partes del barco entre ellas, así como con las fuerzas externas: tanto las aerodinámicas como las hidrodinámicas. El culmen de este enfoque nos llevaría a analizar todo el barco como una estructura integrada en su entorno, y no asumir que el casco es un sólido rígido en su tránsito a través del agua y de las olas, o que la arboladura y las velas tienen una posición estacionaria mientras el barco navega.*

# Appendix B

# Published paper:

## *On the interpolation of normal vectors for triangle meshes*

## Internationa Journal for Numerical Methods in Engineering

**ATTENTION¡¡**

Pages 210 to 232 of the thesis, which contain the article, are available on the editor's web https://onlinelibrary.wiley.com/doi/abs/10.1002/nme.4567

# Appendix C

# Minimization of the membrane (axial) energy of a 2D cubic Bernouilli beam

THE PRESENT APPENDIX DEVELOPS THE FORMULÆ introduced in section 5.4.1 on page 59 to discuss the problem of minimizing the variation of membrane energy of the edge of the curved shell triangle in the construction process.

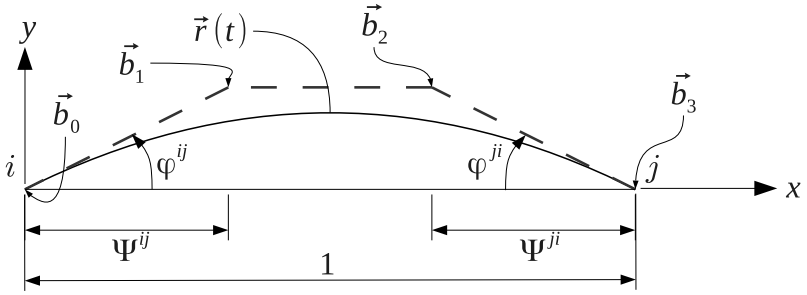


Figure C.1: 2D cubic Bézier curve representing the edge of a cubic Bézier triangle. For the purposes of the exercise and without loss of generality, the distance between the endpoints of the curve will be 1.

Let's state again the problem: if the membrane strain ($\varepsilon$) of the curve depicted in figure C.1 is proportional to the celerity ($c$) of the curve parameter ($t$), then the energy density ($U$) is proportional to the square of the celerity ($c^2$).

$$\vec{r}(t) = (x(t), y(t)) \tag{C.1}$$

$$\vec{r}'(t) = \frac{\partial \vec{r}(t)}{\partial t} \tag{C.2}$$

$$c = \|\vec{r}'(t)\| \tag{C.3}$$

$$\varepsilon \propto c \Rightarrow U \propto \varepsilon^2 \propto c^2 \tag{C.4}$$

The above relationship assumes that the material is linear elastic.

The coordinates of the control points are:

$$\begin{aligned}\vec{b}_0 &= (x_0, y_0) = (0, 0)\\ \vec{b}_1 &= (x_1, y_1) = (\Psi^{ij}, \Psi^{ij} \cdot \tan\varphi^{ij})\\ \vec{b}_2 &= (x_2, y_2) = (1 - \Psi^{ji}, \Psi^{ji} \cdot \tan\varphi^{ji})\\ \vec{b}_3 &= (x_3, y_3) = (1, 0)\end{aligned} \tag{C.5}$$

Using the de Casteljau algorithm and Bernstein functions, the derivative of $\vec{r}$ can be expressed in the following way as a function of the curve parameter $t$.

$$\vec{r}'(t) = (r'_x, r'_y) = (\vec{b}_1 - \vec{b}_0) \cdot (1-t)^2 + (\vec{b}_2 - \vec{b}_1) \cdot 2t(1-t) + (\vec{b}_3 - \vec{b}_2) \cdot t^2 \tag{C.6}$$

$$\begin{aligned}r'_x &= x_1 \cdot (1-t)^2 + (x_2 - x_1) \cdot 2t(1-t) + (1 - x_2) \cdot t^2\\ r'_y &= y_1 \cdot (1-t)^2 + (y_2 - y_1) \cdot 2t(1-t) + y_2 \cdot t^2\end{aligned} \tag{C.7}$$

$$c^2 = r'^2_x + r'^2_y \tag{C.8}$$

Considering the values of $\varphi^{ij}$ and $\varphi^{ji}$ fixed. And maintaining $\Psi^{ij}$ and $\Psi^{ji}$ as variables, then

$$c^2 = c^2(\Psi^{ij}, \Psi^{ji}, t) \tag{C.9}$$

The total membrane elastic energy in the curve can be expressed as:

$$E = \int_0^1 U \,\mathrm{d}t \Rightarrow E \propto \int_0^1 c^2 \,\mathrm{d}t \tag{C.10}$$

The author is interested in minimizing the variation of the energy density along the curve. In order to do that, it is useful to minimize the square of the variation of the energy density along the curve:

$$\int_0^1 \left(\frac{\partial U}{\partial t}\right)^2 \mathrm{d}t \tag{C.11}$$

The minimization is carried out by differentiating the above expression with respect to the two variables of the problem $\Psi^{ij}$ and $\Psi^{ji}$:

$$\left.\begin{aligned}\frac{\partial}{\partial \Psi^{ij}} \int_0^1 \left(\frac{\partial U}{\partial t}\right)^2 \mathrm{d}t = 0\\ \frac{\partial}{\partial \Psi^{ji}} \int_0^1 \left(\frac{\partial U}{\partial t}\right)^2 \mathrm{d}t = 0\end{aligned}\right\} \tag{C.12}$$

Since $U \propto c^2$, the roots of the above system of equations are the same as the roots of

$$\left.\begin{aligned}\frac{\partial}{\partial \Psi^{ij}} \int_0^1 \left(\frac{\partial c^2}{\partial t}\right)^2 \mathrm{d}t = 0\\ \frac{\partial}{\partial \Psi^{ji}} \int_0^1 \left(\frac{\partial c^2}{\partial t}\right)^2 \mathrm{d}t = 0\end{aligned}\right\} \tag{C.13}$$

The expressions in equation (C.13) are polynomials of 4th order with respect to the independent variables $\Psi^{ij}$ and $\Psi^{ji}$. Their graphical solution is presented in figure 5.9 on page 61.

# Appendix D

# Analytic derivatives of some complex expressions

THIS APPENDIX INCLUDES THE ANALYTIC EXPRESSIONS that are not relevant for the understanding of the development of the formulæ in the thesis, or too cumbersome to be included in the main body of the text. Note that Einstein's indicial notation is in full effect.

## D.1 Derivatives of the element normal

The definition of $\boldsymbol{n}$ can be found in equation (5.12) on page 49. Its derivatives with respect to the control points are presented next.

$$\frac{\partial \boldsymbol{n}}{\partial \boldsymbol{p}} = \frac{\partial n_{(i)}}{\partial p_{(mn)}} = \frac{(e_{(ikm)} - n_{(i)} \cdot e_{(jkm)} \cdot n_{(j)}) \cdot p_{(kl)} \cdot (L_{\xi(l)} \cdot L_{\eta(n)} - L_{\eta(l)} \cdot L_{\xi(n)})}{\|(\boldsymbol{p} \cdot \boldsymbol{L}_\xi) \times (\boldsymbol{p} \cdot \boldsymbol{L}_\eta)\|} \tag{D.1}$$

$$\begin{aligned}
\frac{\partial^2 n_{(i)}}{\partial p_{(mn)} \partial p_{(vw)}} = \frac{1}{\|(\boldsymbol{p} \cdot \boldsymbol{L}_\xi) \times (\boldsymbol{p} \cdot \boldsymbol{L}_\eta)\|} \cdot \big[ & (e_{(imv)} + n_{(i)} \cdot e_{(mjv)} \cdot n_{(j)}) \cdot \\
& \cdot (L_{\xi(n)} \cdot L_{\eta(w)} - L_{\eta(n)} \cdot L_{\xi(w)}) - \\
& - \frac{\partial n_{(i)}}{\partial p_{(mn)}} \cdot e_{(jkv)} \cdot n_{(j)} \cdot p_{(kl)} \cdot (L_{\xi(l)} \cdot L_{\eta(w)} - L_{\eta(l)} \cdot L_{\xi(w)}) - \\
& - \frac{\partial n_{(i)}}{\partial p_{(vw)}} \cdot e_{(jkm)} \cdot n_{(j)} \cdot p_{(kl)} \cdot (L_{\xi(l)} \cdot L_{\eta(n)} - L_{\eta(l)} \cdot L_{\xi(n)}) - \\
& - \frac{n_{(i)} \cdot p_{(jl)} \cdot p_{(ko)}}{\|(\boldsymbol{p} \cdot \boldsymbol{L}_\xi) \times (\boldsymbol{p} \cdot \boldsymbol{L}_\eta)\|} \cdot (e_{(tjm)} \cdot e_{(tkv)} + e_{(tjm)} \cdot n_{(t)} \cdot e_{(xkv)} \cdot n_{(x)}) \cdot \\
& \cdot (L_{\xi(l)} \cdot L_{\eta(n)} - L_{\eta(l)} \cdot L_{\xi(n)}) \cdot (L_{\xi(o)} \cdot L_{\eta(w)} - L_{\eta(o)} \cdot L_{\xi(w)}) \big]
\end{aligned} \tag{D.2}$$

Also, the higher derivatives of the expressions defined in equations (6.22) and (6.23) on page 69 are presented below.

$$\begin{aligned}
\frac{\partial \boldsymbol{n}_{,\xi_\alpha}}{\partial \boldsymbol{p}} = \frac{\partial n_{,\xi_\alpha(i)}}{\partial p_{(mn)}} = (\boldsymbol{\delta}_{(ij)} - n_{(i)} \cdot n_{(j)}) \cdot \left( \frac{\partial Lp_{\xi,\xi_\alpha(j)}}{\partial p_{(mn)}} + \frac{\partial Lp_{\eta,\xi_\alpha(j)}}{\partial p_{(mn)}} \right) - \\
- \left( \frac{\partial n_{(i)}}{\partial p_{(mn)}} \cdot n_{(j)} + n_{(i)} \cdot \frac{\partial n_{(j)}}{\partial p_{(mn)}} \right) \cdot (Lp_{\xi,\xi_\alpha(j)} + Lp_{\eta,\xi_\alpha(j)}) \\
\forall \alpha = \{1, 2\}
\end{aligned} \tag{D.3}$$

$$\begin{aligned}
\frac{\partial^2 \boldsymbol{n}_{,\xi_\alpha}}{(\partial \boldsymbol{p})^2} &= \frac{\partial^2 n_{,\xi_\alpha(i)}}{\partial p_{(mn)} \partial p_{(vw)}} = \\
&= (\boldsymbol{\delta}_{(ij)} - n_{(i)} \cdot n_{(j)}) \cdot \left( \frac{\partial^2 Lp_{\xi,\xi_\alpha(j)}}{\partial p_{(mn)} \partial p_{(vw)}} + \frac{\partial^2 Lp_{\eta,\xi_\alpha(j)}}{\partial p_{(mn)} \partial p_{(vw)}} \right) - \\
&\quad - \left( \frac{\partial^2 n_{(i)}}{\partial p_{(mn)} \partial p_{(vw)}} \cdot n_{(i)} + \frac{\partial n_{(i)}}{\partial p_{(mn)}} \cdot \frac{\partial n_{(j)}}{\partial p_{(vw)}} + \right. \\
&\quad \left. + \frac{\partial n_{(i)}}{\partial p_{(vw)}} \cdot \frac{\partial n_{(j)}}{\partial p_{(mn)}} + n_{(i)} \cdot \frac{\partial^2 n_{(j)}}{\partial p_{(mn)} \partial p_{(vw)}} \right) \cdot \left( Lp_{\xi,\xi_\alpha(j)} + Lp_{\eta,\xi_\alpha(j)} \right) - \\
&\quad - \left( \frac{\partial n_{(i)}}{\partial p_{(vw)}} \cdot n_{(j)} + n_{(i)} \cdot \frac{\partial n_{(j)}}{\partial p_{(vw)}} \right) \cdot \left( \frac{\partial Lp_{\xi,\xi_\alpha(j)}}{\partial p_{(mn)}} + \frac{\partial Lp_{\eta,\xi_\alpha(j)}}{\partial p_{(mn)}} \right) - \\
&\quad - \left( \frac{\partial n_{(i)}}{\partial p_{(mn)}} \cdot n_{(j)} + n_{(i)} \cdot \frac{\partial n_{(j)}}{\partial p_{(mn)}} \right) \cdot \left( \frac{\partial Lp_{\xi,\xi_\alpha(j)}}{\partial p_{(vw)}} + \frac{\partial Lp_{\eta,\xi_\alpha(j)}}{\partial p_{(vw)}} \right) \\
&\qquad\qquad \forall \alpha = \{1, 2\}
\end{aligned} \tag{D.4}$$

These expressions are used in equations (7.17) to (7.21) on pages 79–80.

Where

$$\begin{aligned}
\boldsymbol{Lp}_{\xi,\xi_\alpha} &= \frac{(\boldsymbol{p} \cdot \boldsymbol{L}_{\xi,\xi_\alpha}) \times (\boldsymbol{p} \cdot \boldsymbol{L}_\eta)}{\|(\boldsymbol{p} \cdot \boldsymbol{L}_\xi) \times (\boldsymbol{p} \cdot \boldsymbol{L}_\eta)\|} = \frac{e_{(ijk)} \cdot p_{(jl)} \cdot L_{\xi,\xi_\alpha(l)} \cdot p_{(km)} \cdot L_{\eta(m)}}{\|(\boldsymbol{p} \cdot \boldsymbol{L}_\xi) \times (\boldsymbol{p} \cdot \boldsymbol{L}_\eta)\|} \\
&= Lp_{\xi,\xi_\alpha(i)} \qquad \forall \alpha = \{1, 2\}
\end{aligned} \tag{D.5}$$

$$\begin{aligned}
\boldsymbol{Lp}_{\eta,\xi_\alpha} &= \frac{(\boldsymbol{p} \cdot \boldsymbol{L}_\xi) \times (\boldsymbol{p} \cdot \boldsymbol{L}_{\eta,\xi_\alpha})}{\|(\boldsymbol{p} \cdot \boldsymbol{L}_\xi) \times (\boldsymbol{p} \cdot \boldsymbol{L}_\eta)\|} = \frac{e_{(ijk)} \cdot p_{(jl)} \cdot L_{\xi(l)} \cdot p_{(km)} \cdot L_{\eta,\xi_\alpha(m)}}{\|(\boldsymbol{p} \cdot \boldsymbol{L}_\xi) \times (\boldsymbol{p} \cdot \boldsymbol{L}_\eta)\|} \\
&= Lp_{\eta,\xi_\alpha(i)} \qquad \forall \alpha = \{1, 2\}
\end{aligned} \tag{D.6}$$

their first derivatives are expressed in the following way,

$$\begin{aligned}
\frac{\partial Lp_{\xi,\xi_\alpha(i)}}{\partial p_{(mn)}} &= \frac{e_{(ijm)} \cdot p_{(jl)} \cdot (L_{\xi,\xi_\alpha(l)} \cdot L_{\eta(n)} - L_{\eta(l)} \cdot L_{\xi,\xi_\alpha(n)})}{\|(\boldsymbol{p} \cdot \boldsymbol{L}_\xi) \times (\boldsymbol{p} \cdot \boldsymbol{L}_\eta)\|} - \\
&\quad - Lp_{\xi,\xi_\alpha(i)} \cdot \frac{e_{(jkm)} \cdot n_{(j)} \cdot p_{(kl)} \cdot (L_{\xi(l)} \cdot L_{\eta(n)} - L_{\eta(l)} \cdot L_{\xi(n)})}{\|(\boldsymbol{p} \cdot \boldsymbol{L}_\xi) \times (\boldsymbol{p} \cdot \boldsymbol{L}_\eta)\|} \\
&\qquad\qquad \forall \alpha = \{1, 2\}
\end{aligned} \tag{D.7}$$

$$\begin{aligned}
\frac{\partial Lp_{\eta,\xi_\alpha(i)}}{\partial p_{(mn)}} &= \frac{e_{(ijm)} \cdot p_{(jl)} \cdot (L_{\xi(l)} \cdot L_{\eta,\xi_\alpha(n)} - L_{\eta,\xi_\alpha(l)} \cdot L_{\xi(n)})}{\|(\boldsymbol{p} \cdot \boldsymbol{L}_\xi) \times (\boldsymbol{p} \cdot \boldsymbol{L}_\eta)\|} - \\
&\quad - Lp_{\eta,\xi_\alpha(i)} \cdot \frac{e_{(jkm)} \cdot n_{(j)} \cdot p_{(kl)} \cdot (L_{\xi(l)} \cdot L_{\eta(n)} - L_{\eta(l)} \cdot L_{\xi(n)})}{\|(\boldsymbol{p} \cdot \boldsymbol{L}_\xi) \times (\boldsymbol{p} \cdot \boldsymbol{L}_\eta)\|} \\
&\qquad\qquad \forall \alpha = \{1, 2\}
\end{aligned} \tag{D.8}$$

and the expressions of their second derivatives are as follows.

$$\begin{aligned}
&\frac{\partial^2 Lp_{\xi,\xi_\alpha(i)}}{\partial p_{(mn)}\partial p_{(vw)}} = \frac{1}{\|(\boldsymbol{p}\cdot\boldsymbol{L}_\xi)\times(\boldsymbol{p}\cdot\boldsymbol{L}_\eta)\|}\cdot\\
&\cdot\left[e_{(imv)}\cdot(L_{\xi,\xi_\alpha(n)}\cdot L_{\eta(w)} - L_{\eta(n)}\cdot L_{\xi,\xi_\alpha(w)}) - \right.\\
&-\frac{\partial Lp_{\xi,\xi_\alpha(i)}}{\partial p_{(mn)}}\cdot n_{(j)}\cdot e_{(jkv)}\cdot p_{(kl)}\cdot(L_{\xi(l)}\cdot L_{\eta(w)} - L_{\eta(l)}\cdot L_{\xi(w)}) -\\
&-\frac{\partial Lp_{\xi,\xi_\alpha(i)}}{\partial p_{(vw)}}\cdot n_{(j)}\cdot e_{(jkm)}\cdot p_{(kl)}\cdot(L_{\xi(l)}\cdot L_{\eta(n)} - L_{\eta(l)}\cdot L_{\xi(n)}) -\\
&-Lp_{\xi,\xi_\alpha(i)}\cdot\frac{\partial n_{(j)}}{\partial p_{(mn)}}\cdot e_{(jkv)}\cdot p_{(kl)}\cdot(L_{\xi(l)}\cdot L_{\eta(w)} - L_{\eta(l)}\cdot L_{\xi(w)}) -\\
&\left.-Lp_{\xi,\xi_\alpha(i)}\cdot n_{(j)}\cdot e_{(jmv)}\cdot(L_{\xi(n)}\cdot L_{\eta(w)} - L_{\eta(n)}\cdot L_{\xi(w)})\right] \qquad \forall\alpha=\{1,2\}
\end{aligned} \tag{D.9}$$

$$\begin{aligned}
&\frac{\partial^2 Lp_{\eta,\xi_\alpha(i)}}{\partial p_{(mn)}\partial p_{(vw)}} = \frac{1}{\|(\boldsymbol{p}\cdot\boldsymbol{L}_\xi)\times(\boldsymbol{p}\cdot\boldsymbol{L}_\eta)\|}\cdot\\
&\cdot\left[e_{(imv)}\cdot(L_{\xi(n)}\cdot L_{\eta,\xi_\alpha(w)} - L_{\eta,\xi_\alpha(n)}\cdot L_{\xi(w)}) - \right.\\
&-\frac{\partial Lp_{\eta,\xi_\alpha(i)}}{\partial p_{(mn)}}\cdot n_{(j)}\cdot e_{(jkv)}\cdot p_{(kl)}\cdot(L_{\xi(l)}\cdot L_{\eta(w)} - L_{\eta(l)}\cdot L_{\xi(w)}) -\\
&-\frac{\partial Lp_{\eta,\xi_\alpha(i)}}{\partial p_{(vw)}}\cdot n_{(j)}\cdot e_{(jkm)}\cdot p_{(kl)}\cdot(L_{\xi(l)}\cdot L_{\eta(n)} - L_{\eta(l)}\cdot L_{\xi(n)}) -\\
&-Lp_{\eta,\xi_\alpha(i)}\cdot\frac{\partial n_{(j)}}{\partial p_{(mn)}}\cdot e_{(jkv)}\cdot p_{(kl)}\cdot(L_{\xi(l)}\cdot L_{\eta(w)} - L_{\eta(l)}\cdot L_{\xi(w)}) -\\
&\left.-Lp_{\eta,\xi_\alpha(i)}\cdot n_{(j)}\cdot e_{(jmv)}\cdot(L_{\xi(n)}\cdot L_{\eta(w)} - L_{\eta(n)}\cdot L_{\xi(w)})\right] \qquad \forall\alpha=\{1,2\}
\end{aligned} \tag{D.10}$$

## D.2 Derivatives of the system matrix and independent vector to compute the control point locations

The location of the control points is computed by solving a system of equations for each one. These include the control points at the boundaries and the central control point.

### D.2.1 Boundary control points

The general expression of the system of equations to determine the control points of the boundaries is presented in equation (5.15) on page 51. The expression of the derivatives of the system matrix $\boldsymbol{A}_{\boldsymbol{p}}^{ij}$ is presented row by row.

$$\frac{\partial A^{ij}_{p(1l)}}{\partial x^h_{(v)}} = \frac{\partial n^i_{(l)}}{\partial x^h_{(v)}} \tag{D.11}$$

$$\frac{\partial A^{ij}_{p(2l)}}{\partial x^h_{(v)}} = \frac{\partial d^{ij}_{(l)}}{\partial x^h_{(v)}} \tag{D.12}$$

$$\frac{\partial A^{ij}_{p(3l)}}{\partial x^h_{(v)}} = (\boldsymbol{\delta}^{ih} - \boldsymbol{\delta}^{jh}) \cdot \boldsymbol{\delta}_{(lv)} \tag{D.13}$$

The expression of the derivatives of the independent vector is also presented component-wise.

$$\frac{\partial b^{ij}_{p(1)}}{\partial x^h_{(v)}} = x^i_{(l)} \cdot \frac{\partial n^i_{(l)}}{\partial x^h_{(v)}} + \boldsymbol{\delta}^{ih} \cdot n^i_{(v)} \tag{D.14}$$

$$\frac{\partial b^{ij}_{p(2)}}{\partial x^h_{(v)}} = \frac{\partial d^{ij}_{(l)}}{\partial x^h_{(v)}} \cdot x^i_{(l)} + \boldsymbol{\delta}^{ih} \cdot d^{ij}_{(v)} \tag{D.15}$$

$$\begin{aligned}\frac{\partial b^{ij}_{p(3)}}{\partial x^h_{(v)}} &= \boldsymbol{\delta}^{ih} \cdot (x^i_{(v)} - x^j_{(v)}) + (\boldsymbol{\delta}^{ih} - \boldsymbol{\delta}^{jh}) \cdot x^i_{(v)} - \\ &- \|\boldsymbol{x}^i - \boldsymbol{x}^j\|^2 \cdot \frac{\partial \Psi^{ij}}{\partial x^h_{(v)}} - 2(\boldsymbol{\delta}^{ih} - \boldsymbol{\delta}^{jh}) \cdot (x^i_{(v)} - x^j_{(v)}) \cdot \Psi^{ij}\end{aligned} \tag{D.16}$$

And the second derivatives are presented below.

$$\frac{\partial^2 A^{ij}_{p(1l)}}{\partial x^h_{(v)} \partial x^s_{(w)}} = \frac{\partial^2 n^i_{(l)}}{\partial x^h_{(v)} \partial x^s_{(w)}} \tag{D.17}$$

$$\frac{\partial^2 A^{ij}_{p(2l)}}{\partial x^h_{(v)} \partial x^s_{(w)}} = \frac{\partial^2 d^{ij}_{(l)}}{\partial x^h_{(v)} \partial x^s_{(w)}} \tag{D.18}$$

$$\frac{\partial^2 A^{ij}_{p(2l)}}{\partial x^h_{(v)} \partial x^s_{(w)}} = \mathbf{0} \tag{D.19}$$

$$\frac{\partial^2 b^{ij}_{p(1)}}{\partial x^h_{(v)} \partial x^s_{(w)}} = x^i_{(l)} \cdot \frac{\partial^2 n^i_{(l)}}{\partial x^h_{(v)} \partial x^s_{(w)}} + \boldsymbol{\delta}^{ih} \cdot \frac{\partial n^i_{(v)}}{\partial x^s_{(w)}} + \boldsymbol{\delta}^{is} \cdot \frac{\partial n^i_{(w)}}{\partial x^h_{(v)}} \tag{D.20}$$

$$\frac{\partial^2 b^{ij}_{p(2)}}{\partial x^h_{(v)} \partial x^s_{(w)}} = \frac{\partial^2 d^{ij}_{(l)}}{\partial x^h_{(v)} \partial x^s_{(w)}} \cdot x^i_{(l)} + \boldsymbol{\delta}^{is} \cdot \frac{\partial d^{ij}_{(w)}}{\partial x^h_{(v)}} + \boldsymbol{\delta}^{ih} \cdot \frac{\partial d^{ij}_{(v)}}{\partial x^s_{(w)}} \tag{D.21}$$

$$\begin{aligned}\frac{\partial^2 b^{ij}_{p(3)}}{\partial x^h_{(v)} \partial x^s_{(w)}} &= \boldsymbol{\delta}_{(vw)} \cdot [\boldsymbol{\delta}^{ih} \cdot (\boldsymbol{\delta}^{is} - \boldsymbol{\delta}^{js}) + \boldsymbol{\delta}^{is} \cdot (\boldsymbol{\delta}^{ih} - \boldsymbol{\delta}^{jh}) - \\ &- 2 \cdot (\boldsymbol{\delta}^{ih} - \boldsymbol{\delta}^{jh}) \cdot (\boldsymbol{\delta}^{is} - \boldsymbol{\delta}^{js}) \cdot \Psi^{ij}] - \|\boldsymbol{x}^i - \boldsymbol{x}^j\|^2 \cdot \frac{\partial^2 \Psi^{ij}}{\partial x^h_{(v)} \partial x^s_{(w)}} - \\ &- 2 \cdot (\boldsymbol{\delta}^{ih} - \boldsymbol{\delta}^{jh}) \cdot (x^i_{(v)} - x^j_{(v)}) \cdot \frac{\partial \Psi^{ij}}{\partial x^s_{(w)}} - \\ &- 2 \cdot (\boldsymbol{\delta}^{is} - \boldsymbol{\delta}^{js}) \cdot (x^i_{(w)} - x^j_{(w)}) \cdot \frac{\partial \Psi^{ij}}{\partial x^h_{(v)}}\end{aligned} \tag{D.22}$$

The reader will notice that in order to implement these equations we need to develop the expressions of the derivatives of $\boldsymbol{n}^i$ and $\boldsymbol{d}^{ij}$. We will

use the definitions provided in equations (5.3) and (9.7) on page 46 and on page 106, respectively.

The expressions for $\Psi^{ij}$ and its derivatives are provided in equations (9.17) to (9.32) on pages 112–116.

### D.2.2 Central control point candidates

The general expression of the system of equations to determine the central control point candidates is presented in equation (5.19) on page 54. The expression of the first and second derivatives of the system matrix $\boldsymbol{A}_{\boldsymbol{p}}^{0i}$ is presented row by row. However, only the first row presents a challenge, because the expressions for the second and third rows have already been solved in the case of the boundary control points; see equations (D.25) and (D.26).

$$\begin{aligned}\frac{\partial A^{0i}_{p(1l)}}{\partial x^h_{(v)}} = &\left[\left(\frac{\partial p^{jk}_{(m)}}{\partial x^h_{(v)}} - \frac{\partial p^{kj}_{(m)}}{\partial x^h_{(v)}}\right)\cdot n^{jk}_{(m)} + (p^{jk}_{(m)} - p^{kj}_{(m)})\cdot\frac{\partial n^{jk}_{(m)}}{\partial x^h_{(v)}}\right]\cdot(p^{jk}_{(l)} - p^{kj}_{(l)}) + \\ &+ [(p^{jk}_{(m)} - p^{kj}_{(m)})\cdot n^{jk}_{(m)}\cdot\left(\frac{\partial p^{jk}_{(l)}}{\partial x^h_{(v)}} - \frac{\partial p^{kj}_{(l)}}{\partial x^h_{(v)}}\right) - \\ &- 2\cdot\left[(p^{jk}_{(m)} - p^{kj}_{(m)})\cdot\left(\frac{\partial p^{jk}_{(m)}}{\partial x^h_{(v)}} - \frac{\partial p^{kj}_{(m)}}{\partial x^h_{(v)}}\right)\right] n^{jk}_{(l)} - \\ &- (p^{jk}_{(m)} - p^{kj}_{(m)})^2\cdot\frac{\partial n^{jk}_{(l)}}{\partial x^h_{(v)}}\end{aligned} \tag{D.23}$$

$$\frac{\partial^2 A^{0i}_{p(1l)}}{\partial x^h_{(v)}\partial x^s_{(w)}} = \left[\left(\frac{\partial^2 p^{jk}_{(m)}}{\partial x^h_{(v)}\partial x^s_{(w)}} - \frac{\partial^2 p^{kj}_{(m)}}{\partial x^h_{(v)}\partial x^s_{(w)}}\right)\cdot n^{jk}_{(m)} + \left(\frac{\partial p^{jk}_{(m)}}{\partial x^h_{(v)}} - \frac{\partial p^{kj}_{(m)}}{\partial x^h_{(v)}}\right)\cdot\frac{\partial n^{jk}_{(m)}}{\partial x^s_{(w)}} + \right.$$
$$\left. + \left(\frac{\partial p^{jk}_{(m)}}{\partial x^s_{(w)}} - \frac{\partial p^{kj}_{(m)}}{\partial x^s_{(w)}}\right)\cdot\frac{\partial n^{jk}_{(m)}}{\partial x^h_{(v)}} + (p^{jk}_{(m)} - p^{kj}_{(m)})\cdot\frac{\partial^2 n^{jk}_{(m)}}{\partial x^h_{(v)}\partial x^s_{(w)}}\right]\cdot(p^{jk}_{(l)} - p^{kj}_{(l)}) +$$
$$+[(p^{jk}_{(m)} - p^{kj}_{(m)})\cdot n^{jk}_{(m)}]\cdot\left(\frac{\partial^2 p^{jk}_{(l)}}{\partial x^h_{(v)}\partial x^s_{(w)}} - \frac{\partial^2 p^{kj}_{(l)}}{\partial x^h_{(v)}\partial x^s_{(w)}}\right) - (p^{jk}_{(m)} - p^{kj}_{(m)})^2\cdot\frac{\partial^2 n^{jk}_{(l)}}{\partial x^h_{(v)}\partial x^s_{(w)}} +$$
$$+\left[\left(\frac{\partial p^{jk}_{(m)}}{\partial x^h_{(v)}} - \frac{\partial p^{kj}_{(m)}}{\partial x^h_{(v)}}\right)\cdot n^{jk}_{(m)} + (p^{jk}_{(m)} - p^{kj}_{(m)})\cdot\frac{\partial n^{jk}_{(m)}}{\partial x^h_{(v)}}\right]\cdot\left(\frac{\partial p^{jk}_{(l)}}{\partial x^s_{(w)}} - \frac{\partial p^{kj}_{(l)}}{\partial x^s_{(w)}}\right) +$$
$$+\left[\left(\frac{\partial p^{jk}_{(m)}}{\partial x^s_{(w)}} - \frac{\partial p^{kj}_{(m)}}{\partial x^s_{(w)}}\right)\cdot n^{jk}_{(m)} + (p^{jk}_{(m)} - p^{kj}_{(m)})\cdot\frac{\partial n^{jk}_{(m)}}{\partial x^s_{(w)}}\right]\cdot\left(\frac{\partial p^{jk}_{(l)}}{\partial x^h_{(v)}} - \frac{\partial p^{kj}_{(l)}}{\partial x^h_{(v)}}\right) -$$
$$-2\cdot\left[(p^{jk}_{(m)} - p^{kj}_{(m)})\cdot\left(\frac{\partial p^{jk}_{(m)}}{\partial x^h_{(v)}} - \frac{\partial p^{kj}_{(m)}}{\partial x^h_{(v)}}\right)\right]\cdot\frac{\partial n^{jk}_{(l)}}{\partial x^s_{(w)}} -$$
$$-2\cdot\left[(p^{jk}_{(m)} - p^{kj}_{(m)})\cdot\left(\frac{\partial p^{jk}_{(m)}}{\partial x^s_{(w)}} - \frac{\partial p^{kj}_{(m)}}{\partial x^s_{(w)}}\right)\right]\cdot\frac{\partial n^{jk}_{(l)}}{\partial x^h_{(v)}} -$$
$$-2\cdot\left[\left(\frac{\partial p^{jk}_{(m)}}{\partial x^h_{(v)}} - \frac{\partial p^{kj}_{(m)}}{\partial x^h_{(v)}}\right)\cdot\left(\frac{\partial p^{jk}_{(m)}}{\partial x^s_{(w)}} - \frac{\partial p^{kj}_{(m)}}{\partial x^s_{(w)}}\right) + \right.$$
$$\left. + (p^{jk}_{(m)} - p^{kj}_{(m)})\cdot\left(\frac{\partial^2 p^{jk}_{(m)}}{\partial x^h_{(v)}\partial x^s_{(w)}} - \frac{\partial^2 p^{kj}_{(m)}}{\partial x^h_{(v)}\partial x^s_{(w)}}\right)\right]\cdot n^{jk}_{(l)} \quad \text{(D.24)}$$

$$A^{0i}_{p(2l)} = A^{ij}_{p(3l)} \quad \Rightarrow \quad \frac{\partial A^{0i}_{p(2l)}}{\partial x^h_{(v)}} = \frac{\partial A^{ij}_{p(3l)}}{\partial x^h_{(v)}} \quad \Rightarrow \quad \frac{\partial^2 A^{0i}_{p(2l)}}{\partial x^h_{(v)}\partial x^s_{(w)}} = \frac{\partial^2 A^{ij}_{p(3l)}}{\partial x^h_{(v)}\partial x^s_{(w)}} \quad \text{(D.25)}$$

$$A^{0i}_{p(3l)} = A^{ik}_{p(3l)} \quad \Rightarrow \quad \frac{\partial A^{0i}_{p(3l)}}{\partial x^h_{(v)}} = \frac{\partial A^{ik}_{p(3l)}}{\partial x^h_{(v)}} \quad \Rightarrow \quad \frac{\partial^2 A^{0i}_{p(3l)}}{\partial x^h_{(v)}\partial x^s_{(w)}} = \frac{\partial^2 A^{ik}_{p(3l)}}{\partial x^h_{(v)}\partial x^s_{(w)}} \quad \text{(D.26)}$$

## D.3 Derivatives of the normal at the node

Let's use a general expression for a weighted average normal vector at the node.

$$\boldsymbol{n}^i = \frac{\sum\limits_{k=1}^{r_i} w^k\cdot\hat{\boldsymbol{y}}^k}{\left\|\sum\limits_{k=1}^{r_i} w^k\cdot\hat{\boldsymbol{y}}^k\right\|} \quad \text{(D.27)}$$

Then, the general expression for the first derivative is

$$\frac{\partial n^i_{(j)}}{\partial x^h_{(v)}} = \frac{\displaystyle\sum_{k=1}^{r_i}\left(\frac{\partial w^k}{\partial x^h_{(v)}}\hat{y}^k_{(j)} + w^k\,\frac{\partial \hat{y}^k_{(j)}}{\partial x^h_{(v)}}\right) - n^i_{(j)}\,n^i_{(l)}\cdot\displaystyle\sum_{k=1}^{r_i}\left(\frac{\partial w^k}{\partial x^h_{(v)}}\hat{y}^k_{(l)} + w^k\,\frac{\partial \hat{y}^k_{(l)}}{\partial x^h_{(v)}}\right)}{\left\|\displaystyle\sum_{k=1}^{r_i} w^k\cdot\hat{\boldsymbol{y}}^k\right\|} \tag{D.28}$$

and for the second derivative

$$\begin{aligned}\frac{\partial^2 n^i_{(j)}}{\partial x^h_{(v)}\partial x^s_{(w)}} &= \frac{1}{\left\|\displaystyle\sum_{k=1}^{r_i} w^k\cdot\hat{\boldsymbol{y}}^k\right\|}\left[\sum_{k=1}^{r_i}\left(\frac{\partial^2 w^k}{\partial x^h_{(v)}\partial x^s_{(w)}}\hat{y}^k_{(j)} + \frac{\partial w^k}{\partial x^h_{(v)}}\frac{\partial \hat{y}^k_{(j)}}{\partial x^s_{(w)}} + \right.\right.\\
&+\frac{\partial w^k}{\partial x^s_{(w)}}\frac{\partial \hat{y}^k_{(j)}}{\partial x^h_{(v)}} + w^k\,\frac{\partial^2 \hat{y}^k_{(j)}}{\partial x^h_{(v)}\partial x^s_{(w)}}\Bigg) - n^i_{(j)}\,\frac{\partial n^i_{(l)}}{\partial x^s_{(w)}}\sum_{k=1}^{r_i}\left(\frac{\partial w^k}{\partial x^h_{(v)}}\hat{y}^k_{(l)} + w^k\,\frac{\partial \hat{y}^k_{(l)}}{\partial x^h_{(v)}}\right) -\\
&-\frac{\partial n^i_{(j)}}{\partial x^s_{(w)}}\,n^i_{(l)}\sum_{k=1}^{r_i}\left(\frac{\partial w^k}{\partial x^h_{(v)}}\hat{y}^k_{(l)} + w^k\,\frac{\partial \hat{y}^k_{(l)}}{\partial x^h_{(v)}}\right) - \frac{\partial n^i_{(j)}}{\partial x^h_{(v)}}\,n^i_{(l)}\sum_{k=1}^{r_i}\left(\frac{\partial w^k}{\partial x^s_{(w)}}\hat{y}^k_{(l)} + w^k\,\frac{\partial \hat{y}^k_{(l)}}{\partial x^s_{(w)}}\right) -\\
&-n^i_{(j)}\,n^i_{(l)}\sum_{k=1}^{r_i}\left(\frac{\partial^2 w^k}{\partial x^h_{(v)}\partial x^s_{(w)}}\hat{y}^k_{(l)} + \frac{\partial w^k}{\partial x^h_{(v)}}\frac{\partial \hat{y}^k_{(l)}}{\partial x^s_{(w)}} + \frac{\partial w^k}{\partial x^s_{(w)}}\frac{\partial \hat{y}^k_{(l)}}{\partial x^h_{(v)}} + w^k\,\frac{\partial^2 \hat{y}^k_{(l)}}{\partial x^h_{(v)}\partial x^s_{(w)}}\right)\end{aligned} \tag{D.29}$$

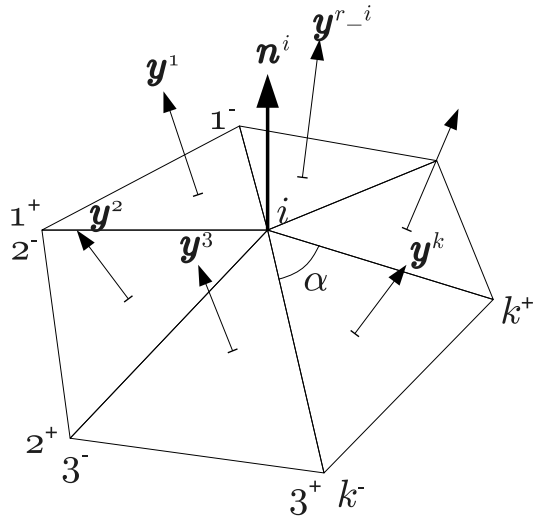


Figure D.1: This figure is a modification of figure 5.1. A new notation is used for the neighboring nodes. Each node has a specific notation depending to the triangle considered and the direction of its normal.

In the case of the weight proposed in equation (5.2) on page 46, we will write the derivatives after rewriting the formula using the nodal coordi-

nates of the neighboring nodes. But first we need to redefine some notation regarding the neighboring nodes. For each triangle $k$ that surrounds node $i$, the two neighboring nodes associated will be named $k^+$ and $k^-$ corresponding to looping them in a counterclockwise order as the normal points towards the observer (see figure D.1 which substitutes figure 5.1 on page 45).

$$w^k_{\alpha/A_\circ} = \frac{\|\boldsymbol{v}^k\|^2}{(\boldsymbol{x}^{k^-} - \boldsymbol{x}^i)^2 (\boldsymbol{x}^{k^+} - \boldsymbol{x}^i)^2 (\boldsymbol{x}^{k^+} - \boldsymbol{x}^{k^-})^2} \cdot \arccos(c_\alpha) \tag{D.30}$$

The first derivative is presented below.

$$\begin{aligned}\frac{\partial w^k_{\alpha/A_\circ}}{\partial x^h_{(v)}} = -2 \cdot w^k_{\alpha/A_\circ} \cdot \Bigg[ & \frac{(x^{k^-}_{(v)} - x^i_{(v)})\,(\boldsymbol{\delta}^{k^-h} - \boldsymbol{\delta}^{ih})}{(\boldsymbol{x}^{k^-} - \boldsymbol{x}^i)^2} + \frac{(x^{k^+}_{(v)} - x^i_{(v)})\,(\boldsymbol{\delta}^{k^+h} - \boldsymbol{\delta}^{ih})}{(\boldsymbol{x}^{k^+} - \boldsymbol{x}^i)^2} + \\ & + \frac{(x^{k^+}_{(v)} - x^{k^-}_{(v)})\,(\boldsymbol{\delta}^{k^+h} - \boldsymbol{\delta}^{k^-h})}{(\boldsymbol{x}^{k^+} - \boldsymbol{x}^{k^-})^2} \Bigg] + \frac{1}{(\boldsymbol{x}^{k^-} - \boldsymbol{x}^i)^2\,(\boldsymbol{x}^{k^+} - \boldsymbol{x}^i)^2\,(\boldsymbol{x}^{k^+} - \boldsymbol{x}^{k-})^2} \cdot \\ & \cdot \left\{ 2 \cdot v^k_{(j)} \cdot \frac{\partial v^k_{(j)}}{\partial x^h_{(v)}} \cdot \arccos(c_\alpha) - \frac{\|\boldsymbol{v}^k\|^2}{\sqrt{1 - c^2_\alpha}} \cdot \frac{\partial c_\alpha}{\partial x^h_{(v)}} \right\}\end{aligned} \tag{D.31}$$

And the second derivative is as follows.

$$\begin{aligned}\frac{\partial^2 w^k_{\alpha/\circ}}{\partial x^h_{(v)} \partial x^s_{(w)}} = & \frac{1}{(\boldsymbol{x}^{k^-} - \boldsymbol{x}^i)^2\,(\boldsymbol{x}^{k^+} - \boldsymbol{x}^i)^2\,(\boldsymbol{x}^{k^+} - \boldsymbol{x}^{k-})^2} \cdot \Bigg[ 2 \cdot \Bigg( \frac{\partial v^k_{(j)}}{\partial x^h_{(v)}} \cdot \frac{\partial v^k_{(j)}}{\partial x^s_{(w)}} + \\ & + v^k_{(j)} \cdot \frac{\partial^2 v^k_{(j)}}{\partial x^s_{(w)}} \Bigg) \cdot \arccos(c_\alpha) - \frac{2 \cdot v^k_{(j)}}{\sqrt{1 - c_\alpha}} \cdot \left( \frac{\partial v^k_{(j)}}{\partial x^h_{(v)}} \cdot \frac{\partial c_\alpha}{\partial x^s_{(w)}} + \frac{\partial v^k_{(j)}}{\partial x^s_{(w)}} \cdot \frac{\partial c_\alpha}{\partial x^h_{(v)}} \right) - \\ & - \frac{\|\boldsymbol{v}^k\|^2}{\sqrt{1 - c^2_\alpha}} \cdot \left( \frac{\partial^2 c_\alpha}{\partial x^h_{(v)} \partial x^s_{(w)}} + \frac{c_\alpha}{1 - c^2_\alpha} \cdot \frac{\partial c_\alpha}{\partial x^h_{(v)}} \cdot \frac{\partial c_\alpha}{\partial x^s_{(w)}} \right) \Bigg] - \\ & - 2 \cdot w^k_{\alpha/A_\circ} \cdot \Bigg[ \frac{\boldsymbol{\delta}_{(vw)} \cdot (\boldsymbol{\delta}^{k^-h} - \boldsymbol{\delta}^{ih}) \cdot (\boldsymbol{\delta}^{k^-s} - \boldsymbol{\delta}^{is})}{(\boldsymbol{x}^{k^-} - \boldsymbol{x}^i)^2} + \frac{\boldsymbol{\delta}_{(vw)} \cdot (\boldsymbol{\delta}^{k^+h} - \boldsymbol{\delta}^{ih}) \cdot (\boldsymbol{\delta}^{k^+s} - \boldsymbol{\delta}^{is})}{(\boldsymbol{x}^{k^+} - \boldsymbol{x}^i)^2} + \\ & + \frac{\boldsymbol{\delta}_{(vw)} \cdot (\boldsymbol{\delta}^{k^+h} - \boldsymbol{\delta}^{k^-h}) \cdot (\boldsymbol{\delta}^{k^+s} - \boldsymbol{\delta}^{k^-s})}{(\boldsymbol{x}^{k^+} - \boldsymbol{x}^{k^-})^2} + \\ & + \frac{2 \cdot (x^{k^-}_{(v)} - x^i_{(v)}) \cdot (\boldsymbol{\delta}^{k^-h} - \boldsymbol{\delta}^{ih}) \cdot (x^{k^+}_{(w)} - x^i_{(w)}) \cdot (\boldsymbol{\delta}^{k^+s} - \boldsymbol{\delta}^{is})}{(\boldsymbol{x}^{k^-} - \boldsymbol{x}^i)^2 \cdot (\boldsymbol{x}^{k^+} - \boldsymbol{x}^i)^2} + \\ & + \frac{2 \cdot (x^{k^-}_{(v)} - x^i_{(v)}) \cdot (\boldsymbol{\delta}^{k^-h} - \boldsymbol{\delta}^{ih}) \cdot (x^{k^+}_{(w)} - x^{k^-}_{(w)}) \cdot (\boldsymbol{\delta}^{k^+s} - \boldsymbol{\delta}^{k^-s})}{(\boldsymbol{x}^{k^-} - \boldsymbol{x}^i)^2 \cdot (\boldsymbol{x}^{k^+} - \boldsymbol{x}^{k^-})^2} + \\ & + \frac{2 \cdot (x^{k^+}_{(v)} - x^i_{(v)}) \cdot (\boldsymbol{\delta}^{k^+h} - \boldsymbol{\delta}^{ih}) \cdot (x^{k^-}_{(w)} - x^i_{(w)}) \cdot (\boldsymbol{\delta}^{k^-s} - \boldsymbol{\delta}^{is})}{(\boldsymbol{x}^{k^-} - \boldsymbol{x}^i)^2 \cdot (\boldsymbol{x}^{k^+} - \boldsymbol{x}^i)^2} + \\ & + \frac{2 \cdot (x^{k^+}_{(v)} - x^i_{(v)}) \cdot (\boldsymbol{\delta}^{k^+h} - \boldsymbol{\delta}^{ih}) \cdot (x^{k^+}_{(w)} - x^{k^-}_{(w)}) \cdot (\boldsymbol{\delta}^{k^+s} - \boldsymbol{\delta}^{k^-s})}{(\boldsymbol{x}^{k^+} - \boldsymbol{x}^i)^2 \cdot (\boldsymbol{x}^{k^+} - \boldsymbol{x}^{k^-})^2} + \\ & + \frac{2 \cdot (x^{k^+}_{(v)} - x^{k^-}_{(v)}) \cdot (\boldsymbol{\delta}^{k^+h} - \boldsymbol{\delta}^{k^-h}) \cdot (x^{k^-}_{(w)} - x^i_{(w)}) \cdot (\boldsymbol{\delta}^{k^-s} - \boldsymbol{\delta}^{is})}{(\boldsymbol{x}^{k^-} - \boldsymbol{x}^i)^2 \cdot (\boldsymbol{x}^{k^+} - \boldsymbol{x}^{k^-})^2} +\end{aligned}$$

$$+\frac{2\cdot(x^{k^+}_{(v)}-x^{k^-}_{(v)})\cdot(\boldsymbol{\delta}^{k^+h}-\boldsymbol{\delta}^{k^-h})\cdot(x^{k^+}_{(w)}-x^{i}_{(w)})\cdot(\boldsymbol{\delta}^{k^+s}-\boldsymbol{\delta}^{is})}{(\boldsymbol{x}^{k^+}-\boldsymbol{x}^{i})^2\cdot(\boldsymbol{x}^{k^+}-\boldsymbol{x}^{k^-})^2}\Bigg]-$$
$$-2\frac{\partial w^k_{\alpha/A_\circ}}{\partial x^s_{(w)}}\cdot\left[\frac{(x^{k^-}_{(v)}-x^{i}_{(v)})\,(\boldsymbol{\delta}^{k^-h}-\boldsymbol{\delta}^{ih})}{(\boldsymbol{x}^{k^-}-\boldsymbol{x}^{i})^2}+\frac{(x^{k^+}_{(v)}-x^{i}_{(v)})\,(\boldsymbol{\delta}^{k^+h}-\boldsymbol{\delta}^{ih})}{(\boldsymbol{x}^{k^+}-\boldsymbol{x}^{i})^2}+\right.$$
$$\left.+\frac{(x^{k^+}_{(v)}-x^{k^-}_{(v)})\,(\boldsymbol{\delta}^{k^+h}-\boldsymbol{\delta}^{k^-h})}{(\boldsymbol{x}^{k^+}-\boldsymbol{x}^{k^-})^2}\right]-2\frac{\partial w^k_{\alpha/A_\circ}}{\partial x^h_{(v)}}\cdot\left[\frac{(x^{k^-}_{(w)}-x^{i}_{(w)})\,(\boldsymbol{\delta}^{k^-s}-\boldsymbol{\delta}^{is})}{(\boldsymbol{x}^{k^-}-\boldsymbol{x}^{i})^2}+\right.$$
$$\left.+\frac{(x^{k^+}_{(w)}-x^{i}_{(w)})\,(\boldsymbol{\delta}^{k^+s}-\boldsymbol{\delta}^{is})}{(\boldsymbol{x}^{k^+}-\boldsymbol{x}^{i})^2}+\frac{(x^{k^+}_{(w)}-x^{k^-}_{(w)})\,(\boldsymbol{\delta}^{k^+s}-\boldsymbol{\delta}^{k^-s})}{(\boldsymbol{x}^{k^+}-\boldsymbol{x}^{k^-})^2}\right] \tag{D.32}$$

Where $c_\alpha$ corresponds to the cosine of the angle formed by the sides of the triangle at the vertex $i$ (see figure D.1).

$$c_\alpha=\frac{(\boldsymbol{x}^{k^-}-\boldsymbol{x}^{i})\cdot(\boldsymbol{x}^{k^+}-\boldsymbol{x}^{i})}{\|\boldsymbol{x}^{k^-}-\boldsymbol{x}^{i}\|\cdot\|\boldsymbol{x}^{k^+}-\boldsymbol{x}^{i}\|} \tag{D.33}$$

$$\frac{\partial c_\alpha}{\partial x^h_{(v)}}=\frac{(x^{k^-}_{(v)}-x^{i}_{(v)})\cdot(\boldsymbol{\delta}^{k^+h}-\boldsymbol{\delta}^{ih})+(x^{k^+}_{(v)}-x^{i}_{(v)})\cdot(\boldsymbol{\delta}^{k^-h}-\boldsymbol{\delta}^{ih})}{\|\boldsymbol{x}^{k^-}-\boldsymbol{x}^{i}\|\cdot\|\boldsymbol{x}^{k^+}-\boldsymbol{x}^{i}\|}-$$
$$-c_\alpha\cdot\left[\frac{(x^{k^-}_{(v)}-x^{i}_{(v)})\cdot(\boldsymbol{\delta}^{k^-h}-\boldsymbol{\delta}^{ih})}{(\boldsymbol{x}^{k^-}-\boldsymbol{x}^{i})^2}+\frac{(x^{k^+}_{(v)}-x^{i}_{(v)})\cdot(\boldsymbol{\delta}^{k^+h}-\boldsymbol{\delta}^{ih})}{(\boldsymbol{x}^{k^+}-\boldsymbol{x}^{i})^2}\right] \tag{D.34}$$

$$\frac{\partial^2 c_\alpha}{\partial x^h_{(v)}\partial x^s_{(w)}}=\boldsymbol{\delta}_{(vw)}\cdot\frac{(\boldsymbol{\delta}^{k^+h}-\boldsymbol{\delta}^{ih})\cdot(\boldsymbol{\delta}^{k^-s}-\boldsymbol{\delta}^{is})+(\boldsymbol{\delta}^{k^-h}-\boldsymbol{\delta}^{ih})\cdot(\boldsymbol{\delta}^{k^+s}-\boldsymbol{\delta}^{is})}{\|\boldsymbol{x}^{k^-}-\boldsymbol{x}^{i}\|\cdot\|\boldsymbol{x}^{k^+}-\boldsymbol{x}^{i}\|}-$$
$$-\frac{\partial c_\alpha}{\partial x^h_{(v)}}\cdot\left[\frac{(x^{k^-}_{(w)}-x^{i}_{(w)})\cdot(\boldsymbol{\delta}^{k^-s}-\boldsymbol{\delta}^{is})}{(\boldsymbol{x}^{k^-}-\boldsymbol{x}^{i})^2}+\frac{(x^{k^+}_{(w)}-x^{i}_{(w)})\cdot(\boldsymbol{\delta}^{k^+s}-\boldsymbol{\delta}^{is})}{(\boldsymbol{x}^{k^+}-\boldsymbol{x}^{i})^2}\right]-$$
$$-\frac{\partial c_\alpha}{\partial x^s_{(w)}}\cdot\left[\frac{(x^{k^-}_{(v)}-x^{i}_{(v)})\cdot(\boldsymbol{\delta}^{k^-h}-\boldsymbol{\delta}^{ih})}{(\boldsymbol{x}^{k^-}-\boldsymbol{x}^{i})^2}+\frac{(x^{k^+}_{(v)}-x^{i}_{(v)})\cdot(\boldsymbol{\delta}^{k^+h}-\boldsymbol{\delta}^{ih})}{(\boldsymbol{x}^{k^+}-\boldsymbol{x}^{i})^2}\right]-$$
$$c_\alpha\cdot\left\{\boldsymbol{\delta}_{(vw)}\cdot\left[\frac{(\boldsymbol{\delta}^{k^-h}-\boldsymbol{\delta}^{ih})\cdot(\boldsymbol{\delta}^{k^-s}-\boldsymbol{\delta}^{is})}{(\boldsymbol{x}^{k^-}-\boldsymbol{x}^{i})^2}+\frac{(\boldsymbol{\delta}^{k^+h}-\boldsymbol{\delta}^{ih})\cdot(\boldsymbol{\delta}^{k^+s}-\boldsymbol{\delta}^{is})}{(\boldsymbol{x}^{k^+}-\boldsymbol{x}^{i})^2}\right]+\right.$$
$$+\frac{(x^{k^-}_{(v)}-x^{i}_{(v)})\cdot(\boldsymbol{\delta}^{k^-h}-\boldsymbol{\delta}^{ih})\cdot(x^{k^+}_{(w)}-x^{i}_{(w)})\cdot(\boldsymbol{\delta}^{k^+s}-\boldsymbol{\delta}^{is})}{(\boldsymbol{x}^{k^-}-\boldsymbol{x}^{i})^2\cdot(\boldsymbol{x}^{k^+}-\boldsymbol{x}^{i})^2}+$$
$$+\frac{(x^{k^+}_{(v)}-x^{i}_{(v)})\cdot(\boldsymbol{\delta}^{k^+h}-\boldsymbol{\delta}^{ih})\cdot(x^{k^-}_{(w)}-x^{i}_{(w)})\cdot(\boldsymbol{\delta}^{k^-s}-\boldsymbol{\delta}^{is})}{(\boldsymbol{x}^{k^-}-\boldsymbol{x}^{i})^2\cdot(\boldsymbol{x}^{k^+}-\boldsymbol{x}^{i})^2}-$$
$$-\frac{(x^{k^-}_{(v)}-x^{i}_{(v)})\cdot(\boldsymbol{\delta}^{k^-h}-\boldsymbol{\delta}^{ih})\cdot(x^{k^-}_{(w)}-x^{i}_{(w)})\cdot(\boldsymbol{\delta}^{k^-s}-\boldsymbol{\delta}^{is})}{(\boldsymbol{x}^{k^-}-\boldsymbol{x}^{i})^{3/2}}-$$
$$\left.-\frac{(x^{k^+}_{(v)}-x^{i}_{(v)})\cdot(\boldsymbol{\delta}^{k^+h}-\boldsymbol{\delta}^{ih})\cdot(x^{k^+}_{(w)}-x^{i}_{(w)})\cdot(\boldsymbol{\delta}^{k^+s}-\boldsymbol{\delta}^{is})}{(\boldsymbol{x}^{k^+}-\boldsymbol{x}^{i})^{3/2}}\right\} \tag{D.35}$$

And $\boldsymbol{v}^k$ is the cross product of the vectors that link the sides of the triangle.

$$\boldsymbol{v}^k = (\boldsymbol{x}^{k^-} - \boldsymbol{x}^i) \times (\boldsymbol{x}^{k^+} - \boldsymbol{x}^i) = e_{(jml)} \cdot \left( x^{k^-}_{(m)} x^{k^+}_{(l)} - x^{k^-}_{(m)} x^i_{(l)} + x^{k^+}_{(m)} x^i_{(l)} \right) = v^k_{(j)} \tag{D.36}$$

$$\frac{\partial v^k_{(j)}}{\partial x^h_{(v)}} = e_{(jmv)} \cdot \left[ \boldsymbol{\delta}^{k^- h} (x^i_{(m)} - x^{k^+}_{(m)}) + \boldsymbol{\delta}^{ih} (x^{k^+}_m - x^{k^-}_{(m)}) + \boldsymbol{\delta}^{k^+ h} (x^{k^-}_{(m)} - x^i_{(m)}) \right] \tag{D.37}$$

$$\frac{\partial^2 v^k_{(j)}}{\partial x^h_{(v)} \partial x^s_{(w)}} = e_{(jvw)} \cdot \left[ \boldsymbol{\delta}^{k^- h} (\boldsymbol{\delta}^{k^+ s} - \boldsymbol{\delta}^{is}) + \boldsymbol{\delta}^{ih} (\boldsymbol{\delta}^{k^- s} - \boldsymbol{\delta}^{k^+ s}) + \boldsymbol{\delta}^{k^+ h} (\boldsymbol{\delta}^{is} - \boldsymbol{\delta}^{k^- s}) \right] \tag{D.38}$$

Then we conclude with the definition of $\hat{\boldsymbol{y}}^k$ and its derivatives.

$$\hat{\boldsymbol{y}}^k = \frac{\boldsymbol{v}^k}{\|\boldsymbol{v}^k\|} \tag{D.39}$$

$$\frac{\hat{y}^k_{(j)}}{\partial x^h_{(v)}} = \|\boldsymbol{v}^k\|^{-1} \cdot \left( \frac{\partial v^k_{(j)}}{\partial x^h_{(v)}} - \hat{y}^k_{(j)} \cdot \hat{y}^k_{(l)} \cdot \frac{\partial v^k_{(l)}}{\partial x^h_{(v)}} \right) \tag{D.40}$$

$$\begin{aligned} \frac{\partial^2 \hat{y}^k_{(j)}}{\partial x^h_{(v)} \partial x^s_{(w)}} = \|\boldsymbol{v}^k\|^{-1} \cdot \Bigg( & \frac{\partial^2 v^k_{(j)}}{\partial x^h_{(v)} \partial x^s_{(w)}} - \frac{\partial \hat{y}^k_{(j)}}{\partial x^h_{(v)}} \cdot y^k_{(l)} \cdot \frac{\partial v^k_{(l)}}{\partial x^s_{(w)}} - \\ - \frac{\partial \hat{y}^k_{(j)}}{\partial x^s_{(w)}} \cdot \hat{y}^k_{(l)} \cdot \frac{\partial v^k_{(l)}}{\partial x^h_{(v)}} & - \hat{y}^k_{(j)} \cdot \frac{\partial \hat{y}^k_{(l)}}{\partial x^s_{(w)}} \cdot \frac{\partial v^k_{(l)}}{\partial x^h_{(v)}} - \hat{y}^k_{(j)} \cdot \hat{y}^k_{(l)} \cdot \frac{\partial^2 v^k_{(l)}}{\partial x^h_{(v)} \partial x^s_{(w)}} \Bigg) \end{aligned} \tag{D.41}$$

## D.4 Derivatives of $d^{ij}$

The vector $\boldsymbol{d}^{ij}$ is the director vector of the plane that bounds the edge of the cubic triangle at the corner nodes. It is defined in item 2 on page 105 and in equation (9.7). Its first derivative is presented below.

$$\begin{aligned} \frac{\partial d^{ij}_{(l)}}{\partial x^h_{(v)}} = {} & e_{(lmk)} \cdot \frac{\partial n^i_{(m)}}{\partial x^h_{(v)}} \cdot (x^i_{(k)} - x^j_{(k)}) \cdot \cos\theta^{ij} + (\boldsymbol{\delta}^{ih} - \boldsymbol{\delta}^{jh}) \cdot e_{(lmv)} \cdot n^i_{(m)} \cdot \cos\theta^{ij} - \\ & - e_{(lmk)} \cdot n^i_{(k)} \cdot (x^i_{(k)} - x^j_{(k)}) \cdot \sin\theta^{ij} \cdot \frac{\partial \theta^{ij}}{\partial x^h_{(v)}} + \frac{\partial n^i_{(l)}}{\partial x^h_{(v)}} \cdot n^i_{(m)} \cdot (x^i_{(m)} - x^j_{(m)}) \cdot \sin\theta^{ij} + \\ & + n^i_{(l)} \cdot \frac{\partial n^i_{(m)}}{\partial x^h_{(v)}} \cdot (x^i_{(m)} - x^j_{(m)}) \cdot \sin\theta^{ij} - (\boldsymbol{\delta}^{ih} - \boldsymbol{\delta}^{jh}) \cdot (\boldsymbol{\delta}_{(lv)} - n^i_{(l)} \cdot n^i_{(v)}) \cdot \sin\theta^{ij} - \\ & - (\boldsymbol{\delta}_{(lm)} - n^i_{(l)} \cdot n^i_{(m)}) \cdot (x^i_{(m)} - x^j_{(m)}) \cdot \cos\theta^{ij} \frac{\partial \theta^{ij}}{\partial x^h_{(v)}} \end{aligned} \tag{D.42}$$

And the expression of the second derivative is included next.

$$\begin{aligned} \frac{\partial^2 d^{ij}_{(l)}}{\partial x^h_{(v)} \partial x^s_{(w)}} = {} & e_{(lmk)} \, (x^i_{(k)} - x^j_{(k)}) \left( \frac{\partial^2 n^i_{(m)}}{\partial x^h_{(v)} \partial x^s_{(w)}} \cos\theta^{ij} - \frac{\partial n^i_{(m)}}{\partial x^h_{(v)}} \sin\theta^{ij} \frac{\partial \theta^{ij}}{\partial x^s_{(w)}} \right) + \\ & + (\boldsymbol{\delta}^{is} - \boldsymbol{\delta}^{js}) \, e_{(lmw)} \frac{\partial n^i_{(m)}}{\partial x^h_{(v)}} \cos\theta^{ij} + (\boldsymbol{\delta}^{ih} - \boldsymbol{\delta}^{jh}) \, e_{(lmv)} \frac{\partial n^i_{(m)}}{\partial x^s_{(w)}} \cos\theta^{ij} - \end{aligned}$$

$$
\begin{aligned}
&- e_{(lmk)}\,\frac{\partial n^i_{(m)}}{\partial x^s_{(w)}}\,(x^i_{(k)}-x^j_{(k)})\,\sin\theta^{ij}\,\frac{\partial\theta^{ij}}{\partial x^h_{(v)}} - (\boldsymbol{\delta}^{ih}\underline{-}\,\boldsymbol{\delta}^{jh})\,e_{(lmv)}\,n^i_{(m)}\,\sin\theta^{ij}\,\frac{\partial\theta^{ij}}{\partial x^s_{(w)}} - \\
&-(\boldsymbol{\delta}^{is}\underline{-}\,\boldsymbol{\delta}^{js})\,e_{(lmw)}\,n^i_{(m)}\,\sin\theta^{ij}\,\frac{\partial\theta^{ij}}{\partial x^h_{(v)}} - e_{(lmk)}\,n^i_{(m)}\,(x^i_{(k)}-x^j_{(k)})\,\cos\theta^{ij}\,\frac{\partial\theta^{ij}}{\partial x^h_{(v)}}\,\frac{\partial\theta^{ij}}{\partial x^s_{(w)}} - \\
&-e_{(lmk)}\,n^i_{(m)}\,(x^i_{(k)}-x^j_{(k)})\,\sin\theta^{ij}\,\frac{\partial^2\theta^{ij}}{\partial x^h_{(v)}\partial x^s_{(w)}} + (x^i_{(m)}-x^j_{(m)})\,\sin\theta^{ij}\,\left(\frac{\partial n^i_{(l)}}{\partial x^h_{(v)}}\,\frac{\partial n^i_{(m)}}{\partial x^s_{(w)}} + \right. \\
&\left. + \frac{\partial n^i_{(l)}}{\partial x^s_{(w)}}\,\frac{\partial n^i_{(m)}}{\partial x^h_{(v)}} + n^i_{(l)}\,\frac{\partial^2 n^i_{(m)}}{\partial x^h_{(v)}\partial x^s_{(w)}} + \frac{\partial^2 n^i_{(l)}}{\partial x^h_{(v)}\partial x^s_{(w)}}\,n^i_{(m)}\right) + \\
&+ (\boldsymbol{\delta}^{is}\underline{-}\,\boldsymbol{\delta}^{js})\,\frac{\partial n^i_{(l)}}{\partial x^h_{(v)}}\,n^i_{(w)}\,\sin\theta^{ij} + (\boldsymbol{\delta}^{ih}\underline{-}\,\boldsymbol{\delta}^{jh})\,\frac{\partial n^i_{(l)}}{\partial x^s_{(w)}}\,n^i_{(v)}\,\sin\theta^{ij} + \\
&+ n^i_{(m)}\,(x^i_{(m)}-x^j_{(m)})\,\cos\theta^{ij}\,\left(\frac{\partial n^i_{(l)}}{\partial x^h_{(v)}}\,\frac{\partial\theta^{ij}}{\partial x^s_{(w)}} + \frac{\partial n^i_{(l)}}{\partial x^s_{(w)}}\,\frac{\partial\theta^{ij}}{\partial x^h_{(v)}}\right) + \\
&+ (\boldsymbol{\delta}^{is}\underline{-}\,\boldsymbol{\delta}^{js})\,n^i_{(l)}\,\frac{\partial n^i_{(w)}}{\partial x^h_{(v)}}\,\sin\theta^{ij} + (\boldsymbol{\delta}^{ih}\underline{-}\,\boldsymbol{\delta}^{jh})\,n^i_{(l)}\,\frac{\partial n^i_{(v)}}{\partial x^s_{(w)}}\,\sin\theta^{ij} + \\
&+ n^i_{(l)}\,(x^i_{(m)}-x^j_{(m)})\,\cos\theta^{ij}\,\left(\frac{\partial n^i_{(m)}}{\partial x^h_{(v)}}\,\frac{\partial\theta^{ij}}{\partial x^s_{(w)}} + \frac{\partial n^i_{(m)}}{\partial x^s_{(w)}}\,\frac{\partial\theta^{ij}}{\partial x^h_{(v)}}\right) - \\
&- (\boldsymbol{\delta}^{ih}\underline{-}\,\boldsymbol{\delta}^{jh})\,(\boldsymbol{\delta}_{(lv)} - n^i_{(l)}\,n^i_{(v)})\,\cos\theta^{ij}\,\frac{\partial\theta^{ij}}{\partial x^s_{(w)}} - \\
&- (\boldsymbol{\delta}^{is}\underline{-}\,\boldsymbol{\delta}^{js})\,(\boldsymbol{\delta}_{(lw)} - n^i_{(l)}\,n^i_{(w)})\,\cos\theta^{ij}\,\frac{\partial\theta^{ij}}{\partial x^h_{(v)}} + \\
&+ (\boldsymbol{\delta}_{(lm)} - n^i_{(l)}\,n^i_{(m)})\,(x^i_{(m)}-x^j_{(m)})\,\sin\theta^{ij}\,\left(\frac{\partial\theta^{ij}}{\partial x^h_{(v)}}\,\frac{\partial\theta^{ij}}{\partial x^s_{(w)}} - \frac{\partial^2\theta^{ij}}{\partial x^h_{(v)}\partial x^s_{(w)}}\right)
\end{aligned}
\tag{D.43}
$$

## D.5 Derivatives of $\theta^{ij}$

$\theta^{ij}$ is the angle of the drilling rotation as defined in equation (9.33). The first and second derivatives are presented below.

$$
\frac{\partial\theta^{ij}}{\partial x^h_{(v)}} = \frac{\partial\alpha^{ij}}{\partial x^h_{(v)}} - \frac{\partial\alpha^{ji}}{\partial x^h_{(v)}} = \frac{1}{z_i}\sum_{\substack{k=1\\k\neq j}}^{z_i}\frac{\partial\beta^{jk}_i}{\partial x^h_{(v)}} - \frac{1}{z_j}\sum_{\substack{k=1\\k\neq i}}^{z_j}\frac{\partial\beta^{ik}_j}{\partial x^h_{(v)}} \tag{D.44}
$$

$$
\begin{aligned}
\frac{\partial^2\theta^{ij}}{\partial x^h_{(v)}\partial x^s_{(w)}} &= \frac{\partial^2\alpha^{ij}}{\partial x^h_{(v)}\partial x^s_{(w)}} - \frac{\partial^2\alpha^{ji}}{\partial x^h_{(v)}\partial x^s_{(w)}} = \\
&= \frac{1}{z_i}\sum_{\substack{k=1\\k\neq j}}^{z_i}\frac{\partial^2\beta^{jk}_i}{\partial x^h_{(v)}\partial x^s_{(w)}} - \frac{1}{z_j}\sum_{\substack{k=1\\k\neq i}}^{z_j}\frac{\partial^2\beta^{ik}_j}{\partial x^h_{(v)}\partial x^s_{(w)}}
\end{aligned}
\tag{D.45}
$$

And $\beta_i^{jk}$ has been defined in equation (9.1).

$$\frac{\partial \beta_i^{jk}}{\partial x_{(v)}^h} = \frac{(\boldsymbol{e}^{ij} \cdot \boldsymbol{e}^{ik}) \cdot \dfrac{\partial |\boldsymbol{e}^{ij} \boldsymbol{e}^{ik} \boldsymbol{n}^i|}{\partial x_{(v)}^h} - |\boldsymbol{e}^{ij} \boldsymbol{e}^{ik} \boldsymbol{n}^i| \cdot \dfrac{\partial (\boldsymbol{e}^{ij} \cdot \boldsymbol{e}^{ik})}{\partial x_{(v)}^h}}{(\boldsymbol{e}^{ij} \cdot \boldsymbol{e}^{ik})^2 + |\boldsymbol{e}^{ij} \boldsymbol{e}^{ik} \boldsymbol{n}^i|^2} \tag{D.46}$$

$$\begin{aligned}
\frac{\partial^2 \beta_i^{jk}}{\partial x_{(v)}^h \partial x_{(w)}^s} = \Bigg\{ & -2 \cdot \frac{\partial \beta_i^{jk}}{\partial x_{(v)}^h} \cdot \left[ (\boldsymbol{e}^{ij} \cdot \boldsymbol{e}^{ik}) \cdot \frac{\partial (\boldsymbol{e}^{ij} \cdot \boldsymbol{e}^{ik})}{\partial x_{(w)}^s} + \right. \\
& \left. + |\boldsymbol{e}^{ij} \boldsymbol{e}^{ik} \boldsymbol{n}^i| \cdot \frac{\partial |\boldsymbol{e}^{ij} \boldsymbol{e}^{ik} \boldsymbol{n}^i|}{\partial x_{(w)}^s} \right] + \frac{\partial (\boldsymbol{e}^{ij} \cdot \boldsymbol{e}^{ik})}{\partial x_{(w)}^s} \cdot \frac{\partial |\boldsymbol{e}^{ij} \boldsymbol{e}^{ik} \boldsymbol{n}^i|}{\partial x_{(v)}^h} - \\
& - \frac{\partial (\boldsymbol{e}^{ij} \cdot \boldsymbol{e}^{ik})}{\partial x_{(v)}^h} \cdot \frac{\partial |\boldsymbol{e}^{ij} \boldsymbol{e}^{ik} \boldsymbol{n}^i|}{\partial x_{(w)}^s} + (\boldsymbol{e}^{ij} \cdot \boldsymbol{e}^{ik}) \cdot \frac{\partial^2 |\boldsymbol{e}^{ij} \boldsymbol{e}^{ik} \boldsymbol{n}^i|}{\partial x_{(v)}^h \partial x_{(w)}^s} - \\
& - |\boldsymbol{e}^{ij} \boldsymbol{e}^{ik} \boldsymbol{n}^i| \cdot \frac{\partial^2 (\boldsymbol{e}^{ij} \cdot \boldsymbol{e}^{ik})}{\partial x_{(v)}^h \partial x_{(w)}^s} \Bigg\} \cdot \left[ (\boldsymbol{e}^{ij} \cdot \boldsymbol{e}^{ik})^2 + |\boldsymbol{e}^{ij} \boldsymbol{e}^{ik} \boldsymbol{n}^i|^2 \right]^{-1}
\end{aligned} \tag{D.47}$$

The vectors $\boldsymbol{e}^{ij}$ and $\boldsymbol{e}^{ik}$ have been defined in equations (9.2) and (9.3); see figure 9.2 on page 103.

$$\frac{\partial |\boldsymbol{e}^{ij} \boldsymbol{e}^{ik} \boldsymbol{n}^i|}{\partial x_{(v)}^h} = \left| \frac{\partial \boldsymbol{e}^{ij}}{\partial x_{(v)}^h} \, \boldsymbol{e}^{ik} \, \boldsymbol{n}^i \right| + \left| \boldsymbol{e}^{ij} \, \frac{\partial \boldsymbol{e}^{ik}}{\partial x_{(v)}^h} \, \boldsymbol{n}^i \right| \tag{D.48}$$

$$\frac{\partial (\boldsymbol{e}^{ij} \cdot \boldsymbol{e}^{ik})}{\partial x_{(v)}^h} = \frac{\partial e_{(l)}^{ij}}{\partial x_{(v)}^h} \cdot e_{(l)}^{ik} + e_{(l)}^{ij} \cdot \frac{\partial e_{(l)}^{ik}}{\partial x_{(v)}^h} \tag{D.49}$$

$$\begin{aligned}
\frac{\partial e_{(l)}^{ij}}{\partial x_{(v)}^h} = & (\boldsymbol{\delta}^{jh} - \boldsymbol{\delta}^{ih}) \cdot (\boldsymbol{\delta}_{(lv)} - n_{(l)}^i \cdot n_{(v)}^i) - \\
& - \left( \frac{\partial n_{(l)}^i}{\partial x_{(v)}^h} \cdot n_{(m)}^i + n_{(l)}^i \cdot \frac{\partial n_{(m)}^i}{\partial x_{(v)}^h} \right) \cdot (x_{(m)}^j - x_{(m)}^i)
\end{aligned} \tag{D.50}$$

$$\begin{aligned}
\frac{\partial^2 |\boldsymbol{e}^{ij} \boldsymbol{e}^{ik} \boldsymbol{n}^i|}{\partial x_{(v)}^h \partial x_{(w)}^s} = & \left| \frac{\partial^2 \boldsymbol{e}^{ij}}{\partial x_{(v)}^h \partial x_{(w)}^s} \, \boldsymbol{e}^{ik} \, \boldsymbol{n}^i \right| + \left| \frac{\partial \boldsymbol{e}^{ij}}{\partial x_{(v)}^h} \, \frac{\partial \boldsymbol{e}^{ik}}{\partial x_{(w)}^s} \, \boldsymbol{n}^i \right| + \left| \frac{\partial \boldsymbol{e}^{ij}}{\partial x_{(v)}^h} \, \boldsymbol{e}^{ik} \, \frac{\partial \boldsymbol{n}^i}{\partial x_{(w)}^s} \right| + \\
& + \left| \boldsymbol{e}^{ij} \, \frac{\partial^2 \boldsymbol{e}^{ik}}{\partial x_{(v)}^h \partial x_{(w)}^s} \, \boldsymbol{n}^i \right| + \left| \frac{\partial \boldsymbol{e}^{ij}}{\partial x_{(w)}^s} \, \frac{\partial \boldsymbol{e}^{ik}}{\partial x_{(v)}^h} \, \boldsymbol{n}^i \right| + \left| \boldsymbol{e}^{ij} \, \frac{\partial \boldsymbol{e}^{ik}}{\partial x_{(w)}^s} \, \frac{\partial \boldsymbol{n}^i}{\partial x_{(v)}^h} \right|
\end{aligned} \tag{D.51}$$

$$\begin{aligned}
\frac{\partial^2 (\boldsymbol{e}^{ij} \cdot \boldsymbol{e}^{ik})}{\partial x_{(v)}^h \partial x_{(w)}^s} = & \frac{\partial^2 e_{(l)}^{ij}}{\partial x_{(v)}^h \partial x_{(w)}^s} \cdot e_{(l)}^{ik} + e_{(l)}^{ij} \cdot \frac{\partial^2 e_{(l)}^{ik}}{\partial x_{(v)}^h \partial x_{(w)}^s} + \\
& + \frac{\partial e_{(l)}^{ij}}{\partial x_{(v)}^h} \cdot \frac{\partial e_{(l)}^{ik}}{\partial x_{(w)}^s} + \frac{\partial e_{(l)}^{ij}}{\partial x_{(w)}^s} \cdot \frac{\partial e_{(l)}^{ik}}{\partial x_{(v)}^h}
\end{aligned} \tag{D.52}$$

$$\begin{aligned}\frac{\partial^2 e^{ij}_{(l)}}{\partial x^h_{(v)}\partial x^s_{(w)}} = &-(\boldsymbol{\delta}^{jh}-\boldsymbol{\delta}^{ih})\cdot\left(\frac{\partial n^i_{(l)}}{\partial x^s_{(w)}}\cdot n^i_{(v)}+n^i_{(l)}\cdot\frac{\partial n^i_{(v)}}{\partial x^s_{(w)}}\right)-\\ &-(\boldsymbol{\delta}^{js}-\boldsymbol{\delta}^{is})\cdot\left(\frac{\partial n^i_{(l)}}{\partial x^h_{(v)}}\cdot n^i_{(w)}+n^i_{(l)}\cdot\frac{\partial n^i_{(w)}}{\partial x^h_{(v)}}\right)-\\ &-\left(\frac{\partial^2 n^i_{(l)}}{\partial x^h_{(v)}\partial x^s_{(w)}}\cdot n^i_{(m)}+\frac{\partial n^i_{(l)}}{\partial x^h_{(v)}}\cdot\frac{\partial n^i_{(m)}}{\partial x^s_{(w)}}+\right.\\ &\left.+\frac{\partial n^i_{(l)}}{\partial x^s_{(w)}}\cdot\frac{\partial n^i_{(m)}}{\partial x^h_{(v)}}+n^i_{(l)}\cdot\frac{\partial^2 n^i_{(m)}}{\partial x^h_{(v)}\partial x^s_{(w)}}\right)\cdot(x^j_{(m)}-x^i_{(m)})\end{aligned} \tag{D.53}$$

## D.6 Derivatives of $\varphi^{ij}$

$\varphi^{ij}$ is the angle of the inclination of the tangent of the curved edge at the node with respect to its chord as defined in equation (9.18). The first and second derivatives are presented below.

$$\begin{aligned}\frac{\partial\varphi^{ij}}{\partial x^h_{(v)}} = &-\frac{\tan\varphi^{ij}}{\|\boldsymbol{x}^i-\boldsymbol{x}^j\|^2}\cdot(\boldsymbol{\delta}^{ih}-\boldsymbol{\delta}^{jh})\cdot(x^i_{(v)}-x^j_{(v)})-\\ &-\frac{\sec\varphi^{ij}}{\|\boldsymbol{x}^i-\boldsymbol{x}^j\|}\cdot\left[(\boldsymbol{\delta}^{ij}-\boldsymbol{\delta}^{jh})\cdot n^i_{(v)}+(x^i_{(k)}-x^j_{(k)})\frac{\partial n^i_{(k)}}{\partial x^h_{(v)}}\right]\end{aligned} \tag{D.54}$$

$$\begin{aligned}\frac{\partial^2\varphi^{ij}}{\partial x^h_{(v)}\partial x^s_{(w)}} = &\tan\varphi^{ij}\cdot\left\{\frac{\partial\varphi^{ij}}{\partial x^h_{(v)}}\cdot\frac{\partial\varphi^{ij}}{\partial x^s_{(w)}}+\frac{(\boldsymbol{\delta}^{ih}-\boldsymbol{\delta}^{jh})(\boldsymbol{\delta}^{is}-\boldsymbol{\delta}^{js})}{\|\boldsymbol{x}^i-\boldsymbol{x}^j\|^2}\cdot\right.\\ &\left.\cdot\left[\frac{(x^i_{(v)}-x^j_{(v)})(x^i_{(w)}-x^j_{(w)})}{\|\boldsymbol{x}^i-\boldsymbol{x}^j\|^2}-\boldsymbol{\delta}_{(vw)}\right]\right\}-\frac{\partial\varphi^{ij}}{\partial x^h_{(v)}}\cdot\frac{(\boldsymbol{\delta}^{is}-\boldsymbol{\delta}^{js})(x^i_{(w)}-x^j_{(w)})}{\|\boldsymbol{x}^i-\boldsymbol{x}^j\|^2}-\\ &-\frac{\partial\varphi^{ij}}{\partial x^s_{(w)}}\cdot\frac{(\boldsymbol{\delta}^{ih}-\boldsymbol{\delta}^{jh})(x^i_{(v)}-x^j_{(v)})}{\|\boldsymbol{x}^i-\boldsymbol{x}^j\|^2}-\frac{\sec\varphi^{ij}}{\|\boldsymbol{x}^i-\boldsymbol{x}^j\|}\cdot\left[(\boldsymbol{\delta}^{ih}-\boldsymbol{\delta}^{jh})\cdot\frac{\partial n^i_{(v)}}{\partial x^s_{(w)}}+\right.\\ &\left.+(\boldsymbol{\delta}^{is}-\boldsymbol{\delta}^{js})\cdot\frac{\partial n^i_{(w)}}{\partial x^h_{(v)}}+(x^i_{(k)}-x^j_{(k)})\frac{\partial^2 n^i_{(k)}}{\partial x^h_{(v)}\partial x^s_{(w)}}\right]\end{aligned} \tag{D.55}$$

# Bibliography


[1] *"ABAQUS Theory Manual, ABAQUS/Standard User's Manual"*. vol. II. ABAQUS. 1998 (cit. on p. 165).

[2] Sohrabuddin Ahmad, Bruce M. Irons, and O. C. Zienkiewicz. "Analysis of thick and thin shell structures by curved finite elements". In: *International Journal for Numerical Methods in Engineering* 2.3 (July 1970), pp. 419–451. ISSN: 0029-5981. DOI: 10.1002/nme.1620020310 (cit. on p. 65).

[3] Alinghi et al. "The Simulation Race for America's Cup. Yacht designers used engineering simulation in a variety of applications to edge out the competition". In: *ANSYS Advantage* 1 (2 2007), pp. 3–6. URL: http://www.ansys.com/magazine/issues/1-2-2007-biomedical/03-americas-cup.pdf (cit. on pp. 202, 203).

[4] *"ANSYS User's Manual"*. Report Version 5.5. ANSYS. 1998 (cit. on p. 165).

[5] Inma Ortigosa Barragán. "Development of a decision support system for the design and adjustment of sailboat rigging". Director: Julio García-Espinosa. PhD thesis. Universitat Politècnica de Catalunya, 2012. URL: http://cataleg.upc.edu/record=b1418440~S1*cat (cit. on p. 20).

[6] Klaus-Jurgen Bathe, Phil-Seung Lee, and Jean-François Hiller. "'Towards improving the MITC9 shell element'". In: *"Computers and Structures"* 81 (2003), pp. 477–489. DOI: 10.1016/S0045-7949(02)00483-2 (cit. on p. 165).

[7] Jean-Pierre Baudet. "Sail of one piece three dimensional laminated fabric having uninterrupted load bearing yarns. A one piece sail is made on a mold and includes an outer impervious layer, such as film, and an inner layer of continuous and uninterrupted yarns disposed in continuous trajectories from one edge of the sail to the other and carrying the majority of the load imposed on the sail." Pat. 5,097,784 (United States). North Sails Group Inc. Aug. 21, 1990. URL: http://patft.uspto.gov/netacgi/nph-Parser?Sect1=PTO1&Sect2=HITOFF&d=PALL&p=1&u=%2Fnetahtml%2FPTO%2Fsrchnum.htm&r=1&f=G&l=50&s1=5,097,784.PN.&OS=PN/5,097,784&RS=PN/5,097,784 (cit. on pp. 5, 202).

[8] Y Bazilevs et al. “Isogeometric analysis using T-splines”. In: *Computer Methods in Applied Mechanics and Engineering* 199.5-8 (Jan. 2010), pp. 229–263. ISSN: 00457825. DOI: 10.1016/j.cma.2009.02.036 (cit. on p. 30).

[9] Ted Belytschko, Wing Kam Liu, and Brian Moran. *Nonlinear Finite Elements for Continua and Structures*. first. Wiley, 2000. ISBN: 978-0471-98774-1. URL: https://www.wiley.com/en-us/Nonlinear+Finite+Elements+for+Continua+and+Structures%2C+2nd+Edition-p-9781118700082 (cit. on pp. 65, 83, 193).

[10] Ted Belytschko et al. “Stress projection for membrane and shear locking in shell finite elements”. In: *"Computer Methods in Applied Mechanics and Engineering"* 51 (1985), pp. 221–258. DOI: 10.1016/0045-7825(85)90035-0 (cit. on pp. 164, 167, 168).

[11] D.J. Benson, Y. Bazilevs, and T.J.R. Hughes. “Isogeometric shell analysis: The Reissner–Mindlin shell”. In: *Computer Methods in Applied Mechanics and Engineering* 199 (5-8 2010): *Computational Geometry and Analysis*, pp. 276–289. DOI: 10.1016/j.cma.2009.05.011 (cit. on pp. 25, 26).

[12] M Bischoff, W A Wall, and E Ramm. “Chapter 3: Models and Finite Elements for Thin-walled Structures”. In: *Encyclopedia of Computational Mechanics. Volume 2: Solids and Structures*. Ed. by Erwin Stein, René de Borst, and Thomas J. R. Hughes. 1921. Chichester, UK: John Wiley & Sons, Ltd, Nov. 2004. Chap. Chapter 3: p. 79. ISBN: 0470846992. DOI: 10.1002/0470091355 (cit. on pp. 65, 85, 198).

[13] Manfred Bischoff and Ekkehard Ramm. “On the physical significance of higher order kinematic and static variables in a three-dimensional shell formulation”. In: *International Journal of Solids and Structures* 37.46-47 (Nov. 2000), pp. 6933–6960. ISSN: 00207683. DOI: 10.1016/S0020-7683(99)00321-2 (cit. on p. 182).

[14] *BOWLER ON MOVISTAR. Farr Yacht Design’s Russel Bowler talks about his first assessment of the damage that resulted in movistar being abandoned*. Volvo Ocean Race 2005-2006. May 25, 2006. URL: http://www.volvooceanrace.com/news/article/2006/may/bowler/index.aspx (cit. on p. 206).

[15] D. Briassoulis. “Testing the asymptotic behaviour of shell elements. Part I: the classical benchmark tests”. In: *International Journal for Numerical Methods in Engineering* 54.3 (May 2002), pp. 421–452. ISSN: 0029-5981. DOI: 10.1002/nme.436 (cit. on p. 56).

[16] D. Briassoulis. “Testing the asymptotic behaviour of shell elements. Part II: New limit tests: analytical solutions and the RFNS element case”. In: *International Journal for Numerical Methods in Engineering* 54.5 (June 2002), pp. 631–670. ISSN: 0029-5981. DOI: 10.1002/nme.435 (cit. on p. 56).

[17] Demetres Briassoulis. “Asymptotic deformation modes of benchmark problems suitable for evaluating shell elements”. In: *Computer Methods in Applied Mechanics and Engineering* 194.21-24 (June 2005), pp. 2385–2405. ISSN: 00457825. DOI: 10.1016/j.cma.2004.07.038 (cit. on p. 56).

[18] Norbert Büchter and Ekkerhard Ramm. “Shell theory vs degeneration—A comparison in large rotation finite element analysis”. In: *International Journal for Numerical Methods in Engineering* 34 (1992), pp. 39–59. DOI: 10.1002/nme.1620340105 (cit. on p. 85).

[19] P. de Casteljau. *Outillages méthodes calcul*. Tech. rep. Paris: A. Citroën, 1959 (cit. on p. 44).

[20] P. de Casteljau. *Courbes et surfaces à pôles*. Tech. rep. Paris: A. Citroën, 1963 (cit. on p. 44).

[21] Pablo Pérez del Castillo and Julio García. *Un modelo numérico para el análisis de velas*. Informe Técnico IT-466. Barcelona: CIMNE, Dec. 2005. 143 pp. (cit. on p. 20).

[22] D. Chapelle and K.J. Bathe. “Fundamental considerations for the finite element analysis of shell structures”. In: *Computers & Structures* 66.1 (Jan. 1998), pp. 19–36. ISSN: 00457949. DOI: 10.1016/S0045-7949(97)00078-3 (cit. on pp. 56, 168, 169).

[23] T. Charvet, F. Hauville, and S. Huberson. “Numerical simulation of the flow over sails in real sailing conditions”. In: *Journal of Wind Engineering and Industrial Aerodynamics* 63 (1996): *Special issue on sail aerodynamics*, pp. 111–129. DOI: 10.1016/S0167-6105(96)00072-4 (cit. on p. 20).

[24] F. Cirak, M. Ortiz, and P. Schröder. “Subdivision surfaces: a new paradigm for thin shell finite-element analysis.” In: *International Journal for Numerical Methods in Engineering* 47.12 (2000), pp. 2039–2072. DOI: 10.1002/(SICI)1097-0207(20000430)47:12%3C2039::AID-NME872%3E3.0.CO;2-1 (cit. on pp. 25, 29, 33, 186).

[25] Fehmi Cirak and Michael Ortiz. “Fully C 1 -conforming subdivision elements for finite deformation thin-shell analysis”. In: *International Journal for Numerical Methods in Engineering* 51.7 (2001), pp. 813–833. DOI: 10.1002/nme.182 (cit. on pp. 29, 186).

[26] Fehmi Cirak et al. “Integrated modeling, finite-element analysis, and engineering design for thin-shell structures using subdivision”. In: *Computer-Aided Design* 34.2 (Feb. 2002), pp. 137–148. ISSN: 00104485. DOI: 10.1016/S0010-4485(01)00061-6 (cit. on pp. 29, 186).

[27] R. Clough and J. Tocher. “Finite element stiffness matrices for analysis of plates in bending”. In: *Proceedings of Conference on Matrix Methods in Structural Analysis*. 1965 (cit. on pp. 23, 28).

[28] *Compass participa en la Copa América de la mano de Alinghi y Great Britain*. 2003. URL: http://www.compassis.com/compass/Compass/Prensa/Copa+america (cit. on pp. 183, 204).

[29] Ronald Cools and Philip Rabinowitz. “Monomial cubature rules since "Stroud": a compilation”. In: *Journal of Computational and Applied Mathematics* 48 (1993), pp. 309–326. DOI: 10.1016/0377-0427(93)90027-9 (cit. on p. 82).

[30] Xiangyang Cui et al. “Analysis of plates and shells using an edge-based smoothed finite element method”. In: *Computational Mechanics* 45 (2010), pp. 141–156. DOI: 10.1007/s00466-009-0429-9 (cit. on p. 177).

[31] Choi D et al. “Membrane locking in the finite element computation of very thin elastic shells”. In: *Modelisation mathematique et analyse numerique* 32.2 (1998), pp. 131–152. URL: http://www.numdam.org/item?id=M2AN_1998__32_2_131_0 (cit. on pp. 99, 101, 162, 173).

[32] Rick Deppe. *Puma breaks boom*. Volvo Ocean Race 2008-2009. Jan. 24, 2009. URL: http://www.youtube.com/watch?v=s9S60G47Ikg (cit. on p. 206).

[33] D.A. Dunavant. “High degree efficient symmetrical Gaussian quadrature rules for the triangle”. In: *International Journal for Numerical Methods in Engineering* 21 (1985), pp. 1129–1148. DOI: 10.1002/nme.1620210612 (cit. on p. 82).

[34] Nguyen Tien Dung and Garth N. Wells. “Geometrically nonlinear formulation for thin shells without rotation degrees of freedom”. In: *Computer Methods in Applied Mechanics and Engineering* 197.33-40 (June 2008), pp. 2778–2788. ISSN: 00457825. DOI: 10.1016/j.cma.2008.01.001 (cit. on p. 30).

[35] *Element types used in structural analysis*. Moldflow Flex. Autodesk. 2016. URL: http://help.autodesk.com/view/MFIWS/2016/ENU/?guid=GUID-C6040A5F-6941-450C-B147-FBC16693CC13 (cit. on p. 24).

[36] J. Burns Fallow. “America’s Cup sail design”. In: *Journal of Wind Engineering and Industrial Aerodynamics* 63 (1996): *Special issue on sail aerodynamics*, pp. 183–192. DOI: 10.1016/S0167-6105(96)00075-X (cit. on p. 202).

[37] G. Farin. *Curves and Surfaces for CAGD. A practical guide*. 5th ed. 340 Pine Street, Sixth Floor, San Francisco, CA 94104-3205, USA: Morgan Kaufmann Publishers, 2002. URL: https://www.elsevier.com/books/curves-and-surfaces-for-cagd/farin/978-1-55860-737-8 (cit. on pp. 23, 44, 52).

[38] Gerald Farin. “Triangular Bernstein-Bézier patches”. In: *Computer Aided Geometric Design* 3.2 (Aug. 1986), pp. 83–127. ISSN: 01678396. DOI: 10.1016/0167-8396(86)90016-6 (cit. on p. 47).

[39] Carlos A. Felippa. “A study of optimal membrane triangles with drilling freedoms”. In: *Computer Methods in Applied Mechanics and Engineering* 192.16-18 (Apr. 2003), pp. 2125–2168. ISSN: 00457825. DOI: 10.1016/S0045-7825(03)00253-6 (cit. on pp. 102, 108).

[40] Richard G.J. Flay. "A twisted flow wind tunnel for testing yacht sails". In: *Journal of Wind Engineering and Industrial Aerodynamics* 63 (1996): *Special issue on sail aerodynamics*, pp. 171–182. DOI: 10.1016/S0167-6105(96)00080-3 (cit. on p. 202).

[41] F. G. Flores and E. Oñate. "Improvements in the membrane behaviour of the three node rotation-free BST shell triangle using an assumed strain approach." In: *Computer Methods in Applied Mechanics and Engineering* 194.6-8 (2005), pp. 907–932. DOI: 10.1016/j.cma.2003.08.012 (cit. on pp. 25, 28, 33, 197).

[42] Fernando G Flores and Eugenio Oñate. "A rotation-free shell triangle for the analysis of kinked and branching shells". In: *International Journal for Numerical Methods in Engineering* 69.7 (Feb. 2007), pp. 1521–1551. ISSN: 00295981. DOI: 10.1002/nme.1823 (cit. on p. 137).

[43] David Flynn. "Code Zero—The new way to close reach". In: *Sailing World* (Mar. 2001), pp. 62–64. URL: http://www.quantumsails.co.za/downloads/Code_Zero.pdf (cit. on p. 6).

[44] Wilhelm Flügge. *Statique et dynamique des coques*. Ed. by Eyrolles. Paris: Eyrolles, 1960. URL: http://cataleg.upc.edu/record=b1036939~S1*cat (cit. on p. 22).

[45] Erez Gal and Robert Levy. "Geometrically Nonlinear Analysis of Shell Structures Using a Flat Triangular Shell Finite Element". In: *Archives of Computational Methods in Engineering* 13.3 (2006), pp. 331–388. DOI: 10.1007/BF02736397 (cit. on p. 21).

[46] J. García-Espinosa, I. Ortigosa, and A. Fernández. "Desarrollo de un sistema de apoyo a la decisión para optimizar el comportamiento de barcos de vela". In: *Revista Internacional de Métodos Numéricos para Cálculo y Diseño en Ingeniería* 31.3 (July 2015), pp. 146–153. ISSN: 02131315. DOI: 10.1016/j.rimni.2014.04.002 (cit. on p. 20).

[47] Julio García-Espinosa, Abel Coll, and Eugenio Oñate. "Advances in the development of an unstructured FEM solver for fluid-structure interaction problems in marine engineering". In: *Computational Methods in Marine Engineering III*. (Trondheim, Norway). Ed. by T. Kvamsdal et al. Barcelona, Spain: CIMNE, 2009, pp. 155–158. ISBN: 978-84-96736-66-5 (cit. on p. 204).

[48] Timothy D. Gatzke and Cindy M. Grimm. "Estimating curvature on triangular meshes". In: *International Journal of Shape Modeling* 12.1 (2006), pp. 1–28. DOI: 10.1142/S0218654306000810 (cit. on pp. 179, 181).

[49] Mattias Gärdsback and Gunnar Tibert. "A comparison of rotation-free triangular shell elements for unstructured meshes". In: *Computer Methods in Applied Mechanics and Engineering* 196 (49-52 2007), pp. 5001–5015. DOI: 10.1016/j.cma.2007.06.017 (cit. on pp. 24, 25, 28, 186).

[50] S. Güzey et al. “Design and development of a discontinuous Galerkin method for shells”. In: *Computer Methods in Applied Mechanics and Engineering* 195.25-28 (May 2006), pp. 3528–3548. ISSN: 00457825. DOI: 10.1016/j.cma.2005.08.001 (cit. on p. 30).

[51] H Hakula, Y Leino, and J. Pitkäranta. “Scale resolution, locking, and high-order finite element modelling of shells”. In: *Computer Methods in Applied Mechanics and Engineering* 133 (1996), pp. 157–182. DOI: 10.1016/0045-7825(95)00939-6 (cit. on pp. 101, 163, 171).

[52] John G. Hamilton and Jocelyn M. Patterson. “Structural Design and Analysis of an America’s Cup Yacht”. In: *SAMPE Journal* 28 (6 1992), pp. 9–13 (cit. on p. 206).

[53] Kevin C. Horrigan. *Bringing a Virtual Wind Tunnel to Market*. Tech. rep. Sponsored by North Sails Performance Resource Group. Thayer School of Engineering, Dartmouth College, Sept. 2003 (cit. on p. 205).

[54] Thomas J.R. Hughes and Wing Kam Liu. “"Nonlinear finite element analysis of shells: Part I. three-dimensional shells"”. In: *"Computer Methods in Applied Mechanics and Engineering"* 26.3 (1981), pp. 331–362. DOI: 10.1016/0045-7825(81)90121-3 (cit. on p. 165).

[55] T.J.R Hughes. *The Finite Element Method; Linear Static and Dynamic Finite Element Analysis*. Englewood Cliffs, New Jersey: Prentice Hall, 1987 (cit. on p. 106).

[56] T.J.R. Hughes, J.A. Cottrell, and Y. Bazilevs. “Isogeometric Analysis: CAD, finite elements, NURBS, exact geometry and mesh refinement.” In: *Computer Methods in Applied Mechanics and Engineering* 194.39-41 (2005), pp. 4135–4195. DOI: 10.1016/j.cma.2004.10.008 (cit. on pp. 25, 30, 33, 44).

[57] Mickey Ickert. “FINNatics - The History and Techniques of Finn Sailing”. In: International Finn Association, 1999. Chap. 32. Plastic Fantastic - a new chapter in sail development, pp. 162–163. URL: http://www.finnclass.org/The%20Finn/Finnatics/%2032_Plasticfantasic_162-163.pdf (cit. on p. 5).

[58] Paul Jones and Rich Korpus. “International America’s Cup Class Yacht Design Using Viscous Flow CFD”. In: *The 15th Cheasapeake Sailing Yacht Symposium*. (Annapolis, MD). Ed. by CSYS. The Cheasapeake Sailing Yacht Symposium. 2001. URL: http://appliedfluidtech.com/publications-pdfs/CSYS_2001_Jones.pdf (cit. on pp. 204, 205).

[59] Frank DeBord Jr. et al. “Design Optimization for the International America’s Cup Class”. In: *SNAME Transactions* (2002) (cit. on pp. 8, 204).

[60] James Stackpole Herman Jr. “A Sail Force Dynamometer: Design, implementation and Data Handling”. Master of Science in Naval Architecture and Marine Engineering. English. Master Thesis. Cambridge, MA: Massachusetts Institute of Technology (MIT), 1988. URL: http://hdl.handle.net/1721.1/14491 (cit. on pp. 201, 202).

[61] William Kahan. “"How Futile are Mindless Assessments of Roundoff in Floating-Point Computation?"” Work in progress. Jan. 2006. URL: http://people.eecs.berkeley.edu/~wkahan/Mindless.pdf (cit. on p. 113).

[62] William Kahan. “"Miscalculating Area and Angles of a Needle-like Triangle"”. from Lecture Notes for Introductory Numerical Analysis Classes. Sept. 2014. URL: https://people.eecs.berkeley.edu/~wkahan/Triangle.pdf (cit. on p. 113).

[63] J Kiendl et al. “Isogeometric shell analysis with Kirchhoff–Love elements”. In: *Computer Methods in Applied Mechanics and Engineering* 198.49-52 (2009), pp. 3902–3914. ISSN: 0045-7825. DOI: 10.1016/j.cma.2009.08.013 (cit. on pp. 26, 30, 33).

[64] Hyun-Jung Kim, Yu-Deok Seo, and Sung-Kie Youn. “Isogeometric analysis for trimmed CAD surfaces”. In: *Computer Methods in Applied Mechanics and Engineering* 198.37-40 (Aug. 2009), pp. 2982–2995. ISSN: 00457825. DOI: 10.1016/j.cma.2009.05.004 (cit. on p. 30).

[65] G.R. Kirchhoff. “"Über das Gleichgewicki und die Bewegung einer elastishem Scheibe"”. In: *"Journal für die Reine und Angewandte Mathematik"* 40 (1850), pp. 51–88 (cit. on p. 22).

[66] Patricia Kranz. “Measuring wealth by the foot”. In: *The New York Times* (Mar. 2008). URL: http://www.nytimes.com/2008/03/16/business/16drop.html?_r=1&scp=1&sq=measuring+wealth+by+the+foot&st=nyt (cit. on p. 199).

[67] E. Kreyszig. *Differential Geometry*. Dover, 1991. URL: https://store.doverpublications.com/0486667219.html (cit. on pp. xxv, 34).

[68] A. Laulusa et al. “Evaluation of some shear deformable shell elements”. In: *International Journal of Solids and Structures* 43 (2006), pp. 5033–5054. DOI: 10.1016/j.ijsolstr.2005.08.006 (cit. on pp. 165, 169, 171).

[69] Leonardo Leonetti and H. Nguyen-Xuan. “"A mixed edge-based smoothed solid-shell finite element method (MES-FEM) for laminated shell structures"”. In: *Composite Structures* 208 (2018), pp. 168–179. DOI: 10.1016/j.compstruct.2018.09.077 (cit. on p. 177).

[70] J Linhard, K.-U. Bletzinger, and M. Firl. “Upgrading Membranes to Shells - The CEG Rotation Free Shell Element and its Applications”. In: *9th US National Congress on Computational Mechanics*. Vol. CD-ROM. University of California at Berkeley, USACM. San Francisco, California, USA, July 2007 (cit. on pp. 38, 43).

[71] Johannes Linhard, Roland Wüchner, and Kai-Uwe Bletzinger. ""Upgrading" membranes to shells—The CEG rotation free shell element and its application in structural analysis". In: *Finite Elements in Analysis and Design* 44.1–2 (2007), pp. 63 –74. ISSN: 0168-874X. DOI: 10.1016/j.finel.2007.09.001 (cit. on pp. 25, 38).

[72] A. E. H. Love. "On the small free vibrations and deformations of elastic shells". In: *Philosophical Transactions of the Royal Society of London*. A 179 (1888), pp. 491–546. URL: http://www.jstor.org/stable/90527 (cit. on p. 22).

[73] Richard H. MacNeal. "Perspective on finite elements for shell analysis". In: *Finite Elements in Analysis and Design* 30 (3 1998), pp. 175–186. DOI: 10.1016/S0168-874X(98)00005-5 (cit. on pp. 21, 23, 24, 33).

[74] Jacquelin Magnay. "London 2012 Olympics: Team GB making waves with new technology". In: *Telegraph.co.uk* (Mar. 2010). URL: http://www.telegraph.co.uk/sport/othersports/sailing/7535609/London-2012-Olympics-Team-GB-making-waves-with-new-technology.html (cit. on p. 200).

[75] George Marsh. "America's Cup – pushing materials to their limits". In: *Reinforced plastics* 45 (10 2001), pp. 48–50. DOI: 10.1016/S0034-3617(01)80389-1 (cit. on p. 206).

[76] George Marsh. "This carbon sail-race winner is 'diabolical'". In: *Reinforced plastics* 50 (9 2006), pp. 20–27. DOI: 10.1016/S0034-3617(06)71126-2 (cit. on p. 206).

[77] Nelson Max. "Weights for computing vertex normals from facet normals". In: *Journal of graphics, gpu and game tools* 4.2 (1999), pp. 1–6. DOI: 10.1080/10867651.1999.10487501 (cit. on p. 187).

[78] O. Le Maître, J.E. Souza de Cursi, and S. Huberson. "Large displacement analysis of ideally flexible sails". In: *European Journal of Mechanics - A/Solids* 17.4 (1998), pp. 619–636. DOI: 10.1016/S0997-7538(99)80025-4 (cit. on p. 19).

[79] Jerome H. Milgram. "Naval Architecture Technology used in Winning the 1992 America's Cup Match". In: *SNAME Transactions* 101 (1993), pp. 399–436 (cit. on pp. 203, 204).

[80] Jerome H. Milgram. "Fluid mechanics for sailing vessel design". In: *Annu. Rev. Fluid Mech.* 30 (1998), pp. 613–653. DOI: 10.1146/annurev.fluid.30.1.613 (cit. on p. 207).

[81] R.D. Mindlin. "Influence of rotary inertia and shear on flexural motions of isotropic elastic plates". In: *Journal of Applied Mechanics* 18 (1951) (cit. on p. 23).

[82] R.a.S. Moreira and J. Dias Rodrigues. "A non-conforming plate facet-shell finite element with drilling stiffness". In: *Finite Elements in Analysis and Design* 47.9 (Sept. 2011), pp. 973–981. ISSN: 0168874X. DOI: 10.1016/j.finel.2011.03.013 (cit. on pp. 117, 143, 144).

[83] Gustav Morin. *ERICSSON 3 EMAIL: 'A FOUR-METER CRACK AND AN OPEN HOLE IN THE HULL'*. Volvo Ocean Race 2008-2009. Jan. 27, 2009. URL: http://www.volvooceanrace.com/news/article/2009/January/EMAIL-ERT3-L4-D10-0952/ (cit. on p. 206).

[84] *Movistar abandons ship*. Volvo Ocean Race 2005-2006. May 21, 2006. URL: http://www.volvooceanrace.com/news/article/2006/may/abandon/index.aspx (cit. on p. 206).

[85] Jari Mäkinen. "A Formulation for Flexible Multibody Mechanics". PhD thesis. Tampere University of Technology, 2004. ISBN: 9521512881. URL: http://butler.cc.tut.fi/~jmamakin/vk.pdfhttp://butler.cc.tut.fi/~jmamakin/tutkimus/Raportti.htm (cit. on p. 33).

[86] L. Noels and R. Radovitzky. "A new discontinuous Galerkin method for Kirchhoff–Love shells". In: *Computer Methods in Applied Mechanics and Engineering* 197.33-40 (June 2008), pp. 2901–2929. ISSN: 00457825. DOI: 10.1016/j.cma.2008.01.018 (cit. on p. 30).

[87] Bastian Oesterle, Ekkerhard Ramm, and Manfred Bischoff. "A shear deformable, rotation-free isogeometric shear formulation". In: *Computer Methods in Applied Mechanics and Engineering* 307 (Aug. 2016), pp. 235–255. DOI: 10.1016/j.cma.2016.04.015 (cit. on p. 181).

[88] S. Oller. *Análisis y Cálculo de Estructuras de Materiales Compuestos*. Ref. L60. Barcelona: CIMNE, 2002. 576 pp. ISBN: 84-95999-06-4. URL: http://www.cimne.upc.es/tiendaCIMNE/ProductosCon.asp?id_prod=960 (cit. on p. 206).

[89] S. Oller. *Simulación Numérica del Comportamiento Mecánico de los Materiales Compuestos*. Ref. M74. Barcelona: CIMNE, 2003. 193 pp. ISBN: 84-95999-24-2. URL: http://www.cimne.upc.es/tiendaCIMNE/ProductosCon.asp?id_prod=994 (cit. on p. 206).

[90] Peter van Oossanen. "Predicting the Speed of Sailing Yachts". In: *SNAME Transactions* 101 (1993), pp. 337–397 (cit. on p. 204).

[91] *ORC VPP Documentation 2009*. Version 1.3. Offshore Racing Congress. 2009. URL: http://www.orc.org/rules/ORC%20VPP%20Documentation%202009.pdf (cit. on p. 8).

[92] E. Oñate. "A Review of some Finite Element Families for Thick and Thin Plante and Shell Analysis". In: *Recent Developments in Finite element Analysis*. A book dedicated to Robert L. Taylor. Ed. by T.J.R. Hughes, E. Oñate, and O.C. Zienkiewicz. Barcelona: CIMNE, 1994, pp. 98–111. ISBN: 84-87867-45-6. URL: https://books.cimne.com/shop/recent-developments-in-finite-element-analysis-a-book-dedicated-to-robert-l-taylor/ (cit. on p. 28).

[93] E. Oñate. *Structural Analysis with the Finite Element Method*. Vol. 2 Plates and Shells. CIMNE-Springer, 2009. URL: https://books.cimne.com/shop/structural-analysis-with-the-finite-element-method-linear-statics-volume-2-beams-plates-and-shells/ (cit. on pp. 20, 21, 23, 24, 33, 82, 101, 181).

[94] E. Oñate and M. Cervera. "Derivation of Thin Plate Bending Elements with One Degree of Freedom per Node: A Simple Three Node Triangle". In: *Engineering Computations* 10.6 (1993), pp. 543–561. ISSN: 0264-4401. DOI: 10.1108/eb023924 (cit. on p. 29).

[95] E. Oñate and F. Flores. "Advances in the formulation of the rotation-free basic shell triangle." In: *Computer Methods in Applied Mechanics and Engineering* 194.21-24 (2005), pp. 2406–2443. DOI: 10.1016/j.cma.2004.07.039 (cit. on pp. 25, 28, 33, 165).

[96] E. Oñate and F. Zárate. "Rotation-free triangular plate and shell elements." In: *International Journal for Numerical Methods in Engineering* 47 (2000), pp. 557–603. DOI: 10.1002/(SICI)1097-0207(20000110/30)47:1/3%3C557::AID-NME784%3E3.0.CO;2-9 (cit. on pp. 25, 28, 33, 41, 176, 186).

[97] Eugenio Oñate, Julio García, and Sergio Idelsohn. "Ship Hydrodynamics". In: *Encyclopedia Of Computational Mechanics*. Ed. by Erwin Stein, René de Borst, and Thomas J.R. Hughes. Vol. 3 Fluids. Chichester: John Wiley & Sons, Ltd., 2004. Chap. 18, pp. 579–610. DOI: 10.1002/0470091355.ecm070 (cit. on p. 204).

[98] Nicola Parolini and Alfio Quarteroni. "Mathematical models and numerical simulations for the America's Cup". In: *Computational Methods in Applied Mechanics and Engineering* (194 2005), pp. 1001–1026. DOI: 10.1016/j.cma.2004.06.020 (cit. on p. 203).

[99] Lara Pellegrini. "Desarrollo y validación de un sistema para el cálculo de velas de barcos mediante el método de los elementos finitos". Máster en Métodos Numéricos para Cálculo y Diseño en Ingeniería. Spanish. Tesis de Máster. Barcelona: Universitat Politècnica de Catalunya (UPC), 2000 (cit. on p. 4).

[100] R. Phaal and C. R. Calladine. "Simple class of finite elements for plate and shell problems. II: An element for thin shells, with only translational degrees of freedom". In: *International Journal for Numerical Methods in Engineering* 35.5 (1992), pp. 979–996. ISSN: 00295981. URL: http://www.scopus.com/inward/record.url?eid=2-s2.0-0026925349\&partnerID=tZOtx3y1 (cit. on pp. 28, 140).

[101] Quoc-Hoa Pham et al. ""Geometrically nonlinear analysis of functionally graded shells using an edge-based smoothed MITC3 (ES-MITC3) finite elements"". In: *Engineering with Computers* (2019), pp. 1–14. DOI: 10.1007/s00366-019-00750-z (cit. on p. 177).

[102] B. Philipp et al. “Integrated design and analysis of structural membranes using the Isogeometric B-Rep Analysis”. In: *Computer Methods in Applied Mechanics and Engineering* 303 (2016), pp. 312–340. ISSN: 00457825. DOI: 10.1016/j.cma.2016.02.003 (cit. on p. 26).

[103] E. Ramm and W. A. Wall. “Shell structures—a sensitive interrelation between physics and numerics”. In: *International Journal for Numerical Methods in Engineering* 60.1 (2004), pp. 381–427. ISSN: 1097-0207. DOI: 10.1002/nme.967 (cit. on p. 21).

[104] Ekkehard Ramm. “Heinz Isler Schalen”. In: ed. by E. Ramm and E. Schunck. Verlag, 1986. Chap. Form und Tragverhalten, pp. 29–34 (cit. on p. 21).

[105] Fernando Rastellini et al. “Composite materials non-linear modelling for long fibre-reinforced laminates: Continuum basis, computational aspects and validations”. In: *Computers & Structures* 86 (9 2008), pp. 879–896. DOI: 10.1016/j.compstruc.2007.04.009 (cit. on p. 206).

[106] Robert Razenbach and Zhenlong Xu. “Sail Aero-Structures: Studying Primary Load Paths and Distortion”. In: *The 17th Cheasapeake Sailing Yacht Symposium*. Ed. by CSYS. The Cheasapeake Sailing Yacht Symposium. Mar. 2005, pp. 193–204 (cit. on pp. 20, 205).

[107] E. Reissner. “On the theory of bending of elastic plates”. In: *Journal of Mathematical Physics* 23 (1944), pp. 184–191 (cit. on p. 23).

[108] E. Reissner. “The effect of transverse shear deformation on the bending of elastic plates”. In: *Journal of Applied Mechanics* 12 (1945), A69–A77 (cit. on p. 23).

[109] Hee Yuel Roh and Maenghyo Cho. “The application of geometrically exact shell elements to B-spline surfaces”. In: *Computer Methods in Applied Mechanics and Engineering* 193.23-26 (June 2004), pp. 2261–2299. ISSN: 00457825. DOI: 10.1016/j.cma.2004.01.019 (cit. on p. 31).

[110] Hee Yuel Roh and Maenghyo Cho. “Integration of geometric design and mechanical analysis using B-spline functions on surface”. In: *International Journal for Numerical Methods in Engineering* 62.14 (Apr. 2005), pp. 1927–1949. ISSN: 0029-5981. DOI: 10.1002/nme.1254 (cit. on p. 31).

[111] Riccardo Rossi et al. “Simulation of light-weight membrane structures by wrinkling model”. In: *International Journal for Numerical Methods in Engineering* 62 (15 2005), pp. 2127–2153. DOI: 10.1002/nme.1266 (cit. on p. 20).

[112] Francis Sabourin and Michel Brunet. “Detailed formulation of the rotation-free triangular element “S3” for general purpose shell analysis”. In: *Engineering Computations* 23.5 (2006), pp. 469–502. ISSN: 0264-4401. DOI: 10.1108/02644400610671090 (cit. on pp. 28, 38).

[113] Nils Salvesen, Martin Fritts, and Michael Meinhold. “Technology and Design for Stars & Stripes”. In: *Finite elements in Analysis and Design* 4 (1 1988): *Special Issue on Unification of Finite Element Methods in Theory and Test*, pp. 79–82. DOI: 10.1016/0168-874X(88)90025-X (cit. on p. 200).

[114] Robert Schmidt, Roland Wüchner, and Kai-Uwe Bletzinger. “Isogeometric analysis of trimmed NURBS geometries”. In: *Computer Methods in Applied Mechanics and Engineering* 241-244 (Oct. 2012), pp. 93–111. ISSN: 00457825. DOI: 10.1016/j.cma.2012.05.021 (cit. on p. 30).

[115] A. Shenoi et al., eds. *Sailing Yacht Design*. Vol. 2: *17th International Ship and Offshore Structures Congress*. (Seoul, Korea). ISSC. 2009. Chap. Committee V.8, pp. 433–493. URL: http://139.30.101.246/ISSC2012/Material/2009/SAILING%20YACHT%20DESIGN.pdf (cit. on p. 206).

[116] J. C. Simo and M. S. Rifai. “A class of assumed strain methods and the method of incompatible modes”. In: *International Journal for Numerical Methods in Engineering* 29 (1990), pp. 1595–1638. DOI: 10.1002/nme.1620290802 (cit. on p. 106).

[117] J. C. Simo, R. L. Taylor, and K. s. Pister. “Variational and Projection Methods for the volume constraint in finite deformation elasto-plasticity”. In: *Computer Methods in Applied Mechanics and Engineering* 51 (1985), pp. 177–208. DOI: 10.1016/0045-7825(85)90033-7 (cit. on p. 106).

[118] J.C. Simo and D.D. Fox. “On a stress resultant geometrically exact shell model. Part I: Formulation and optimal parametrization”. In: *Computer Methods in Applied Mechanics and Engineering* 72.3 (Mar. 1989), pp. 267–304. ISSN: 00457825. DOI: 10.1016/0045-7825(89)90002-9 (cit. on pp. 65, 66).

[119] Dan Spurr. “The Hydrodynamicist. Winged Victory”. In: *Professional Boatbuilder* 121 (2009), pp. 50–61. URL: https://www.proboat.com/2009/09/winged-victory/ (cit. on p. 200).

[120] Gary Mitchell Stanley. “Continuum-based shell elements”. PhD thesis. Stanford University, 1985, p. 515. URL: http://searchworks.stanford.edu/view/1190339 (cit. on pp. 33, 65, 82, 193, 194).

[121] Hanryk Stolarski, Ted Belytschko, and Sang-Ho Lee. “A review of shell finite elements and corotational theories”. In: *Computational Mechanics Advances* 2.2 (1995), pp. 125–212. ISSN: "0927-7951" (cit. on pp. 21, 33).

[122] D.J. Struik. *Lectures on Classical Differential Geometry*. 2nd ed. Dover, 1988. URL: https://store.doverpublications.com/0486656098.html (cit. on pp. xxv, 34).

[123] R.L. Taylor, E. Oñate, and P.-A. Ubach. "Textile Composites and Inflatable Structures". In: ed. by E. Oñate and B. Kröplin. Vol. 3. Computational Methods in Applied Sciences. P.O. Box 17, 3300 AA Dordrecht, The Nederlands: Springer, 2005. Chap. Finite Element Analysis of Membrane Structures, pp. 47–68. DOI: 10.1007/1-4020-3317-6 (cit. on pp. 3, 4, 20, 35).

[124] Alexander Tessler, Marco Di Sciuva, and Marco Gherlone. "A consistent refinement of first-order shear deformation theory for laminated composite and sandwich plates using improved zigzag kinematics". In: *Journal of Mechanics of Materials and Structures* 5.2 (Aug. 2010), pp. 341–367. ISSN: 1559-3959. DOI: 10.2140/jomms.2010.5.341 (cit. on p. 181).

[125] Alexander Tessler, David W. Sleight, and John T. Wang. "Effective Modelling and Nonlinear Shell Analysis of Thin Membranes Exhibiting Structural Wrinkling". In: *Journal of Spacecraft and Rockets* 42.2 (2005), pp. 287–298. DOI: 10.2514/1.3915 (cit. on p. 20).

[126] Alexander Tessler et al. *Refinement of Timoshenko Beam Theory for Composite and Sandwich Beams Using Zigzag Kinematics*. Tech. rep. NASA/TP-2007-215086. Hampton, VA: NASA Langley Research Center, Nov. 2007, p. 45. URL: http://ntrs.nasa.gov/search.jsp?R=20070035078 (cit. on p. 181).

[127] Stephen Timoshenko and S. Woinowsky-Krieger. *Teoria de placas y láminas*. Ed. by Urmo. Bilbao: Urmo, 1975. URL: http://cataleg.upc.edu/record=b1030550~S1*cat (cit. on pp. 22, 158, 160, 162).

[128] Daniele Trimarchi et al. "Fluid-structure interactions of anisotropic thin composite materials for application to sail aerodynamics of a yacht in waves". In: *12th Numerical Towing Tank Symposium 2009 (NuTTS'09)*. (Cortona, Italy). Numerical Towing Tank Symposium. Curran Associates, Inc., 2009. ISBN: 9781615676149. URL: http://eprints.soton.ac.uk/69141/ (cit. on p. 20).

[129] P.-A. Ubach, C. Estruch, and J. García-Espinosa. "On the interpolation of normal vectors for triangle meshes". In: *International Journal for Numerical Methods in Engineering* 96.4 (Sept. 2013), pp. 247–268. ISSN: 00295981. DOI: 10.1002/nme.4567 (cit. on pp. 44, 46, 158, 179, 187).

[130] P.-A. Ubach and E. Oñate. "New Rotation-Free Composite Shell Triangle using Accurate Geometrical Data". In: *WCCM VII. 7th World Congress on Computational Mechanics*. Vol. CD-ROM. UCLA, iacm, Northwestern University. Los Angeles, California, USA, July 2006 (cit. on p. 38).

[131] P.-A. Ubach and E. Oñate. "Advances of the New Rotation-Free Finite Element Shell Triangle Using Accurate Geometrical Data". In: *9th US National Congress on Computational Mechanics*. Vol. CD-ROM. University of California at Berkeley, USACM. San Francisco, California, USA, July 2007 (cit. on p. 38).

[132] P.-A. Ubach and E. Oñate. "New Rotation-Free Finite Element Shell Triangle Accurately Using Geometrical Data". In: *Computer Methods in Applied Mechanics and Engineering* 199 (5-8 2009): *Computational Geometry and Analysis*, pp. 383–391. DOI: 10.1016/j.cma.2009.01.006 (cit. on pp. 27, 54, 55, 159).

[133] Pere-Andreu Ubach. "Análisis y cálculo de membranas mediante el método de los elementos finitos. Búsqueda de la aproximación inicial." Tesina Final de Carrera. Escola Tècnica Superior d'Enginyers de Camins, Canals i Ports de Barcelona, Sept. 2001. URL: http://bibliotecnica.upc.es/cddecma/colleccions/tesines/Divulgacio/Tesines/F2001/EC/Resums/Ubach_Fuentes.htm (cit. on pp. 3, 4, 20).

[134] J.G. Valdés, E. Oñate, and J. Miquel. *Nonlinear Analysis of Orthotropic Membrane and Shell Structures Including Fluid-Structure Interaction*. Monograph 107. Barcelona: CIMNE, Dec. 2007. 216 pp. ISRN: 978-84-96736-37-5. URL: https://books.cimne.com/shop/nonlinear-analysis-of-orthotropic-membrane-and-shell-structures-including-fluid-structure-interaction/ (cit. on p. 20).

[135] Eduard Ventsel and Theodor Krauthammer. *Thin Plates and Shells: Theory, Analysis, and Applications*. Ed. by Pennsylvania State University. New York: Taylor & Francis, 2001. ISBN: 0824705750. DOI: 10.1201/9780203908723 (cit. on pp. 22, 160).

[136] Charles M. Vest. *"Pursuing the Endless Frontier: Essays on MIT and the Role of Research Universities"*. "The MIT Press", 2005. ISBN: 0-262-22072-5. URL: https://mitpress.mit.edu/books/pursuing-endless-frontier (cit. on p. 175).

[137] Ignazio Maria Viola, Raffaele Ponzini, and Giuseppe Passoni. "Sailing Past a Billion". In: *ANSYS Advantage* 3 (2 2009), pp. 47–48. URL: http://www.ansys.com/magazine/issues/vol3-iss2-2009/cilea.pdf (cit. on p. 205).

[138] Gerald Wempner. "Finite elements, finite rotations and small strains of flexible shells". In: *International Journal of Solids and Structures* 5.2 (1969), pp. 117–153. DOI: 10.1016/0020-7683(69)90025-0 (cit. on p. 83).

[139] E. L. Wilson et al. "Incompatible displacement models". In: *Numerical and Computer Methods in Structural Mechanics* (1973), pp. 43–57. DOI: 10.1016/B978-0-12-253250-4.50008-7 (cit. on p. 106).

[140] K. Wisniewski and E. Turska. "Enhanced Allman quadrilateral for finite drilling rotations". In: *Computer Methods in Applied Mechanics and Engineering* 195.44-47 (Sept. 2006), pp. 6086–6109. ISSN: 00457825. DOI: 10.1016/j.cma.2005.11.003. URL: http://linkinghub.elsevier.com/retrieve/pii/S0045782505004913 (cit. on p. 102).

[141] Henry T Y Yang et al. "A survey of recent shell finite elements". In: *International Journal for Numerical Methods in Engineering* 47.1-3 (Jan. 2000), pp. 101–127. ISSN: 0029-5981. DOI: 10.1002/(SICI)1097-0207(20000110/30)47:1/3<101::AID-NME763>3.0.CO;2-C (cit. on pp. 21, 24, 83).

[142] Y.X. Zhou and K.Y. Sze. "A geometric nonlinear rotation-free triangle and its application to drape simulation". In: *International Journal for Numerical Methods in Engineering* 89.4 (Jan. 2012), pp. 509–536. ISSN: 00295981. DOI: 10.1002/nme.3250 (cit. on pp. 25, 28, 29, 140).

[143] O.C. Zienkiewicz and R.L. Taylor. *Finite Element Method*. 5th ed. Vol. 2. Oxford, UK: Butterworth-Heinemann, 2000. URL: https://www.elsevier.com/books/the-finite-element-method-for-solid-and-structural-mechanics/zienkiewicz/978-0-08-045558-7 (cit. on p. 33).

[144] O.C. Zienkiewicz and R.L. Taylor. *El Método de los Elementos Finitos*. Ed. by E. Oñate. 5th ed. Vol. 2. CIMNE, 2004. URL: https://books.cimne.com/shop/el-metodo-de-los-elementos-finitos-vol-2-mecanica-de-solidos/ (cit. on pp. 20, 21).

[145] Francisco Zárate and Eugenio Oñate. "Extended rotation-free shell triangles with transverse shear deformation effects". In: *Computational Mechanics* 49.4 (Nov. 2011), pp. 487–503. ISSN: 0178-7675. DOI: 10.1007/s00466-011-0653-y (cit. on pp. 16, 165).